

SMALL MOLECULE 20S PROTEASOME ACTIVATION: A TARGETED PROTEIN  
DEGRADATION PATHWAY FOR NEURODEGENERATION THERAPEUTICS.

By

Charles Anamoah

A DISSERTATION

Submitted to  
Michigan State University  
in partial fulfillment of the requirements  
for the degree of

Chemistry – Doctor of Philosophy

2025

## ABSTRACT

The ubiquitin-proteasome system (UPS) represents a critical pathway in maintaining cellular proteostasis by regulating protein degradation. Dysregulation in this system is implicated in neurodegenerative diseases, where the accumulation of misfolded proteins exacerbates proteotoxic stress. This dissertation investigates small-molecule activators of the 20S proteasome, leveraging its unique capacity to degrade intrinsically disordered proteins (IDPs) independent of ubiquitination. Through systematically exploring the structural and biochemical dynamics of proteasomal activation, the work delineates the therapeutic potential of targeting the 20S proteasome for neurodegenerative conditions. Initial studies characterized the interplay between protein aggregation, oxidative stress, and proteostasis disruption in diseases like Parkinson's and Alzheimer's. A focus was placed on  $\alpha$ -synuclein ( $\alpha$ -syn), an IDP whose aggregation is central to Parkinson's pathology. Chapter Two describes the design, synthesis, and biological evaluation of third-generation chlorpromazine analogs, highlighting their efficacy in promoting 20S proteasome-mediated degradation of  $\alpha$ -syn aggregates. Structure-activity relationships (SARs) were established, demonstrating the importance of specific substitutions in enhancing selectivity and minimizing off-target effects.

Subsequent investigations in Chapter Three assessed these compounds in cellular models of oxidative stress. The results revealed that 20S proteasome activators mitigate oxidative damage by selectively degrading carbonylated proteins while preserving mitochondrial function.

Chapter Four extends this work by introducing a novel piperazinone-based scaffold for 20S proteasome activators. These studies underscore the therapeutic promise of modulating proteasomal activity, providing a framework for future drug development to restore proteostasis and combat neurodegenerative diseases.

This dissertation advances our understanding of proteasomal regulation and offers a compelling strategy to address the molecular underpinnings of protein misfolding disorders. The findings pave the way for developing clinically viable interventions targeting proteostasis networks, with significant implications for treating age-related neurodegenerative diseases.

## **ACKNOWLEDGEMENTS**

Wow, what an epic journey. When I started this process, I had yet to learn what I was getting myself into. I'm glad I did, and it's worth it. I would do it again in a heartbeat.

First, thanks to the Almighty God for helping me through this challenging but fulfilling experience. I want to say a big thank you to my advisor, Dr. Tepe. I am thrilled that you allowed me to join your lab. Thank you for your time, patience, and guidance during my academic journey. Your belief in my scientific instincts has significantly contributed to my growth as a confident researcher. Lastly, thank you for bringing together such an exceptional, kind, fun, and intellectually stimulating group of individuals I have collaborated with over the last few years. In addition, I am grateful for building such an incredible group. A popular African adage goes, "It takes a village to raise a child." My rendition is "It takes a group to train a scientist," and you have built a very supportive and inclusive group.

My gratitude goes to my committee members, Dr. Wulff, Dr. Borhan, and Dr. Draths. Thank you for your guidance, patience, and support throughout my academic journey. Your directions and constructive criticisms have had a positive impact on both my professional and personal life.

To the Tepe group, past and present, you have become like family to me, and I would not have navigated this journey without your support. Sophie and Allison, I can't express how thankful I am to both of you. It is incredible how often I approached both of you for advice on various issues. Your patience in dealing with me has not only made an impact on my professional career but also inspired me to be a better person. Taylor, your calm disposition in dealing with me has been refreshing. To Katarina, I appreciate your time and effort in helping me settle in when I first joined the lab. Your regular check-in with me when the science was not working kept me going. To Grace, thank you for your kind words and advice. To Konika, no one understands my story more than you do. Thanks for all the advice and suggestions. It kept me going. Dare, thanks for all our wonderful times in the lab and on the soccer pitch. Those assists kept me going, literally. Thank you to Shafaat, Daniel, Evan, Shannon, Sydney, Miracle, and Lihn for your support and encouragement. Working with all of you was a great honor and privilege.

And to my friends, Sterling, Emmanuel, Dr. Banahene, Dr. Kavey, Julius, and Daniel, thank you for being there for me. Bismarck, I genuinely appreciate your friendship, help, and gregarious disposition on the soccer field.

I thank my family back home for their prayers and support. I would also like to thank my mother, Mary Eyiah, for all the sacrifices she made so that I could get an education. I thank my uncle, James Abbuah, and his entire family for their immense support throughout my high school and college education. I'm immensely grateful to my parents-in-law, Steve and Lynn Surdock, for their incredible support. Thank you to my siblings: Beatrice, Eunice, Jeniffer, Ebenezer, and Bismack.

I want to thank my partner, Alayna, for being there for me through thick and thin, and for relocating across the state with me to complete my program. Your thoughtfulness, patience, and affection for me kept me going during the most stressful part of my PhD journey. I want to thank my wonderful son, Grayson. Your presence gives me the strength and energy to continue when all hope is lost. You have enlightened my world, and I am blessed to have you.

Finally, I would like to thank the entire faculty at the MSU chemistry department for their incredible dedication to scientific research. I am also grateful to all the administrative and support staff in the chemistry department. Your tireless work keeps the department running.



## TABLE OF CONTENTS

|  |     |
|--|-----|
| <b>LIST OF ABBREVIATIONS</b> .....   | vi  |
| <b>CHAPTER ONE: Targeting Proteostasis via the Ubiquitin-Proteasome System: A<br/>Therapeutic Avenue for Neurodegenerative Diseases</b> .....      |     |
| 1.1 The Proteostasis Network .....   | 2   |
| 1.2 The Ubiquitin-Proteasome System .....  | 4   |
| REFERENCES .....   | 21  |
| <b>CHAPTER TWO: Design, Synthesis, and Biological Evaluation of Chlorpromazine-<br/>Based 20S Proteasome Activators</b> .....                      |     |
| 2.1 Introduction .....   | 37  |
| 2.2 Design and Synthesis of Third-Generation Chlorpromazine Analogs .....  | 43  |
| 2.3 Conclusion .....   | 55  |
| REFERENCES .....   | 57  |
| APPENDIX .....   | 65  |
| <b>CHAPTER THREE: 20S Proteasome Activation as a Therapeutic Strategy: Mitigating<br/>Oxidative Stress and Proteotoxicity in HT-22 cells</b> ..... |     |
| 3.1 Introduction .....   | 110 |
| 3.2 Rational .....   | 113 |
| 3.3 Results and Discussion .....   | 114 |
| 3.4 Conclusions .....  | 130 |
| APPENDIX .....   | 140 |
| <b>CHAPTER FOUR: Development of Novel Small Molecule Activators of the 20S<br/>Proteasome Based on Piperazinone Scaffold</b> .....                 |     |
| 4.1 Introduction .....   | 144 |
| 4.2 Rational .....   | 146 |
| 4.3 Design and synthesis of analogs .....  | 148 |
| 4.4 Biological Evaluation of Synthesized Analogs .....   | 152 |
| 4.5 Conclusion .....   | 156 |
| REFERENCES .....   | 158 |
| APPENDIX .....   | 162 |
| <b>CHAPTER FIVE: Materials and Miscellaneous</b> .....   |     |
| 5.1 Materials .....  | 206 |
| 5.2 Miscellaneous .....  | 209 |

## LIST OF ABBREVIATIONS

|                 |   |
|-----------------|---|
| 11S/PA28        | 11S Proteasome Activator Complex (also known as PA28)   |
| 13-Å            | 13 Ångström (unit of length used in molecular biology)  |
| 19S             | 19S Regulatory Particle of the Proteasome               |
| 20S             | 20S Core Particle of the Proteasome                     |
| 26S             | 26S Proteasome (composed of 20S core and 19S regulator) |
| AAA             | ATPases Associated with diverse cellular Activities     |
| ABBV-0805       | A monoclonal antibody targeting $\alpha$ -synuclein     |
| AD              | Alzheimer's Disease                                     |
| ANOVA           | Analysis of variance                                    |
| ATP             | Adenosine Triphosphate                                  |
| BCA             | Bicinchoninic Acid                                      |
| Boc-LRR-AMC     | Boc-Ler-Arg-Arg-7-amido-4-Methylcoumarin                |
| CD4+            | Cluster of Differentiation 4 Positive (T-helper cells)  |
| BTZ             | Bortezomib  |
| CO <sub>2</sub> | Carbon Dioxide  |
| COMT            | Catechol-O-Methyltransferase                            |
| COP9            | Constitutive Photomorphogenesis 9 Signalosome           |
| CPZ             | Chlorpromazine  |
| CP              | Core Particle (of the proteasome)                       |
| CT-L            | Chymotrypsin-like                                       |
| DBS             | Deep Brain Stimulation                                  |
| DMF             | Dimethylformamide                                       |
| DMSO            | Dimethyl Sulfoxide                                      |
| DNA             | Deoxyribonucleic Acid                                   |
| DNPH            | Dinitrophenylhydrazine                                  |
| DTT             | Dithiothreitol  |
| E1              | Ubiquitin-Activating Enzyme                             |
| E2              | Ubiquitin-Conjugating Enzyme                            |

|          |   |
|----------|---|
| E3       | Ubiquitin Ligase  |
| ECL      | Enhanced Chemiluminescence                                |
| ETC      | Electron Transport Chain                                  |
| FBS      | Dinitrophenylhydrazine                                    |
| FCCP     | Carbonyl cyanide-p-trifluoromethoxyphenylhydrazone        |
| GAPDH    | Glyceraldehyde 3-Phosphate Dehydrogenase                  |
| GBA      | Glucocerebrosidase (gene associated with PD)              |
| GSH      | Reduced Glutathione                                       |
| GSSG     | Oxidized Glutathione                                      |
| HBSS     | Hanks' Balanced Salt Solution                             |
| HD       | Huntington's Disease                                      |
| HT-22    | Mouse Hippocampal Cell Line                               |
| HECT     | Homologous to E6-AP Carboxyl Terminus                     |
| HEK      | Human Embryonic Kidney                                    |
| HEPS     | 4-(2-hydroxyethyl)-1-piperazineethanesulfonic acid        |
| HRMS     | High-Resolution Mass Spectrometry                         |
| HSR      | Heat Shock Response                                       |
| IDP      | Intrinsically Disordered Protein                          |
| IL-8     | Interleukin 8   |
| IUBMB    | International Union of Biochemistry and Molecular Biology |
| K48      | Lysine 48   |
| LC-MS/MS | Liquid Chromatography–Tandem Mass Spectrometry            |
| LRRK2    | Leucine-Rich Repeat Kinase 2                              |
| MAO-B    | Monoamine Oxidase B                                       |
| Mdm2     | Mouse Double Minute 2                                     |
| MHC      | Major Histocompatibility Complex                          |
| MPO      | Multi-parameter Optimization                              |
| MSA      | Multiple System Atrophy                                   |
| MS       | Multiple Sclerosis  |
| NADPH    | Nicotinamide Adenine Dinucleotide Phosphate               |
| NIH      | National Institutes of Health                             |

|                   |   |
|-------------------|---|
| NMDA              | N-Methyl-D-Aspartate                                      |
| NMR               | Nuclear Magnetic Resonance                                |
| NO                | Nitric Oxide  |
| ONOO <sup>-</sup> | Peroxynitrite   |
| NOS               | Nitric Oxide Synthase                                     |
| NQO1              | NAD(P)H Quinone Dehydrogenase 1                           |
| RIPA              | Radioimmunoprecipitation Assay                            |
| PA28              | Proteasome Activator 28                                   |
| PA200             | Proteasome Activator 200                                  |
| PBS               | Phosphate-Buffered Saline                                 |
| PD                | Parkinson's Disease                                       |
| PN                | Proteostasis Network                                      |
| PVDF              | Polyvinylidene Difluoride                                 |
| P53               | Tumor Protein P53   |
| P73               | Tumor Protein P73   |
| PPI               | Protein-Protein Interaction                               |
| RNA               | Ribonucleic Acid  |
| RNS               | Reactive Nitrogen Species                                 |
| ROS               | Reactive Oxygen Species                                   |
| RPA               | Replication Protein A                                     |
| RP                | Regulatory Particle (of the proteasome)                   |
| RT                | Room Temperature  |
| SDS-PAGE          | Sodium Dodecyl Sulfate Polyacrylamide Gel Electrophoresis |
| SOD               | Superoxide Dismutase                                      |
| SNCA              | Synuclein Alpha (gene encoding $\alpha$ -synuclein)       |
| Suc-LLVY-AMC_     | Suc-Leu-Leu-Val-Tyr-7-amido-4-Methylcoumarin              |
| TBHP              | Tert-Butyl Hydroperoxide                                  |
| TCA               | Trichloroacetic Acid                                      |
| TCH-165           | A small molecule proteasome activator                     |
| TEA               | Triethylamine   |

|           |   |
|-----------|---|
| THF       | Tetrahydrofuran                                 |
| T-L       | Trypsin-like                                    |
| TMRM      | Tetramethylrhodamine, Methyl Ester, Perchlorate |
| TMT       | Tandem Mass Tag                                 |
| UBA       | Ubiquitin-Associated Domain                     |
| UBL       | Ubiquitin-Like Domain                           |
| UPR       | Unfolded Protein Response                       |
| UPS       | Ubiquitin-Proteasome System                     |
| USP14     | Ubiquitin-Specific Protease 14                  |
| USP7      | Ubiquitin-Specific Protease 7                   |
| Z-LLE-AMC | Z-Leu-Leu-Glu-7-amido-4-Methylcoumarin          |

**CHAPTER ONE:** Targeting Proteostasis via the Ubiquitin-Proteasome System: A  
Therapeutic Avenue for Neurodegenerative Diseases

## 1.1 The Proteostasis Network

Proteostasis, or protein homeostasis, is the delicate balance of processes that manage the synthesis, folding, trafficking, and degradation of proteins to maintain a functional and stable proteome.<sup>1</sup> This balance is critical for cellular health. It enables adaptation to various physiological and environmental conditions while preventing the toxic accumulation of misfolded or aggregated proteins.<sup>2</sup>

Protein synthesis, managed by ribosomes and translation machinery, produces polypeptides, laying the foundation for proteostasis. This process is tightly regulated to ensure fidelity and efficiency. Molecular chaperones, such as heat shock proteins (HSPs), play a central role by facilitating the correct folding of nascent polypeptides, preventing aggregation, and refolding misfolded proteins under stress conditions (**Figure 1.1**).<sup>3</sup>

Degradation pathways are equally critical. The ubiquitin-proteasome system (UPS) targets damaged or misfolded proteins for proteasomal degradation in a ubiquitin-dependent manner.<sup>4–6</sup> Complementing this, the autophagy-lysosome pathway clears long-lived proteins, aggregates, and damaged organelles, providing a secondary defense against proteotoxic stress.<sup>7</sup> Stress response pathways, including the unfolded protein response (UPR) and the heat shock response (HSR), detect and mitigate disruptions in proteostasis by upregulating protective proteins and molecular chaperones.<sup>8,9</sup> These components work interconnectedly, adapting dynamically to cellular needs and environmental changes.<sup>10</sup> Together, they safeguard the proteome, ensuring cellular health and preventing the accumulation of toxic protein aggregates, a hallmark of several age-related and neurodegenerative diseases.<sup>11–13</sup>

The proteostasis network (PN) maintains cellular metabolism, signaling, and structural integrity, enabling long-term tissue functionality. It helps cells adapt to proteotoxic stresses, such as oxidative damage or nutrient imbalance, ensuring proteome quality across an organism's lifespan.<sup>14,15</sup>

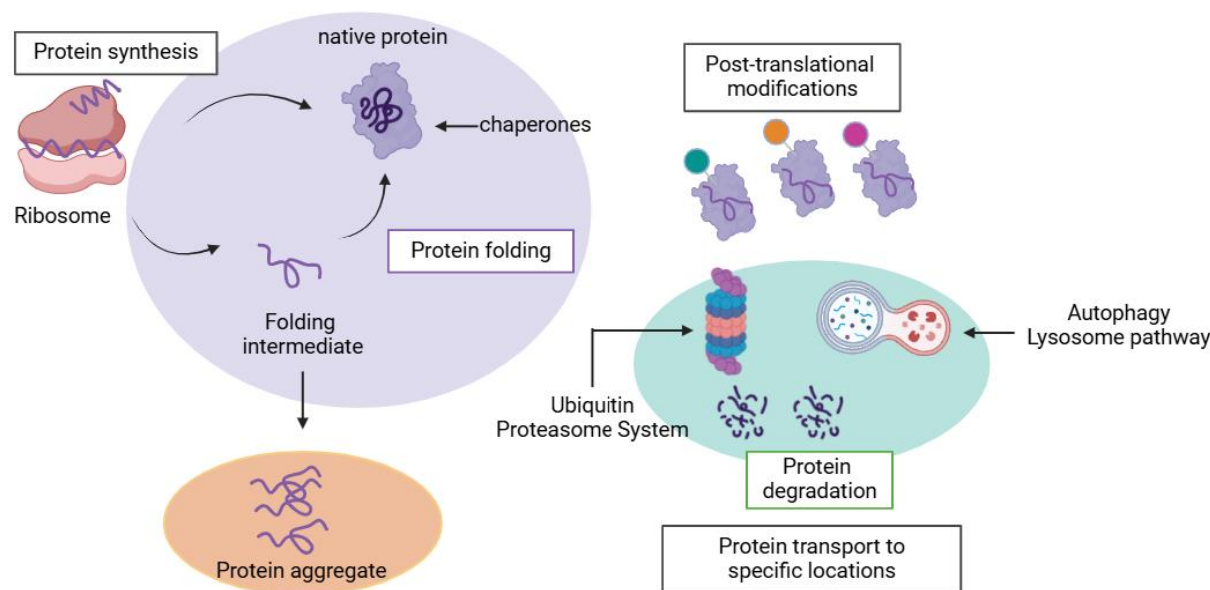


**Figure 1.1: Schematic Representation of the Proteostasis Network and Its Regulatory Components.**

Maintaining proteostasis relies on the intricate balance between protein folding and degradation. While specific proteins can achieve their functional native conformation spontaneously, the folding of many others is facilitated by molecular chaperones, which play a critical role in ensuring proper protein structure and function within the cellular environment.

However, disruptions in proteostasis can lead to the accumulation of aberrant protein aggregates, which are strongly linked to neurodegenerative diseases. For example, Alzheimer's disease (AD) is marked by  $\beta$ -amyloid plaques and tau tangles, while Huntington's and Parkinson's diseases (PD) involve the aggregation of huntingtin and  $\alpha$ -synuclein, respectively.<sup>16–18</sup> Aging exacerbates these challenges, as the PN's capacity to manage proteotoxic stress declines, contributing to the onset and progression of age-related conditions like neurodegeneration and cancer.<sup>19</sup> Understanding the PN's dynamics provides valuable insights into developing therapeutic strategies. Targeting pathways like the UPS or autophagy could help restore proteostasis, offering potential treatments for these debilitating disorders. The proteostasis network remains a



cornerstone of cellular health and a critical area of focus for combating age-related and neurodegenerative diseases.

## 1.2 The Ubiquitin-Proteasome System

The 26S proteasome is large, approximately 2.5 MDa.<sup>20</sup> It is an ATP-dependent proteolytic complex that degrades ubiquitinated proteins, playing a central role in maintaining cellular protein homeostasis.<sup>21</sup> It comprises a 20S core particle (CP) and one or two 19S regulatory particles (RPs). The 20S CP provides proteolytic activity, housing three catalytic sites responsible for cleaving substrates with distinct specificities (**Figure 1.2 A**). The RPs recognize polyubiquitinated substrates, unfold them, and translocate them into the core for degradation.<sup>14,22</sup>

Structurally, the CP is a cylindrical, multimeric complex that functions as the catalytic core of the proteasome system. It comprises four stacked heptameric rings arranged symmetrically, forming a structure that facilitates the highly regulated degradation of proteins. The outer two rings consist of  $\alpha$ -subunits, while  $\beta$ -subunits form the inner two rings. Together, these subunits create a central proteolytic chamber, a hallmark of the proteasome's unique design, ensuring specificity and efficiency in protein degradation.<sup>4,23,24</sup> The  $\alpha$ -subunits, denoted as  $\alpha 1$ - $\alpha 7$ , constitute the outer rings of the CP. These subunits are not catalytically active but serve as critical gatekeepers of the proteasome.<sup>20</sup> Their primary role is to regulate access to the proteolytic chamber, ensuring that substrates enter only under appropriate conditions. The amino-terminal (N-terminal) tails of the  $\alpha$ -subunits form a dynamic "gate" that occludes the 13-Å central pore, effectively restricting entry to the catalytic chamber.<sup>20</sup> This structural arrangement is termed the "closed-gate" conformation. Within this conformation, the N-terminal ends harbor a highly conserved tyrosine-aspartate-arginine (YDR) motif, facilitating the formation of inter-subunit salt bridges (**Figure 1.2 C**).<sup>14,25</sup> These interactions stabilize the occlusive architecture by anchoring the tails in a position that obstructs the pores.

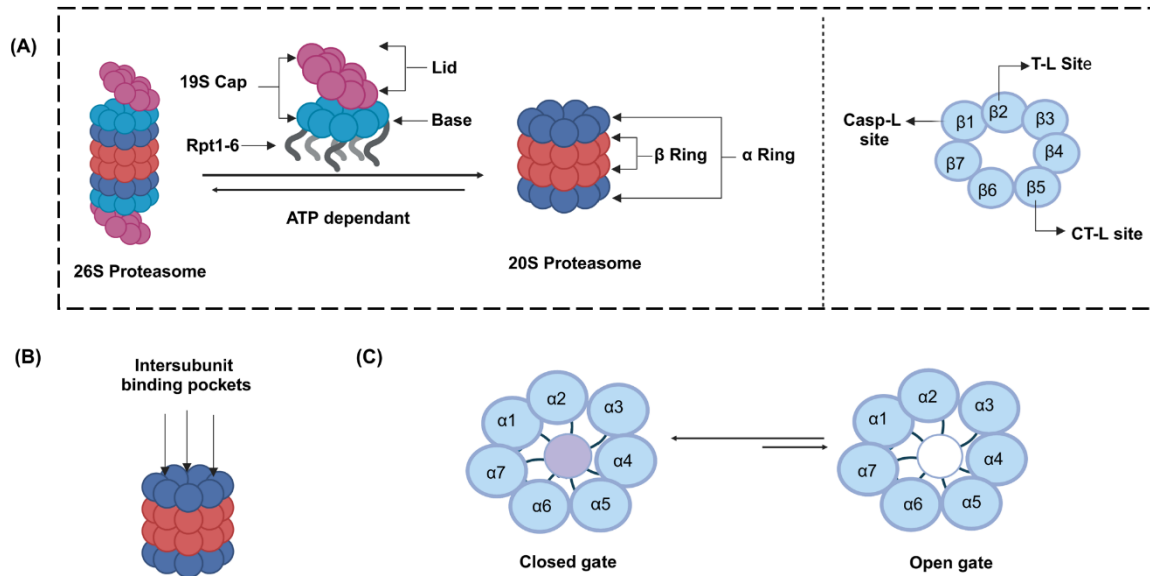


### **Figure 1.2: The Structural Components of the Ubiquitin-Proteasome System (UPS).**

The 20S proteasome, in its low-activity or latent state, contains three distinct catalytic sites within the  $\beta$ -rings: chymotrypsin-like ( $\beta 5$ ), trypsin-like ( $\beta 2$ ), and caspase-like ( $\beta 1$ ). A dynamic equilibrium exists between the 20S proteasome and the fully active 26S proteasome, which assembles through ATP-dependent docking of the 19S regulatory particle (RP). (B) 20S proteasome CP showing the intersubunit pockets where the rpt tails of the 19S cap bind to initiate gate opening. (C) A top view of the  $\alpha$ -ring shows the closed and opened gate conformation of the 20S proteasome. The N-terminal tails of  $\alpha$ -subunits obstruct access to the proteolytic chamber in the closed conformation. Transition to the open conformation, where these tails are displaced, permits substrate entry to the catalytic sites.

Among the  $\alpha$ -subunits, the N-terminal tail of the  $\alpha 3$  subunit plays a pivotal role in maintaining the integrity of the closed gate. Deletion of this specific tail has been demonstrated to significantly compromise gate stability, thereby increasing substrate accessibility to the proteolytic sites.<sup>26,27</sup> Although the CP exists predominantly in the closed-gate conformation under physiological conditions, it exists in dynamic equilibrium with an open-gate state (**Figure 1.2 C**). In this latter state, the N-terminal tails transiently disengage from their inhibitory position, permitting periodic substrate access to the proteolytic core.

An insightful study by Osmulski and Gaczynska, utilizing the precision of atomic force microscopy, demonstrated that the proteasome gates can open independently of additional protein binding or external activators. Notably, approximately 25% of yeast 20S proteasomes were found to adopt an 'open' conformation naturally.<sup>28</sup> In addition, when it interacts with regulatory particles such as the 19S cap or alternative activators like PA28/11S, the gate undergoes conformational changes, allowing substrate entry.<sup>29</sup> This regulatory function is central to maintaining proteasome fidelity and preventing unwarranted proteolytic activity.<sup>30–32</sup>

The  $\beta$ -subunits, designated as  $\beta$ 1– $\beta$ 7, form the two inner rings of the 20S proteasome and house the active sites responsible for proteolytic activity. Among these, three subunits— $\beta$ 1,  $\beta$ 2, and  $\beta$ 5—are catalytically active, exhibiting distinct substrate specificities.<sup>22</sup> The  $\beta$ 1 subunit mediates caspase-like activity, preferentially cleaving peptide bonds after acidic residues. The  $\beta$ 2 subunit exhibits trypsin-like activity, cleaving after basic residues. The  $\beta$ 5 subunit performs chymotrypsin-like activity, targeting hydrophobic residues.<sup>23</sup> This division of labor among the  $\beta$ -subunits allows the proteasome to degrade a wide array of protein substrates rapidly.<sup>33</sup>

The catalytic  $\beta$ -subunits undergo a tightly regulated maturation process during proteasome assembly. Initially synthesized as inactive precursors, these subunits possess *N*-terminal propeptides that block their active sites. Autocatalytic cleavage removes these propeptides, exposing the catalytic threonine residues essential for peptide bond hydrolysis.<sup>34,35</sup> This threonine-based mechanism is a unique feature of the proteasome, differentiating it from other proteases and ensuring that proteolytic activity is activated only under controlled conditions.

The remaining  $\beta$ -subunits— $\beta$ 3,  $\beta$ 4,  $\beta$ 6, and  $\beta$ 7—are not catalytically active but contribute to the proteasome's structural integrity. These subunits help stabilize the cylindrical architecture and facilitate the spatial organization of the catalytic subunits, optimizing the proteasome's function.<sup>22,24</sup> In specialized forms of the proteasome, such as the immunoproteasome, certain  $\beta$ -subunits, including  $\beta$ 1i,  $\beta$ 2i, and  $\beta$ 5i, replace their standard counterparts.<sup>36,37</sup> This substitution alters the proteasome's substrate specificity, enabling the generation of peptides suitable for antigen presentation via the major histocompatibility complex (MHC) class I pathway.<sup>38</sup> Such adaptations underscore the

proteasome's versatility and ability to respond to physiological and immunological demands.

The intricate arrangement of the  $\alpha$ - and  $\beta$ -subunits forms a highly specialized proteolytic chamber. This enclosed environment ensures that proteolytic activity is restricted to targeted substrates, minimizing collateral damage to other cellular components. Furthermore, the interaction between the  $\alpha$ -subunits and regulatory particles, such as the 19S cap, allows the proteasome to adapt its activity to cellular needs, enabling the degradation of ubiquitinated proteins under ATP-dependent conditions.

The **19S regulatory particle (RP)** is an essential component of the 26S proteasome, playing a critical role in substrate recognition, unfolding, and translocation into the 20S proteolytic core. Structurally, the 19S RP is a highly dynamic assembly divided into two functional subcomplexes: the base and the lid, each performing distinct yet interdependent roles crucial for proteasomal activity (**Figure 1.2A**). This structural organization ensures the efficient degradation of ubiquitinated proteins and the maintenance of cellular proteostasis.<sup>39</sup>

The **base subcomplex** is primarily responsible for engaging the 20S core particle and facilitating substrate translocation.<sup>40</sup> It comprises six ATPases (Rpt1–Rpt6) arranged in a heterohexameric ring and non-ATPase components, such as Rpn1 and Rpn2.<sup>31</sup> These ATPases utilize energy from ATP hydrolysis to drive conformational changes necessary for substrate unfolding and translocation.<sup>41</sup> Their C-terminal tails dock into intersubunit pockets of the  $\alpha$ -ring in the 20S core using a conserved hydrophobic-tyrosine-any residue (HbYX) motif.<sup>30</sup> This interaction induces an open-gate conformation, granting substrates access to the proteolytic chamber. Rpn1 and Rpn2 act as scaffolds and ubiquitin-binding hubs, anchoring ubiquitinated substrates and facilitating subsequent processing.<sup>42</sup> This intricate arrangement underscores the functional complexity of the base in proteasomal activity.

The **lid subcomplex**, comprising nine non-ATPase subunits, complements the base by mediating substrate deubiquitination. Key components of the lid include Rpn3, Rpn5–Rpn9, Rpn11, Rpn12, and Sem1, among which Rpn11 plays a pivotal role.<sup>43,44</sup> Rpn11, a  $\text{Zn}^{2+}$ -dependent metalloprotease, cleaves polyubiquitin chains from substrates in an ATP-independent manner, enabling the recycling of ubiquitin and ensuring that only the target

protein is translocated for degradation.<sup>45</sup> The lid subunits exhibit evolutionary conservation, with structural homology to components of the COP9 signalosome, further highlighting their regulatory significance.<sup>46</sup> The lid's integration with the base and its interactions with accessory proteins underscores its central role in substrate processing and proteolytic specificity.

Functionally, the 19S RP exhibits remarkable dynamism, with ATP binding and hydrolysis driving structural transitions in the ATPase ring. These conformational changes propagate the mechanical force required for substrate unfolding and movement into the 20S core. The RP also incorporates multiple ubiquitin receptors, including Rpn10 and Rpn13, which enhance its ability to recognize and process substrates tagged with diverse ubiquitin chain types and lengths.<sup>41</sup> This versatility allows the proteasome to degrade various protein substrates, adapting to the cellular environment's demands.

### **1.2.1 Ubiquitin-dependent proteasome degradation pathway**

The ubiquitin-proteasome system (UPS) is the principal pathway for targeted protein degradation in eukaryotic cells.<sup>47</sup> The UPS ensures cellular homeostasis and proper functionality by selectively removing damaged, misfolded, or redundant proteins.<sup>15,20,48</sup> This intricate system integrates substrate tagging with ubiquitin, recognition by proteasomal receptors, and subsequent degradation.<sup>49</sup> Below, I delve into substrate requirements, ubiquitination mechanisms, substrate recognition, and the role of initiation regions in the degradation process.

For efficient degradation, substrates must be tagged with ubiquitin, a conserved 76-residue polypeptide, via a process known as ubiquitination.<sup>50,51</sup> Ubiquitin is conjugated to lysine residues on target proteins through isopeptide bonds, forming either mono- or polyubiquitin chains.<sup>52</sup> The classical understanding is that ubiquitin chains formed via linkage at Lys48 serve as a signal for proteasomal degradation.<sup>53–55</sup> Biochemical studies have demonstrated that the proteasome requires a minimum chain length of four ubiquitin molecules for effective recognition.<sup>53</sup> Lys11 and other mixed linkage chains can also serve regulatory roles in specific contexts.<sup>2,15,20,56</sup> Substrates must also contain disordered regions, termed initiation regions, which are critical for engaging the proteasome's ATPase motor.<sup>57–59</sup> These regions facilitate substrate unfolding and translocation into the proteolytic chamber, ensuring that only appropriately modified proteins are targeted.

Ubiquitination involves a highly regulated enzymatic cascade comprising three key enzyme classes: E1 ubiquitin-activating enzymes, E2 ubiquitin-conjugating enzymes, and E3 ubiquitin ligases.<sup>7,60</sup> The process begins with E1 activating ubiquitin in an ATP-dependent reaction, forming a high-energy thiol ester bond between ubiquitin's C-terminal glycine and the cysteine residue of E1. Activated ubiquitin is then transferred to an E2 enzyme, which collaborates with an E3 ligase to attach ubiquitin to the substrate. E3 ligases determine substrate specificity by recognizing degrons—short sequence motifs or structural features that signal degradation.<sup>61,62</sup> Distinct E3 ligase families employ varied mechanisms to transfer ubiquitin. For example, Cullin-RING ligases (CRLs) facilitate direct ubiquitin transfer from E2 to the substrate, while HECT domain (homologous to E6-associated protein C terminus) E3 ligases form an intermediate ubiquitin-thioester complex before conjugation.<sup>60</sup> Polyubiquitination occurs by sequentially adding ubiquitin moieties, forming chains linked at specific lysine residues **Figure 1.3**). The structure and topology of these chains, governed by E2-E3 combinations, determine substrate fate. K48-linked chains typically signal proteasomal degradation, while alternative linkages can modulate cellular signaling or trafficking.<sup>63</sup>

Proteasomal degradation begins with substrate recognition by ubiquitin receptors located within the regulatory particle (RP) of the 26S proteasome. Rpn10 and Rpn13 are the primary ubiquitin-binding receptors for K48-linked ubiquitination.<sup>64</sup> These receptors interact with polyubiquitin chains via their ubiquitin-interacting motifs (UIMs), with Rpn10 showing specificity for K48-linked chains and Rpn13 displaying broader binding capabilities.<sup>65</sup> Rpn1, another receptor, is a docking site for shuttle proteins like Rad23 and Dsk2, facilitating substrate delivery.<sup>66</sup>

Shuttle proteins play a critical role in expanding the proteasome's substrate repertoire. For instance, Rad23 contains ubiquitin-associated (UBA) domains that bind polyubiquitin chains and ubiquitin-like (UBL) domains that interact with the proteasome.<sup>66</sup> These proteins bridge substrates to the proteasome, streamlining delivery and ensuring efficient processing. Rpn10 and Rpn13 can also act synergistically, enhancing polyubiquitin binding and substrate capture.<sup>67</sup>

Deubiquitination before proteolysis is a critical regulatory step in the ubiquitin-proteasome system, partly mediated by the proteasomal deubiquitinating subunit Rpn11.<sup>68</sup>

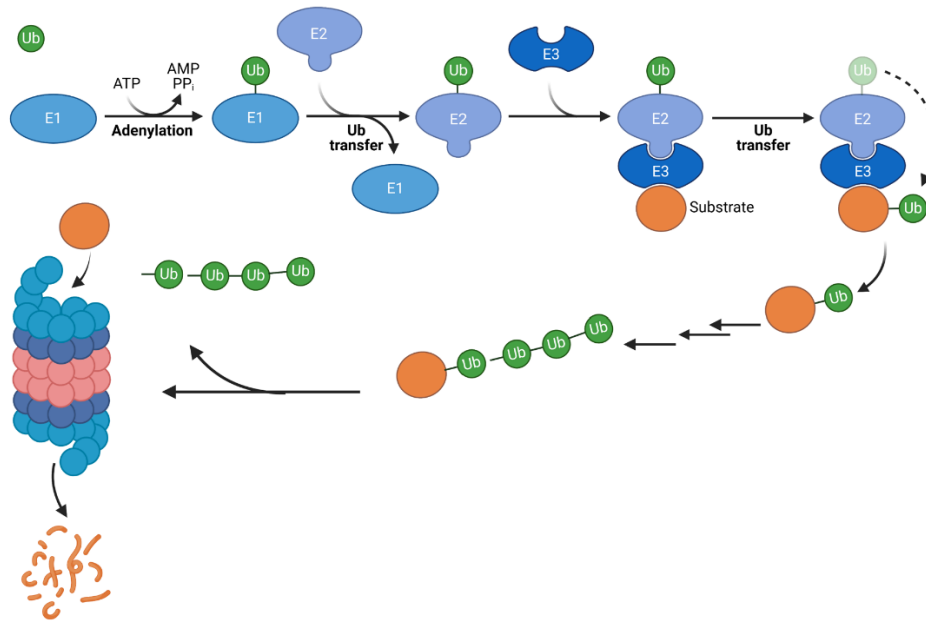


**Figure 1.3: Mechanism of Ubiquitination.**

This is an illustration of the ubiquitination mechanism, showing E1 activating ubiquitin, E2 transferring it, and E3 ligase attaching ubiquitin to a substrate protein, forming a polyubiquitin chain.

This metalloprotease within the 19S regulatory particle cleaves ubiquitin chains from substrates as they are translocated into the 20S core for degradation.<sup>46</sup> Other deubiquitinating enzymes (DUBs), such as USP14 and USP7, may act earlier to edit or remove ubiquitin chains, preventing excessive ubiquitination or rescuing substrates from degradation.<sup>69</sup> This process ensures the selective turnover of properly marked proteins and recycles ubiquitin, maintaining cellular ubiquitin homeostasis.

Initiation regions within substrates are indispensable for successful degradation. These disordered regions serve as entry points for the proteasome's ATPase motor, enabling substrate unfolding and translocation into the proteolytic chamber.<sup>70</sup> The interplay between ubiquitin chains and initiation regions ensures precise substrate processing. Proteasomal ubiquitin receptors align the ubiquitin tag with the initiation site, facilitating substrate engagement and degradation. Substrates with well-exposed initiation regions are processed efficiently, while those with buried or inaccessible initiation sites may require further modifications to engage the proteasome effectively.<sup>71,72</sup>

Once a substrate protein is translocated to the proteolytic sites within the CP of the proteasome, its peptide bonds are hydrolytically cleaved by the proteasome's catalytic activities. These catalytic sites, classified as chymotrypsin-like, trypsin-like, and caspase-like, work synergistically to degrade the substrate into small peptide fragments of varying lengths.<sup>35</sup> These fragments are subsequently released into the cytosol, where they can undergo further processing. Cytosolic peptidases recycle some peptides into amino acids, providing building blocks for new protein synthesis.<sup>73</sup> In contrast, others may be used as signaling molecules or presented as antigens in immune surveillance.<sup>74,75</sup> This degradation process is tightly regulated to maintain proteostasis and cellular function.

### **1.2.2 Ubiquitin-independent proteasome degradation pathway**

The 20S proteasome ubiquitin-independent proteasomal degradation (UblnPD) pathway is a critical mechanism that ensures protein homeostasis under physiological and stress conditions. At the center of this pathway is the 20S core particle (20S CP), a barrel-shaped catalytic particle capable of degrading proteins without ubiquitin tagging or ATP-dependent unfolding, as required by the 26S proteasome.<sup>6,76,77</sup> The UblnPD relies on proteins' intrinsic properties, such as structural disorder, oxidative modifications, or specific sequence motifs, to highlight the proteasome system's adaptability and versatility in managing diverse cellular challenges.<sup>78–81</sup>

Unlike the 26S proteasome, which depends on ATP-driven regulators for substrate processing, the UblnPD operates autonomously.<sup>82</sup> This autonomy allows it to directly degrade structurally disordered or oxidatively damaged proteins, making it indispensable in stress responses, particularly during oxidative stress.<sup>83,84</sup>

Substrate recognition in UblnPD primarily depends on the structural properties of target proteins. Proteins with intrinsically disordered regions (IDRs) or intrinsically disordered proteins (IDPs) are especially susceptible to UblnPD (**Figure 1.3**).<sup>85</sup> These proteins lack stable tertiary structures, enabling them to pass through the proteasome's narrow gating aperture without prior unfolding.<sup>86</sup> Studies have shown that IDPs, particularly those involved in RNA processing, splicing, and translation, are enriched among UblnPD substrates.<sup>87,88</sup> Such proteins often contain prion-like domains or low-complexity sequences, which increase their susceptibility to degradation. The 20S proteasome plays



a vital role in cellular quality control and adaptation by targeting these dynamic and transiently disordered molecules.

Oxidative modifications also play a significant role in substrate recognition. Oxidative stress leads to modifications such as carbonylation and glutathionylation, destabilizing protein conformations and making them prone to aggregation and toxicity (**Figure 1.3**).<sup>89–</sup>

<sup>92</sup> Unlike the 26S proteasome, which is susceptible to oxidative inactivation, the 20S proteasome remains functional under these conditions.<sup>93</sup> This resilience enables the 20S proteasome to act as a frontline defense against proteotoxic stress, clearing damaged proteins and preventing their accumulation into aggregates that could compromise cellular integrity.

In addition to structural disorder and oxidative damage, specific sequence-specific motifs, such as C-terminal degrons (C-degrons), facilitate substrate recognition.<sup>94</sup> These degrons are molecular tags that guide proteins to the 20S proteasome for degradation. Recent studies have identified a growing repertoire of proteins reliant on such motifs, underscoring the specificity and efficiency of ubiquitin-independent protein degradation.<sup>95</sup> For instance, tert-butyl carbamate (Boc<sub>3</sub>)-protected arginine (B<sub>3</sub>A)-linked tags have been used to induce glutathione S-transferase alpha (GST-α) degradation by the 20S proteasome.<sup>96</sup> Furthermore, endogenous proteasomal activators, including PA28 and PA200, enhance the 20S proteasome's ability to degrade oxidized or partially unfolded proteins.<sup>29,97</sup> These activators interact with the α-subunits, promoting gate opening and facilitating substrate entry, thereby broadening the proteasome's substrate repertoire.

The 20S proteasome's adaptability is further illustrated by its dynamic response to cellular stress. The 26S proteasome often disassembles during oxidative stress into its 20S core and 19S regulatory components.<sup>52,98</sup> This disassembly can also be facilitated by proteasome-interacting proteins such as Ecm29, which increases the availability of free 20S particles and prioritizes the degradation of oxidatively modified proteins.<sup>99</sup> This redistribution of proteasomal activity ensures that cells can rapidly address protein damage while conserving energy, as 20S proteasome-mediated processes do not require ATP. Such flexibility underscores the proteasome's role in cellular resilience and stress adaptation.

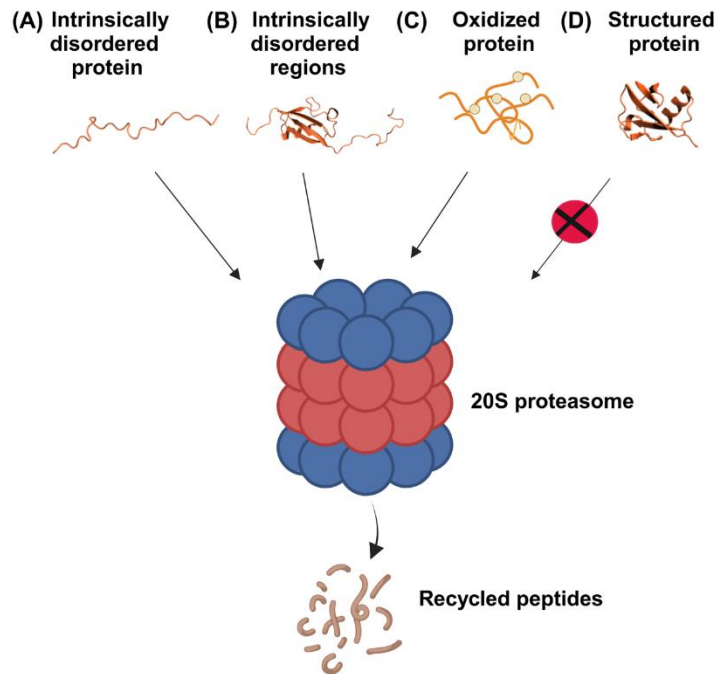


**Figure 1.4: Substrate Requirement for Ubiquitin-Independent Proteasome Degradation.**

Proteins that are (A) intrinsically disordered, (B) have disordered regions, or (C) oxidatively damaged under ubiquitin-independent proteasome degradation. (D) Structured proteins do not undergo ubiquitin-independent proteasome degradation.

The UbInPD also contributes significantly to cellular regulation and aging.<sup>2,14,87,88</sup> For example, proteins such as p53, which is integral to cell cycle control and stress responses and has unstructured N- and C-termini, are subject to UbInPD.<sup>102</sup> However, p53 typically escapes degradation under physiological conditions by the proteasome. This resistance is attributed to regulatory mechanisms that stabilize its structure or mask its unstructured regions. One critical regulator is the NAD(P)H quinone oxidoreductase 1 (NQO1), which binds p53 in an NADH-dependent manner, shielding it from the proteasome.<sup>103,104</sup> This interaction prevents p53 from entering the 20S catalytic chamber, effectively protecting it from degradation. Disruption of this interaction using NQO1 inhibitors, such as dicoumarol, destabilizes p53, making it susceptible to ubiquitin-independent degradation.<sup>105</sup> This enables precise modulation of their levels, allowing dynamic responses to environmental and intracellular cues. Although UbInPD has long been taught to proceed without ubiquitination, Lee and coworkers showed that an open-gate mutant 20S

proteasome enhanced ubiquitin-conjugate degradation compared to wild-type.<sup>26</sup> Similar studies using mutants in model organisms such as *Caenorhabditis elegans* have shown that enhancing 20S proteasome activity extends lifespan and increases resistance to proteotoxic stress.<sup>27</sup> These findings suggest that promoting UbInPD could be a promising therapeutic approach for age-related diseases and disorders characterized by protein aggregation, such as Alzheimer's, Parkinson's, and Huntington's.<sup>15,106–109</sup>

The evolutionary significance of UbInPD further underscores its importance in cellular biology. The 20S proteasome's ability to degrade unstructured proteins without ubiquitination reflects its primordial role as an ancestral proteolytic system.<sup>110</sup> This capability predates the evolution of ubiquitination, highlighting the 20S proteasome as a fundamental pathway in protein quality control. The coexistence of ubiquitin-dependent and ubiquitin-independent degradation mechanisms in modern cells illustrates the proteasome's remarkable adaptability and essential role in maintaining proteostasis across diverse biological contexts.

### **1.2.3 Proteostasis impairment in neurodegenerative diseases**

Neurodegenerative diseases, including Alzheimer's disease (AD), Parkinson's disease (PD), and Huntington's disease (HD), are among the most debilitating conditions of aging populations. These disorders, characterized by progressive neuronal loss, significantly impact cognitive, motor, and behavioral functions. Globally, over 55 million people live with dementia, with AD accounting for 60–70% of cases. PD affects more than 10 million people worldwide, while HD, though rare, affects approximately 5–10 individuals per 100,000. Aging is the primary risk factor for these diseases, with AD and PD predominantly manifesting after age 60, while HD often presents between ages 30 and 50 due to its genetic etiology.<sup>111–113</sup>

The role of aging in neurodegenerative diseases is profound. Aging is associated with genomic instability<sup>114</sup>, telomere attrition<sup>13,115</sup>, mitochondrial dysfunction, and the accumulation of oxidative damage.<sup>17,116</sup> These processes disrupt cellular homeostasis and render neurons vulnerable to degeneration. Oxidative stress, a hallmark of aging, arises from an imbalance between the production of reactive oxygen species (ROS) and the body's antioxidant defenses. This imbalance damages lipids, proteins, and DNA, exacerbating neuronal dysfunction and cell death.<sup>101,117</sup>

Protein aggregation is a defining pathological feature of neurodegenerative diseases. In AD, extracellular plaques of amyloid-beta ( $A\beta$ ) and intracellular neurofibrillary tangles of hyperphosphorylated tau protein accumulate, disrupting synaptic function and inducing inflammation.<sup>118–120</sup> PD is marked by the aggregation of alpha-synuclein ( $\alpha$ -syn) into Lewy bodies, primarily affecting dopaminergic neurons in the substantia nigra.<sup>121–123</sup> HD, caused by a genetic mutation leading to the production of a mutant huntingtin protein, involves intracellular aggregates that interfere with neuronal processes.<sup>124</sup> These aggregates result from disrupted proteostasis, the cellular balance of protein synthesis, folding, and degradation.

The onset and progression of these diseases vary. AD typically manifests as memory impairment and cognitive decline, progressing to affect behavior, visuospatial abilities, and daily functioning. The average age of onset is 65 years, with prevalence doubling every five years in older age groups.<sup>120</sup> PD often begins around age 60, with early symptoms including tremors, rigidity, and bradykinesia.<sup>125</sup> Cognitive decline may follow in advanced stages<sup>126</sup>. HD differs in its earlier onset, often presenting with motor disturbances, such as chorea, alongside psychiatric symptoms and cognitive decline.

Current treatment strategies aim to alleviate symptoms and improve quality of life, as no cures exist for these diseases. For AD, medications like cholinesterase inhibitors (e.g., donepezil, rivastigmine) and the *N*-methyl-D-aspartate (NMDA) receptor antagonist memantine can modestly improve cognitive symptoms.<sup>16,126</sup> Emerging therapies targeting amyloid plaques and tau protein, such as monoclonal antibodies like aducanumab, aim to slow disease progression.<sup>127</sup> Non-pharmacological approaches, including cognitive training and lifestyle interventions, also show promise. PD treatments focus on managing motor symptoms. Levodopa, often combined with carbidopa, remains the gold standard, replenishing dopamine levels in the brain.<sup>128</sup> Dopamine agonists, monoamine oxidase-B (MAO-B), and catechol-O-methyltransferase (COMT) inhibitors offer additional symptom relief.<sup>129</sup> Advanced therapies, such as deep brain stimulation (DBS), significantly benefit patients with severe motor fluctuations.<sup>130</sup> Non-motor symptoms, including depression and sleep disturbances, are managed with supportive medications. In HD, treatments primarily address symptoms. Antidopaminergic medications, such as tetrabenazine, can reduce chorea, while antidepressants and antipsychotics help manage psychiatric

symptoms.<sup>131</sup> Physical therapy and supportive care are vital in maintaining mobility and quality of life.<sup>132</sup>

The decline in proteostasis is a shared feature of neurodegenerative diseases.<sup>11,19</sup> These systems become less efficient with aging and disease, accumulating toxic protein aggregates.<sup>133,134</sup> Strategies to enhance proteostasis, such as proteasome activators, represent a promising avenue for therapeutic development. Next, the role of intrinsically disordered protein (IDP) accumulation in the progression of Parkinson's disease (PD) will be examined in greater depth.

As stated previously,  $\alpha$ -syn plays a central role in the pathogenesis of PD, with its aggregation being a defining pathological feature.  $\alpha$ -syn was discovered as the main component of Lewy bodies, the hallmark protein aggregates in PD pathology.<sup>121–123</sup> In addition, a missense point mutation in the SNCA gene was found in patients with familial PD.<sup>135,136</sup>  $\alpha$ -syn is a small 140 amino acid (14 kDa) intrinsically disordered protein (IDP) that resides predominantly in presynaptic terminals.<sup>137</sup> Under physiological conditions, it regulates synaptic vesicle dynamics, neurotransmitter release, and dopamine homeostasis.<sup>137,138</sup> The formation of  $\alpha$ -syn aggregates begins with a nucleation event where monomers transition into oligomers.<sup>139,140</sup> The small oligomers are considered the most toxic species, interfering with cellular functions by disrupting membranes and impairing mitochondrial function and dopamine homeostasis.<sup>141,142,143</sup> One critical mechanism linking  $\alpha$ -syn aggregation to neuronal degeneration is proteasome impairment. The ubiquitin-proteasome system (UPS) maintains protein homeostasis by degrading misfolded or damaged proteins. Aggregated  $\alpha$ -syn binds to and inhibits the 20S core of the proteasome, preventing the degradation of ubiquitinated substrates. This proteasomal dysfunction results in the accumulation of misfolded proteins, exacerbating cellular stress and aggregation.<sup>141</sup>

The role of  $\alpha$ -syn in PD pathogenesis has been elucidated through various approaches, including genetic studies, animal models, and postmortem brain analyses. Genetic mutations, such as A53T and E46K, have enhanced  $\alpha$ -syn aggregation and accelerated disease onset in familial PD.<sup>144</sup> Animal models expressing mutant or aggregated  $\alpha$ -syn recapitulate many features of PD, including dopaminergic neuron loss and motor dysfunction, providing insights into the molecular pathways involved.<sup>145</sup> Moreover, studies

using  $\alpha$ -syn preformed fibrils (PFFs) have highlighted the prion-like behavior of  $\alpha$ -syn. PFFs can induce the misfolding and aggregation of endogenous  $\alpha$ -syn in neighboring neurons, propagating pathology across brain regions.<sup>142</sup> This mechanism is thought to underlie the progressive spread of Lewy pathology observed in PD patients, as described by Braak's staging. Despite advances in understanding the role of  $\alpha$ -syn in PD, therapeutic strategies targeting  $\alpha$ -syn aggregation remain challenging.

Given the significant role of  $\alpha$ -syn in the pathogenesis of Parkinson's disease (PD), there is a growing interest in therapeutic strategies to target this protein to overcome the absence of disease-modifying treatments. Current methods for targeting  $\alpha$ -syn include inhibiting its aggregation, enhancing its clearance, employing immunotherapeutic interventions, and reducing its expression levels.

Antibody-based therapies targeting  $\alpha$ -syn represent a promising avenue for disease-modifying interventions in PD.<sup>146</sup> Passive immunization strategies, such as monoclonal antibodies, are designed to bind and neutralize toxic  $\alpha$ -syn species, with some explicitly targeting oligomers or fibrils. One notable example is **Prasinezumab**, a monoclonal antibody targeting aggregated  $\alpha$ -syn.<sup>147</sup> Although its phase 2 trial showed safety and tolerability, it failed to demonstrate significant clinical efficacy in slowing motor symptom progression, highlighting challenges in clinical translation.<sup>148,149</sup> Another antibody, **Cinpanemab**, an *N*-terminally directed monoclonal antibody, was investigated in a randomized trial. Like Prasinezumab, Cinpanemab exhibited dose-dependent increases in cerebrospinal fluid levels but did not yield significant improvements in clinical or imaging endpoints, leading to the discontinuation of its development.<sup>149</sup> In contrast, experimental antibodies like **ABBV-0805**, which preferentially target oligomers and protofibrils, have shown promise in preclinical models.<sup>150</sup> By reducing  $\alpha$ -syn pathology and microgliosis while improving motor function, these antibodies underscore the therapeutic potential of selectively targeting toxic aggregation intermediates.<sup>151</sup>

Despite setbacks, these efforts exemplify the growing focus on antibody-based approaches to address the underlying pathophysiology of PD. The field continues to advance, with ongoing refinements in antibody specificity, delivery methods, and combination therapies aimed at overcoming previous limitations and realizing the full potential of immunotherapy for PD.

Another strategy involves preventing  $\alpha$ -syn aggregation into toxic oligomers and fibrils. Small molecules and peptides that inhibit  $\alpha$ -syn aggregation are under active investigation.<sup>152–154</sup> For instance, an engineered peptide, Tat- $\beta$ syn-degron, promotes the degradation of  $\alpha$ -syn aggregates through proteasomal pathways and has shown promise in animal models by mitigating neuronal damage and reducing motor impairments.<sup>155</sup>

Another promising avenue is enhancing the clearance of  $\alpha$ -syn aggregates through cellular proteostasis mechanisms, such as the ubiquitin-proteasome system. Compounds like ambroxol have been shown to activate glucocerebrosidase, an enzyme that facilitates lysosomal clearance of aggregated proteins, including  $\alpha$ -syn.<sup>156</sup> Similarly, enhancing autophagic pathways through the modulation of mTOR signaling has been investigated to promote the degradation of pathological  $\alpha$ -syn inclusions.

An alternative approach emphasizes reducing  $\alpha$ -syn expression to limit the protein pool for pathological aggregation. Gene-silencing technologies, including antisense oligonucleotides (ASOs) and RNA interference (RNAi), have been developed to decrease the transcription and translation of SNCA, the gene encoding  $\alpha$ -syn.<sup>157</sup> These approaches have demonstrated efficacy in preclinical models by protecting dopaminergic neurons from degeneration.

In addition to these direct interventions, targeting upstream modulators of  $\alpha$ -syn pathology is also being explored. Mutations in genes such as GBA and LRRK2, linked to familial and sporadic forms of PD, have been implicated in exacerbating  $\alpha$ -syn aggregation.<sup>157,158</sup> Therapies that normalize the function of these genes or their associated pathways may indirectly mitigate  $\alpha$ -syn toxicity.

The Tepe lab has leveraged the ability of 20S proteasome to degrade IDPs without ubiquitination to target  $\alpha$ -syn as therapy for PD. Targeting  $\alpha$ -syn via small molecule activation of the 20S proteasome has progressively emerged as a promising therapeutic avenue for PD. The concept utilizes the unique ability of the 20S proteasome to degrade IDPs such as  $\alpha$ -syn without needing ubiquitination, making it a strong candidate for addressing proteostasis disturbances in neurodegenerative diseases.

The discovery of TCH-165 represented a significant milestone.<sup>159</sup> This molecule modulated the equilibrium between 26S and 20S proteasomes, favoring 20S assembly and activity. It effectively prevented  $\alpha$ -syn accumulation and aggregation in cellular

models by enhancing proteasomal degradation. The mechanism of activation was attributed to its ability to induce allosteric activation of the 20S proteasome by stabilizing its open-gate conformation.<sup>160</sup> This led to enhanced degradation of IDPs, including  $\alpha$ -syn, and delayed aggregation in vitro.<sup>159,161</sup> These findings laid the groundwork for exploring targeted activators that could increase proteasomal activity and selectively clear pathological proteins.

Subsequently, a high-throughput screen identified chlorpromazine as a lead compound capable of activating the 20S proteasome. Chemical modifications of chlorpromazine yielded phenothiazine derivatives that retained proteasome-enhancing activity while abrogating off-target interactions with dopamine receptors.<sup>161</sup> These analogs demonstrated robust activation of the 20S proteasome, effectively reducing the burden of  $\alpha$ -syn oligomers and aggregates in neuronal models.<sup>162</sup>

Dihydroquinazoline derivatives further advanced this therapeutic strategy. A library of these compounds was developed to probe structure-activity relationships, leading to the identification of potent 20S activators that induced degradation of  $\alpha$ -syn in both in vitro and cellular systems. These compounds exhibited remarkable selectivity for the 20S proteasome, sparing structured proteins while targeting IDPs for degradation.<sup>163</sup>

More recently, fluspirilene and its derivatives have shown exceptional promise. These compounds achieved up to a 10-fold enhancement in 20S proteasome activity and demonstrated the ability to restore proteasome function impaired by  $\alpha$ -syn oligomers.<sup>164</sup> By overcoming proteasome inhibition and facilitating the clearance of mutant and aggregated  $\alpha$ -syn, these molecules represent a novel approach to mitigating proteostasis impairment in PD. While these findings highlight the potential of 20S proteasome activators, challenges remain. Translating preclinical successes into clinically viable therapies requires optimizing pharmacokinetics, achieving effective blood-brain barrier penetration, and ensuring long-term safety. Nevertheless, the chronological progression of these studies underscores the growing feasibility of targeting the 20S proteasome to treat  $\alpha$ -syn associated pathologies, offering hope for disease-modifying interventions in PD.

In Chapter 2, I will detail our collaborative efforts to design, synthesize, and systematically evaluate third-generation chlorpromazine analogs as activators of the 20S proteasome.



This chapter will comprehensively analyze these analogs' structure-activity relationships (SARs). It will highlight their ability to modulate proteasome activity and target the degradation of intrinsically disordered proteins such as  $\alpha$ -syn.

Chapter 3 will focus on applying these optimized analogs to mitigate the detrimental effects of oxidative stress, a key contributor to proteostasis impairment in neurodegenerative diseases. This discussion will include mechanistic studies on how these compounds enhance proteasome activity under conditions of oxidative damage and their potential therapeutic implications for cellular homeostasis.

In Chapter 4, I will present my identification of a novel scaffold for 20S proteasome activation and the subsequent design, synthesis, and evaluation of innovative analogs derived from this scaffold. This chapter will include detailed investigations into these analogs' biochemical and cellular activities, their efficacy in promoting proteasome-mediated degradation of pathological proteins, and their potential advantages over existing proteasome activators.

## REFERENCES

- (1) Jayaraj, G. G.; Hipp, M. S.; Ulrich Hartl, F. Functional Modules of the Proteostasis Network. *Cold Spring Harb. Perspect. Biol.* **2020**, *12* (1). <https://doi.org/10.1101/cshperspect.a033951>.
- (2) Labbadia, J.; Morimoto, R. I. The Biology of Proteostasis in Aging and Disease. *Annu. Rev. Biochem.* **2015**, *84*, 435–464. <https://doi.org/10.1146/annurev-biochem-060614-033955>.
- (3) Kim, Y. E.; Hipp, M. S.; Bracher, A.; Hayer-Hartl, M.; Ulrich Hartl, F. *Molecular Chaperone Functions in Protein Folding and Proteostasis*; 2013; Vol. 82. <https://doi.org/10.1146/annurev-biochem-060208-092442>.
- (4) Smalle, J.; Vierstra, R. D. The Ubiquitin 26S Proteasome Proteolytic Pathway. *Annu. Rev. Plant Biol.* **2004**, *55*, 555–590. <https://doi.org/10.1146/annurev-arplant.55.031903.141801>.
- (5) Brandon Croft, G. R. Ubiquitin-Proteasome System in Neurodegenerative Disorders. *J. Drug Metab. Toxicol.* **2015**, *06* (04). <https://doi.org/10.4172/2157-7609.1000187>.
- (6) Baugh, J. M.; Viktorova, E. G.; Pilipenko, E. V. Proteasomes Can Degrade a Significant Proportion of Cellular Proteins Independent of Ubiquitination. *J. Mol. Biol.* **2009**, *386* (3), 814–827. <https://doi.org/10.1016/j.jmb.2008.12.081>.
- (7) Dikic, I. Proteasomal and Autophagic Degradation Systems. *Annu. Rev. Biochem.* **2017**, *86*, 193–224. <https://doi.org/10.1146/annurev-biochem-061516-044908>.
- (8) Read, A.; Schröder, M. The Unfolded Protein Response: An Overview. *Biology (Basel)*. **2021**, *10* (5), 1–10. <https://doi.org/10.3390/biology10050384>.
- (9) Hetz, C.; Zhang, K.; Kaufman, R. J. Mechanisms, Regulation and Functions of the Unfolded Protein Response. *Nat. Rev. Mol. Cell Biol.* **2020**, *21* (8), 421–438. <https://doi.org/10.1038/s41580-020-0250-z>.
- (10) Lang, B. J.; Guerrero, M. E.; Prince, T. L.; Okusha, Y.; Bonorino, C.; Calderwood, S. K. The Functions and Regulation of Heat Shock Proteins; Key Orchestrators of Proteostasis and the Heat Shock Response. *Arch. Toxicol.* **2021**, *95* (6), 1943–1970. <https://doi.org/10.1007/s00204-021-03070-8>.
- (11) Farooqui, T.; Farooqui, A. A. Aging: An Important Factor for the Pathogenesis of Neurodegenerative Diseases. *Mech. Ageing Dev.* **2009**, *130* (4), 203–215. <https://doi.org/10.1016/j.mad.2008.11.006>.
- (12) Childs, B. G.; Durik, M.; Baker, D. J.; Van Deursen, J. M. Cellular Senescence in Aging and Age-Related Disease: From Mechanisms to Therapy. *Nat. Med.* **2015**, *21* (12), 1424–1435. <https://doi.org/10.1038/nm.4000>.
- (13) Baker, D. J.; Petersen, R. C. Cellular Senescence in Brain Aging and Neurodegenerative Diseases: Evidence and Perspectives. *J. Clin. Invest.* **2018**, *128* (4), 1208–1216. <https://doi.org/10.1172/JCI95145>.

- (14) Thibaut, T. A.; Smith, D. M. A Practical Review of Proteasome Pharmacology. *Pharmacol. Rev.* **2019**, *71* (2), 170–197. <https://doi.org/10.1124/pr.117.015370>.
- (15) Bedford, L.; Paine, S.; Sheppard, P. W.; Mayer, R. J.; Roelofs, J. Assembly, Structure, and Function of the 26S Proteasome. *Trends Cell Biol.* **2010**, *20* (7), 391–401. <https://doi.org/10.1016/j.tcb.2010.03.007>.
- (16) Hou, Y.; Dan, X.; Babbar, M.; Wei, Y.; Hasselbalch, S. G.; Croteau, D. L.; Bohr, V. A. Ageing as a Risk Factor for Neurodegenerative Disease. *Nat. Rev. Neurol.* **2019**, *15* (10), 565–581. <https://doi.org/10.1038/s41582-019-0244-7>.
- (17) Cenini, G.; Lloret, A.; Cascella, R. Oxidative Stress in Neurodegenerative Diseases: From a Mitochondrial Point of View. *Oxid. Med. Cell. Longev.* **2019**, *2019*. <https://doi.org/10.1155/2019/2105607>.
- (18) Sweeney, P.; Park, H.; Baumann, M.; Dunlop, J.; Frydman, J.; Kopito, R.; McCampbell, A.; Leblanc, G.; Venkateswaran, A.; Nurmi, A.; Hodgson, R. Protein Misfolding in Neurodegenerative Diseases: Implications and Strategies. *Transl. Neurodegener.* **2017**, *6* (1), 1–13. <https://doi.org/10.1186/s40035-017-0077-5>.
- (19) Hipp, M. S.; Kasturi, P.; Hartl, F. U. The Proteostasis Network and Its Decline in Ageing. *Nat. Rev. Mol. Cell Biol.* **2019**, *20* (7), 421–435. <https://doi.org/10.1038/s41580-019-0101-y>.
- (20) Harris, J. R.; Marles-Wright Editors, J. *Subcellular Biochemistry 96 Macromolecular Protein Complexes III: Structure and Function*; 2020.
- (21) Livneh, I.; Cohen-Kaplan, V.; Cohen-Rosenzweig, C.; Avni, N.; Ciechanover, A. The Life Cycle of the 26S Proteasome: From Birth, through Regulation and Function, and onto Its Death. *Cell Res.* **2016**, *26* (8), 869–885. <https://doi.org/10.1038/cr.2016.86>.
- (22) Groll, M.; Heinemeyer, W.; Jäger, S.; Ullrich, T.; Bochtler, M.; Wolf, D. H.; Huber, R. The Catalytic Sites of 20S Proteasomes and Their Role in Subunit Maturation: A Mutational and Crystallographic Study. *Proc. Natl. Acad. Sci. U. S. A.* **1999**, *96* (20), 10976–10983. <https://doi.org/10.1073/pnas.96.20.10976>.
- (23) Harris, J. L.; Alper, P. B.; Li, J.; Rechsteiner, M.; Backes, B. J. Substrate Specificity of the Human Proteasome. *Chem. Biol.* **2001**, *8* (12), 1131–1141. [https://doi.org/10.1016/S1074-5521\(01\)00080-1](https://doi.org/10.1016/S1074-5521(01)00080-1).
- (24) Schmidtke, G.; Kraft, R.; Kostka, S.; Henklein, P.; Frömmel, C.; Löwe, J.; Huber, R.; Kloetzel, P. M.; Schmidt, M. Analysis of Mammalian 20S Proteasome Biogenesis: The Maturation of  $\beta$ -Subunits Is an Ordered Two-Step Mechanism Involving Autocatalysis. *EMBO J.* **1996**, *15* (24), 6887–6898. <https://doi.org/10.1002/j.1460-2075.1996.tb01081.x>.
- (25) Groll Michael; Bajorek Monica; Köhler Alwin; Moroder Luis; Rubin David M.; Huber Rober; Glickman Michael H.; Finley Daniel. A Gated Channel into the Proteasome Core Particle. *Nat. Struct. Biol.* **2000**, *7* (11), 1062–1067.
- (26) Choi, W. H.; De Poot, S. A. H.; Lee, J. H.; Kim, J. H.; Han, D. H.; Kim, Y. K.; Finley,

- D.; Lee, M. J. Open-Gate Mutants of the Mammalian Proteasome Show Enhanced Ubiquitin-Conjugate Degradation. *Nat. Commun.* **2016**, *7*. <https://doi.org/10.1038/ncomms10963>.
- (27) Anderson, R. T.; Bradley, T. A.; Smith, D. M. Hyperactivation of the Proteasome in *Caenorhabditis Elegans* Protects against Proteotoxic Stress and Extends Lifespan. *J. Biol. Chem.* **2022**, *298* (10), 102415. <https://doi.org/10.1016/j.jbc.2022.102415>.
  - (28) Sakata-Kaneko, S.; Wakatsuki, Y.; Matsunaga, Y.; Usui, T.; Kita, T. Altered Th1/Th2 Commitment in Human CD4<sup>+</sup> T Cells with Ageing. *Clin. Exp. Immunol.* **2000**, *120* (2), 267–273. <https://doi.org/10.1046/j.1365-2249.2000.01224.x>.
  - (29) Thomas, T.; Salcedo-Tacuma, D.; Smith, D. M. Structure, Function, and Allosteric Regulation of the 20S Proteasome by the 11S/PA28 Family of Proteasome Activators. *Biomolecules* **2023**, *13* (9). <https://doi.org/10.3390/biom13091326>.
  - (30) Sahu, I.; Glickman, M. H. Proteasome in Action: Substrate Degradation by the 26S Proteasome. *Biochem. Soc. Trans.* **2021**, *49* (2), 629–644. <https://doi.org/10.1042/BST20200382>.
  - (31) Rabl, J.; Smith, D. M.; Yu, Y.; Chang, S. C.; Goldberg, A. L.; Cheng, Y. Mechanism of Gate Opening in the 20S Proteasome by the Proteasomal ATPases. *Mol. Cell* **2008**, *30* (3), 360–368. <https://doi.org/10.1016/j.molcel.2008.03.004>.
  - (32) Yu, Z.; Yu, Y.; Wang, F.; Myasnikov, A. G.; Coffino, P.; Cheng, Y. Allosteric Coupling between  $\alpha$ -Rings of the 20S Proteasome. *Nature Communications*. 2020. <https://doi.org/10.1038/s41467-020-18415-7>.
  - (33) Chondrogianni, N.; Voutetakis, K.; Kapetanou, M.; Delitsikou, V.; Papaevgeniou, N.; Sakellari, M.; Lefaki, M.; Filippopoulou, K.; Gonos, E. S.; Im, E.; Chung, K. C.; Fleury, D.; Walker, J. M.; Scott, M. R.; Meador-Woodruff, J. H.; Shachrai, I. *Book on Proteostasis*; 2016; Vol. 49.
  - (34) Huber, E. M.; Heinemeyer, W.; Li, X.; Arendt, C. S.; Hochstrasser, M.; Groll, M. A Unified Mechanism for Proteolysis and Autocatalytic Activation in the 20S Proteasome. *Nat. Commun.* **2016**, *7*, 1–10. <https://doi.org/10.1038/ncomms10900>.
  - (35) Chen, P.; Hochstrasser, M. Autocatalytic Subunit Processing Couples Active Site Formation in the 20S Proteasome to Completion of Assembly. *Cell* **1996**, *86* (6), 961–972. [https://doi.org/10.1016/S0092-8674\(00\)80171-3](https://doi.org/10.1016/S0092-8674(00)80171-3).
  - (36) Kimura, H.; Caturegli, P.; Takahashi, M.; Suzuki, K. New Insights into the Function of the Immunoproteasome in Immune and Nonimmune Cells. *J. Immunol. Res.* **2015**, *2015*. <https://doi.org/10.1155/2015/541984>.
  - (37) Ferrington, D. A.; Gregerson, D. S. *Immunoproteasomes: Structure, Function, and Antigen Presentation*; 2012; Vol. 109. <https://doi.org/10.1016/B978-0-12-397863-9.00003-1>.
  - (38) Murata, S.; Takahama, Y.; Kasahara, M.; Tanaka, K. The Immunoproteasome and Thymoproteasome: Functions, Evolution and Human Disease. *Nat. Immunol.* **2018**, *19* (9), 923–931. <https://doi.org/10.1038/s41590-018-0186-z>.

- (39) Sharon, M.; Taverner, T.; Ambroggio, X. I.; Deshaies, R. J.; Robinson, C. V. Structural Organization of the 19S Proteasome Lid: Insights from MS of Intact Complexes. *PLoS Biol.* **2006**, *4* (8), 1314–1323. <https://doi.org/10.1371/journal.pbio.0040267>.
- (40) Rosenzweig, R.; Osmulski, P. A.; Gaczynska, M.; Glickman, M. H. The Central Unit within the 19S Regulatory Particle of the Proteasome. *Nat. Struct. Mol. Biol.* **2008**, *15* (6), 573–580. <https://doi.org/10.1038/nsmb.1427>.
- (41) Martinez-Fonts, K.; Davis, C.; Tomita, T.; Elsasser, S.; Nager, A. R.; Shi, Y.; Finley, D.; Matouschek, A. The Proteasome 19S Cap and Its Ubiquitin Receptors Provide a Versatile Recognition Platform for Substrates. *Nat. Commun.* **2020**, *11* (1). <https://doi.org/10.1038/s41467-019-13906-8>.
- (42) Rosenzweig, R.; Bronner, V.; Zhang, D.; Fushman, D.; Glickman, M. H. Rpn1 and Rpn2 Coordinate Ubiquitin Processing Factors at Proteasome. *J. Biol. Chem.* **2012**, *287* (18), 14659–14671. <https://doi.org/10.1074/jbc.M111.316323>.
- (43) Saeki, Y.; Toh-e, A.; Kudo, T.; Kawamura, H.; Tanaka, K. Multiple Proteasome-Interacting Proteins Assist the Assembly of the Yeast 19S Regulatory Particle. *Cell* **2009**, *137* (5), 900–913. <https://doi.org/10.1016/j.cell.2009.05.005>.
- (44) Glickman, M. H.; Rubin, D. M.; Fried, V. A.; Finley, D. The Regulatory Particle of the *Saccharomyces Cerevisiae* Proteasome. *Mol. Cell. Biol.* **1998**, *18* (6), 3149–3162. <https://doi.org/10.1128/mcb.18.6.3149>.
- (45) Verma, R.; Aravind, L.; Oania, R.; McDonald, W. H.; Yates, J. R.; Koonin, E. V.; Deshaies, R. J. Role of Rpn11 Metalloprotease in Deubiquitination and Degradation by the 26S Proteasome. *Science* (80-. ). **2002**, *298* (5593), 611–615. <https://doi.org/10.1126/science.1075898>.
- (46) Worden, E. J.; Dong, K. C.; Martin, A. An AAA Motor-Driven Mechanical Switch in Rpn11 Controls Deubiquitination at the 26S Proteasome. *Mol. Cell* **2017**, *67* (5), 799–811.e8. <https://doi.org/10.1016/j.molcel.2017.07.023>.
- (47) Franić, D.; Zubčić, K.; Boban, M. Nuclear Ubiquitin-Proteasome Pathways in Proteostasis Maintenance. *Biomolecules* **2021**, *11* (1), 1–16. <https://doi.org/10.3390/biom11010054>.
- (48) Coux, O.; Tanaka, K.; Goldberg, A. L. Structure and Functions of the 20S and 26S Proteasomes. *Annu. Rev. Biochem.* **1996**, *65*, 801–847. <https://doi.org/10.1146/annurev.bi.65.070196.004101>.
- (49) Wilkinson, K. D. The Discovery of Ubiquitin-Dependent Proteolysis. *Proc. Natl. Acad. Sci. U. S. A.* **2005**, *102* (43), 15280–15282. <https://doi.org/10.1073/pnas.0504842102>.
- (50) Dikic, I.; Wakatsuki, S.; Walters, K. J. Ubiquitin-Binding Domains from Structures to Functions. *Nat. Rev. Mol. Cell Biol.* **2009**, *10* (10), 659–671. <https://doi.org/10.1038/nrm2767>.
- (51) Pickart, C. M.; Eddins, M. J. Ubiquitin: Structures, Functions, Mechanisms.

*Biochim. Biophys. Acta - Mol. Cell Res.* **2004**, 1695 (1–3), 55–72.  
<https://doi.org/10.1016/j.bbamcr.2004.09.019>.

- (52) Mattioli, F.; Sixma, T. K. Lysine-Targeting Specificity in Ubiquitin and Ubiquitin-like Modification Pathways. *Nat. Struct. Mol. Biol.* **2014**, *21* (4), 308–316. <https://doi.org/10.1038/nsmb.2792>.
- (53) Komander, D.; Rape, M. The Ubiquitin Code. *Annu. Rev. Biochem.* **2012**, *81*, 203–229. <https://doi.org/10.1146/annurev-biochem-060310-170328>.
- (54) Inobe, T.; Matouschek, A. Paradigms of Protein Degradation by the Proteasome. *Curr. Opin. Struct. Biol.* **2014**, *24* (1), 156–164. <https://doi.org/10.1016/j.sbi.2014.02.002>.
- (55) Le Guerroué, F.; Youle, R. J. Ubiquitin Signaling in Neurodegenerative Diseases: An Autophagy and Proteasome Perspective. *Cell Death Differ.* **2021**, *28* (2), 439–454. <https://doi.org/10.1038/s41418-020-00667-x>.
- (56) Arkinson, C.; Dong, K. C.; Gee, C. L.; Martin, A. Mechanisms and Regulation of Substrate Degradation by the 26S Proteasome. *Nat. Rev. Mol. Cell Biol.* <https://doi.org/10.1038/s41580-024-00778-0>.
- (57) Davis, C.; Spaller, B. L.; Matouschek, A. Mechanisms of Substrate Recognition by the 26S Proteasome. *Curr. Opin. Struct. Biol.* **2021**, *67*, 161–169. <https://doi.org/10.1016/j.sbi.2020.10.010>.
- (58) Mao, Y. Structure, Dynamics and Function of the 26S Proteasome. *Subcell. Biochem.* **2021**, *96*, 1–151. [https://doi.org/10.1007/978-3-030-58971-4\\_1](https://doi.org/10.1007/978-3-030-58971-4_1).
- (59) Babu, M. M. The Contribution of Intrinsically Disordered Regions to Protein Function, Cellular Complexity, and Human Disease. *Biochem. Soc. Trans.* **2016**, *44* (5), 1185–1200. <https://doi.org/10.1042/BST20160172>.
- (60) Liu, J.; Nussinov, R. The Mechanism of Ubiquitination in the Cullin-RING E3 Ligase Machinery: Conformational Control of Substrate Orientation. *PLoS Comput. Biol.* **2009**, *5* (10). <https://doi.org/10.1371/journal.pcbi.1000527>.
- (61) Shabek, N.; Herman-Bachinsky, Y.; Ciechanover, A. Ubiquitin Degradation with Its Substrate, or as a Monomer in a Ubiquitination-Independent Mode, Provides Clues to Proteasome Regulation. *Proc. Natl. Acad. Sci. U. S. A.* **2009**, *106* (29), 11907–11912. <https://doi.org/10.1073/pnas.0905746106>.
- (62) Pickart, C. M. Mechanisms Underlying Ubiquitination. *Annual Review of Biochemistry*, *70*(1), 503–533. <https://doi.org/10.1146/annurev-biochem-070101-000000>.
- (63) Rahman, S.; Wolberger, C. Breaking the K48-Chain: Linking Ubiquitin beyond Protein Degradation. *Nat. Struct. Mol. Biol.* **2024**, *31* (2), 216–218. <https://doi.org/10.1038/s41594-024-01221-w>.
- (64) Saeki, Y.; Saitoh, A.; Toh-e, A.; Yokosawa, H. Ubiquitin-like Proteins and Rpn10

- Play Cooperative Roles in Ubiquitin-Dependent Proteolysis. *Biochem. Biophys. Res. Commun.* **2002**, 293 (3), 986–992. [https://doi.org/10.1016/S0006-291X\(02\)00340-6](https://doi.org/10.1016/S0006-291X(02)00340-6).
- (65) Liu, Z.; Dong, X.; Yi, H. W.; Yang, J.; Gong, Z.; Wang, Y.; Liu, K.; Zhang, W. P.; Tang, C. Structural Basis for the Recognition of K48-Linked Ub Chain by Proteasomal Receptor Rpn13. *Cell Discov.* **2019**, 5 (1). <https://doi.org/10.1038/s41421-019-0089-7>.
- (66) Iii, J. W. 35661. **1998**, 391 (February), 715–718.
- (67) Hamazaki, J.; Hirayama, S.; Murata, S. Redundant Roles of Rpn10 and Rpn13 in Recognition of Ubiquitinated Proteins and Cellular Homeostasis. *PLoS Genet.* **2015**, 11 (7), 1–20. <https://doi.org/10.1371/journal.pgen.1005401>.
- (68) Trulsson, F.; Akimov, V.; Robu, M.; van Overbeek, N.; Berrocal, D. A. P.; Shah, R. G.; Cox, J.; Shah, G. M.; Blagoev, B.; Vertegaal, A. C. O. Deubiquitinating Enzymes and the Proteasome Regulate Preferential Sets of Ubiquitin Substrates. *Nat. Commun.* **2022**, 13 (1). <https://doi.org/10.1038/s41467-022-30376-7>.
- (69) Hu, M.; Li, P.; Song, L.; Jeffrey, P. D.; Chenova, T. A.; Wilkinson, K. D.; Cohen, R. E.; Shi, Y. Structure and Mechanisms of the Proteasome-Associated Deubiquitinating Enzyme USP14. *EMBO J.* **2005**, 24 (21), 3747–3756. <https://doi.org/10.1038/sj.emboj.7600832>.
- (70) Tomita, T.; Matouschek, A. Substrate Selection by the Proteasome through Initiation Regions. *Protein Sci.* **2019**, 28 (7), 1222–1232. <https://doi.org/10.1002/pro.3642>.
- (71) Prakash, S.; Tian, L.; Ratliff, K. S.; Lehotzky, R. E.; Matouschek, A. An Unstructured Initiation Site Is Required for Efficient Proteasome-Mediated Degradation. *Nat. Struct. Mol. Biol.* **2004**, 11 (9), 830–837. <https://doi.org/10.1038/nsmb814>.
- (72) Yu, H.; Kago, G.; Yellman, C. M.; Matouschek, A. Ubiquitin-like Domains Can Target to the Proteasome but Proteolysis Requires a Disordered Region. *EMBO J.* **2016**, 35 (14), 1522–1536. <https://doi.org/10.15252/embj.201593147>.
- (73) Glickman, M. H.; Ciechanover, A. The Ubiquitin-Proteasome Proteolytic Pathway: Destruction for the Sake of Construction. *Physiol. Rev.* **2002**, 82 (2), 373–428. <https://doi.org/10.1152/physrev.00027.2001>.
- (74) Pishesha, N.; Harmand, T. J.; Ploegh, H. L. A Guide to Antigen Processing and Presentation. *Nat. Rev. Immunol.* **2022**, 22 (12), 751–764. <https://doi.org/10.1038/s41577-022-00707-2>.
- (75) Neefjes, J.; Jongsma, M. L. M.; Paul, P.; Bakke, O. Towards a Systems Understanding of MHC Class I and MHC Class II Antigen Presentation. *Nat. Rev. Immunol.* **2011**, 11 (12), 823–836. <https://doi.org/10.1038/nri3084>.
- (76) Ben-Nissan, G.; Sharon, M. *Regulating the 20S Proteasome Ubiquitin-Independent Degradation Pathway*; 2014; Vol. 4. <https://doi.org/10.3390/biom4030862>.

- (77) Asher, G.; Reuven, N.; Shaul, Y. 20S Proteasomes and Protein Degradation “by Default.” *BioEssays* **2006**, *28* (8), 844–849. <https://doi.org/10.1002/bies.20447>.
- (78) Shang, F.; Taylor, A. Ubiquitin-Proteasome Pathway and Cellular Responses to Oxidative Stress. *Free Radic. Biol. Med.* **2011**, *51* (1), 5–16. <https://doi.org/10.1016/j.freeradbiomed.2011.03.031>.
- (79) Raynes, R.; Pomatto, L. C. D.; Davies, K. J. A. Degradation of Oxidized Proteins by the Proteasome: Distinguishing between the 20S, 26S, and Immunoproteasome Proteolytic Pathways. *Mol. Aspects Med.* **2016**, *50*, 41–55. <https://doi.org/10.1016/j.mam.2016.05.001>.
- (80) Jung, T.; Grune, T. The Proteasome and Its Role in the Degradation of Oxidized Proteins. *IUBMB Life* **2008**, *60* (11), 743–752. <https://doi.org/10.1002/iub.114>.
- (81) Jung, T.; Grune, T. The Proteasome and the Degradation of Oxidized Proteins: Part I-Structure of Proteasomes. *Redox Biol.* **2013**, *1* (1), 178–182. <https://doi.org/10.1016/j.redox.2013.01.004>.
- (82) Deshmukh, F. K.; Yaffe, D.; Olshina, M. A.; Ben-Nissan, G.; Sharon, M. The Contribution of the 20s Proteasome to Proteostasis. *Biomolecules* **2019**, *9* (5). <https://doi.org/10.3390/biom9050190>.
- (83) Reinheckel, T.; Sitte, N.; Ullrich, O.; Kuckelkorn, U.; Davies, K. J. A.; Grune, T. Comparative Resistance of the 20 S and 26 S Proteasome to Oxidative Stress. *Biochem. J.* **1998**, *335* (3), 637–642. <https://doi.org/10.1042/bj3350637>.
- (84) Lefaki, M.; Papaevgeniou, N.; Chondrogianni, N. Redox Regulation of Proteasome Function. *Redox Biol.* **2017**, *13* (July), 452–458. <https://doi.org/10.1016/j.redox.2017.07.005>.
- (85) Sahu, I.; Glickman, M. H. Structural Insights into Substrate Recognition and Processing by the 20s Proteasome. *Biomolecules* **2021**, *11* (2), 1–15. <https://doi.org/10.3390/biom11020148>.
- (86) Ukmar-Godec, T.; Fang, P.; Ibáñez de Opakua, A.; Henneberg, F.; Godec, A.; Pan, K. T.; Cima-Omori, M. S.; Chari, A.; Mandelkow, E.; Urlaub, H.; Zweckstetter, M. Proteasomal Degradation of the Intrinsically Disordered Protein Tau at Single-Residue Resolution. *Sci. Adv.* **2020**, *6* (30), 1–12. <https://doi.org/10.1126/sciadv.aba3916>.
- (87) Wright, P. E.; Dyson, H. J. Intrinsically Disordered Proteins in Cellular Signalling and Regulation. *Nat. Rev. Mol. Cell Biol.* **2015**, *16* (1), 18–29. <https://doi.org/10.1038/nrm3920>.
- (88) Tompa, P. The Interplay between Structure and Function in Intrinsically Unstructured Proteins. *FEBS Lett.* **2005**, *579* (15), 3346–3354. <https://doi.org/10.1016/j.febslet.2005.03.072>.



- (89) Martínez-Orgado, J.; Martínez-Vega, M.; Silva, L.; Romero, A.; de Hoz-Rivera, M.; Villa, M.; del Pozo, A. Protein Carbonylation as a Biomarker of Oxidative Stress and a Therapeutic Target in Neonatal Brain Damage. *Antioxidants* **2023**, *12* (10), 1–13. <https://doi.org/10.3390/antiox12101839>.
- (90) Akagawa, M. Protein Carbonylation: Molecular Mechanisms, Biological Implications, and Analytical Approaches. *Free Radic. Res.* **2021**, *55* (4), 307–320. <https://doi.org/10.1080/10715762.2020.1851027>.
- (91) Frijhoff, J.; Winyard, P. G.; Zarkovic, N.; Davies, S. S.; Stocker, R.; Cheng, D.; Knight, A. R.; Taylor, E. L.; Oettrich, J.; Ruskovska, T.; Gasparovic, A. C.; Cuadrado, A.; Weber, D.; Poulsen, H. E.; Grune, T.; Schmidt, H. H. H. W.; Ghezzi, P. Clinical Relevance of Biomarkers of Oxidative Stress. *Antioxidants Redox Signal.* **2015**, *23* (14), 1144–1170. <https://doi.org/10.1089/ars.2015.6317>.
- (92) Ezraty, B.; Gennaris, A.; Barras, F.; Collet, J. F. Oxidative Stress, Protein Damage and Repair in Bacteria. *Nat. Rev. Microbiol.* **2017**, *15* (7), 385–396. <https://doi.org/10.1038/nrmicro.2017.26>.
- (93) Shringarpure, R.; Grune, T.; Davies, K. J. A. Cellular and Molecular Life Sciences Protein Oxidation and 20S Proteasome-Dependent Proteolysis in Mammalian Cells. *Cell. Mol. life Sci.* **2001**, *58*, 1442–1450.
- (94) Makaros, Y.; Raiff, A.; Timms, R. T.; Wagh, A. R.; Gueta, M. I.; Bekturova, A.; Guez-Haddad, J.; Brodsky, S.; Opatowsky, Y.; Glickman, M. H.; Elledge, S. J.; Koren, I. Ubiquitin-Independent Proteasomal Degradation Driven by C-Degron Pathways. *Mol. Cell* **2023**, *83* (11), 1921–1935.e7. <https://doi.org/10.1016/j.molcel.2023.04.023>.
- (95) Huang, W. C.; Yeh, C. W.; Hsu, S. Y.; Lee, L. T.; Chu, C. Y.; Yen, H. C. S. *Characterization of Degradation Signals at Protein C-Termini*, 1st ed.; Elsevier Inc., 2023; Vol. 686. <https://doi.org/10.1016/bs.mie.2023.02.009>.
- (96) Shi, Y.; Long, M. J. C.; Rosenberg, M. M.; Li, S.; Kobjack, A.; Lessans, P.; Coffey, R. T.; Hedstrom, L. Boc3Arg-Linked Ligands Induce Degradation by Localizing Target Proteins to the 20S Proteasome. *ACS Chem. Biol.* **2016**, *11* (12), 3328–3337. <https://doi.org/10.1021/acscchembio.6b00656>.
- (97) Zhao, J.; Makhija, S.; Zhou, C.; Zhang, H.; Wang, Y. Q.; Muralidharan, M.; Huang, B.; Cheng, Y. Structural Insights into the Human PA28–20S Proteasome Enabled by Efficient Tagging and Purification of Endogenous Proteins. *Proc. Natl. Acad. Sci. U. S. A.* **2022**, *119* (33), 1–8. <https://doi.org/10.1073/pnas.2207200119>.
- (98) Hugo, M.; Korovila, I.; Köhler, M.; García-García, C.; Cabrera-García, J. D.; Marina, A.; Martínez-Ruiz, A.; Grune, T. Early Cysteine-Dependent Inactivation of 26S Proteasomes Does Not Involve Particle Disassembly. *Redox Biol.* **2018**, *16* (December 2017), 123–128. <https://doi.org/10.1016/j.redox.2018.02.016>.
- (99) Wang, X.; Chemmama, I. E.; Yu, C.; Huszagh, A.; Xu, Y.; Viner, R.; Block, S. A.; Cimermancic, P.; Rychnovsky, S. D.; Ye, Y.; Sali, A.; Huang, L. The Proteasome-Interacting Ecm29 Protein Disassembles the 26S Proteasome in Response to

- Oxidative Stress. *J. Biol. Chem.* **2017**, 292 (39), 16310–16320. <https://doi.org/10.1074/jbc.M117.803619>.
- (100) Morimoto, R. I.; Cuervo, A. M. Protein Homeostasis and Aging: Taking Care of Proteins from the Cradle to the Grave. *Journals Gerontol. - Ser. A Biol. Sci. Med. Sci.* **2009**, 64 (2), 167–170. <https://doi.org/10.1093/gerona/gln071>.
- (101) Baraibar, M. A.; Liu, L.; Ahmed, E. K.; Friguet, B. Protein Oxidative Damage at the Crossroads of Cellular Senescence, Aging, and Age-Related Diseases. *Oxid. Med. Cell. Longev.* **2012**, 2012. <https://doi.org/10.1155/2012/919832>.
- (102) Tsvetkov, P.; Reuven, N.; Shaul, Y. Ubiquitin-Independent P53 Proteasomal Degradation. *Cell Death Differ.* **2010**, 17 (1), 103–108. <https://doi.org/10.1038/cdd.2009.67>.
- (103) Anwar, A.; Dehn, D.; Siegel, D.; Kepa, J. K.; Tang, L. J.; Pietenpol, J. A.; Ross, D. Interaction of Human NAD(P)H:Quinone Oxidoreductase 1 (NQO1) with the Tumor Suppressor Protein P53 in Cells and Cell-Free Systems. *J. Biol. Chem.* **2003**, 278 (12), 10368–10373. <https://doi.org/10.1074/jbc.M211981200>.
- (104) Asher, G.; Lotem, J.; Tsvetkov, P.; Reiss, V.; Sachs, L.; Shaul, Y. P53 Hot-Spot Mutants Are Resistant to Ubiquitin-Independent Degradation by Increased Binding to NAD(P)H:Quinone Oxidoreductase 1. *Proc. Natl. Acad. Sci. U. S. A.* **2003**, 100 (25), 15065–15070. <https://doi.org/10.1073/pnas.2436329100>.
- (105) Asher, G.; Tsvetkov, P.; Kahana, C.; Shaul, Y. A Mechanism of Ubiquitin-Independent Proteasomal Degradation of the Tumor Suppressors P53 and P73. *Genes Dev.* **2005**, 19 (3), 316–321. <https://doi.org/10.1101/gad.319905>.
- (106) Chondrogianni, N.; Voutetakis, K.; Kapetanou, M.; Delitsikou, V.; Papaevgeniou, N.; Sakellari, M.; Lefaki, M.; Filippopoulou, K.; Gonos, E. S. Proteasome Activation: An Innovative Promising Approach for Delaying Aging and Retarding Age-Related Diseases. *Ageing Res. Rev.* **2015**, 23 (PA), 37–55. <https://doi.org/10.1016/j.arr.2014.12.003>.
- (107) Staerz, S. D.; Anamoah, C.; Tepe, J. J. 20S Proteasome Enhancers Prevent Cytotoxic Tubulin Polymerization-Promoting Protein Induced  $\alpha$ -Synuclein Aggregation. *iScience* **2024**, 27 (7), 110166. <https://doi.org/10.1016/j.isci.2024.110166>.
- (108) Ben-Nissan, G.; Katzir, N.; Füzesi-Levi, M. G.; Sharon, M. Biology of the Extracellular Proteasome. *Biomolecules* **2022**, 12 (5). <https://doi.org/10.3390/biom12050619>.
- (109) Krüger, E.; Kloetzel, P. M.; Enenkel, C. 20S Proteasome Biogenesis. *Biochimie* **2001**, 83 (3–4), 289–293. [https://doi.org/10.1016/S0300-9084\(01\)01241-X](https://doi.org/10.1016/S0300-9084(01)01241-X).
- (110) Naujokat, C.; Šarić, T. Concise Review: Role and Function of the Ubiquitin-Proteasome System in Mammalian Stem and Progenitor Cells. *Stem Cells* **2007**, 25 (10), 2408–2418. <https://doi.org/10.1634/stemcells.2007-0255>.
- (111) 2024 Alzheimer's Disease Facts and Figures. *Alzheimer's Dement.* **2024**, 20 (5),

- (112) Brookmeyer, R.; Evans, D. A.; Hebert, L.; Langa, K. M.; Heeringa, S. G.; Plassman, B. L.; Kukull, W. A. National Estimates of the Prevalence of Alzheimer's Disease in the United States. *Alzheimer's Dement.* **2011**, *7* (1), 61–73. <https://doi.org/10.1016/j.jalz.2010.11.007>.
- (113) Nichols, E.; Steinmetz, J. D.; Vollset, S. E.; Fukutaki, K.; Chalek, J.; Abd-Allah, F.; Abdoli, A.; Abualhasan, A.; Abu-Gharbieh, E.; Akram, T. T.; Al Hamad, H.; Alahdab, F.; Alanezi, F. M.; Alipour, V.; Almustanyir, S.; Amu, H.; Ansari, I.; Arabloo, J.; Ashraf, T.; Astell-Burt, T.; Ayano, G.; Ayuso-Mateos, J. L.; Baig, A. A.; Barnett, A.; Barrow, A.; Baune, B. T.; Béjot, Y.; Mequanint Bezabhe, W. M.; Bezabih, Y. M.; Bhagavathula, A. S.; Bhaskar, S.; Bhattacharyya, K.; Bijani, A.; Biswas, A.; Bolla, S. R.; Boloor, A.; Brayne, C.; Brenner, H.; Burkart, K.; Burns, R. A.; Cámara, L. A.; Cao, C.; Carvalho, F.; Castro-De-Araujo, L. F. S.; Catalá-López, F.; Cerin, E.; Chavan, P. P.; Cherbuin, N.; Chu, D. T.; Costa, V. M.; Couto, R. A. S.; Dadras, O.; Dai, X.; Dandona, L.; Dandona, R.; De la Cruz-Góngora, V.; Dhamnetiya, D.; da Silva, D. D.; Diaz, D.; Douiri, A.; Edvardsson, D.; Ekholuenetale, M.; El Sayed, I.; El-Jaafary, S. I.; Eskandari, K.; Eskandarieh, S.; Esmaeilnejad, S.; Fares, J.; Faro, A.; Farooque, U.; Feigin, V. L.; Feng, X.; Fereshtehnejad, S. M.; Fernandes, E.; Ferrara, P.; Filip, I.; Fillit, H.; Fischer, F.; Gaidhane, S.; Galluzzo, L.; Ghashghaee, A.; Ghith, N.; Gialluisi, A.; Gilani, S. A.; Glavan, I. R.; Gnedovskaya, E. V.; Golechha, M.; Gupta, R.; Gupta, V. B.; Gupta, V. K.; Haider, M. R.; Hall, B. J.; Hamidi, S.; Hanif, A.; Hankey, G. J.; Haque, S.; Hartono, R. K.; Hasaballah, A. I.; Hasan, M. T.; Hassan, A.; Hay, S. I.; Hayat, K.; Hegazy, M. I.; Heidari, G.; Heidari-Soureshjani, R.; Herteliu, C.; Househ, M.; Hussain, R.; Hwang, B. F.; Iacoviello, L.; Iavicoli, I.; Ilesanmi, O. S.; Ilic, I. M.; Ilic, M. D.; Irvani, S. S. N.; Iso, H.; Iwagami, M.; Jabbarinejad, R.; Jacob, L.; Jain, V.; Jayapal, S. K.; Jayawardena, R.; Jha, R. P.; Jonas, J. B.; Joseph, N.; Kalani, R.; Kandel, A.; Kandel, H.; Karch, A.; Kasa, A. S.; Kassie, G. M.; Keshavarz, P.; Khan, M. A. B.; Khatib, M. N.; Khoja, T. A. M.; Khubchandani, J.; Kim, M. S.; Kim, Y. J.; Kisa, A.; Kisa, S.; Kivimäki, M.; Koroshetz, W. J.; Koyanagi, A.; Kumar, G. A.; Kumar, M.; Lak, H. M.; Leonardi, M.; Li, B.; Lim, S. S.; Liu, X.; Liu, Y.; Logroscino, G.; Lorkowski, S.; Lucchetti, G.; Saute, R. L.; Magnani, F. G.; Malik, A. A.; Massano, J.; Mehndiratta, M. M.; Menezes, R. G.; Meretoja, A.; Mohajer, B.; Ibrahim, N. M.; Mohammad, Y.; Mohammed, A.; Mokdad, A. H.; Mondello, S.; Moni, M. A.; Moniruzzaman, M.; Mossie, T. B.; Nagel, G.; Naveed, M.; Nayak, V. C.; Kandel, S. N.; Nguyen, T. H.; Oancea, B.; Otstavnov, N.; Otstavnov, S. S.; Owolabi, M. O.; Panda-Jonas, S.; Kan, F. P.; Pasovic, M.; Patel, U. K.; Pathak, M.; Peres, M. F. P.; Perianayagam, A.; Peterson, C. B.; Phillips, M. R.; Pinheiro, M.; Piradov, M. A.; Pond, C. D.; Potashman, M. H.; Potttoo, F. H.; Prada, S. I.; Radfar, A.; Raggi, A.; Rahim, F.; Rahman, M.; Ram, P.; Ranasinghe, P.; Rawaf, D. L.; Rawaf, S.; Rezaei, N.; Rezapour, A.; Robinson, S. R.; Romoli, M.; Roshandel, G.; Sahathevan, R.; Sahebkar, A.; Sahraian, M. A.; Sathian, B.; Sattin, D.; Sawhney, M.; Saylan, M.; Schiavolin, S.; Seylani, A.; Sha, F.; Shaikh, M. A.; Shaji, K. S.; Shannawaz, M.; Shetty, J. K.; Shigematsu, M.; Shin, J. I.; Shiri, R.; Santos Silva, D. A.; Silva, J. P.; Silva, R.; Singh, J. A.; Skryabin, V. Y.; Skryabina, A. A.; Smith, A. E.; Soshnikov, S.; Spurlock, E. E.; Stein, D. J.; Sun,

- J.; Tabarés-Seisdedos, R.; Thakur, B.; Timalisina, B.; Tovani-Palone, M. R.; Tran, B. X.; Tsegaye, G. W.; Tahbaz, S. V.; Valdez, P. R.; Venketasubramanian, N.; Vlassov, V.; Vu, G. T.; Vu, L. G.; Wang, Y. P.; Wimo, A.; Winkler, A. S.; Yadav, L.; Jabbari, S. H. Y.; Yamagishi, K.; Yang, L.; Yano, Y.; Yonemoto, N.; Yu, C.; Yunusa, I.; Zadey, S.; Zastrozhin, M. S.; Zastrozhina, A.; Zhang, Z. J.; Murray, C. J. L.; Vos, T. Estimation of the Global Prevalence of Dementia in 2019 and Forecasted Prevalence in 2050: An Analysis for the Global Burden of Disease Study 2019. *Lancet Public Heal.* **2022**, 7 (2), e105–e125. [https://doi.org/10.1016/S2468-2667\(21\)00249-8](https://doi.org/10.1016/S2468-2667(21)00249-8).
- (114) Maslov, A. Y.; Vijg, J. Genome Instability, Cancer and Aging. *Biochim. Biophys. Acta - Gen. Subj.* **2009**, 1790 (10), 963–969. <https://doi.org/10.1016/j.bbagen.2009.03.020>.
- (115) Rossiello, F.; Jurk, D.; Passos, J. F.; d'Adda di Fagagna, F. Telomere Dysfunction in Ageing and Age-Related Diseases. *Nat. Cell Biol.* **2022**, 24 (2), 135–147. <https://doi.org/10.1038/s41556-022-00842-x>.
- (116) Wu, Y.; Chen, M.; Jiang, J. Mitochondrial Dysfunction in Neurodegenerative Diseases and Drug Targets via Apoptotic Signaling. *Mitochondrion* **2019**, 49 (July), 35–45. <https://doi.org/10.1016/j.mito.2019.07.003>.
- (117) Rodríguez-García, A.; García-Vicente, R.; Morales, M. L.; Ortiz-Ruiz, A.; Martínez-López, J.; Linares, M. Protein Carbonylation and Lipid Peroxidation in Hematological Malignancies. *Antioxidants* **2020**, 9 (12), 1–30. <https://doi.org/10.3390/antiox9121212>.
- (118) Sadigh-Eteghad, S.; Sabermarouf, B.; Majdi, A.; Talebi, M.; Farhoudi, M.; Mahmoudi, J. Amyloid-Beta: A Crucial Factor in Alzheimer's Disease. *Med. Princ. Pract.* **2015**, 24 (1), 1–10. <https://doi.org/10.1159/000369101>.
- (119) Hampel, H.; Hardy, J.; Blennow, K.; Chen, C.; Perry, G.; Kim, S. H.; Villemagne, V. L.; Aisen, P.; Vendruscolo, M.; Iwatsubo, T.; Masters, C. L.; Cho, M.; Lannfelt, L.; Cummings, J. L.; Vergallo, A. The Amyloid- $\beta$  Pathway in Alzheimer's Disease. *Molecular Psychiatry*. 2021, pp 5481–5503. <https://doi.org/10.1038/s41380-021-01249-0>.
- (120) Li, M.; Chen, L.; Lee, D. H. S.; Yu, L. C.; Zhang, Y. The Role of Intracellular Amyloid  $\beta$  in Alzheimer's Disease. *Progress in Neurobiology*. 2007, pp 131–139. <https://doi.org/10.1016/j.pneurobio.2007.08.002>.
- (121) Spillantini, M. G.; Schmidt, M. L.; Lee, V. M. Y.; Trojanowski, J. Q.; Jakes, R.; Goedert, M.  $\alpha$ -Synuclein in Lewy Bodies [8]. *Nature* **1997**, 388 (6645), 839–840. <https://doi.org/10.1038/42166>.
- (122) Yang, Y.; Shi, Y.; Schweighauser, M.; Zhang, X.; Kotecha, A.; Murzin, A. G.; Garringer, H. J.; Cullinane, P. W.; Saito, Y.; Foroud, T.; Warner, T. T.; Hasegawa, K.; Vidal, R.; Murayama, S.; Revesz, T.; Ghetti, B.; Hasegawa, M.; Lashley, T.; Scheres, S. H. W.; Goedert, M. Structures of  $\alpha$ -Synuclein Filaments from Human Brains with Lewy Pathology. *Nature*. 2022, pp 791–795.

<https://doi.org/10.1038/s41586-022-05319-3>.

- (123) Volpicelli-Daley, L. A.; Luk, K. C.; Patel, T. P.; Tanik, S. A.; Riddle, D. M.; Stieber, A.; Meaney, D. F.; Trojanowski, J. Q.; Lee, V. M. Y. Exogenous  $\alpha$ -Synuclein Fibrils Induce Lewy Body Pathology Leading to Synaptic Dysfunction and Neuron Death. *Neuron* **2011**, 72 (1), 57–71. <https://doi.org/10.1016/j.neuron.2011.08.033>.
- (124) Illarioshkin, S. N.; Klyushnikov, S. A.; Vigont, V. A.; Seliverstov, Y. A.; Kaznacheyeva, E. V. Molecular Pathogenesis in Huntington's Disease. *Biochem.* **2018**, 83 (9), 1030–1039. <https://doi.org/10.1134/s0006297918090043>.
- (125) Pagano, G.; Ferrara, N.; Brooks, D. J.; Pavese, N. Age at Onset and Parkinson Disease Phenotype. *Neurology* **2016**, 86 (15), 1400–1407. <https://doi.org/10.1212/WNL.0000000000002461>.
- (126) Aborode, A. T.; Pustake, M.; Awuah, W. A.; Alwerdani, M.; Shah, P.; Yarlagadda, R.; Ahmad, S.; Silva Correia, I. F.; Chandra, A.; Nansubuga, E. P.; Abdul-Rahman, T.; Mehta, A.; Ali, O.; Amaka, S. O.; Zuñiga, Y. M. H.; Shkodina, A. D.; Inya, O. C.; Shen, B.; Alexiou, A. Targeting Oxidative Stress Mechanisms to Treat Alzheimer's and Parkinson's Disease: A Critical Review. *Oxid. Med. Cell. Longev.* **2022**, 2022. <https://doi.org/10.1155/2022/7934442>.
- (127) Beshir, S. A.; Aadithsoorya, A. M.; Parveen, A.; Goh, S. S. L.; Hussain, N.; Menon, V. B. Aducanumab Therapy to Treat Alzheimer's Disease: A Narrative Review. *Int. J. Alzheimers. Dis.* **2022**, 2022. <https://doi.org/10.1155/2022/9343514>.
- (128) Probst, D.; Batchu, K.; Younce, J. R.; Sode, K. Levodopa: From Biological Significance to Continuous Monitoring. *ACS Sensors* **2024**, 9 (8), 3828–3839. <https://doi.org/10.1021/acssensors.4c00602>.
- (129) Baweja, G. S.; Gupta, S.; Kumar, B.; Patel, P.; Asati, V. Recent Updates on Structural Insights of MAO-B Inhibitors: A Review on Target-Based Approach. *Molecular Diversity*. 2024, pp 1823–1845. <https://doi.org/10.1007/s11030-023-10634-6>.
- (130) Xu, W.; Wang, J.; Li, X. N.; Liang, J.; Song, L.; Wu, Y.; Liu, Z.; Sun, B.; Li, W. G. Neuronal and Synaptic Adaptations Underlying the Benefits of Deep Brain Stimulation for Parkinson's Disease. *Transl. Neurodegener.* **2023**, 12 (1), 1–21. <https://doi.org/10.1186/s40035-023-00390-w>.
- (131) Frank, S. Tetrabenazine: The First Approved Drug for the Treatment of Chorea in US Patients with Huntington Disease. *Neuropsychiatr. Dis. Treat.* **2010**, 657. <https://doi.org/10.2147/ndt.s6430>.
- (132) Radder, D. L. M.; Sturkenboom, I. H.; van Nimwegen, M.; Keus, S. H.; Bloem, B. R.; de Vries, N. M. Physical Therapy and Occupational Therapy in Parkinson's Disease. *Int. J. Neurosci.* **2017**, 127 (10), 930–943. <https://doi.org/10.1080/00207454.2016.1275617>.
- (133) Ciechanover, A.; Kwon, Y. T. Degradation of Misfolded Proteins in Neurodegenerative Diseases: Therapeutic Targets and Strategies. *Exp. Mol. Med.*

- 2015**, 47 (3), e147. <https://doi.org/10.1038/EMM.2014.117>.
- (134) Soto, C.; Estrada, L. D. Protein Misfolding and Neurodegeneration. *Arch. Neurol.* **2008**, 65 (2), 184–189. <https://doi.org/10.1001/archneurol.2007.56>.
- (135) Polymeropoulos, M. H.; Lavedan, C.; Leroy, E.; Ide, S. E.; Dehejia, A.; Dutra, A.; Pike, B.; Root, H.; Rubenstein, J.; Boyer, R.; Stenroos, E. S.; Chandrasekharappa, S.; Athanassiadou, A.; Papapetropoulos, T.; Johnson, W. G.; Lazzarini, A. M.; Duvoisin, R. C.; Di Iorio, G.; Golbe, L. I.; Nussbaum, R. L. Mutation in the  $\alpha$ -Synuclein Gene Identified in Families with Parkinson's Disease. *Science* (80-. ). **1997**, 276 (5321), 2045–2047. <https://doi.org/10.1126/science.276.5321.2045>.
- (136) Ohgita, T.; Namba, N.; Kono, H.; Shimanouchi, T.; Saito, H. Mechanisms of Enhanced Aggregation and Fibril Formation of Parkinson's Disease-Related Variants of  $\alpha$ -Synuclein. *Sci. Rep.* **2022**, 12 (1), 1–13. <https://doi.org/10.1038/s41598-022-10789-6>.
- (137)  $\alpha$ -Synuclein in Synaptic Function.Pdf.
- (138) de Oliveira, G. A. P.; Silva, J. L. Alpha-Synuclein Stepwise Aggregation Reveals Features of an Early Onset Mutation in Parkinson's Disease. *Commun. Biol.* **2019**, 2 (1). <https://doi.org/10.1038/s42003-019-0598-9>.
- (139) Hijaz, B. A.; Volpicelli-Daley, L. A. Initiation and Propagation of  $\alpha$ -Synuclein Aggregation in the Nervous System. *Molecular Neurodegeneration*. 2020. <https://doi.org/10.1186/s13024-020-00368-6>.
- (140) Afitska, K.; Fucikova, A.; Shvadchak, V. V.; Yushchenko, D. A. Modification of C Terminus Provides New Insights into the Mechanism of  $\alpha$ -Synuclein Aggregation. *Biophys. J.* **2017**, 113 (10), 2182–2191. <https://doi.org/10.1016/j.bpj.2017.08.027>.
- (141) Thibaut, T. A.; Anderson, R. T.; Smith, D. M. A Common Mechanism of Proteasome Impairment by Neurodegenerative Disease-Associated Oligomers. *Nat. Commun.* **2018**, 9 (1), 1–13. <https://doi.org/10.1038/s41467-018-03509-0>.
- (142) Dong-Chen, X.; Yong, C.; Yang, X.; Chen-Yu, S. T.; Li-Hua, P. Signaling Pathways in Parkinson's Disease: Molecular Mechanisms and Therapeutic Interventions. *Signal Transduct. Target. Ther.* **2023**, 8 (1). <https://doi.org/10.1038/s41392-023-01353-3>.
- (143) Benskey, M. J.; Perez, R. G.; Manfredsson, F. P. The Contribution of Alpha Synuclein to Neuronal Survival and Function - Implications for Parkinson's Disease. *J. Neurochem.* **2016**, 137 (3), 331–359. <https://doi.org/10.1111/jnc.13570>.
- (144) Conway, K. A.; Lee, S. J.; Rochet, J. C.; Ding, T. T.; Williamson, R. E.; Lansbury, P. T. Acceleration of Oligomerization, Not Fibrillization, Is a Shared Property of Both  $\alpha$ -Synuclein Mutations Linked to Early-Onset Parkinson's Disease: Implications for Pathogenesis and Therapy. *Proc. Natl. Acad. Sci. U. S. A.* **2000**, 97 (2), 571–576. <https://doi.org/10.1073/pnas.97.2.571>.
- (145) Flagmeier, P.; Meisl, G.; Vendruscolo, M.; Knowles, T. P. J.; Dobson, C. M.; Buell, A. K.; Galvagnion, C. Mutations Associated with Familial Parkinson's Disease Alter

- the Initiation and Amplification Steps of  $\alpha$ -Synuclein Aggregation. *Proc. Natl. Acad. Sci. U. S. A.* **2016**, *113* (37), 10328–10333. <https://doi.org/10.1073/pnas.1604645113>.
- (146) Yu, Y. J.; Watts, R. J. Developing Therapeutic Antibodies for Neurodegenerative Disease. *Neurotherapeutics* **2013**, *10* (3), 459–472. <https://doi.org/10.1007/s13311-013-0187-4>.
- (147) Espay, A. J.; McFarthing, K. Alpha-Synuclein and the Parkinson's Disease Drug Pipeline. *Park. Relat. Disord.* **2023**, *111* (April), 105432. <https://doi.org/10.1016/j.parkreldis.2023.105432>.
- (148) Castonguay, A. M.; Gravel, C.; Lévesque, M. Treating Parkinson's Disease with Antibodies: Previous Studies and Future Directions. *J. Parkinsons. Dis.* **2021**, *11* (1), 71–92. <https://doi.org/10.3233/JPD-202221>.
- (149) Kharel, S.; Ojha, R. Future of Monoclonal Antibody Therapy in Parkinson's Disease. *Ann. Neurosci.* **2023**, *30* (1), 8–10. <https://doi.org/10.1177/09727531221136349>.
- (150) Nordström, E.; Eriksson, F.; Sigvardson, J.; Johannesson, M.; Kasrayan, A.; Jones-Kostalla, M.; Appelkvist, P.; Söderberg, L.; Nygren, P.; Blom, M.; Rachalski, A.; Nordenankar, K.; Zachrisson, O.; Amandius, E.; Osswald, G.; Moge, M.; Ingelsson, M.; Bergström, J.; Lannfelt, L.; Möller, C.; Giorgetti, M.; Färling, J. ABBV-0805, a Novel Antibody Selective for Soluble Aggregated  $\alpha$ -Synuclein, Prolongs Lifespan and Prevents Buildup of  $\alpha$ -Synuclein Pathology in Mouse Models of Parkinson's Disease. *Neurobiology of Disease*. 2021. <https://doi.org/10.1016/j.nbd.2021.105543>.
- (151) Tonges, L.; Zella, M. Antibody-Based Immunotherapies for Parkinsonian Syndromes. *Neural Regen. Res.* **2019**, *14* (11), 1903–1904. <https://doi.org/10.4103/1673-5374.259613>.
- (152) Pujols, J.; Peña-Díaz, S.; Lázaro, D. F.; Peccati, F.; Pinheiro, F.; González, D.; Carija, A.; Navarro, S.; Conde-Giménez, M.; García, J.; Guardiola, S.; Giralt, E.; Salvatella, X.; Sancho, J.; Sodupe, M.; Outeiro, T. F.; Dalfó, E.; Ventura, S. Small Molecule Inhibits  $\alpha$ -Synuclein Aggregation, Disrupts Amyloid Fibrils, and Prevents Degeneration of Dopaminergic Neurons. *Proceedings of the National Academy of Sciences of the United States of America*. 2018, pp 10481–10486. <https://doi.org/10.1073/pnas.1804198115>.
- (153) Horne, R. I.; Andrzejewska, E. A.; Alam, P.; Brotzakis, Z. F.; Srivastava, A.; Aubert, A.; Nowinska, M.; Gregory, R. C.; Staats, R.; Possenti, A.; Chia, S.; Sormanni, P.; Ghetti, B.; Caghey, B.; Knowles, T. P. J.; Vendruscolo, M. Discovery of Potent Inhibitors of  $\alpha$ -Synuclein Aggregation Using Structure-Based Iterative Learning. *Nature Chemical Biology*. 2024, pp 634–645. <https://doi.org/10.1038/s41589-024-01580-x>.
- (154) Chia-et-Al-2022-Structure-Based-Discovery-of-Small-Molecule-Inhibitors-of-the-Autocatalytic-Proliferation-of- $\alpha$ .Pdf.
- (155) Jin, J. W.; Fan, X.; del Cid-Pellitero, E.; Liu, X. X.; Zhou, L.; Dai, C.; Gibbs, E.; He,

- W.; Li, H.; Wu, X.; Hill, A.; Leavitt, B. R.; Cashman, N.; Liu, L.; Lu, J.; Durcan, T. M.; Dong, Z.; Fon, E. A.; Wang, Y. T. Development of an  $\alpha$ -Synuclein Knockdown Peptide and Evaluation of Its Efficacy in Parkinson's Disease Models. *Communications Biology*. 2021. <https://doi.org/10.1038/s42003-021-01746-6>.
- (156) Silveira, C. R. A.; MacKinley, J.; Coleman, K.; Li, Z.; Finger, E.; Bartha, R.; Morrow, S. A.; Wells, J.; Borrie, M.; Tirona, R. G.; Rupar, C. A.; Zou, G.; Hegele, R. A.; Mahuran, D.; MacDonald, P.; Jenkins, M. E.; Jog, M.; Pasternak, S. H. Ambroxol as a Novel Disease-Modifying Treatment for Parkinson's Disease Dementia: Protocol for a Single-Centre, Randomized, Double-Blind, Placebo-Controlled Trial. *BMC Neurol.* **2019**, 19 (1), 1–10. <https://doi.org/10.1186/s12883-019-1252-3>.
- (157) Baggett, D.; Olson, A.; Parmar, M. S. Novel Approaches Targeting  $\alpha$ -Synuclein for Parkinson's Disease: Current Progress and Future Directions for the Disease-Modifying Therapies. *Brain Disord.* **2024**, 16 (September), 100163. <https://doi.org/10.1016/j.dscb.2024.100163>.
- (158) Jasutkar, H. G.; Oh, S. E.; Mouradian, M. M. Therapeutics in the Pipeline Targeting  $\alpha$ -Synuclein for Parkinson's Disease. *Pharmacological Reviews*. 2022, pp 207–237. <https://doi.org/10.1124/PHARMREV.120.000133>.
- (159) Njomen, E.; Osmulski, P. A.; Jones, C. L.; Gaczynska, M.; Tepe, J. J. Small Molecule Modulation of Proteasome Assembly. *Biochemistry* **2018**, 57 (28), 4214–4224. <https://doi.org/10.1021/acs.biochem.8b00579>.
- (160) Njomen, E.; Osmulski, P. A.; Jones, C. L.; Gaczynska, M.; Tepe, J. J. Small Molecule Modulation of Proteasome Assembly. *Biochemistry* **2018**, 57 (28), 4214–4224. <https://doi.org/10.1021/acs.biochem.8b00579>.
- (161) Staerz, S. D.; Jones, C. L.; Tepe, J. J. Design, Synthesis, and Biological Evaluation of Potent 20S Proteasome Activators for the Potential Treatment of  $\alpha$ -Synucleinopathies. *Journal of Medicinal Chemistry*. 2022, pp 6631–6642. <https://doi.org/10.1021/acs.jmedchem.1c02158>.
- (162) Jones, C. L.; Njomen, E.; Sjögren, B.; Dexheimer, T. S.; Tepe, J. J. Small Molecule Enhancement of 20S Proteasome Activity Targets Intrinsically Disordered Proteins. *ACS Chem. Biol.* **2017**, 12 (9), 2240–2247. <https://doi.org/10.1021/acschembio.7b00489>.
- (163) Fiolek, T. J.; Magyar, C. L.; Wall, T. J.; Davies, S. B.; Campbell, M. V.; Savich, C. J.; Tepe, J. J.; Mosey, R. A. Dihydroquinazolines Enhance 20S Proteasome Activity and Induce Degradation of  $\alpha$ -Synuclein, an Intrinsically Disordered Protein Associated with Neurodegeneration. *Bioorganic Med. Chem. Lett.* **2021**, 36. <https://doi.org/10.1016/j.bmcl.2021.127821>.
- (164) Fiolek, T. J.; Keel, K. L.; Tepe, J. J. Fluspirilene Analogs Activate the 20S Proteasome and Overcome Proteasome Impairment by Intrinsically Disordered Protein Oligomers. *ACS Chem. Neurosci.* **2021**, 12 (8), 1438–1448. <https://doi.org/10.1021/acschemneuro.1c00099>.



## **CHAPTER TWO:** Design, Synthesis, and Biological Evaluation of Chlorpromazine-Based 20S Proteasome Activators

## 2.1 Introduction

Despite being the second most common neurodegenerative disease (ND), Parkinson's disease (PD) is very prevalent in North America, with an estimated 930,000 individuals aged  $\geq 45$  years living with PD in 2020<sup>1</sup>. This number is projected to increase to 1,238,000 by 2030.<sup>2</sup> PD belongs to a group of disorders known collectively as neurodegenerative diseases characterized by progressive neuronal loss and simultaneous accumulation of misfolded or aggregated proteins.<sup>3–5</sup> NDs include Alzheimer's disease (AD), Huntington's disease (HD), amyotrophic lateral sclerosis (ALS), and multiple system atrophy (MSA), with each affecting different parts of the central nervous system. Despite extensive research, the causes of NDs remain unclear, with genetic, environmental, and age-related factors all implicated.<sup>6–8</sup> The slow disease progression, coupled with the lack of early diagnosis, makes them challenging to treat. Current treatment options target symptoms rather than the underlying causes with no definitive cure.<sup>9,10</sup>

One general feature of NDs is the accumulation of misfolded or aggregated proteins.<sup>5,11</sup> These misfolded proteins, such as amyloid beta<sup>12</sup> in Alzheimer's disease and  $\alpha$ -synuclein<sup>11,13–15</sup> ( $\alpha$ -syn) in Parkinson's disease have been shown to form toxic aggregates that are believed to interfere with cellular functions. A common mechanism has been reported whereby soluble oligomeric forms derived from these IPDs bind and inhibit the proteasome, exacerbating their toxic effects.<sup>4</sup> In addition, the cells' failure to degrade protein aggregates leads to proteotoxic stress, which triggers inflammation and neuronal death.<sup>3,15,16</sup> Moreover, when misfolded proteins accumulate inside cells, they can spread between cells in a prion-like fashion, worsening disease progression.<sup>17,18</sup>

Additionally, the loss of dopaminergic neurons in the substantia nigra pars compacta and the abnormal accumulation of  $\alpha$ -syn in Lewy Bodies and Lewy neurites are vital pathological features of PD.<sup>19,20</sup> Although most PD are considered to be idiopathic, a single missense mutation has been linked to a familial form of PD.<sup>21</sup> This mutant  $\alpha$ -syn, A53T, is known to have a higher propensity to aggregates than the wild type.<sup>21,22</sup> The key role of  $\alpha$ -syn in Parkinson's disease has driven intense research to find therapies that reduce its aggregation and toxicity.<sup>13,14,23</sup>

However, the lack of a stable 3D-conformation of  $\alpha$ -syn makes it harder to target this protein directly using traditional drug discovery approaches.<sup>24–26</sup> Current therapeutic

strategies targeting  $\alpha$ -syn aim to mitigate the toxic effects of its accumulation and subsequent aggregation.

Immunotherapy has emerged as an attractive strategy. This strategy uses antibodies to target and neutralize  $\alpha$ -syn aggregates. Active and passive immunotherapies have shown promise in reducing  $\alpha$ -syn load in preclinical models by promoting clearance through immune-mediated pathways.<sup>27</sup> In clinical trials, these therapies demonstrated good tolerability and some efficacy in reducing  $\alpha$ -syn levels, though challenges with brain delivery remain.<sup>13,14</sup> Another promising approach involves small molecules that prevent  $\alpha$ -syn from misfolding and aggregating. These molecules bind to  $\alpha$ -syn, stabilizing its structure and preventing the formation of harmful fibrils.<sup>28</sup>

Protein clearance mechanisms also play a vital role in current therapeutic strategies. The autophagy-lysosomal pathway, responsible for degrading misfolded proteins like  $\alpha$ -syn, is often impaired in PD.<sup>29,30</sup> Enhancing this pathway through small molecules that boost autophagy or lysosomal activity can facilitate the degradation of  $\alpha$ -syn aggregates.<sup>31</sup> By improving protein clearance, these treatments aim to reduce the burden of toxic aggregates on neurons.

Another pathway through which  $\alpha$ -syn clearance has been achieved is the proteasome-mediated protein degradation. The study of small molecules capable of modulating proteasomal activity began with identifying inhibitors, with bortezomib being the first proteasome inhibitor approved to treat multiple myeloma.<sup>32,33</sup> However, the idea of enhancing proteasome function, specifically the 20S proteasome, emerged later motivated by the potential to counteract diseases associated with protein aggregation. Tanaka and co-workers were the first to demonstrate that the 20S proteasome could be activated using the small molecule detergent, sodium dodecyl sulfate (SDS), and polylysine.<sup>34</sup> The study found that SDS can activate these latent proteasomes in the presence of a substrate, enhancing their ability to degrade proteins. This activation is reversible, as the proteasomes return to their latent state when SDS is diluted.<sup>35</sup> However, without a substrate, SDS causes irreversible inactivation of proteasomes. Substrates are critical in maintaining the active state and protecting proteasomes from SDS-induced inactivation. Subsequently, lipids, fatty acids<sup>36</sup>, and the natural product, oleuropein<sup>37</sup> have been shown to exhibit SDS-like proteasome activation. Although their observed dose-response is

attenuated in physiologically relevant systems, they are still essential tools for *in vitro* studies.<sup>38</sup> Haung *et al.*,<sup>39</sup> discovered the triterpenoid betulinic acid as a proteasome activator. However, an attempt to improve its activity through chemical modification led to the generation of a proteasome inhibitor. To discover new bona fide 20S proteasome activators, Kodadek and co-workers screened the NIH Clinical Collection (NCC) library. Although a dozen compounds stimulated the degradation of small fluorogenic peptides, only two compounds, AM-404 and MK-886, activated the proteasome under physiologically relevant conditions.<sup>40</sup> Following up on this work, the Trader lab developed small molecules 20S proteasome activators derivatives based on AM-404 and oleic amide, respectively.<sup>41</sup>

The Tepe lab has explored using small molecules to activate the 20S proteasome to degrade IDPs as a novel approach to treating NDs. TCH-165, an imidazoline, increased the proteolytical activity of the 20S proteasome by favoring the open gate conformation of the 20S complex.<sup>42</sup> Subsequent studies expanded the repertoire of the 20S proteasome activator class to include the dihydroquinazolines<sup>43</sup> and analogs of the FDA-approved antipsychotic agent fluspirilene<sup>44</sup>. Recently, novel classes of 20S proteasome activators, including peptide-based activators, have been introduced.<sup>45,46</sup> A notable example is the development of HIV-1 Tat protein-derived peptides, which were shown to enhance proteasome activity by binding to specific  $\alpha$ -ring subunit interfaces.<sup>47</sup> These peptides demonstrated *in vitro* proteasome activation and the ability to cross the blood-brain barrier, which is crucial for targeting neurodegenerative diseases.<sup>47</sup> Although the field of 20S proteasome activation has seen significant attention in recent years, the level of activity displayed by current agents needs to be improved significantly before any relevant clinical studies can be initiated.

To tackle this, the Tepe lab screened the NIH, clinical, and Prestwick libraries and identified chlorpromazine (CPZ), an FDA-approved antipsychotic, as a 20S proteasome activator.<sup>48</sup> CPZ was serendipitously discovered in the early 1950s as an antipsychotic agent.<sup>49</sup> Initially developed as a surgical anesthetic, its profound effects on behavior led to its use in psychiatric treatment, marking a significant breakthrough in schizophrenia management. Structurally, chlorpromazine belongs to the phenothiazine class, and its therapeutic action is primarily attributed to its ability to block dopamine receptors in the

brain, particularly the dopamine D2 receptors (D2R).<sup>50</sup> The planarity of the phenothiazine ring in CPZ mimics the conformation of dopamine molecules, which allows them to bind to dopamine receptors and prevent dopamine from exerting its effects.<sup>51,52</sup> Furthermore, the protonation of the alkylamine side chain in CPZ is crucial for its interaction with dopamine D2 receptors (D2R). This interaction is critical to CPZ's neuroleptic activity, as it allows CPZ to effectively block D2R, reducing dopamine signaling and alleviating symptoms of psychosis.<sup>52</sup>

Implementing CPZ analogs as 20S proteasome activators requires structural modifications to achieve two key goals: (i) improving the observed 20S proteasome activity and (ii) abolishing the observed neuroleptic properties. Dr. Jones achieved this aim by modifying the alkylamine side chain of CPZ, a critical structural feature responsible for its neuroleptic effects. Substituting the amine chain with aryl ester led to CJ-4-72, which retained proteasome activation but had diminished affinity for D2R (**Figure 2.1 B and C**). In addition, molecular docking tools were implemented, which predicted that CJ-4-72 interacted with the  $\alpha 1/\alpha 2$  inter-subunit pockets of the  $\alpha$ -rings of the 20S proteasome, inducing an open-gate conformation, which allowed IDPs access to the proteolytic core for subsequent degradation.<sup>48</sup> CJ-4-72 exhibited 20S proteasome activation, which provided a good lead for further exploration and insight into the mechanism of 20S gate regulation.

Buoyed by this success, Dr. Staerz aimed to design a potent and selective 20S proteasome activator based on the Chlorpromazine analogs. Dr. Staerz pursued the design and synthesis of additional pendant groups featuring aromatic structures to enhance interaction with the 20S proteasome. The final design iteration, SS-2-71 (**Figure 2.1 C**), was crafted to mimic the disubstituted amine group found in CPZ. However, the nitrogen in this new structure was electron-depleted (acylated) and effectively suppressing its N-protonation potential (**Figure 2.1 A vs C**). This modification was intended to reduce any residual affinity for dopamine D2 receptors whose interaction with CPZ requires protonation of the free tertiary amine. Hence, this will prevent neuroleptic side effects while enhancing compound SS-2-71's interaction within the 20S proteasome's  $\alpha$ -ring. Each structural modification in the pendant group was made to fine-

tune the compound's electronic properties and spatial arrangement, maximizing the efficacy of proteasome activation.

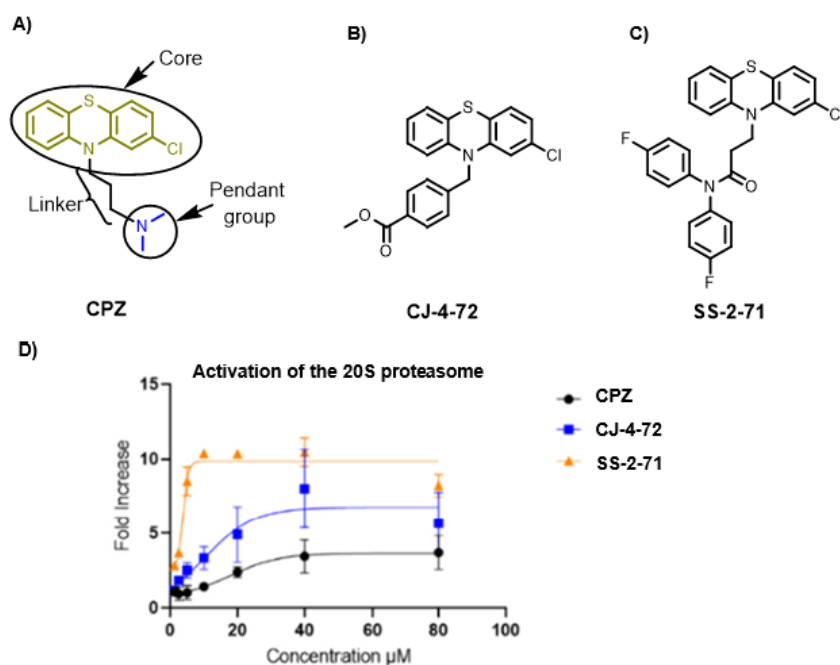


**Figure 2.1: Chlorpromazine Analog and Their Functional Group Modifications.**

(A) The structure of chlorpromazine highlights the core, linker, and pendant groups. The structure analogs are (B) CJ-7-42, (C) SS-2-71, and (D) the comparison of the enhancement of the 20S proteasome by CPZ, CJ-7-42, and SS-2-71.

Through molecular docking, the potent activity of SS-2-71 as a 20S proteasome activator was predicted to rely on its precise interactions with tyrosine 159 (Y159) and cysteine 161 (C161) within the  $\alpha 1/\alpha 2$  inter-subunit pocket.<sup>53</sup> The interactions with these residues were predicted to stabilize the open-gate conformation necessary for enhanced proteolysis. Y159, an aromatic residue, engages in  $\pi$ - $\pi$  stacking with the electron-deficient aromatic ring, creating both parallel and T-shaped stacking configurations. Parallel stacking is especially critical, as it offers optimal orbital overlap and a more substantial stabilizing effect than T-shaped stacking. The electron-poor nature of the diphenyl tail of the pendant group also enhances "aromatic donor-acceptor" interactions with the electron-rich Y159, further strengthening binding affinity.

This specific  $\pi$ - $\pi$  stacking configuration is crucial to compound high activation potency, providing an interaction strength not seen in less electron-deficient analogs. C161, on the

other hand, provides a unique sulfur atom capable of forming strong edge-on  $\pi$ -sulfur interactions with the aromatic system. This edge-on configuration stabilizes the ligand-proteasome complexes and positions them effectively within the binding site. Unlike sulfur-alkyl interactions observed in less active compounds,  $\pi$ -sulfur interactions with C161 anchor SS-2-71 stabilize the  $\alpha$ -ring's open conformation and facilitate proteasome activation.

Despite the ability of SS-2-71 to activate the 20S proteasome, it required higher micromolar concentrations (10  $\mu$ M) for significant activity in cellular assays, requiring the development of more potent compounds.<sup>54</sup> Furthermore, phenothiazines, like CPZ, have well-documented interactions with dopamine receptors (D2R), leading to potential central nervous system side effects, mainly because of their neuroleptic activity.<sup>55–57</sup> Phenothiazines undergo complex hepatic biotransformation mediated primarily by the cytochrome P450 enzyme system, encompassing several distinct metabolic pathways.<sup>58</sup> *N*-Demethylation, predominantly facilitated by cytochrome P450 2D6 (CYP2D), generates secondary amine derivatives with attenuated pharmacological activity.<sup>59,60</sup> Concurrently, aromatic ring hydroxylation, often mediated by CYP1A2, yields hydroxylated metabolites, which may subsequently conjugate with glucuronic acid or sulfates, leading to hepatotoxicity. Another major pathway, S-oxidation, converts the sulfur atom in the thiazine ring to sulfoxides.<sup>59</sup> It is catalyzed by multiple isoforms, including CYP2D6, CYP3A4, and flavin-containing monooxygenases. A notable aspect of phenothiazine metabolism is the bioactivation process, wherein hydroxylated intermediates undergo further oxidation to form electrophilic iminoquinone species.<sup>61</sup> These reactive metabolites can conjugate with glutathione or covalently bind to cellular macromolecules, potentially precipitating idiosyncratic hepatotoxicity. This intricate metabolic profile, influenced by both genetic polymorphisms and co-administered drugs, underscores the variability in therapeutic response and adverse effects observed with phenothiazine use.<sup>62</sup> Hence, the following sections of this chapter will describe the collaborative efforts of Dr. Sophie D. Staerz and me toward the design, synthesis, and biological evaluation of third-generation chlorpromazine analogs for 20S proteasome activation.

## 2.2 Design and Synthesis of Third-Generation Chlorpromazine Analogs

### 2.2.1 Rational

The design of the third generation chlorpromazine analogs was conceived to investigate two hypotheses: i) the effect of linker length on 20S proteasome activation and ii) different heterocyclic cores to replace the phenothiazine core. We implemented the same pendant group found in SS-2-71 and varied the linker using one and two carbon chains.<sup>54</sup> The heterocyclic cores included tricyclic, bicyclic, and monocyclic cores with different heterocyclic atoms. To differentiate compounds prepared by Dr. Staerz and in this collaborative effort, Dr. Staerz synthesized and characterized all compounds with an asterisk against their number identifier.

### 2.2.2 Synthesis

The design and synthesis of small molecules described in this work were guided by two main objectives: (1) replacing the phenothiazine core and (2) investigating the effect of linker length on 20S proteasome activation. To achieve these aims, the *N,N*-bis(4-fluorophenyl)amine pendant group was synthesized by adding *p*-fluorophenylboronic acid to a mixture of *p*-fluorophenylalanine, CuOAc<sub>2</sub>, TEA, and 4 Å molecular sieves in DCM (**Scheme 2.1**) giving the coupled product, compound **1** with varying yields of 48%-73%.<sup>63</sup> The yields were sensitive to the reaction scale, with a reaction scale higher than 1 gram giving lower yields. The methylene linker length was explored to examine its influence on proteasome activation. The synthesized *N,N*-bis(4-fluorophenyl)amine, compound **1** was functionalized by coupling it with either a one- or two-methylene-linked *N,N*-bis(4-fluorophenyl)amide linker, which were subsequently attached as pendant groups to various heterocyclic cores. The amide synthesis involved treating *N,N*-bis(4-fluorophenyl)amine with triethylamine (TEA) and either 2-chloroacetyl chloride or 3-bromopropanoyl chloride, yielding compounds **2** and **3** in 67% and 88% yield, respectively (**Figure 2.1**).<sup>64</sup> This approach facilitated the preparation of versatile derivatives for further exploration.

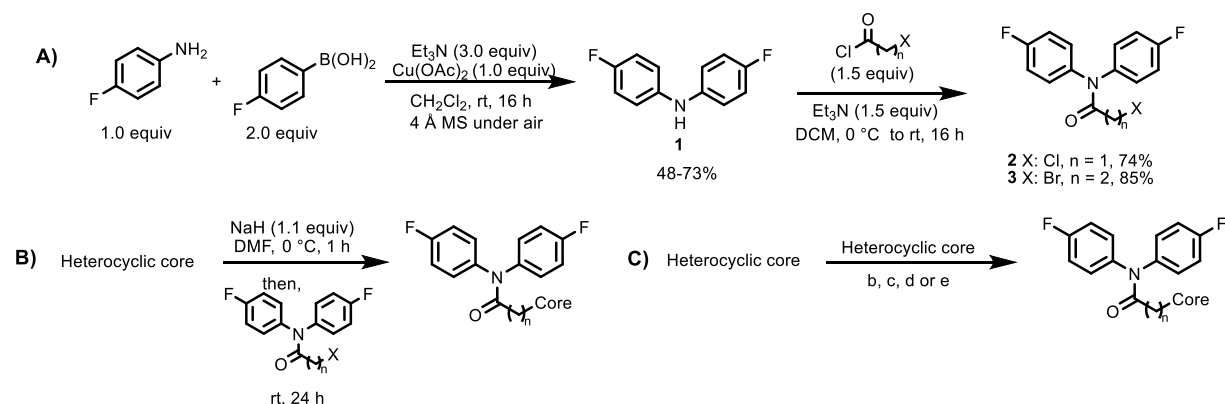
The impact of different heterocyclic cores on proteasome activation was examined using bi- and tricyclic systems. The investigation was initiated by coupling the amide tails (**2** and **3**) to carbazole-containing cores, focusing on the role of ring size and the absence of sulfur. The carbazole-containing core was first treated with sodium hydride (NaH),



followed by the subsequent addition of the respective linker to yield the unsubstituted and 2-chlorocarbazole derivatives. The reactions with **3** produced compounds **4** (59%) and **6** (88%), while the coupling with **2** produced compounds **5** and **7** in 92% and 58% respectively (**Scheme 2.1**).

Next, we explored the influence of electron-poor aromatic systems by coupling the amide tails with a  $\beta$ -carboline core. The electron-deficient nature of  $\beta$ -carboline was hypothesized to affect proteasome activation by altering electronic interactions with the target protein. The synthesis yielded compounds **8** (38%) and **9** (65%), indicating that the two-methylene linker **3** may provide a more favorable conformation for interaction with the proteasome. To assess whether a tricyclic core is necessary for proteasome activation, a series of activators with various bicyclic heterocyclic cores were synthesized. Indole derivatives were chosen due to their structural similarity to carbazoles but with fewer fused rings. Using NaH as the base, indole was coupled with the one- and two-methylene amide linkers, resulting in compounds **10** and **11** in 65% and 60%, respectively (**Scheme 2.1**). The comparable yields of **10** and **11** suggest that indole maintains adequate reactivity, even with a more straightforward core structure.

To further understand the effect of halogen substitution, 2-chloroindole derivatives were synthesized. Compounds **12** (62%) and **13** (77%) were obtained using the two- and one-methylene linkers, respectively. The higher yield of **13** may indicate that the shorter linker favors a more optimal spatial orientation for coupling.



| No   | Heterocycle core | n | X  | Yield |
|------|------------------|---|----|-------|
| * 4  |                  | 2 | Br | 59%   |
| 5    |                  | 1 | Cl | 92%   |
| 6    |                  | 2 | Br | 88%   |
| * 7  |                  | 1 | Cl | 58%   |
| * 8  |                  | 2 | Br | 38%   |
| 9    |                  | 1 | Cl | 65%   |
| * 10 |                  | 2 | Br | 65%   |
| * 11 |                  | 1 | Cl | 60%   |
| * 12 |                  | 2 | Br | 62%   |
| 13   |                  | 1 | Cl | 77%   |
| 14   |                  | 2 | Br | 98%   |
| 15   |                  | 1 | Cl | 80%   |

Synthesized using reaction condition B above.

| No   | Heterocycle core | n | X  | Yield            |
|------|------------------|---|----|------------------|
| * 16 |                  | 2 | Br | 47% <sup>b</sup> |
| * 17 |                  | 1 | Cl | 70% <sup>b</sup> |
| 18   |                  | 2 | Br | 46% <sup>c</sup> |
| 19   |                  | 1 | Cl | 84% <sup>c</sup> |
| -    |                  | - | -  | -                |
| 20   |                  | 1 | Cl | 36% <sup>e</sup> |
| 21   |                  | 2 | Br | 44% <sup>b</sup> |
| 22   |                  | 1 | Cl | 70% <sup>b</sup> |
| * 23 |                  | 2 | Br | 36% <sup>b</sup> |
| * 24 |                  | 1 | Cl | 30% <sup>b</sup> |
| * 25 |                  | 2 | Br | 64% <sup>d</sup> |
| * 26 |                  | 1 | Cl | 48% <sup>d</sup> |

<sup>b</sup> TEA (4.0 equiv) in toluene, refluxed for 24 h. <sup>c</sup> K<sub>2</sub>CO<sub>3</sub> in CH<sub>3</sub>CN or DMF at 80 °C for 24 h. <sup>d</sup> TEA (1.2 equiv) in THF at room temperature for 24 hours. <sup>e</sup> TBAB (10 mol%), K<sub>2</sub>CO<sub>3</sub> (1.5 equiv) in DMF, room temperature for 24 hours.

## **Scheme 2.1: The Synthetic Routes to Access Compounds (A) 1- 3, (B) 4-14, and (C) 16-26.**

In an effort to mimic the sulfur found in the phenothiazine core, 3-oxo-3,4-dihydro-2H-1,4-benzothiazine was employed as a replacement. Compounds **14** (98%) and **15** (80%) were synthesized using NaH, demonstrating high yields and underscoring the robustness of the reaction conditions with this core structure.

Next, the impact of hydrogen bond acceptors within the core structure was investigated. Compounds **16** (47%) and **17** (70%) were synthesized by refluxing 3,4-dihydro-2H-

benzo[b][1,4] oxazine in toluene using TEA as the base in the presence of one-methylene (**2**) and two-methylene (**3**) linker respectively.

We then investigated the role of hetero atoms on 20S proteasome activation. To achieve these, two cores bearing three hetero atoms were each coupled with the one and two methylene linkers. The 2-benzoxazolinone core was coupled with the two-methylene linker to produce compound **18** in 46% while coupling with the one-methylene linker yielded compound **19** (84%). The marked difference in yields suggests a significant effect of the linker length on the efficiency of the reaction. In addition, refluxing the two-methylene linker (**3**) eliminated HBr to yield *N,N* bis(4-fluorophenyl)acrylamide as a side product, explaining the lower yields under such reaction conditions. When 1,3-dihydro-2H-benzo[d]imidazole-2-one was reacted with one methylene linker (**2**) in the presence of K<sub>2</sub>CO<sub>3</sub> as base and tetrabutylammonium bromide as phase transfer agent yielded compound **20** in 36%. Efforts to produce the two-methylene linker counterpart proved futile. The reaction resulted in complex mixtures which with no not isolated.

To determine if an aromatic core is necessary for proteasome activation, we synthesized derivatives based on non-aromatic piperazine-2-one and morpholine cores. Piperazin-2-one was reacted with the amide linkers (**3** and **2**) using TEA as a base, yielding compounds **21** and **22** in 44% and 70%, respectively (**Scheme 2.1**). The morpholine derivatives were accessed similarly to produce compounds **23** (36%) and **24** (30%). The lower yields of the morpholine derivatives (**23** and **24**) may imply a reduced ability to engage in  $\pi$ -stacking interactions, which could be crucial for binding to the proteasome active site. Finally, we synthesized compounds **25** and **26** by coupling the amide linkers with a dimethyl amine moiety, similar to the structure of chlorpromazine. The reactions, conducted in the presence of TEA in THF, yielded compound **25** (64%) with the two-methylene linker and compound **26** (48%) with the one-methylene linker (**Scheme 2.1**).

### 2.2.3 Evaluation of analogs towards the Activation of 20S proteasome

Having synthesized compounds **4-26**, we tested them for their ability to activate the 20S proteasome in a small fluorogenic peptide assay. In this assay, a fluorescent 7-amino-methyl coumarin (AMC) tag was attached to peptides that mimic the preferred cleavage sites of the three catalytic subunits of the 20S proteasome: chymotrypsin-like (Suc-LLVY-AMC), caspase-like (Z-LLE-AMC), and trypsin-like (Boc-LRR-AMC) sites using an

excitation and emission wavelengths of 380 nm and 460nm, respectively.<sup>40,65–67</sup> Upon the proteasome cleavage of these peptides, the AMC tag is released, emitting a fluorescent signal (**Figure 2.2**). This signal was measured every 5 minutes for one hour to monitor the degradation rate of the peptides, indicating the proteasome activity.<sup>43,54</sup>

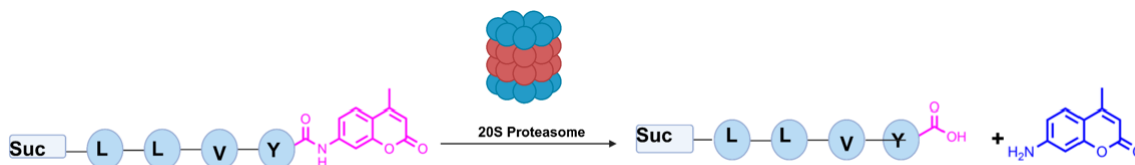


**Figure 2.2: Schematic Diagram for Small Peptide Assay.**

The 26S proteasome cleaves the AMC probe, releasing the AMC fluorophore, which is monitored by a plate reader at 480 nm.

An equimolar mix of these probes was used to assess the effect of each test compound on the overall 20S proteasome function. The proteasome was incubated with various concentrations of the compounds alongside a vehicle control (DMSO-treated sample) for 20 minutes at 37 °C. A mixture of the fluorogenic probes (13.3  $\mu$ M each) was added, and fluorescence was monitored over time. In a 96-well plate setup, purified human 20S proteasome (0.5 nM) was exposed to concentrations of 30  $\mu$ M, 15  $\mu$ M, 7.5  $\mu$ M, and 3.75  $\mu$ M of each compound, with DMSO serving as the vehicle (2% final concentration). The increase in proteasome activity was quantified by calculating the fold change in degradation rate compared to the untreated control. The concentration required to achieve a two-fold increase ( $EC_{200}$ ) was determined through a range of doses. Compounds with an  $EC_{200}$  below 3.75  $\mu$ M underwent additional testing across a 9-point concentration gradient (30  $\mu$ M to 0.16  $\mu$ M). The results are summarized in **Figure 2.3**. Compounds featuring a tricyclic heterocycle structure exhibited varying degrees of proteasome activation. The length of the methylene linker did not significantly impact activity, as demonstrated by the comparable performance of carbazole-based molecules **4** and **5**. Compound **4**, with a two-methylene linker, showed strong activation with an  $EC_{200}$  of 1.6  $\mu$ M and a maximal fold increase of 8.8 at 30  $\mu$ M. Conversely, compound **5**, having a one-methylene linker, displayed lower potency, with an  $EC_{200}$  of 3.8  $\mu$ M and a maximal fold increase of 5.1 at 30  $\mu$ M. Interestingly, this trend reversed when the core structure was changed to 2-chlorocarbazole. In this case, the one-methylene-linked

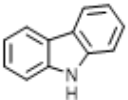
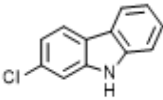
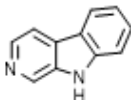
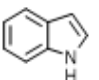
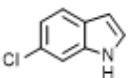
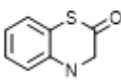
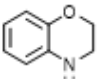
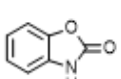
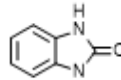
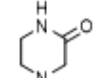
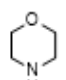
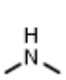
compound **7** outperformed its two-methylene counterpart, compound **6**. Compound **7** had an EC<sub>200</sub> of 1.2  $\mu$ M and a maximal enhancement of 6.1-fold, while compound **6** showed an EC<sub>200</sub> of 0.9  $\mu$ M but a lower fold enhancement of 4.5 (**Figure 2.3**).

Both carbolines (compounds **8** and **9**) demonstrated similar potencies, with EC<sub>200</sub> values of 3.8  $\mu$ M and 2.0  $\mu$ M, respectively. However, the two-methylene-linked carboline (compound **8**) showed a higher maximal fold increase (12) compared to the one-methylene variant (compound **9**), which had a maximal fold increase of 5.5. These observations suggest that chlorine at the 2-position influences the interaction of these molecules with the proteasome, affecting their activation potential (**Figure 2.3**).

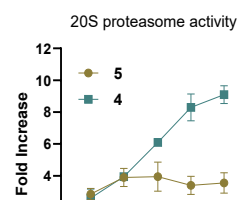
In contrast to tricyclic derivatives, bicyclic compounds exhibited lower efficacy and potency overall. Both unsubstituted indole derivatives, compounds **10** and **11**, showed poor potency with an EC<sub>200</sub> of 7.5  $\mu$ M and max folds of 3.5 and 4.4, respectively. Only compound **12**, a two-methylene-linked 2-chloroindole, achieved an EC<sub>200</sub> below 1  $\mu$ M, demonstrating strong activity with an EC<sub>200</sub> of 0.9  $\mu$ M and a 4.4-fold increase in proteasome activation. The one-methylene-linked analog, compound **13**, showed similar efficiency, with an EC<sub>200</sub> of 1.6  $\mu$ M (**Figure 2.3**). Compounds **16** and **17** had comparable activation effects with an EC<sub>200</sub> of 9.0  $\mu$ M and 8.0  $\mu$ M respectively. These indoles were predicted to bind the  $\alpha$ 1/2 pocket of the proteasome, interacting with cysteine-161 through a  $\pi$ -alkyl interaction. Previous studies have shown that such interactions typically result in weaker EC<sub>200</sub> values and reduced maximal fold increases.<sup>53</sup>

Increased flexibility in the bicyclic analogs, as observed in compounds **16** and **17**, resulted in diminished potency, with EC<sub>200</sub> values of 9.0  $\mu$ M and 8.0  $\mu$ M, respectively. Incorporating hydrogen bond acceptors enhanced activity when linked to a two-methylene spacer, as seen with compound **18**, which had an EC<sub>200</sub> of 1.3  $\mu$ M. However, the proteasome activation was lost entirely when the acceptors were attached to a one-methylene linker, as in compound **19**.

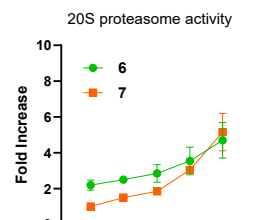
A.

| No | Heterocyclic core   | n | Max fold   | EC <sub>200</sub> (μM) |
|----|---|---|------------|------------------------|
| 4  |    | 2 | 5.8 ± 1.4  | 1.6 ± 0.8              |
| 5  |   | 1 | 5.1 ± 1.1  | 3.8 ± 0.6              |
| 6  |    | 2 | 4.5 ± 1.2  | 0.9 ± 0.5              |
| 7  |   | 1 | 6.1 ± 2.7  | 1.2 ± 0.8              |
| 8  |    | 2 | 12.0 ± 2.6 | 3.8 ± 1.2              |
| 9  |   | 1 | 5.5 ± 2.2  | 2.0 ± 0.9              |
| 10 |    | 2 | 3.5 ± 0.9  | 7.5 ± 1.6              |
| 11 |   | 1 | 4.4 ± 1.4  | 7.5 ± 2.2              |
| 12 |    | 2 | 4.4 ± 2.7  | 0.9 ± 0.6              |
| 13 |   | 1 | 4.0 ± 1.4  | 1.6 ± 1.5              |
| 14 |    | 2 | ---        | > 30                   |
| 15 |   | 1 | 4.3 ± 1.3  | 15.0 ± 3.3             |
| 16 |   | 2 | 5.0 ± 0.4  | 9.0 ± 3.5              |
| 17 |   | 1 | 5.1 ± 0.9  | 8.0 ± 0.6              |
| 18 |  | 2 | 4.8 ± 1.1  | 1.3 ± 0.3              |
| 19 |   | 1 | ---        | >30                    |
| -  |  | - | -          | -                      |
| 20 |   | 1 | 6.5 ± 1.3  | 4.0 ± 1.2              |
| 21 |  | 2 | ---        | >30                    |
| 22 |   | 1 | ---        | >30                    |
| 23 |  | 2 | ---        | >30                    |
| 24 |   | 1 | ---        | > 30                   |
| 25 |  | 2 | ---        | >30                    |
| 26 |   | 1 | ---        | >30                    |

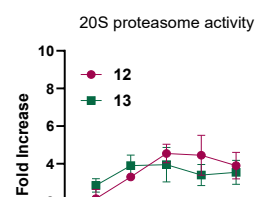
B.



C.



D.



E.

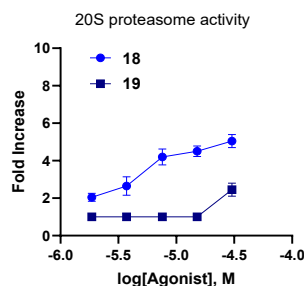


**Figure 2.3: 20S Proteasome Activity of Compounds 4-26.**

(A) The table shows the EC<sub>200</sub> and max fold increase of 20S proteasome-mediated proteolysis induced by compounds 4-26.

### **Figure 2.3 (Cont'd):**

EC<sub>200</sub> depicts the concentration of compounds that increase the proteolytic degradation rate of fluorogenic peptide by 200%. The 20S proteasome activity graphs of compounds (B) **4-5**, (C) **6-7**, (D) **12-13**, and (E) **18-19**.

Interestingly, the one-methylene linker derivative of **19**, which has the oxygen replaced with nitrogen (compound **20**) was active with an EC<sub>200</sub> of 4.0  $\mu$ M. This underscores how subtle changes can significantly impact analogs' ability to activate the 20S proteasome. However, the inability to access the two methylene-linked counterparts means a reasonable conclusion could not be drawn regarding the effect of chain lengths. The removal of the aromatic group from the heterocyclic core, as in compounds **21-26**, led to a complete loss of proteasome activity, emphasizing the critical role of the aromatic moiety in the interaction with the proteasome's active sites.

#### **2.2.4 Evaluation of analogs towards the proteolytic degradation of pathologically relevant substrate**

The pathological aggregation of alpha-synuclein ( $\alpha$ -synuclein) is a defining feature of Parkinson's disease (PD) and related synucleinopathies, including dementia with Lewy bodies.<sup>68-71</sup> This presynaptic protein plays a pivotal role in neurotransmitter regulation.<sup>72</sup> However, its misfolding and subsequent aggregation result in toxic oligomer and fibril formation, disrupting cellular homeostasis.<sup>73,74</sup> Key pathological mechanisms include mitochondrial dysfunction, oxidative stress, and impaired proteasomal activity, ultimately culminating in the degeneration of dopaminergic neurons within the substantia nigra pars compacta. Targeting  $\alpha$ -synuclein aggregation has emerged as a promising therapeutic strategy to address the underlying pathophysiology of PD, potentially slowing disease progression.<sup>14,15,75,76</sup> Building upon efforts to identify potent 20S proteasome activators capable of degrading  $\alpha$ -synuclein, we focused on a subset of molecules demonstrating robust activity in initial fluorogenic peptide assays. Compounds with an EC<sub>200</sub> value below 1  $\mu$ M were prioritized for further evaluation. Additionally, methylene linker variants were included as controls to assess the impact of linker length on 20S proteasome activation, particularly with physiologically relevant substrates.

To refine our analysis, two concentrations of each compound (5  $\mu$ M and 15  $\mu$ M) were examined. The putative 20S proteasome activator TCH-165<sup>77,78</sup> was a positive control,

while dimethyl sulfoxide (DMSO)-treated proteasome functioned as the vehicle control. The purified 20S proteasome was diluted to a final concentration of 10 nM in a buffer comprising 50 mM HEPES and 5 mM DTT (pH 7.2). The desired compounds or controls were added to the proteasome solution and incubated at 37°C for 45 minutes. Subsequently, purified  $\alpha$ -synuclein (final concentration: 300 nM) was introduced, and the reaction proceeded at 37°C for 3.5 hours. The degradation of  $\alpha$ -synuclein was assessed through immunoblotting, quantifying full-length  $\alpha$ -synuclein depicted in **Figure 2.4**.

TCH-165 demonstrated effective enhancement of 20S proteasome-mediated degradation of  $\alpha$ -synuclein, leaving 60% and 40% of the substrate intact at concentrations of 5  $\mu$ M and 15  $\mu$ M, respectively (**Figure 2.4**).

Remarkably, at 15  $\mu$ M, several test compounds surpassed the performance of TCH-165, with compounds **4** and **5** also exhibiting superior activity at the lower concentration of 5  $\mu$ M. Specifically, compound **4** facilitated significant degradation, leaving only 45% and 28% of  $\alpha$ -synuclein intact at 5  $\mu$ M and 15  $\mu$ M, respectively (**Figure 2.4**). Similarly, the two 2-chlorocarbazole analogs, compounds **6** and **7**, displayed comparable efficacy at 15  $\mu$ M, reducing intact  $\alpha$ -synuclein levels to 33% (**Figure 2.4 B**).

However, compound **7** underperformed relative to compound **6** at 5  $\mu$ M, with 58%  $\alpha$ -synuclein remaining. Interestingly, compound **12** did not enhance the degradation of  $\alpha$ -synuclein at both 15  $\mu$ M and 5  $\mu$ M despite having an EC<sub>200</sub> 0.9  $\mu$ M in the small fluorogenic peptide assay (**Figure 2.4 B**). Unsurprisingly, the one methylene linker counterpart of the 2-chloroindole compound **13** did not display any activity in agreement with the small peptide assay results (**Figure 2.3 and 2.4 B**).

In addition, at 5  $\mu$ M concentrations, compounds **6**, **12**, and **5** failed to significantly impact the proteolytic degradation of  $\alpha$ -synuclein (**Figure 2.3 A and B**).



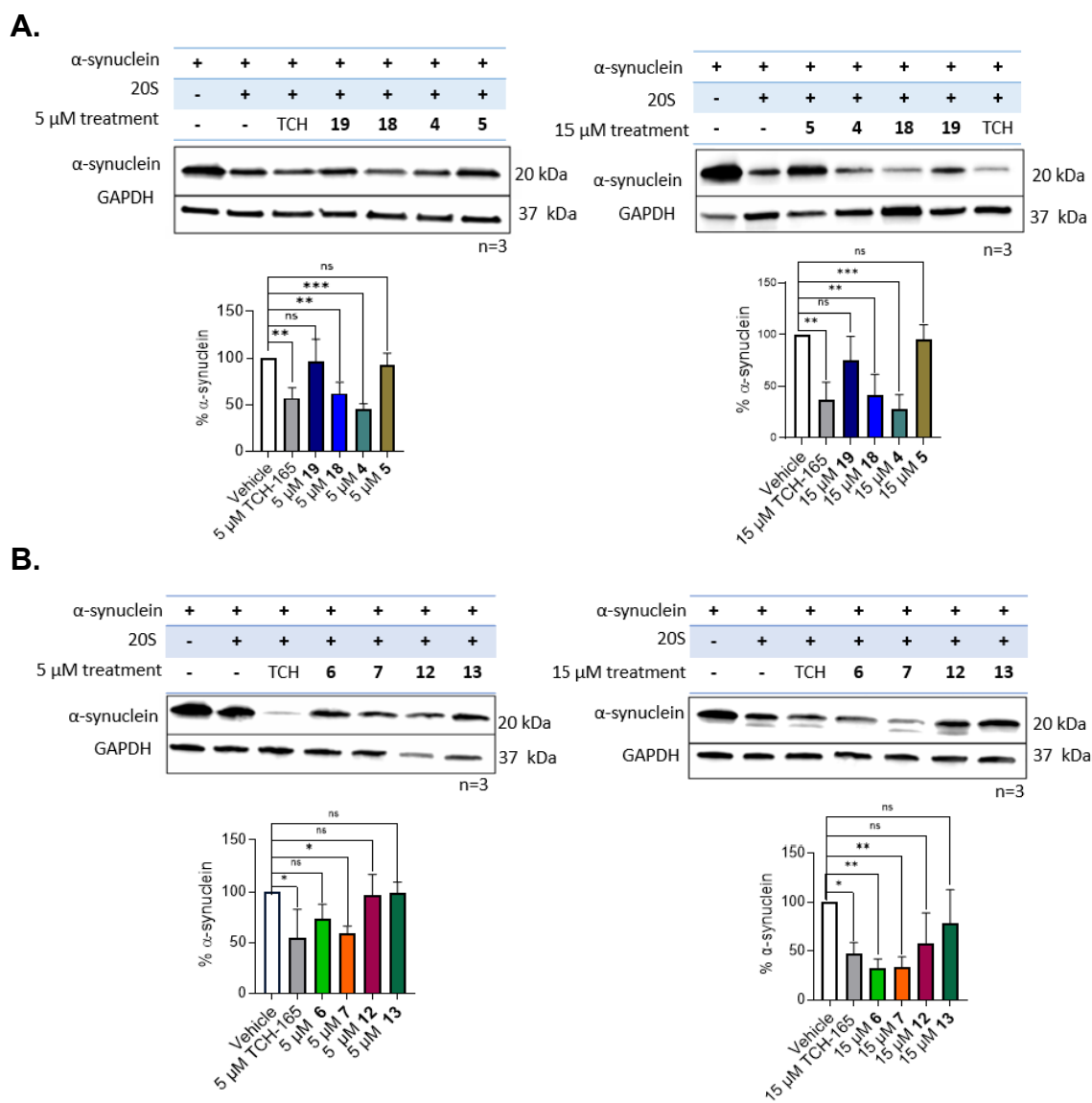


**Figure 2.4: Evaluation of In Vitro 20S Proteasome-Mediated Degradation of  $\alpha$ -Synuclein Degradation.**

(A and B) The degradation of purified  $\alpha$ -synuclein by the 20S proteasome treated with (A) 5  $\mu$ M and (B) 15  $\mu$ M of compounds 4-9, 9, 12, 13, 18, 19, or the positive control, TCH-165. GAPDH was added as a loading control. Each set of assays was done in triplicate. Error bars denote standard deviation. One-way ANOVA statistical analysis was used to determine statistical significance (ns = not significant, \* $p < 0.05$ , \*\* $p < 0.01$ , \*\*\* $p < 0.001$ , \*\*\*\* $p < 0.0001$ ). Error bars based on standard deviation. n denotes the number of replicates.

Given their superior degradation capabilities at both tested concentrations, compounds **4** and **7** were selected for further investigations. These findings underscore the potential of 20S proteasome activators in mitigating  $\alpha$ -synuclein aggregation, paving the way for novel therapeutic interventions in synucleinopathies.

### **2.2.5 Evaluation of Compounds 4 and 7 for Cellular Degradation of A53T $\alpha$ -Synuclein**

To determine whether the enhanced 20S proteasome activity mediated by compounds **4** and **7** translates to cellular systems, we employed HEK-293T cells transiently transfected with an A53T  $\alpha$ -synuclein plasmid. The A53T mutation is associated with familial Parkinson's disease (PD) due to its propensity to destabilize the native alpha-helical structure of  $\alpha$ -synuclein, accelerating its transition to toxic  $\beta$ -sheet aggregates, oligomers, and fibrils. These features make it a pathological model for assessing potential therapeutic interventions.

After 48 hours of transfection, cells expressing A53T  $\alpha$ -synuclein were treated with varying concentrations (1, 5, 10, and 15  $\mu$ M) of compounds **4** and **7** for 16 hours, followed by lysis and immunoblotting to quantify A53T  $\alpha$ -synuclein levels. Positive and negative controls included 10  $\mu$ M TCH-165, 15  $\mu$ M of an inactive structural analog (**19**), 30 nM of the proteasome inhibitor Bortezomib (BTZ)<sup>79,80</sup>, and DMSO as a vehicle control. Compound **4** significantly reduced A53T  $\alpha$ -synuclein levels in a dose-dependent manner. At the lowest concentration (1  $\mu$ M), 64% of A53T  $\alpha$ -synuclein remained, while at the highest concentration (15  $\mu$ M), only 21% remained (**Figure 4.5 B**).

By comparison, the positive control TCH-165 at 10  $\mu$ M left 52%  $\alpha$ -synuclein intact. The inactive control (**19**) had no significant effect, whereas BTZ, as expected, increased A53T  $\alpha$ -synuclein levels by 148%, underscoring its role in inhibiting the proteasome (**Figure 4.5 B**). These results highlight compound **4**'s capacity to promote proteasomal degradation of A53T  $\alpha$ -synuclein. Compound **7** exhibited equal or superior efficacy compared to compound **4**. At 1  $\mu$ M, 67% of  $\alpha$ -synuclein was degraded, while at 5  $\mu$ M, only 30% remained, outperforming compound **4** at this concentration (**Figure 4.5 C**). At higher concentrations (10 and 15  $\mu$ M), compound **4** further reduced  $\alpha$ -synuclein levels to 14% and 11%, respectively. TCH-165 (10  $\mu$ M) achieved an average of 40% remaining  $\alpha$ -

synuclein, while the inactive control compound **19** remained ineffective. BTZ increased  $\alpha$ -synuclein levels by 135%, confirming its inhibitory effect on the proteasome.

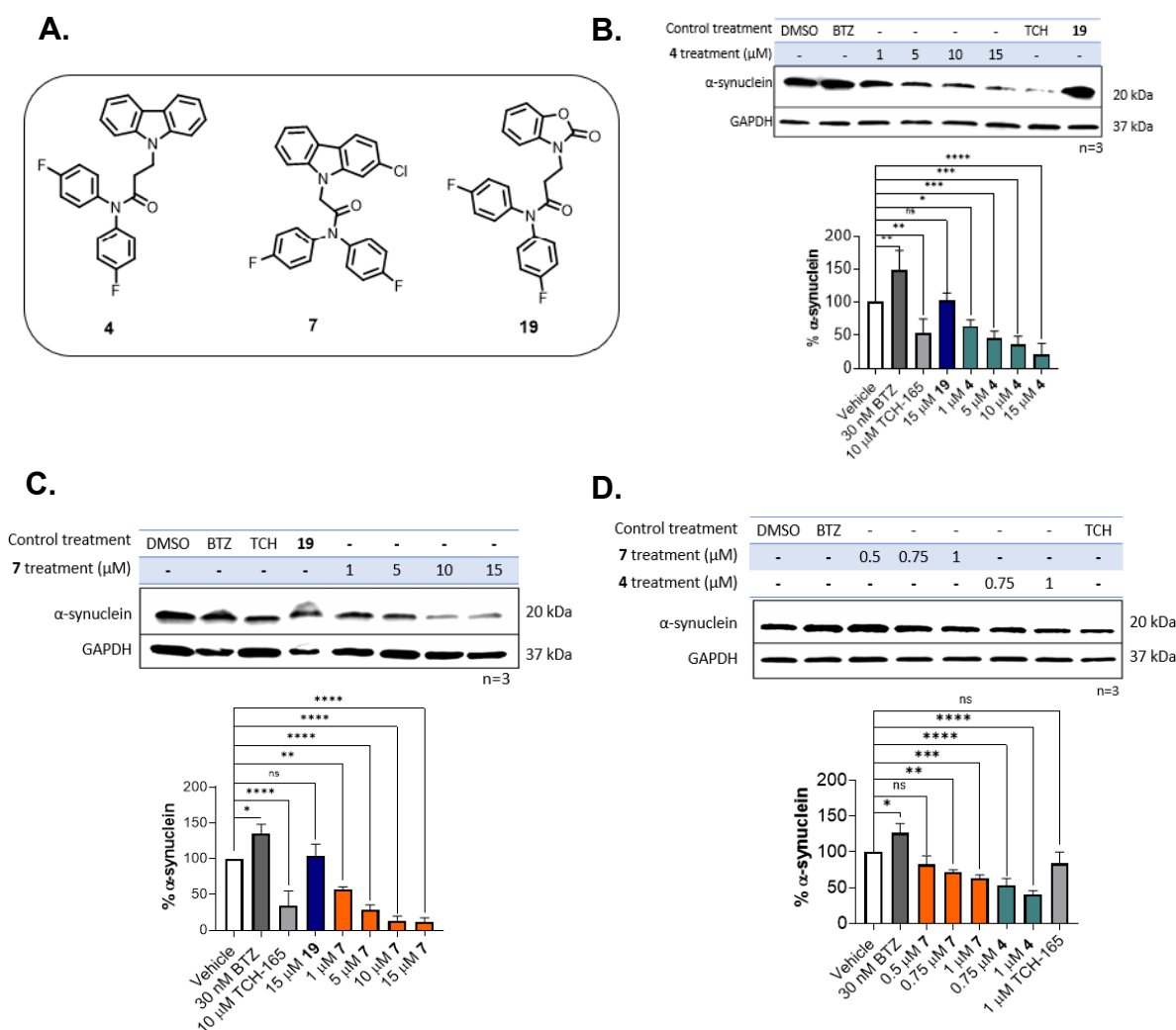


**Figure 2.5: Compounds **4** and **7** Enhance the Proteolytic Degradation of Mutant A53T  $\alpha$ -Synuclein in HEK Cells.**

(A) Structures of compounds **4**, **7** and **19**. The evaluation of A53T  $\alpha$ -synuclein levels in HEK-293T cells once they have been treated with 1, 5, 10, or 15  $\mu$ M of compounds (B) **4** and (C) **7**, and with 15  $\mu$ M of an inactive control (**19**), 10  $\mu$ M of positive control, TCH-165, and 30 nM of a proteasome inhibitor, BTZ, and (D) The experimental set up was repeated, with 0.5, 0.75, and 1  $\mu$ M of compound **7**, and 0.75 and 1  $\mu$ M of compound **4**.

### **Figure 2.5: (Cont'd )**

Each set of assays was done in triplicate. Error bars denote standard deviation. One-way ANOVA statistical analysis was used to determine statistical significance (ns = not significant, \* $p < 0.05$ , \*\* $p < 0.01$ , \*\*\* $p < 0.001$ , \*\*\*\* $p < 0.0001$ ). Error bars based on standard deviation. n denotes the number of replicates.

HEK-293T cells were treated with 0.75  $\mu\text{M}$  of compounds **4** and **7** to evaluate activity at lower concentrations. Both compounds demonstrated notable activity even at this sub-micromolar dose, with 55% and 72% of A53T  $\alpha$ -synuclein remaining (**Figure 4.5 D**). These results suggest that the potency observed in the fluorogenic peptide assays translates effectively to cellular contexts. Compounds **4** and **7** exhibited strong 20S proteasome-activating properties that translated to robust cellular degradation of the pathologically relevant A53T  $\alpha$ -synuclein. Compared to controls, their dose-dependent and sub-micromolar efficacy underscores their potential as therapeutic candidates for mitigating  $\alpha$ -synuclein pathology in PD. These findings and a follow-up study of compounds **4** and **7** in a physiologically relevant multiple system atrophy model have been published in IScience.<sup>81</sup>

### **2.3 Conclusion**

This study elucidates the systematic design, synthesis, and evaluation of third-generation chlorpromazine analogs as 20S proteasome activators to address the proteotoxic burden characteristic of neurodegenerative diseases, particularly Parkinson's disease. Through the development of these analogs, specific structural modifications were explored to optimize proteasome activation, reduce off-target neuroleptic effects, and enhance substrate specificity. The integration of heterocyclic cores and varying linker lengths allowed a comprehensive evaluation of the influence of structural parameters on proteasome modulation. The rational design process underscored the critical role of  $\pi$ - $\pi$  stacking interactions with proteasomal residues, such as tyrosine-159, and sulfur-mediated stabilization through cysteine-161, exemplified by the lead compounds SS-2-71 and its derivatives.<sup>42,48,54</sup> These interactions are hypothesized to facilitate the open-gate conformation of the 20S proteasome, thereby promoting the degradation of intrinsically disordered proteins like  $\alpha$ -synuclein. Notably, the lead analogs, compounds **4** and **7**, demonstrated significant activation of the 20S proteasome, with distinct patterns

of efficacy tied to the length of methylene linkers and the electronic properties of the pendant groups.

Functional assays revealed the robust activity of these compounds in proteasome-mediated degradation of synthetic fluorogenic peptides and physiologically relevant substrates such as  $\alpha$ -synuclein. Compounds **4** and **7** emerged as particularly promising candidates, displaying superior efficacy in degrading A53T  $\alpha$ -synuclein, a pathogenic variant associated with familial Parkinson's disease.<sup>14,21,82–84</sup> These findings highlight the translational potential of these compounds, particularly in the context of cellular systems where their activity was dose-dependent and exhibited sub-micromolar potency. These analogs (compounds **4** and **7**) are currently the most potent 20S proteasome activators developed in the Tepe lab. Several lab members are using them as tools for exploring the impact of 20S proteasome activation in different disease-relevant systems. Despite these advancements, limitations remain. The variable efficacy of different analogs, the dependence on specific structural motifs, and the challenge of achieving optimal proteasome activation at lower concentrations suggest further refinement. Additionally, the complexity of phenothiazine metabolism and its potential for off-target effects necessitate a cautious approach to therapeutic development. Future studies should focus on enhancing the pharmacokinetic properties of these analogs, ensuring their stability and bioavailability while minimizing the risk of neuroleptic side effects.

In conclusion, this work provides a foundational framework for developing targeted 20S proteasome activators as therapeutic agents for neurodegenerative diseases. The insights gained from the structure-activity relationship studies and the demonstrated ability of these analogs to degrade pathological  $\alpha$ -synuclein aggregates represent significant strides toward addressing the proteotoxic stress underlying synucleinopathies. Continued optimization and preclinical evaluation of these compounds could pave the way for novel therapeutic strategies to combat Parkinson's disease and related disorders.

## REFERENCES

1. Willis, A.W., Roberts, E., Beck, J.C., Fiske, B., Ross, W., Savica, R., Van Den Eeden, S.K., Tanner, C.M., Marras, C., Alcalay, R., et al. (2022). Incidence of Parkinson disease in North America. *npj Park. Dis.* 8. 10.1038/s41531-022-00410-y.
2. Marras, C., Beck, J.C., Bower, J.H., Roberts, E., Ritz, B., Ross, G.W., Abbott, R.D., Savica, R., Van Den Eeden, S.K., Willis, A.W., et al. (2018). Prevalence of Parkinson's disease across North America. *npj Park. Dis.* 4, 1–7. 10.1038/s41531-018-0058-0.
3. Sweeney, P., Park, H., Baumann, M., Dunlop, J., Frydman, J., Kopito, R., McCampbell, A., Leblanc, G., Venkateswaran, A., Nurmi, A., et al. (2017). Protein misfolding in neurodegenerative diseases: Implications and strategies. *Transl. Neurodegener.* 6, 1–13. 10.1186/s40035-017-0077-5.
4. Thibaut, T.A., Anderson, R.T., and Smith, D.M. (2018). A common mechanism of proteasome impairment by neurodegenerative disease-associated oligomers. *Nat. Commun.* 9, 1–13. 10.1038/s41467-018-03509-0.
5. Ross, C.A., and Poirier, M.A. (2004). Protein aggregation and neurodegenerative disease. *Nat. Med.* 10, S10. 10.1038/nm1066.
6. Pihlström, L., Wiethoff, S., and Houlden, H. (2018). Genetics of neurodegenerative diseases: an overview. *Handb. Clin. Neurol.* 145, 309–323. 10.1016/B978-0-12-802395-2.00022-5.
7. Hou, Y., Dan, X., Babbar, M., Wei, Y., Hasselbalch, S.G., Croteau, D.L., and Bohr, V.A. (2019). Ageing as a risk factor for neurodegenerative disease. *Nat. Rev. Neurol.* 15, 565–581. 10.1038/s41582-019-0244-7.
8. Brown, R.C., Lockwood, A.H., and Sonawane, B.R. (2005). Neurodegenerative diseases: An overview of environmental risk factors. *Environ. Health Perspect.* 113, 1250–1256. 10.1289/ehp.7567.
9. Akhtar, A., Andleeb, A., Waris, T.S., Bazzar, M., Moradi, A.R., Awan, N.R., and Yar, M. (2021). Neurodegenerative diseases and effective drug delivery: A review of challenges and novel therapeutics. *J. Control. Release* 330, 1152–1167. 10.1016/j.jconrel.2020.11.021.
10. Alzheimer, T., Journal, B.M., Chen, R., Society, T.R., Challenge, G., Gov-, U.K., Barna-, P., Szigeti, K., and York, N. (2020). Overcoming gaps in the treatment of neurodegenerative disease. *EBioMedicine* 60. 10.1016/j.ebiom.2020.103088.
11. Ohgita, T., Namba, N., Kono, H., Shimanouchi, T., and Saito, H. (2022). Mechanisms of enhanced aggregation and fibril formation of Parkinson's disease-related variants of  $\alpha$ -synuclein. *Sci. Rep.* 12, 1–13. 10.1038/s41598-022-10789-6.
12. Tseng, B.P., Green, K.N., Chan, J.L., Blurton-Jones, M., and LaFerla, F.M. (2008). A $\beta$  inhibits the proteasome and enhances amyloid and tau accumulation, 10.1016/j.neurobiolaging.2007.04.014 10.1016/j.neurobiolaging.2007.04.014.

13. Magalhães, P., and Lashuel, H.A. (2022). Opportunities and challenges of alpha-synuclein as a potential biomarker for Parkinson's disease and other synucleinopathies. *npj Park. Dis.* 8. 10.1038/s41531-022-00357-0.
14. Fields, C.R., Bengoa-Vergniory, N., and Wade-Martins, R. (2019). Targeting Alpha-Synuclein as a Therapy for Parkinson's Disease. *Front. Mol. Neurosci.* 12, 1–14. 10.3389/fnmol.2019.00299.
15. Wong, Y.C., and Krainc, D. (2017).  $\alpha$ -synuclein toxicity in 1. Wong, Y. C., and D. Krainc. 2017.  $\alpha$ -synuclein toxicity in neurodegeneration : mechanism and therapeutic strategies. *Nat. Publ. Gr.* 23: 1–13. neurodegeneration : mechanism and therapeutic strategies.
16. Oh, S., Hong, H.S., Hwang, E., Sim, H.J., Lee, W., Shin, S.J., and Mook-Jung, I. (2005). Amyloid peptide attenuates the proteasome activity in neuronal cells. *Mech. Ageing Dev.* 126, 1292–1299. 10.1016/j.mad.2005.07.006.
17. Butler, Y.R., Liu, Y., Kumbhar, R., Zhao, P., Gadhav, K., Wang, N., Li, Y., Mao, X., and Wang, W. Prion-Like A -Synuclein Spreading in Mice.
18. Vargas, J.Y., Grudina, C., and Zurzolo, C. (2019). The prion-like spreading of  $\alpha$ -synuclein: From in vitro to in vivo models of Parkinson's disease, 10.1016/j.arr.2019.01.012 10.1016/j.arr.2019.01.012.
19. Gibb WRG, and Lees AJ (1998). Occasional review: the relevance of the Lewy body to the pathogenesis of idiopathic Parkinson's disease. *J Neurol Neurosurg Psychiatry* 51, 745–752.
20. Osterhaus, A., Groen, J., Bildt, M. Van De, Martina, B., Vos, J., and Egmond, H. Van (1997). A -Synuclein In Lewy Bodies. *Nature* 388, 839–840.
21. Polymeropoulos, M.H., Lavedan, C., Leroy, E., Ide, S.E., Dehejia, A., Dutra, A., Pike, B., Root, H., Rubenstein, J., Boyer, R., et al. (1997). Mutation in the  $\alpha$ -synuclein gene identified in families with Parkinson's disease. *Science* (80-. ). 276, 2045–2047. 10.1126/science.276.5321.2045.
22. Spira, P.J., Sharpe, D.M., Halliday, G., Cavanagh, J., and Nicholson, G.A. (2001). Clinical and pathological features of a Parkinsonian syndrome in a family with an Ala53Thr  $\alpha$ -synuclein mutation, 10.1002/ana.67 10.1002/ana.67.
23. Gómez-Benito, M., Granado, N., García-Sanz, P., Michel, A., Dumoulin, M., and Moratalla, R. (2020). Modeling Parkinson's Disease With the Alpha-Synuclein Protein. *Front. Pharmacol.* 11, 1–15. 10.3389/fphar.2020.00356.
24. Meade, R.M., Fairlie, D.P., and Mason, J.M. (2019). Alpha-synuclein structure and Parkinson's disease - Lessons and emerging principles. *Mol. Neurodegener.* 14, 1–14. 10.1186/s13024-019-0329-1.
25. Yang, Y., Shi, Y., Schweighauser, M., Zhang, X., Kotecha, A., Murzin, A.G., Garringer, H.J., Cullinane, P.W., Saito, Y., Foroud, T., et al. (2022). Structures of  $\alpha$ -synuclein filaments from human brains with Lewy pathology, 10.1038/s41586-022-05319-3 10.1038/s41586-022-05319-3.

26. Bisi, N., Feni, L., Peqini, K., Pérez-Peña, H., Ongerì, S., Pieraccini, S., and Pellegrino, S. (2021).  $\alpha$ -Synuclein: An All-Inclusive Trip Around its Structure, Influencing Factors and Applied Techniques, 10.3389/fchem.2021.666585 10.3389/fchem.2021.666585.
27. Yu, Y.J., and Watts, R.J. (2013). Developing Therapeutic Antibodies for Neurodegenerative Disease. *Neurotherapeutics* 10, 459–472. 10.1007/s13311-013-0187-4.
28. Fonseca-Ornelas, L., Eisbach, S.E., Paulat, M., Giller, K., Fernández, C.O., Outeiro, T.F., Becker, S., and Zweckstetter, M. (2014). Small molecule-mediated stabilization of vesicle-associated helical  $\alpha$ -synuclein inhibits pathogenic misfolding and aggregation, 10.1038/ncomms6857 10.1038/ncomms6857.
29. Harris, H., and Rubinsztein, D.C. (2012). Control of autophagy as a therapy for neurodegenerative disease. *Nat. Rev. Neurol.* 8, 108–117. 10.1038/nrneurol.2011.200.
30. Ajoolabady, A., Aslkhodapasandhokmabad, H., Henninger, N., Demillard, L.J., Nikanfar, M., Nourazarian, A., and Ren, J. (2021). Targeting autophagy in neurodegenerative diseases: From molecular mechanisms to clinical therapeutics. *Clin. Exp. Pharmacol. Physiol.* 48, 943–953. 10.1111/1440-1681.13500.
31. Zhang, K., Zhu, S., Li, J., Jiang, T., Feng, L., Pei, J., Wang, G., Ouyang, L., and Liu, B. (2021). Targeting autophagy using small-molecule compounds to improve potential therapy of Parkinson's disease. *Acta Pharm. Sin. B* 11, 3015–3034. 10.1016/j.apsb.2021.02.016.
32. Roccaro, A., Hideshima, T., Richardson, P., Russo, D., Ribatti, D., Vacca, A., Dammacco, F., and Anderson, K. (2006). Bortezomib as an Antitumor Agent. *Curr. Pharm. Biotechnol.* 7, 441–448. 10.2174/138920106779116865.
33. Mujtaba, T., and Dou, Q.P. (2011). Advances in the understanding of mechanisms and therapeutic use of bortezomib. *Discov. Med.* 12, 471–480.
34. Tanaka, K., Yoshimura, T., and Ichihara, A. (1989). Role of substrate in reversible activation of proteasomes (multi-protease complexes) by sodium dodecyl sulfate. *J. Biochem.* 106, 495–500. 10.1093/oxfordjournals.jbchem.a122880.
35. Yamada, S., Hojo, K., Yoshimura, H., and Ishikawa, K. (1995). Reaction of 20S proteasome: Shift of SDS-dependent activation profile by divalent cations. *J. Biochem.* 117, 1162–1169. 10.1093/oxfordjournals.jbchem.a124839.
36. Watanabe, N., and Yamada, S. (1996). Activation of 20S proteasomes from spinach leaves by fatty acids. *Plant Cell Physiol.* 37, 147–151. 10.1093/oxfordjournals.pcp.a028925.
37. Katsiki, M., Chondrogianni, N., Chinou, I., Rivett, A.J., and Gonos, E.S. (2007). The olive constituent oleuropein exhibits proteasome stimulatory properties in vitro and confers life span extension of human embryonic fibroblasts.



- Rejuvenation Res. 10, 157–172. 10.1089/rej.2006.0513.
38. Njomen, E., and Tepe, J.J. (2019). Proteasome Activation as a New Therapeutic Approach to Target Proteotoxic Disorders. *J. Med. Chem.* 62, 6469–6481. 10.1021/acs.jmedchem.9b00101.
  39. Huang, L., Ho, P., and Chen, C.H. (2007). Activation and inhibition of the proteasome by betulinic acid and its derivatives. *FEBS Lett.* 581, 4955–4959. 10.1016/j.febslet.2007.09.031.
  40. Trader, D.J., Simanski, S., Dickson, P., and Kodadek, T. (2017). Establishment of a suite of assays that support the discovery of proteasome stimulators. *Biochim. Biophys. Acta - Gen. Subj.* 1861, 892–899. 10.1016/j.bbagen.2017.01.003.
  41. Halder, S., Macatangay, N.J., Zervas, B.L., Salazar-Chaparro, A.F., and Trader, D.J. (2022). Oleic amide derivatives as small molecule stimulators of the human proteasome's core particle. *RSC Med. Chem.* 13, 1077–1081. 10.1039/d2md00133k.
  42. Njomen, E., Osmulski, P.A., Jones, C.L., Gaczynska, M., and Tepe, J.J. (2018). Small Molecule Modulation of Proteasome Assembly. *Biochemistry* 57, 4214–4224. 10.1021/acs.biochem.8b00579.
  43. Fiolek, T.J., Magyar, C.L., Wall, T.J., Davies, S.B., Campbell, M. V., Savich, C.J., Tepe, J.J., and Mosey, R.A. (2021). Dihydroquinazolines enhance 20S proteasome activity and induce degradation of  $\alpha$ -synuclein, an intrinsically disordered protein associated with neurodegeneration. *Bioorganic Med. Chem. Lett.* 36. 10.1016/j.bmcl.2021.127821.
  44. Fiolek, T.J., Keel, K.L., and Tepe, J.J. (2021). Fluspirilene Analogs Activate the 20S Proteasome and Overcome Proteasome Impairment by Intrinsically Disordered Protein Oligomers. *ACS Chem. Neurosci.* 12, 1438–1448. 10.1021/acchemneuro.1c00099.
  45. Dal Vechio, F.H., Cerqueira, F., Augusto, O., Lopes, R., and Demasi, M. (2014). Peptides that activate the 20S proteasome by gate opening increased oxidized protein removal and reduced protein aggregation. *Free Radic. Biol. Med.* 67, 304–313. 10.1016/j.freeradbiomed.2013.11.017.
  46. Gizińska, M., Witkowska, J., Karpowicz, P., Rostankowski, R., Chocron, E.S., Pickering, A.M., Osmulski, P., Gaczynska, M., and Jankowska, E. (2019). Proline- and Arginine-Rich Peptides as Flexible Allosteric Modulators of Human Proteasome Activity. *J. Med. Chem.* 62, 359–370. 10.1021/acs.jmedchem.8b01025.
  47. Osmulski, P.A., Karpowicz, P., Jankowska, E., Bohmann, J., Pickering, A.M., and Gaczynska, M. (2020). New peptide-based pharmacophore activates 20S proteasome. *Molecules* 25. 10.3390/molecules25061439.
  48. Jones, C.L., Njomen, E., Sjögren, B., Dexheimer, T.S., and Tepe, J.J. (2017). Small Molecule Enhancement of 20S Proteasome Activity Targets Intrinsically

- Disordered Proteins. *ACS Chem. Biol.* **12**, 2240–2247. 10.1021/acscchembio.7b00489.
49. Froimowitz, M., and Cody, V. (1993). c-OCO 4. 2219–2227. 10.1021/jm00067a019.
  50. Wilson, J.M., Sanyal, S., and Van Tol, H.H.M. (1998). Dopamine D2 and D4 receptor ligands: Relation to antipsychotic action. *Eur. J. Pharmacol.* **351**, 273–286. 10.1016/S0014-2999(98)00312-4.
  51. Feinberg, A.P., and Snyder, S.H. (1975). Phenothiazine drugs: structure activity relationships explained by a conformation that mimics dopamine. *Proc. Natl. Acad. Sci. U. S. A.* **72**, 1899–1903. 10.1073/pnas.72.5.1899.
  52. Jaszczyszyn, A., Gąsiorowski, K., Świątek, P., Malinka, W., Cieślík-Boczula, K., Petrus, J., and Czarnik-Matusiewicz, B. (2012). Chemical structure of phenothiazines and their biological activity. *Pharmacol. Reports* **64**, 16–23. 10.1016/S1734-1140(12)70726-0.
  53. Staerz, S.D., Jones, C.L., and Tepe, J.J. (2022). Design, Synthesis, and Biological Evaluation of Potent 20S Proteasome Activators for the Potential Treatment of  $\alpha$ -Synucleinopathies, 10.1021/acs.jmedchem.1c02158 10.1021/acs.jmedchem.1c02158.
  54. Staerz, S.D., Jones, C.L., and Tepe, J.J. (2022). Design, Synthesis, and Biological Evaluation of Potent 20S Proteasome Activators for the Potential Treatment of  $\alpha$ -Synucleinopathies. *J. Med. Chem.* **65**, 6631–6642. 10.1021/acs.jmedchem.1c02158.
  55. Ohlow, M.J., and Moosmann, B. (2011). Phenothiazine: The seven lives of pharmacology's first lead structure. *Drug Discov. Today* **16**, 119–131. 10.1016/j.drudis.2011.01.001.
  56. Samara, M.T., Cao, H., Helfer, B., Davis, J.M., and Leucht, S. (2014). Chlorpromazine versus every other antipsychotic for schizophrenia: A systematic review and meta-analysis challenging the dogma of equal efficacy of antipsychotic drugs. *Eur. Neuropsychopharmacol.* **24**, 1046–1055. 10.1016/j.euroneuro.2014.03.012.
  57. Salie, S., Hsu, N.J., Semenya, D., Jardine, A., and Jacobs, M. (2014). Novel non-neuroleptic phenothiazines inhibit mycobacterium tuberculosis replication. *J. Antimicrob. Chemother.* **69**, 1551–1558. 10.1093/jac/dku036.
  58. Wójcikowski, J., Basińska, A., and Daniel, W.A. (2014). The cytochrome P450-catalyzed metabolism of levomepromazine: A phenothiazine neuroleptic with a wide spectrum of clinical application. *Biochem. Pharmacol.* **90**, 188–195. 10.1016/j.bcp.2014.05.005.
  59. Yeung, P.K.F., Hubbard, J.W., Korchinski, E.D., and Midha, K.K. (1993). Pharmacokinetics of chlorpromazine and key metabolites. *Eur. J. Clin. Pharmacol.* **45**, 563–569. 10.1007/BF00315316.

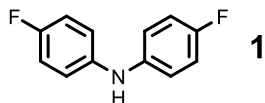
60. Daniel, W.A., Syrek, M., and Haduch, A. (2002). The contribution of cytochrome P-450 isoenzymes to the metabolism of phenothiazine neuroleptics. *Eur. Neuropsychopharmacol.* *12*, 371–377. 10.1016/S0924-977X(02)00053-6.
61. Wen, B., and Zhou, M. (2009). Metabolic activation of the phenothiazine antipsychotics chlorpromazine and thioridazine to electrophilic iminoquinone species in human liver microsomes and recombinant P450s. *Chem. Biol. Interact.* *181*, 220–226. 10.1016/j.cbi.2009.05.014.
62. Boyd-Kimball, D., Gonczy, K., Lewis, B., Mason, T., Siliko, N., and Wolfe, J. (2019). Classics in Chemical Neuroscience: Chlorpromazine. *ACS Chem. Neurosci.* *10*, 79–88. 10.1021/acschemneuro.8b00258.
63. Vantourout, J.C., Miras, H.N., Isidro-Llobet, A., Sproules, S., and Watson, A.J.B. (2017). Spectroscopic Studies of the Chan-Lam Amination: A Mechanism-Inspired Solution to Boronic Ester Reactivity. *J. Am. Chem. Soc.* *139*, 4769–4779. 10.1021/jacs.6b12800.
64. Dual Probes for the Dopamine Transporter and  $\sigma_1$  Receptors Novel Piperazinyl Alkyl-bis(4'-fluorophenyl)amine Analogues as Potential Cocaine-Abuse Therapeutic Agents.pdf.
65. Liggett, A., Crawford, L.J., Walker, B., Morris, T.C.M., and Irvine, A.E. (2010). Methods for measuring proteasome activity: Current limitations and future developments. *Leuk. Res.* *34*, 1403–1409. 10.1016/j.leukres.2010.07.003.
66. Kisselev, A.F., and Goldberg, A.L. (2005). Monitoring activity and inhibition of 26S proteasomes with fluorogenic peptide substrates. *Methods Enzymol.* *398*, 364–378. 10.1016/S0076-6879(05)98030-0.
67. Coleman, R.A., and Trader, D.J. (2019). Methods to discover and evaluate proteasome small molecule stimulators. *Molecules* *24*. 10.3390/molecules24122341.
68. Benskey, M.J., Perez, R.G., and Manfredsson, F.P. (2016). The contribution of alpha synuclein to neuronal survival and function - Implications for Parkinson's disease. *J. Neurochem.* *137*, 331–359. 10.1111/jnc.13570.
69. Calabresi, P., Mechelli, A., Natale, G., Volpicelli-Daley, L., Di Lazzaro, G., and Ghiglieri, V. (2023). Alpha-synuclein in Parkinson's disease and other synucleinopathies: from overt neurodegeneration back to early synaptic dysfunction. *Cell Death Dis.* *14*, 176. 10.1038/s41419-023-05672-9.
70. Su, R., and Zhou, T. (2021). Alpha-Synuclein Induced Immune Cells Activation and Associated Therapy in Parkinson's Disease. *Front. Aging Neurosci.* *13*, 1–10. 10.3389/fnagi.2021.769506.
71. Villar-Piqué, A., Lopes da Fonseca, T., and Outeiro, T.F. (2016). Structure, function and toxicity of alpha-synuclein: the Bermuda triangle in synucleinopathies. *J. Neurochem.* *139*, 240–255. 10.1111/jnc.13249.
72. Burré, J. (2015). The synaptic function of  $\alpha$ -synuclein. *J. Parkinsons. Dis.* *5*, 699–

713. 10.3233/JPD-150642.
73. Hipp, M.S., Park, S.H., and Hartl, U.U. (2014). Proteostasis impairment in protein-misfolding and -aggregation diseases. *Trends Cell Biol.* 24, 506–514. 10.1016/j.tcb.2014.05.003.
74. Goldberg, A.L. (2003). Protein degradation and protection against misfolded or damaged proteins. *Nature* 426, 895–899. 10.1038/nature02263.
75. Espay, A.J., and McFarthing, K. (2023). Alpha-synuclein and the Parkinson's disease drug pipeline. *Park. Relat. Disord.* 111, 105432. 10.1016/j.parkreldis.2023.105432.
76. Rodger, A.T., ALNasser, M., and Carter, W.G. (2023). Are Therapies That Target  $\alpha$ -Synuclein Effective at Halting Parkinson's Disease Progression? A Systematic Review, 10.3390/ijms241311022 10.3390/ijms241311022.
77. Njomen, E., Osmulski, P.A., Jones, C.L., Gaczynska, M., and Tepe, J.J. (2018). Small Molecule Modulation of Proteasome Assembly 10.1021/acs.biochem.8b00579.
78. Tepe, J.J., Staerz, S.D., Lisabeth, E.M., Njomen, E., Dexheimer, T.S., and Neubig, R.R. (2023). Development of a Cell-Based AlphaLISA Assay for High-Throughput Screening for Small Molecule Proteasome Modulators. *ACS Omega* 8, 15650–15659. 10.1021/acsomega.3c01158.
79. Adams, J. (2002). Development of the Proteasome Inhibitor PS-341. *Oncologist* 7, 9–16. 10.1634/theoncologist.7-1-9.
80. Chauhan, D., Catley, L., Li, G., Podar, K., Hideshima, T., Velankar, M., Mitsiades, C., Mitsiades, N., Yasui, H., Letai, A., et al. (2005). A novel orally active proteasome inhibitor induces apoptosis in multiple myeloma cells with mechanisms distinct from Bortezomib. *Cancer Cell* 8, 407–419. 10.1016/j.ccr.2005.10.013.
81. Staerz, S.D., Anamoah, C., and Tepe, J.J. (2024). 20S proteasome enhancers prevent cytotoxic tubulin polymerization-promoting protein induced  $\alpha$ -synuclein aggregation. *iScience* 27, 110166. 10.1016/j.isci.2024.110166.
82. Li, J., Uversky, V.N., and Fink, A.L. (2001). Effect of familial Parkinson's disease point mutations A30P and A53T on the structural properties, aggregation, and fibrillation of human  $\alpha$ -synuclein. *Biochemistry* 40, 11604–11613. 10.1021/bi010616g.
83. de Oliveira, G.A.P., and Silva, J.L. (2019). Alpha-synuclein stepwise aggregation reveals features of an early onset mutation in Parkinson's disease. *Commun. Biol.* 2. 10.1038/s42003-019-0598-9.
84. Kuwahara, T., Koyama, A., Gengyo-Ando, K., Masuda, M., Kowa, H., Tsunoda, M., Mitani, S., and Iwatsubo, T. (2006). Familial Parkinson mutant  $\alpha$ -synuclein causes dopamine neuron dysfunction in transgenic *Caenorhabditis elegans*. *J. Biol. Chem.* 281, 334–340. 10.1074/jbc.M504860200.

85. Raghuvanshi, D.S., Gupta, A.K., and Singh, K.N. (2012). Nickel-mediated N-arylation with arylboronic acids: An avenue to Chan-Lam coupling. *Org. Lett.* *14*, 4326–4329. 10.1021/ol3021836.

## APPENDIX

### Chemistry



#### Bis(4-fluorophenyl)amine (**1**)

Compound **1** was synthesized using the previously described method.<sup>3</sup> A 100 mL round bottom flask containing a 4 Å molecular sieve was added 4- fluorophenylboronic acid (10 mmol), 30 mL of dried DCM, and 4-fluoroaniline (10 mmol). After that, triethyl amine (10 mmol) and Copper acetate (5 mmol) were added to the reaction mixture. The mixture was stirred at room temperature under air for 16 h. The reaction was stopped, and the mixture dried over a celite plug. The crude mixture was purified *using automated Combiflash chromatography* (silica gel, 20-40 microns, gradient 0-15% ethyl acetate in hexane). The compound was isolated as a dark yellowish oil (549 mg, 50%). IR: 3401, 2908  $\text{cm}^{-1}$ .  $^1\text{H}$  NMR ( $\text{CD}_2\text{Cl}_2$ , 500 MHz)  $\delta$  6.98-6.97(m, 4H), 6.96 – 6.95 (m, 4H), 5.60 (s, 1H).  $^{13}\text{C}\{^1\text{H}\}$  NMR ( $\text{CD}_2\text{Cl}_2$ , 126 MHz)  $\delta$  159.6 (d,  $J_{\text{CF}} = 241.0$  Hz), 140.0 (d,  $J_{\text{CF}} = 2.4$  Hz), 119.8 (d,  $J_{\text{CF}} = 8.0$  Hz), 116.1 (d,  $J_{\text{CF}} = 22.8$  Hz). HRMS (ESI-TOF)  $m/z$ :  $[(\text{M}+\text{H})^+]$  calcd for ( $\text{C}_{12}\text{H}_{10}\text{FN}_2^+$ ) 206.0781; found, 206.0783.

#### General acylation procedure

The bis(fluorophenyl) amine (1.0 equiv) and TEA (1.3 equiv) were dissolved in DCM (15.0 mL) and cooled to 0 °C, and the desired acyl halide (1.2 equiv) was added dropwise. The reaction mixture was warmed to room temperature and stirred for 12 hours under inert  $\text{N}_2$  gas. The crude reaction was washed with brine (2 x 10 mL) and extracted with DCM (2 x 10 mL). The organic layer was dried over anhydrous  $\text{Na}_2\text{SO}_4$ , filtered, and concentrated under reduced pressure. The desired product was purified using an automated CombiFlash chromatography (silica gel, 20-40 microns, 20–40  $\mu\text{m}$ , with a gradient mobile phase of 0% - 40% EtOAc in Hexane).

### General procedure A

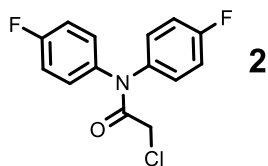
The desired heterocycle (1.0 equiv) was dissolved in DMF (3.0 mL) and cooled to 0 °C. Then, NaH (1.1 equiv) was added, and the mixture stirred at 0 °C for one hour. The corresponding *N,N*-bis(4-fluorophenyl) amide (2 equiv) was added, and the reaction was slowly warmed to room temperature and stirred for 24 hours under inert N<sub>2</sub> gas. The crude mixture was washed with LiBr (3 x 9 mL), and the organic layer was extracted with EtOAc (1 x 10 mL). The organic layer was dried over anhydrous Na<sub>2</sub>SO<sub>4</sub>, filtered, concentrated under reduced pressure, and purified using an automated CombiFlash chromatography (silica gel, 20–40 µm, with a gradient mobile phase of 0% - 20% EtOAc in Hexane).

### General procedure B

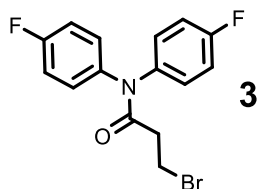
The desired heterocycle (1.0 equiv) and the corresponding *N,N*-bis(4-fluorophenyl) amide (1.0 equiv) were dissolved in toluene (5.0 mL). Then, TEA (4.0 equiv) was added dropwise, and the solution was refluxed for 24 hours under inert N<sub>2</sub> gas. The crude mixture was washed with brine (3 x 5 mL), and the organic layer was extracted with DCM (1 x 10 mL). The organic layer was dried over anhydrous Na<sub>2</sub>SO<sub>4</sub>, filtered, concentrated under reduced pressure, and purified using an automated CombiFlash chromatography (silica gel, 20–40 µm, with a gradient mobile phase of 0% - 20% EtOAc in Hexane).

### General procedure C

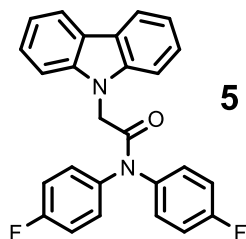
The corresponding *N,N*-bis(4-fluorophenyl) amide (1.0 equiv) was dissolved in THF (5 mL), and TEA (1.2 equiv) was added dropwise. Then, 2 M dimethyl amine in THF (2.0 equiv) was added dropwise, and the solution was stirred for 24 hours at room temperature under inert N<sub>2</sub> gas. The crude mixture was washed with brine (3 x 5 mL), and the organic layer was extracted with DCM (10 mL). The crude mixture was dried over Na<sub>2</sub>SO<sub>4</sub>, filtered, concentrated under reduced pressure, and purified using an automated CombiFlash chromatography (silica gel, 20–40 µm, with a gradient mobile phase of 0 - 30% EtOAc in Hexane).



General acylation procedure produced a light-yellow solid (67%). MP: 95-97 °C.  $^1\text{H}$  NMR ( $\text{CD}_2\text{Cl}_2$ , 500 MHz)  $\delta$  7.32-7.27 (m, 4H), 7.16-7.08 (m, 4H), 4.02 (s, 2H).  $^{13}\text{C}\{^1\text{H}\}$  NMR ( $\text{DMSO}-d_6$ , 126 MHz)  $\delta$  166.0, 139.2, 138.2, 131.4, 129.3, 117.2, 116.3, 43.7. IR: 3067  $\text{cm}^{-1}$ , 2980  $\text{cm}^{-1}$ , 1686  $\text{cm}^{-1}$ , 1503  $\text{cm}^{-1}$ . HRMS (APCI)  $m/z$ :  $[\text{M}+\text{H}]^+$  calc'd for ( $\text{C}_{14}\text{H}_{11}\text{ClF}_2\text{NO}^+$ ) 282.0492; Found 282.0338.  $^1\text{H}$  NMR and  $^{13}\text{C}\{^1\text{H}\}$  NMR were run in different solvents for better resolution of the observed peaks.



General acylation procedure produced a pale pink solid (88%). MP: 94-96 °C.  $^1\text{H}$  NMR ( $\text{CD}_2\text{Cl}_2$ , 500 MHz)  $\delta$  7.29-7.25 (m, 4H), 7.17-7.03 (m, 4H), 3.64 (t,  $J = 6.7$  Hz, 2H), 2.82 (t,  $J = 6.7$  Hz, 2H).  $^{13}\text{C}\{^1\text{H}\}$  NMR ( $\text{CD}_2\text{Cl}_2$ , 126 MHz)  $\delta$  170.2, 138.9, 130.9, 128.5, 117.4 (d,  $J_{\text{CF}} = 22.6$  Hz), 116.1 (d,  $J_{\text{CF}} = 22.6$  Hz), 38.3, 28.1. IR: 3117  $\text{cm}^{-1}$ , 2950  $\text{cm}^{-1}$ , 1600  $\text{cm}^{-1}$ , 1425  $\text{cm}^{-1}$ . HRMS (APCI)  $m/z$ :  $[\text{M}+\text{H}]^+$  calc'd for ( $\text{C}_{15}\text{H}_{13}\text{BrF}_2\text{NO}^+$ ) 340.0143; Found 340.0063.

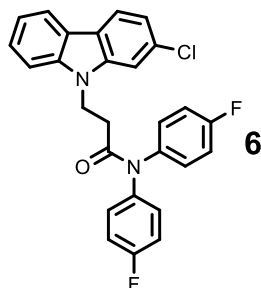


#### 2-(9H-carbazol-9-yl)-N,N-bis(4-fluorophenyl)acetamide (**5**)

General Procedure A produced a white solid (92%). MP: 189-190 °C.  $^1\text{H}$  NMR ( $\text{CDCl}_3$ , 500 MHz)  $\delta$  8.05 (d,  $J = 7.7$  Hz, 2H), 7.41 (t,  $J = 7.7$  Hz, 2H), 7.26-7.20 (m, 4H), 7.15-6.93 (m, 8H), 5.01 (s, 2H).  $^{13}\text{C}\{^1\text{H}\}$  NMR ( $\text{CDCl}_3$ , 126 MHz)  $\delta$  168.0, 140.2, 138.3, 136.9, 129.4, 127.5, 125.7, 123.1, 120.3, 119.6, 117.1, 115.9, 108.3, 46.8. IR: 3069  $\text{cm}^{-1}$ , 2978  $\text{cm}^{-1}$ ,

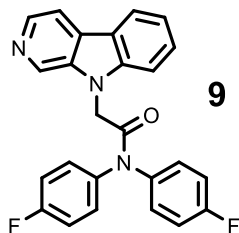


1668  $\text{cm}^{-1}$ , 1501  $\text{cm}^{-1}$ . (APCI)  $m/z$ :  $[\text{M}+\text{H}]^+$  calc'd for  $(\text{C}_{26}\text{H}_{19}\text{F}_2\text{N}_2\text{O}^+)$  413.1460; Found 413.1466.



3-(2-chloro-9H-carbazol-9-yl)-N,N-bis(4-fluorophenyl)propanamide (**6**)

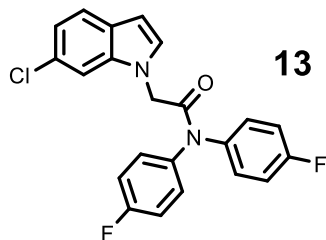
General procedure A produced a white solid in 88% yield. MP: 133-134 °C.  $^1\text{H}$  NMR ( $\text{DMSO}-d_6$ , 500 MHz)  $\delta$  8.17 (dd,  $J$  = 8.1, 1.5 Hz, 2H), 7.57 (d,  $J$  = 1.8 Hz, 1H), 7.51 (d,  $J$  = 8.2 Hz, 1H), 7.45-7.42 (m, 1H), 7.25-7.20 (m, 2H), 7.14-7.00 (m, 8H), 4.64 (t,  $J$  = 6.8 Hz, 2H), 2.66 (t,  $J$  = 6.8 Hz, 2H).  $^{13}\text{C}\{^1\text{H}\}$  NMR ( $\text{CDCl}_3$ , 126 MHz)  $\delta$  171.0, 140.4, 140.3, 137.92, 137.89, 131.7, 129.6 (d,  $J$  = 8.6 Hz), 128.0 (d,  $J$  = 8.8 Hz), 126.2, 122.3, 121.5, 121.2, 120.3, 119.9, 119.8, 116.6 (d,  $J$  = 22.8 Hz), 116.0 (d,  $J$  = 22.5 Hz), 109.2, 109.0, 40.0, 33.3. IR: 3030  $\text{cm}^{-1}$ , 2865  $\text{cm}^{-1}$ , 1605  $\text{cm}^{-1}$ , 1320  $\text{cm}^{-1}$ . HRMS (APCI)  $m/z$ :  $[\text{M}+\text{H}]^+$  calc'd for  $(\text{C}_{27}\text{H}_{20}\text{ClF}_2\text{N}_2\text{O}^+)$  462.1227; Found 462.1157.  $^1\text{H}$  NMR and  $^{13}\text{C}\{^1\text{H}\}$  NMR were run in different solvents to better resolve the observed peaks.



N,N-bis(4-fluorophenyl)-2-(9H-pyrido[3,4-b]indol-9-yl)acetamide (**9**)

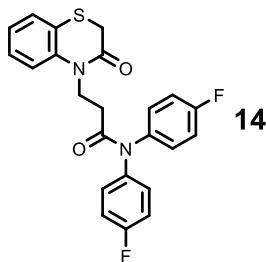
General procedure A produced a light-yellow solid (65%). MP: 161-162 °C.  $^1\text{H}$  NMR ( $\text{CDCl}_3$ , 500 MHz)  $\delta$  8.76 (s, 1H), 8.44 (d,  $J$  = 5.3 Hz, 1H), 8.12 (dt,  $J$  = 7.9, 1.0 Hz, 1H), 7.94-7.93 (m, 1H), 7.60-7.57 (m, 1H), 7.36 (dt,  $J$  = 8.3, 0.9 Hz, 1H), 7.33-7.29 (m, 1H), 7.24-7.18 (m, 8H), 5.08 (s, 2H).  $^{13}\text{C}\{^1\text{H}\}$  NMR ( $\text{CDCl}_3$ , 126 MHz)  $\delta$  166.9, 141.5, 138.6, 137.8, 136.8, 136.4, 131.0, 129.7, 129.3, 128.9, 127.5, 122.1, 121.3, 120.6, 117.6 (d,  $J$  = 22.5 Hz), 116.0 (d,  $J$  = 22.5 Hz), 114.7, 109.3, 46.6. IR: 3062  $\text{cm}^{-1}$ , 2954  $\text{cm}^{-1}$ , 1686  $\text{cm}^{-1}$ .

<sup>1</sup>, 1450 cm<sup>-1</sup>. HRMS (APCI) *m/z*: [M+H]<sup>+</sup> calc'd for (C<sub>25</sub>H<sub>18</sub>F<sub>2</sub>N<sub>3</sub>O<sup>+</sup>) 414.1412; Found 414.1446.



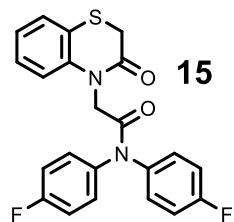
2-(6-chloro-1H-indol-1-yl)-N,N-bis(4-fluorophenyl)acetamide (**13**)

General procedure A produced a white solid (77%). MP: 144-145 °C. <sup>1</sup>H NMR (CD<sub>2</sub>Cl<sub>2</sub>, 500 MHz) δ 7.55 (d, *J* = 8.4 Hz, 1H), 7.38-7.22 (m, 6H), 7.18 (dt, *J* = 1.5, 0.7 Hz, 1H), 7.10 (dd, *J* = 8.4, 1.9 Hz, 2H), 7.02 (d, *J* = 3.3 Hz, 2H), 6.52 (dd, *J* = 3.2, 0.9 Hz, 1H), 4.77 (s, 2H). <sup>13</sup>C{<sup>1</sup>H} NMR (CD<sub>2</sub>Cl<sub>2</sub>, 126 MHz) δ 167.3, 138.5, 137.5, 137.2, 130.7 (d, *J* = 8.2 Hz), 129.9, 128.04, 128.01, 127.5, 122.2, 120.6, 117.9 (d, *J* = 23.9 Hz), 116.2 (d, *J* = 22.9 Hz), 109.4, 102.6, 49.6. IR: 3056 cm<sup>-1</sup>, 2979 cm<sup>-1</sup>, 1669 cm<sup>-1</sup>, 1499 cm<sup>-1</sup>. HRMS (APCI) *m/z*: [M+H]<sup>+</sup> calc'd for (C<sub>22</sub>H<sub>16</sub>F<sub>2</sub>ClN<sub>2</sub>O<sup>+</sup>) 397.0914; Found 397.0916.



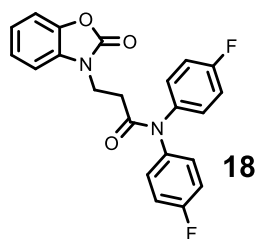
N,N-bis(4-fluorophenyl)-3-(3-oxo-2,3-dihydro-4H-benzo[b][1,4]thiazin-4-yl)propanamide (**14**)

General procedure A produced a fluffy white solid (98%) with THF as the solvent in place of DMF. MP: 150-151 °C. <sup>1</sup>H NMR (CD<sub>2</sub>Cl<sub>2</sub>, 500 MHz) δ 7.40 (dd, *J* = 7.7, 1.6 Hz, 1H), 7.27-7.23 (m, 5H), 7.14-7.04 (m, 6H), 4.33 (t, *J* = 6.8 Hz, 2H), 3.35 (s, 2H), 2.62 (t, *J* = 6.8 Hz, 2H). <sup>13</sup>C{<sup>1</sup>H} NMR (CD<sub>2</sub>Cl<sub>2</sub>, 126 MHz) δ 170.3, 165.0, 139.3, 138.6, 138.5, 130.3, 128.5, 128.2, 127.3, 123.9, 123.4, 117.6, 116.9 (d, *J* = 23.2 Hz), 115.7 (d, *J* = 22.8 Hz), 41.5, 32.8, 31.5. IR: 3067 cm<sup>-1</sup>, 2966 cm<sup>-1</sup>, 1677 cm<sup>-1</sup>, 1656 cm<sup>-1</sup>, 1497 cm<sup>-1</sup>. HRMS (APCI) *m/z*: [M+H]<sup>+</sup> calc'd for (C<sub>23</sub>H<sub>19</sub>F<sub>2</sub>O<sub>2</sub>N<sub>2</sub>S<sup>+</sup>) 425.1130; Found 425.1173.



N,N-bis(4-fluorophenyl)-2-(3-oxo-2,3-dihydro-4H-benzo[b][1,4]thiazin-4-yl)acetamide (**15**)

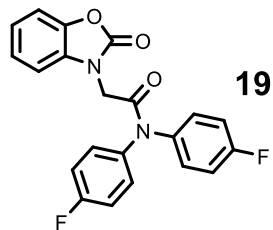
General procedure A produced a fluffy white solid (80%) with THF as the solvent in place of DMF. MP: 90-92 °C.  $^1\text{H}$  NMR ( $\text{CD}_2\text{Cl}_2$ , 500 MHz)  $\delta$  7.47 (s, 2H), 7.39 (dd,  $J$  = 7.7, 1.5 Hz, 1H), 7.28-7.25 (m, 3H), 7.18 (s, 2H), 7.06 (td,  $J$  = 7.6, 1.2 Hz, 3H), 6.99 (dd,  $J$  = 8.2, 1.2 Hz, 1H), 4.51 (s, 2H), 3.42 (s, 2H).  $^{13}\text{C}\{^1\text{H}\}$  NMR ( $\text{CD}_2\text{Cl}_2$ , 126 MHz)  $\delta$  167.5, 166.2, 140.2, 138.7, 137.7, 130.9, 128.7, 128.1, 127.7, 124.0, 123.9, 117.8, 117.7 (d,  $J$  = 23.1 Hz), 116.1 (d,  $J$  = 21.8 Hz), 49.2, 31.6. IR: 3065  $\text{cm}^{-1}$ , 2983  $\text{cm}^{-1}$ , 1660  $\text{cm}^{-1}$ , 1499  $\text{cm}^{-1}$ . HRMS (APCI)  $m/z$ :  $[\text{M}+\text{H}]^+$  calc'd for ( $\text{C}_{22}\text{H}_{17}\text{F}_2\text{O}_2\text{N}_2\text{S}^+$ ) 411.0973; Found 411.0974.



N,N-bis(4-fluorophenyl)-3-(2-oxobenzo[d]oxazol-3(2H)-yl)propanamide (**18**)

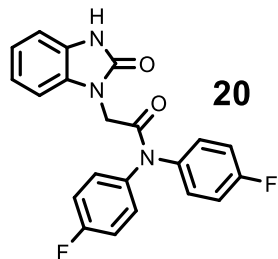
To a solution of benzo[d]oxazol-2(3H)-one (1.0 equiv) in  $\text{CH}_3\text{CN}$  (5 mL),  $\text{K}_2\text{CO}_3$  (1.5 equiv) and **3** (1.15 equiv) were each added. The reaction mixture was stirred for 24 hours at 80 °C under inert  $\text{N}_2$  gas. The reaction was then cooled to room temperature and concentrated under reduced pressure. The crude mixture was washed with water (2 x 10 mL) and extracted with DCM (20 mL). The organic layer was dried over  $\text{Na}_2\text{SO}_4$ , filtered, concentrated under reduced pressure, and purified using automated Combiflash chromatography (silica gel, 20-40 microns using a mobile phase of 0%-20% EtOAc in Hexane), yielding a white solid (46%). MP: 141-142 °C  $^1\text{H}$  NMR ( $\text{CD}_2\text{Cl}_2$ , 500 MHz)  $\delta$  7.25-7.20 (m, 6H), 7.16-7.12 (m, 4H), 7.05 (t,  $J$  = 8.5 Hz, 2H), 4.15 (t,  $J$  = 6.7 Hz, 2H), 2.77 (t,  $J$  = 6.7 Hz, 2H).  $^{13}\text{C}\{^1\text{H}\}$  NMR ( $\text{CD}_2\text{Cl}_2$ , 126 MHz)  $\delta$  170.0, 154.2, 142.6, 138.4, 138.2, 131.1, 130.3 (d,  $J$  = 8.8 Hz), 128.2 (d,  $J$  = 8.4 Hz), 123.8, 122.3, 117.1 (d,  $J$  = 22.9 Hz), 115.8 (d,  $J$  = 22.7 Hz), 109.7, 109.0, 38.6, 33.0. IR: 3069  $\text{cm}^{-1}$ , 2926  $\text{cm}^{-1}$ , 1760  $\text{cm}^{-1}$ , 1666

cm<sup>-1</sup>, 1501 cm<sup>-1</sup>. HRMS (APCI) *m/z*: [M+H]<sup>+</sup> calc'd for (C<sub>22</sub>H<sub>17</sub>F<sub>2</sub>N<sub>2</sub>O<sub>3</sub><sup>+</sup>) 395.1202; Found 392.1208.



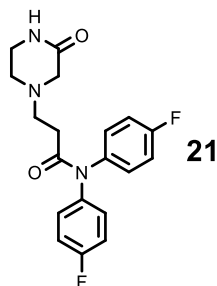
N,N-bis(4-fluorophenyl)-2-(2-oxobenzo[d]oxazol-3(2H)-yl)acetamide (**19**)

The procedure detailed for compound **18** was followed, but the CH<sub>3</sub>CN solvent was replaced with DMF, yielding a white solid (84 %). MP: 155-156 °C. <sup>1</sup>H NMR (CDCl<sub>3</sub>, 500 MHz) δ 7.40 (s, 2H), 7.25-7.15 (m, 6H), 7.13 (td, *J* = 7.8, 1.3 Hz, 1H), 7.00 (t, *J* = 8.2 Hz, 2H), 6.95-6.93 (m, 1H), 4.47 (s, 2H). <sup>13</sup>C{<sup>1</sup>H} NMR (CDCl<sub>3</sub>, 126 MHz) δ 165.3, 154.5, 142.6, 137.6, 136.6, 131.0, 130.3, 127.3, 123.9, 122.8, 117.8 (d, *J* = 23.1 Hz), 116.0 (d, *J* = 22.9 Hz), 110.2, 108.6, 44.6 IR: 3065 cm<sup>-1</sup>, 2930 cm<sup>-1</sup>, 1764 cm<sup>-1</sup>, 1666 cm<sup>-1</sup>. HRMS (APCI) *m/z*: [M+H]<sup>+</sup> calc'd for (C<sub>21</sub>H<sub>15</sub>F<sub>2</sub>N<sub>2</sub>O<sub>3</sub><sup>+</sup>) 381.1045; Found 381.1070.



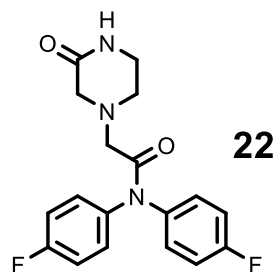
To a stirred solution of 1,3-dihydro-2H-benzo[d]imidazol-2-one (119.8 mg, 0.89 mmol) in DMF (10 mL) was added potassium carbonate (69.5 mg, 0.50 mmol). Tertbutyl ammonium bromide (5.4 mg, 17 μmol) was added to the solution and stirred for 5 minutes at rt. Acetamide **2** (138.16 mg, 0.49 mmol) was added in 3 portions over 10 minutes. The mixture was stirred at rt for a further 24 h and filtered. The solvent was removed under reduced pressure, and the resulting solid was dissolved in 30 mL of DCM and washed with deionized water (4X, 10 mL). The organic layer was dried over sodium sulfate concentrated into silica gel and purified by flash chromatography (50% ethyl acetate in hexane). The compound was isolated as a white solid (50.5 mg, 36%). MP: 194-195 °C. IR: 3069, 1686, 1501 cm<sup>-1</sup>. <sup>1</sup>H NMR (CD<sub>3</sub>SO, 500 MHz) δ 10.86 (s, 1H), 7.75 (br s, 2H), 7.36 (br s, 4H), 7.21 (br s, 2H), 7.11-7.09 (m, 1H), 7.01-7.16 (m, 2H), 4.45 (s, 2H). <sup>13</sup>C{<sup>1</sup>H}

NMR (CD<sub>2</sub>Cl<sub>2</sub>, 125 MHz)  $\delta$  166.7, 154.8, 131.1, 121.4, 121.0, 109.2, 43.4. HRMS (ESI-TOF)  $m/z$ : [(M+H)<sup>+</sup>] calcd for (C<sub>21</sub>H<sub>16</sub>F<sub>2</sub>N<sub>3</sub>O<sub>2</sub><sup>+</sup>) 380.1211; found, 380.1212.



*N,N*-bis(4-fluorophenyl)-3-(3-oxopiperazin-1-yl)propanamide (**21**)

General procedure B produced an off-white solid (44%). MP: 94-95 °C. IR: 3174, 3058, 1659, 1496 cm<sup>-1</sup>. <sup>1</sup>H NMR (CD<sub>2</sub>Cl<sub>2</sub>, 500 MHz)  $\delta$  7.26-7.21 (m, 4H), 7.13-7.04 (m, 4H), 6.07 (s, 1H), 3.30-3.27 (m, 2H), 2.98 (s, 2H), 2.75 (t, *J* = 7.2 Hz, 2H), 2.59 (t, *J* = 5.5 Hz, 2H), 2.42 (t, *J* = 7.2 Hz, 2H). <sup>13</sup>C{<sup>1</sup>H} NMR (CD<sub>2</sub>Cl<sub>2</sub>, 126 MHz)  $\delta$  171.7, 169.1, 139.2, 130.7, 128.6, 117.2, 116.1, 57.2, 53.7, 49.8, 41.7, 32.2. HRMS (ESI-TOF)  $m/z$ : [(M+H)<sup>+</sup>] calcd for (C<sub>19</sub>H<sub>20</sub>F<sub>2</sub>N<sub>3</sub>O<sub>2</sub><sup>+</sup>) 360.1524; found, 360.1538.



*N,N*-bis(4-fluorophenyl)-3-(3-oxopiperazin-1-yl)propanamide (**22**)

General procedure B produced an off-white solid (70%). MP: 73-75 °C. IR: 3215, 3066, 1664, 1499 cm<sup>-1</sup>. <sup>1</sup>H NMR (CDCl<sub>3</sub>, 500 MHz)  $\delta$  7.30-7.26 (m, 4H), 7.13-7.04 (m, 4H), 3.28-3.25 (m, 2H), 3.18 (s, 2H), 3.18 (s, 2H), 3.18 (s, 2H), 2.76-2.74 (m, 2H). <sup>13</sup>C{<sup>1</sup>H} NMR (CD<sub>2</sub>Cl<sub>2</sub>, 125 MHz)  $\delta$  169.3, 168.4, 138.8, 138.3, 116.7, 115.7, 58.7, 56.3, 48.8, 41.1. HRMS (ESI-TOF)  $m/z$ : [(M+H)<sup>+</sup>] calcd for (C<sub>18</sub>H<sub>18</sub>F<sub>2</sub>N<sub>3</sub>O<sub>2</sub><sup>+</sup>) 346.1367; found, 346.1415.

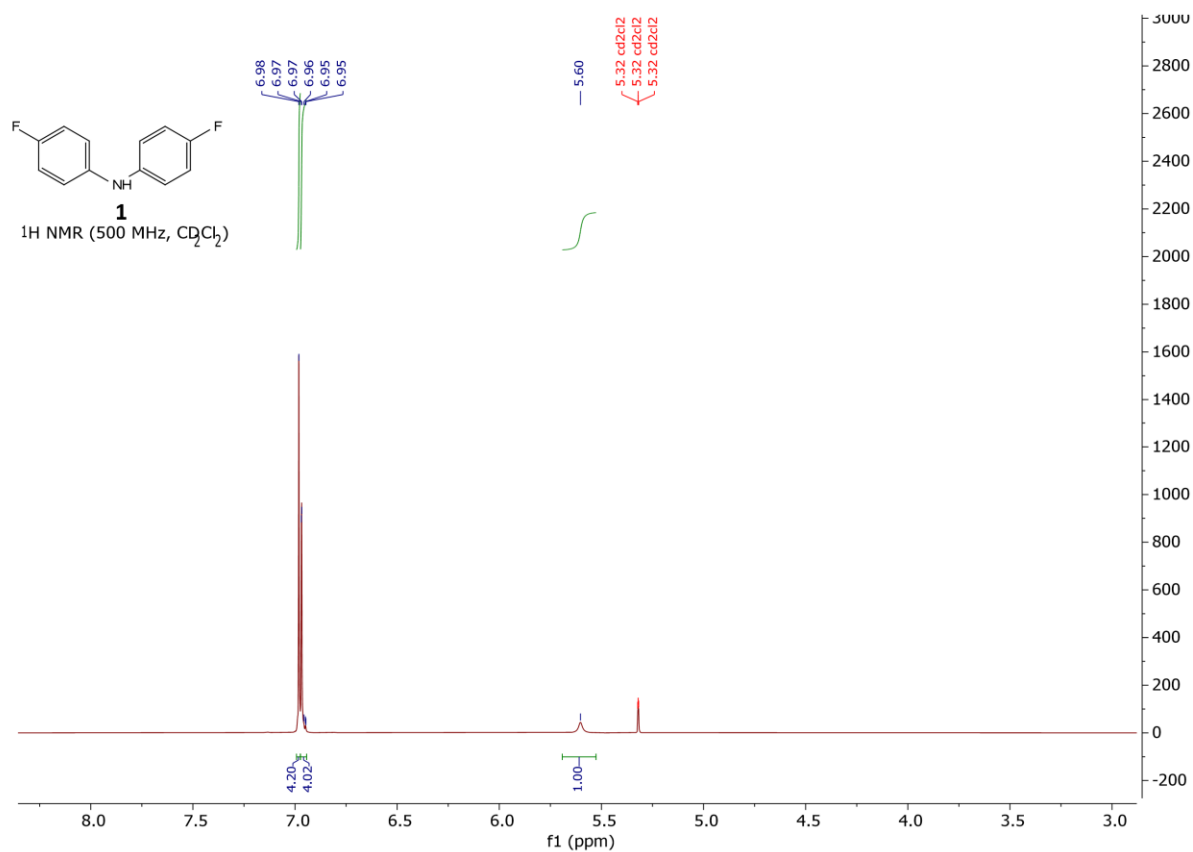


**Figure 2.6: Proton NMR of compound 1. Related to Scheme 2.1.**

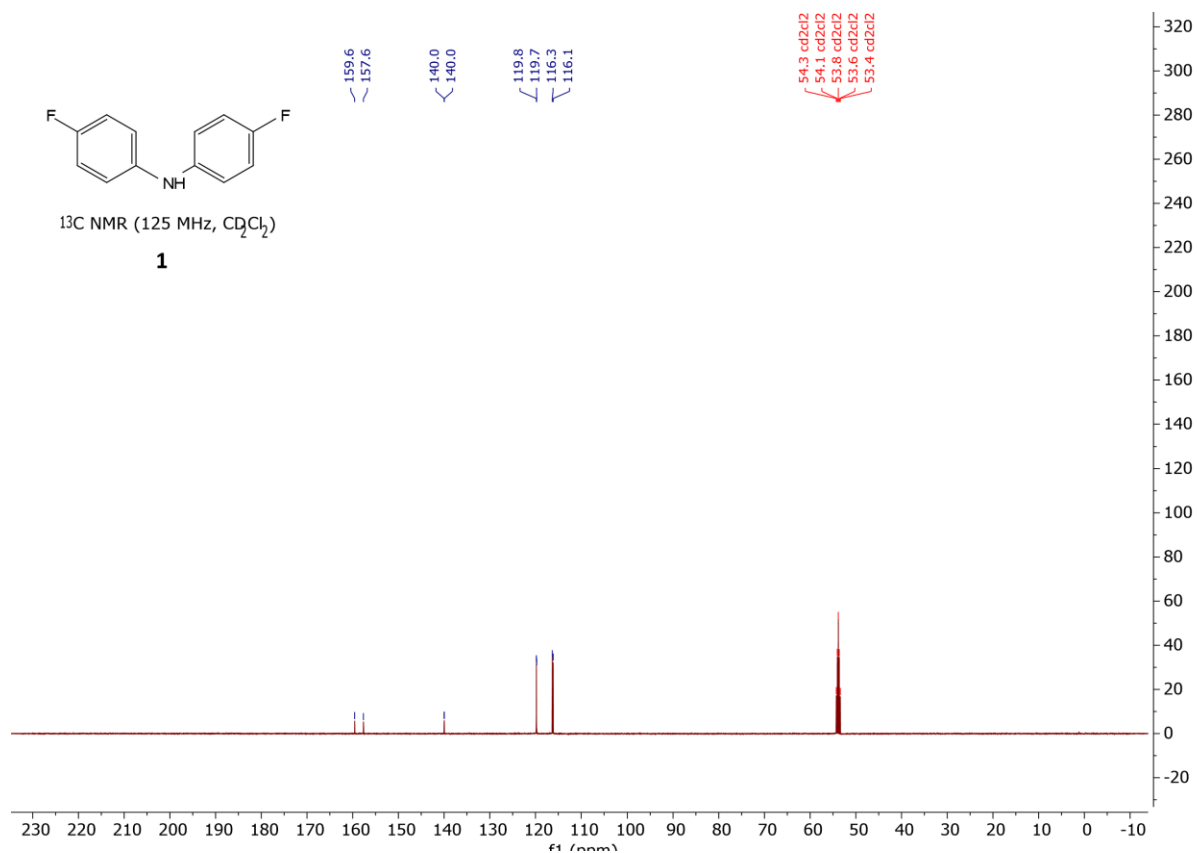


**Figure 2.7: Carbon-13 NMR of compound 1. Related to Scheme 2.1.**

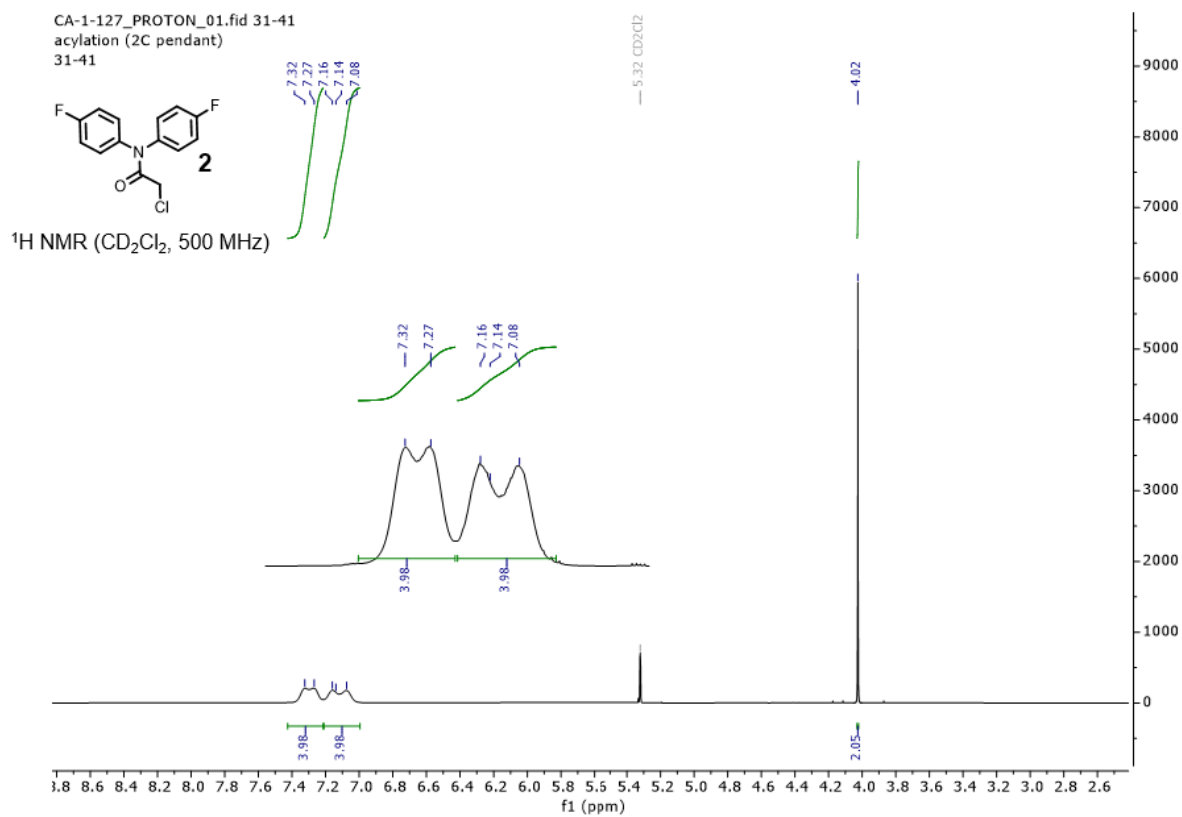


**Figure 2.8: Proton NMR of compound 2. Related to Scheme 2.1.**



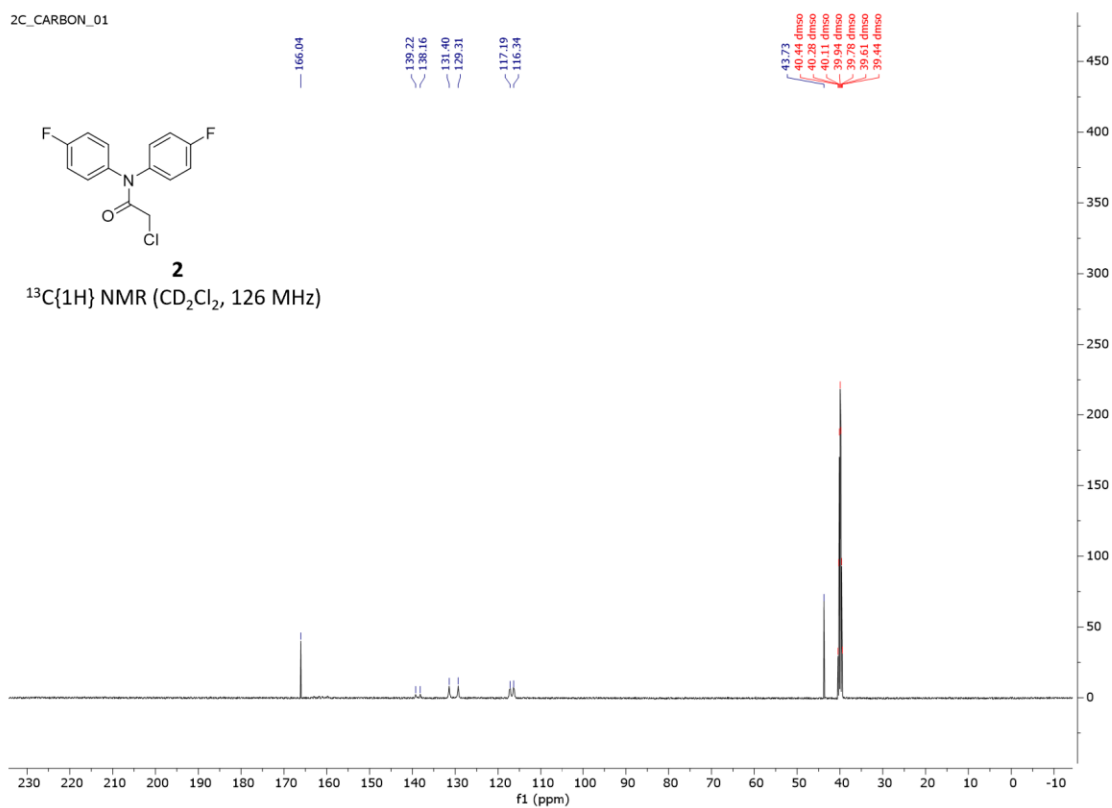


**Figure 2.9: Carbon-13 NMR of compound 2. Related to Scheme 2.1.**

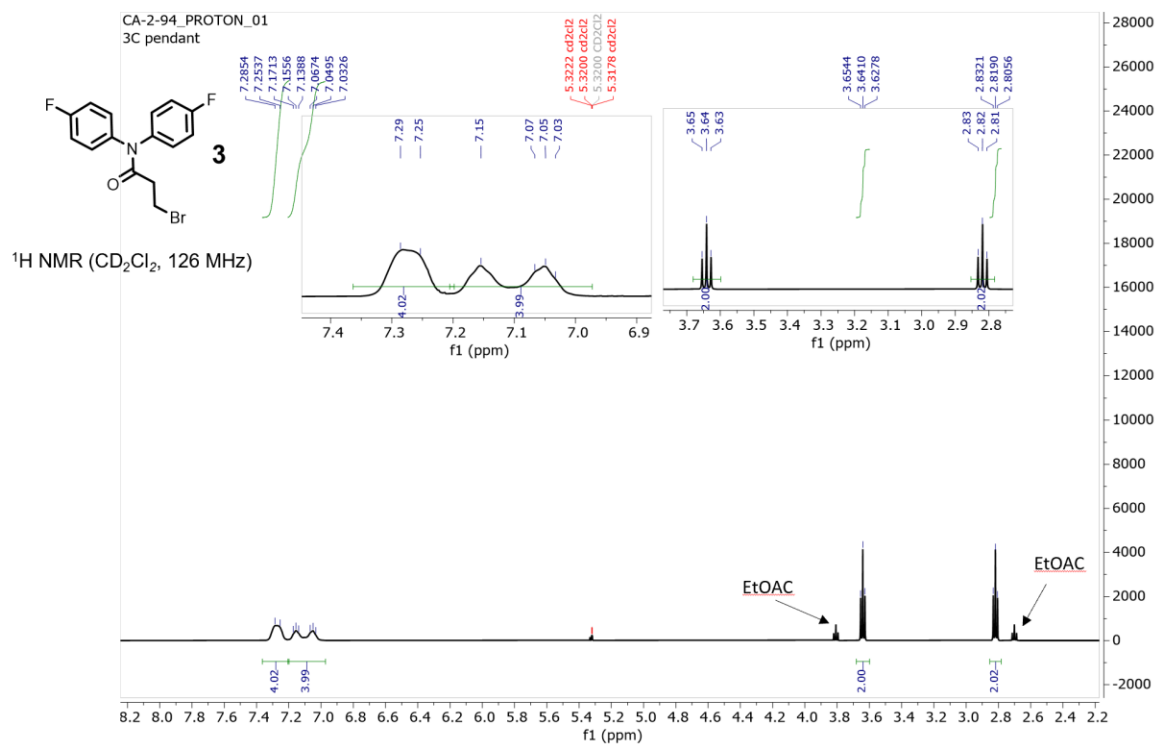


**Figure 2.10: Proton NMR of compound 3. Related to Scheme 2.1.**

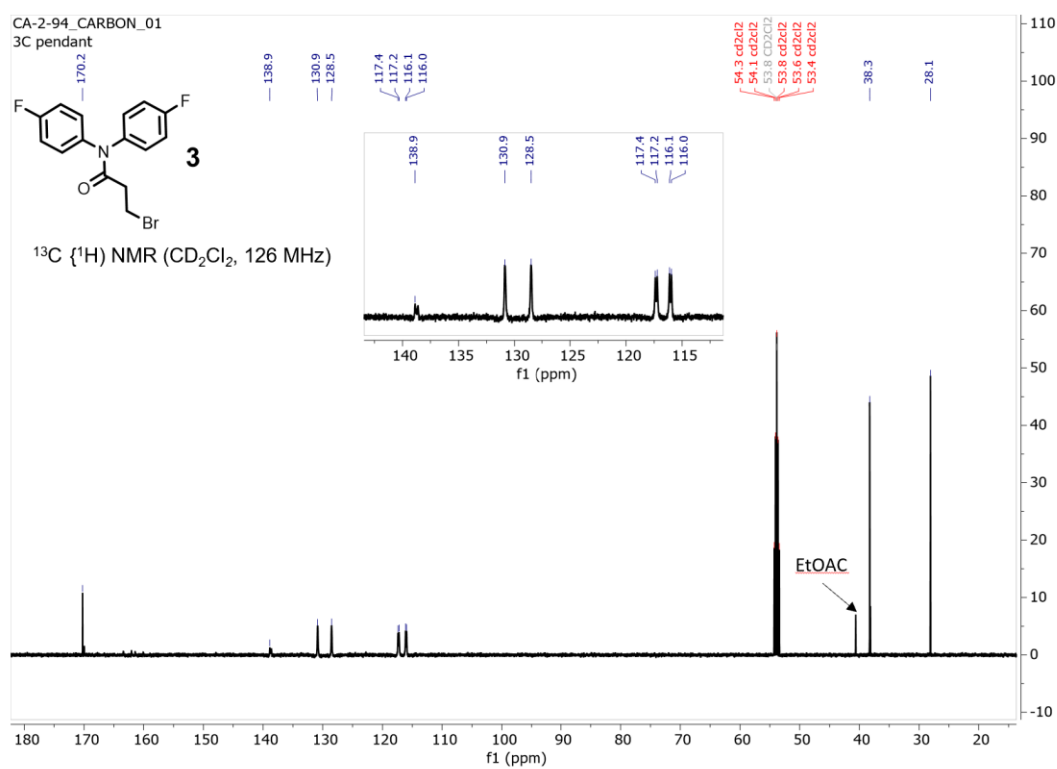


**Figure 2.11: Carbon-13 NMR of compound 3. Related to Scheme 2.1.**

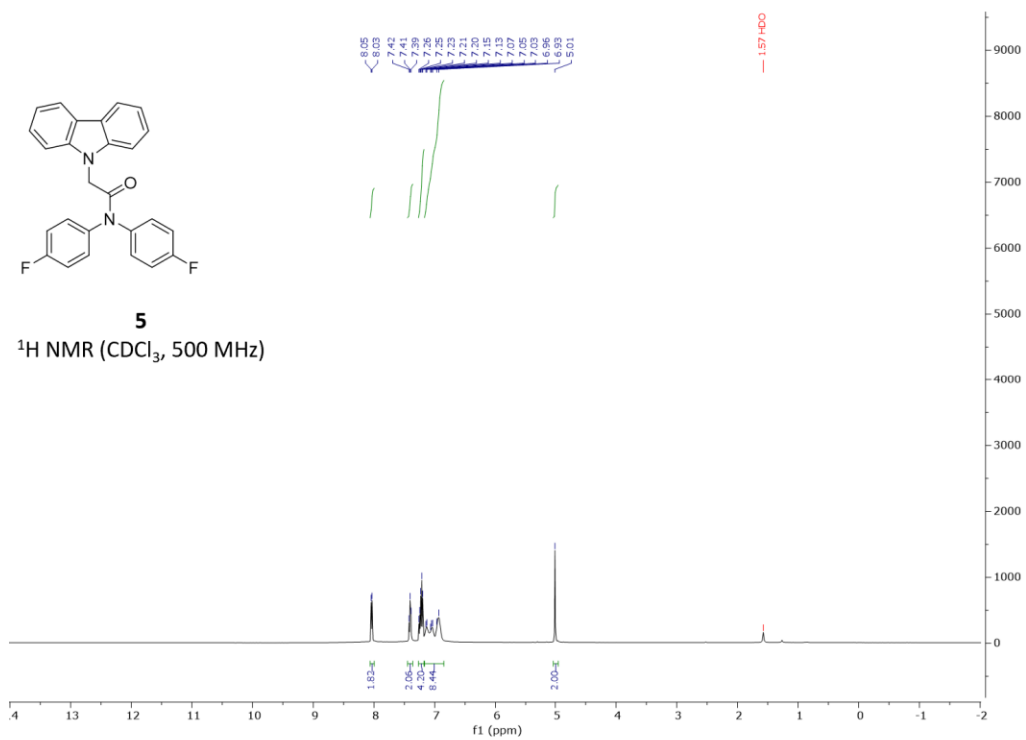


**Figure 2.12: Proton NMR of compound 5. Related to Scheme 2.1.**

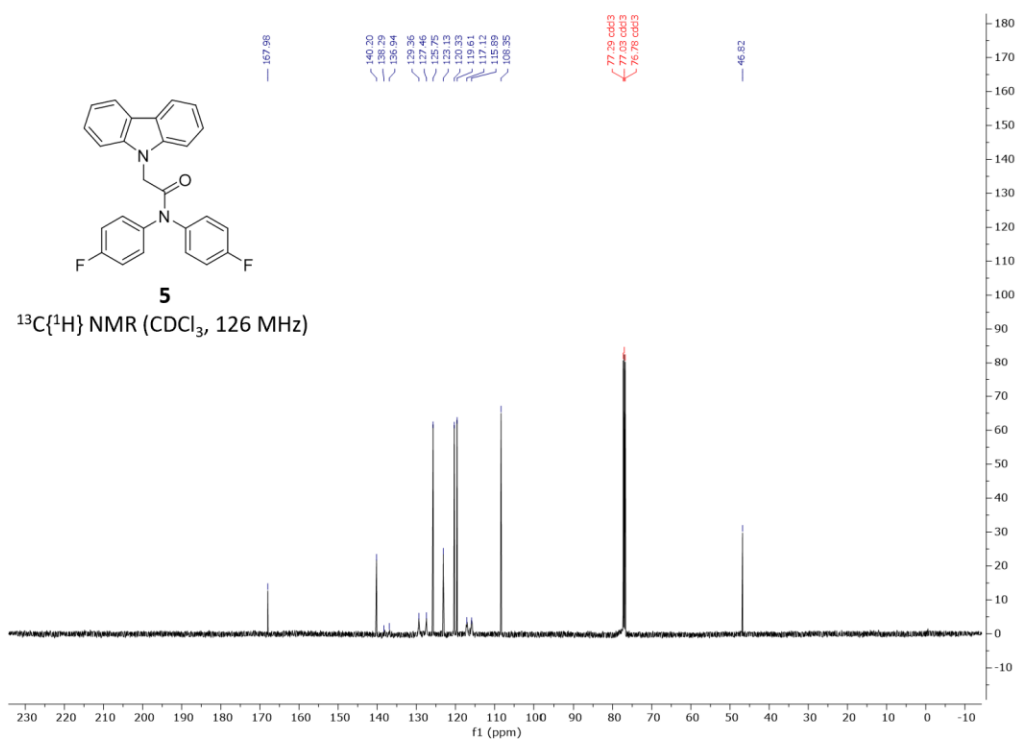


**Figure 2.13: Carbon-13 NMR of compound 5. Related to Scheme 2.1.**



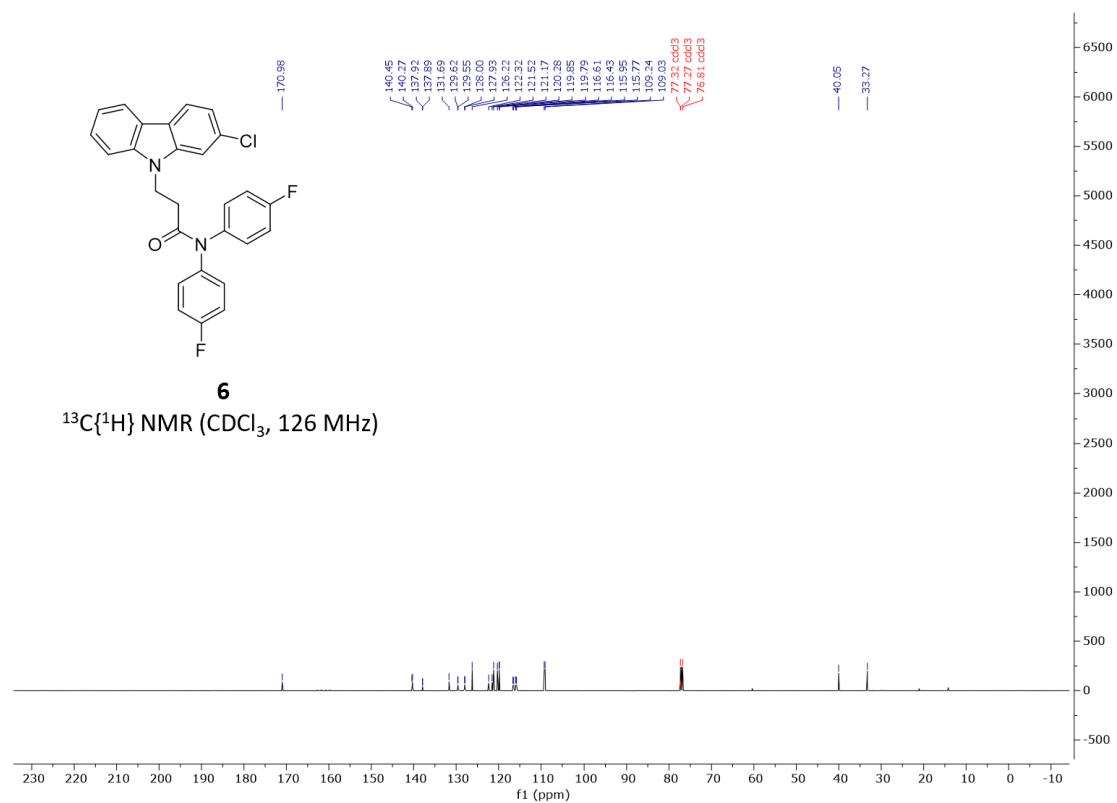


**Figure 2.15: Proton NMR of compound 6. Related to Scheme 2.1.**





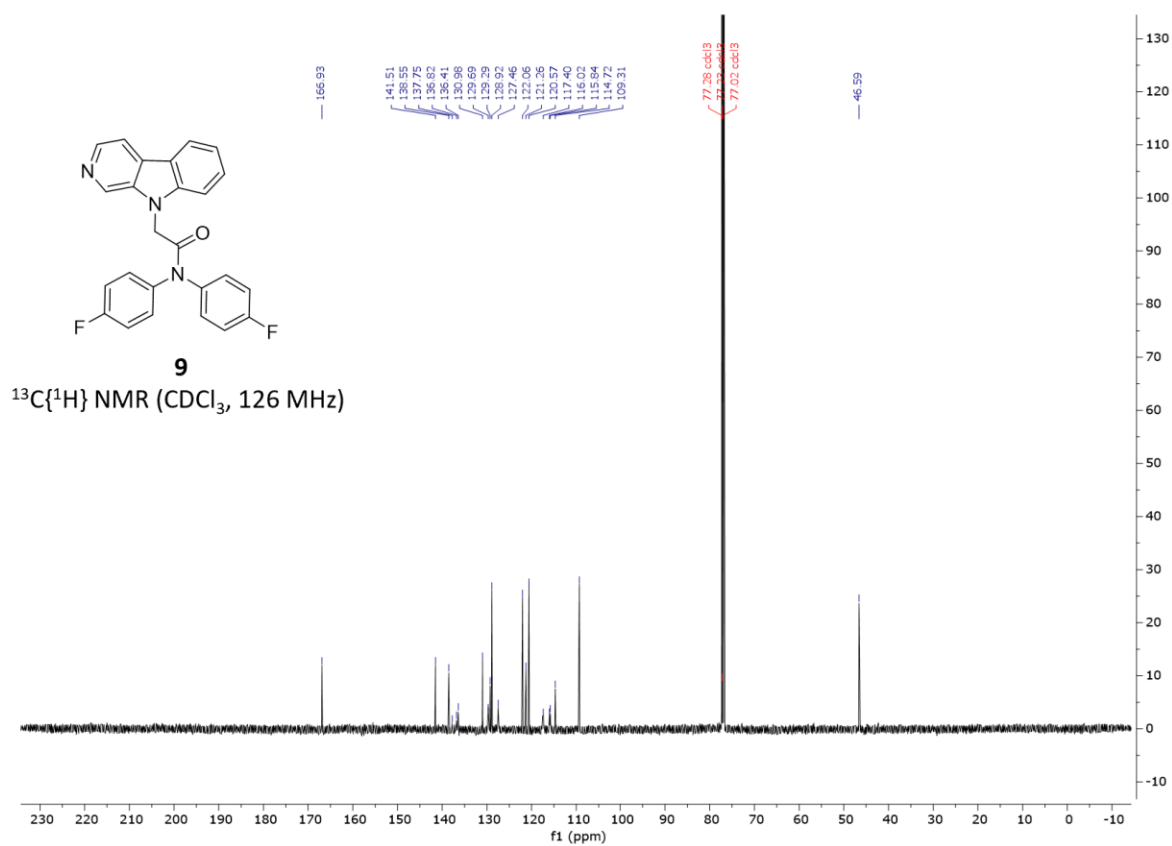


**Figure 2.17: Carbon-13 NMR of compound 9. Related to Scheme 2.1.**

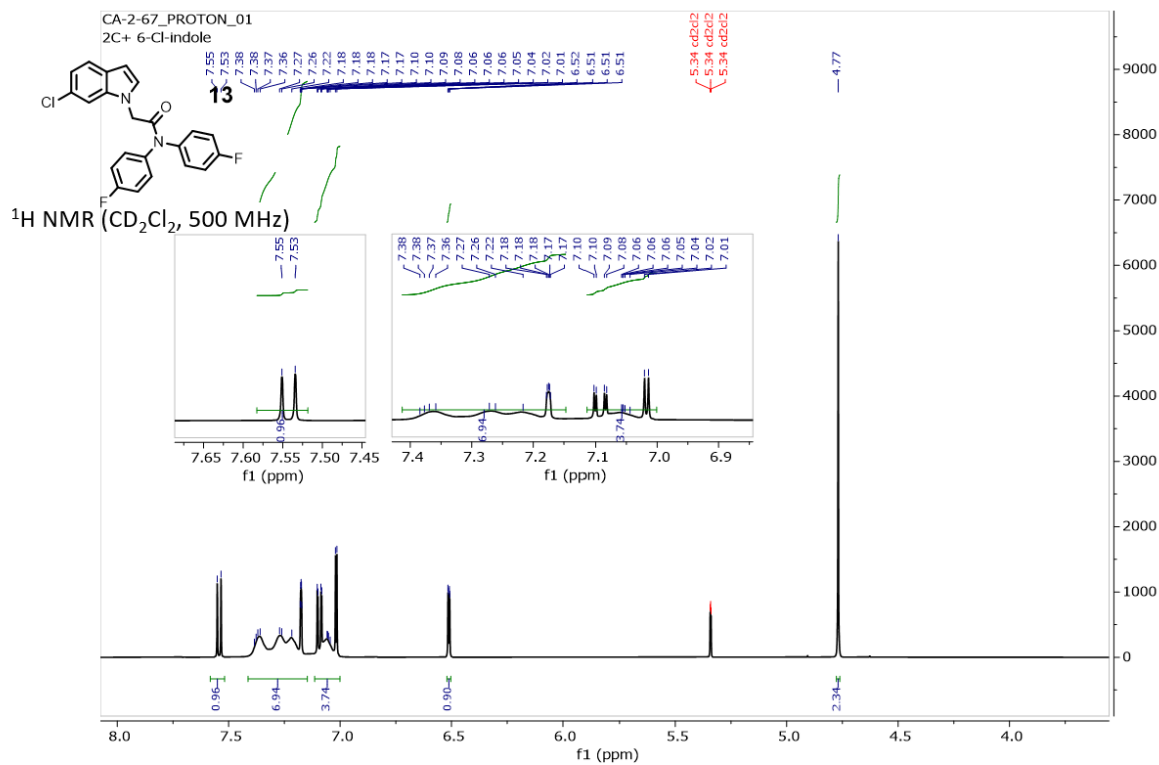


**Figure 2.18: Proton NMR of compound 13. Related to Scheme 2.1**

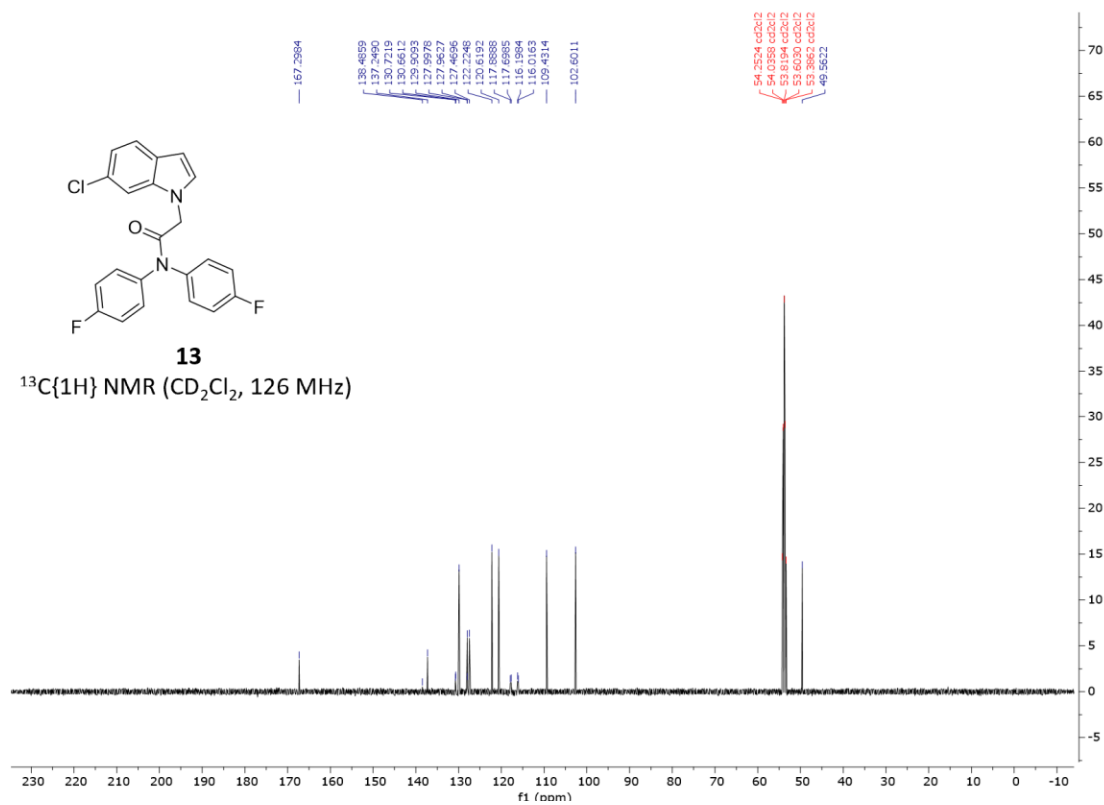


**Figure 2.19: Carbon-13 NMR of compound 13. Related to Scheme 2.1**

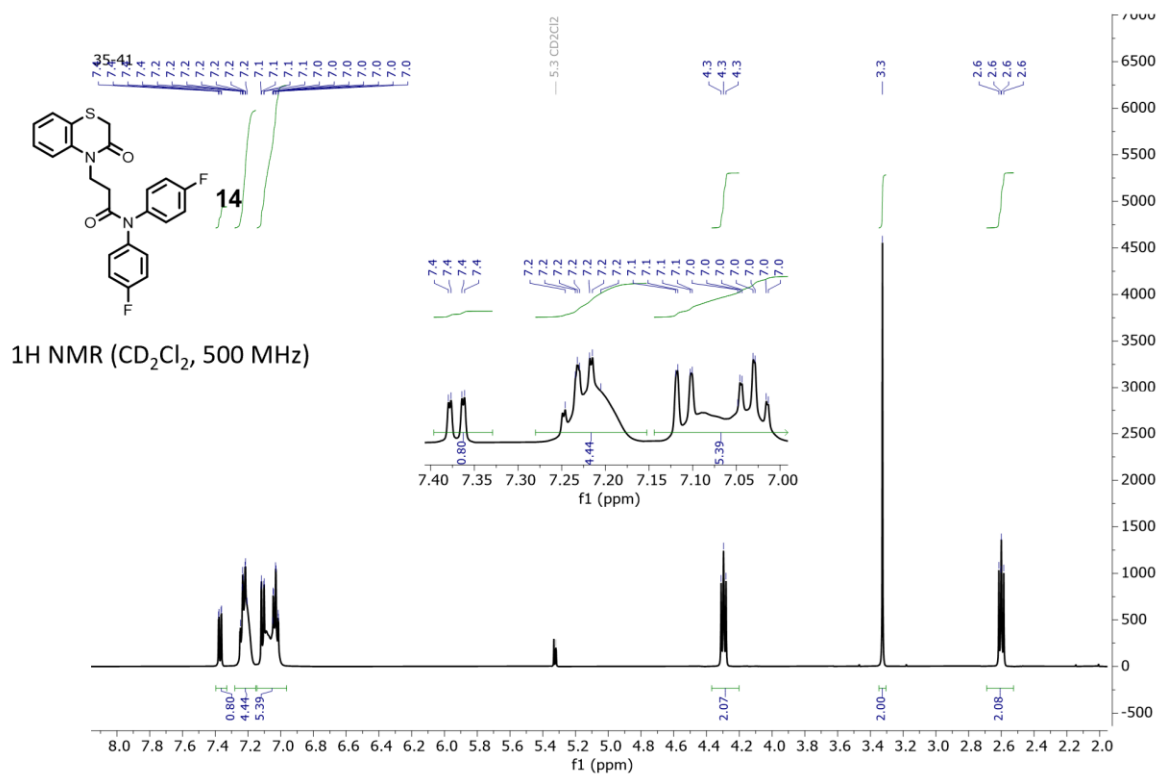


**Figure 2.20: Proton NMR of compound 14. Related to Scheme 2.1**

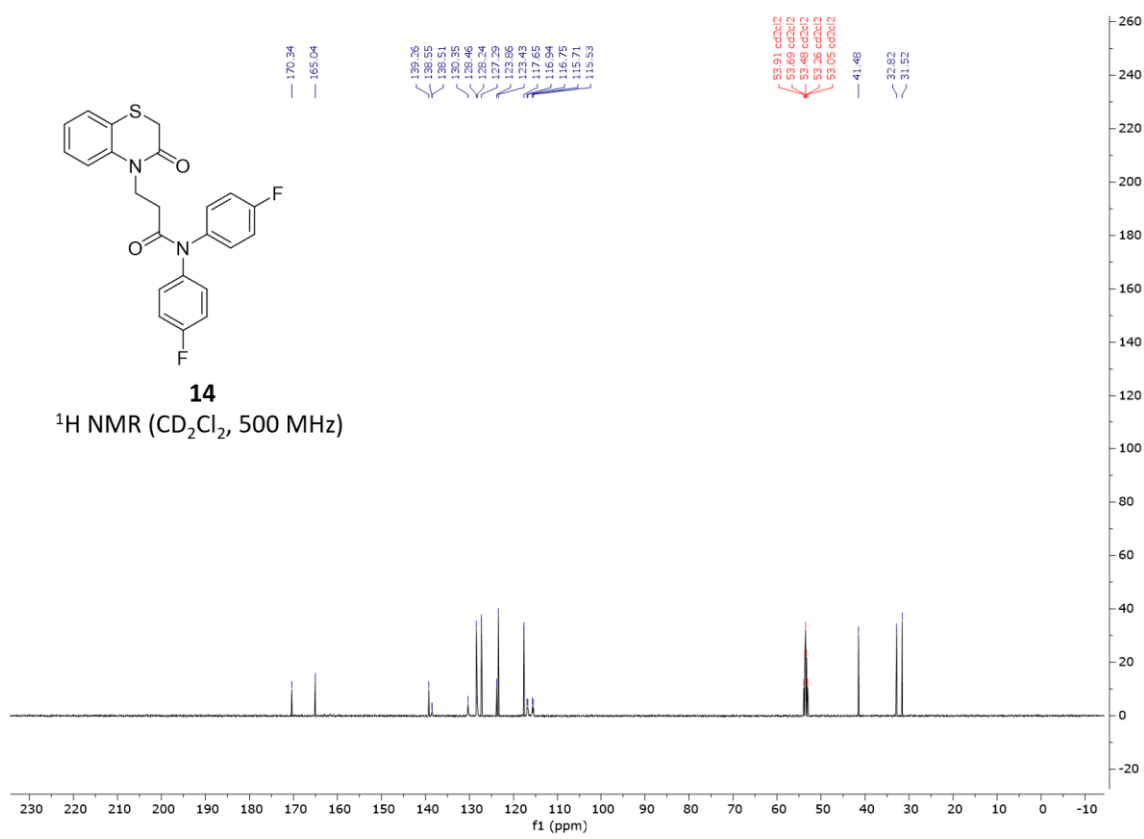


**Figure 2.21: Carbon-13 NMR of compound 14. Related to Scheme 2.1**

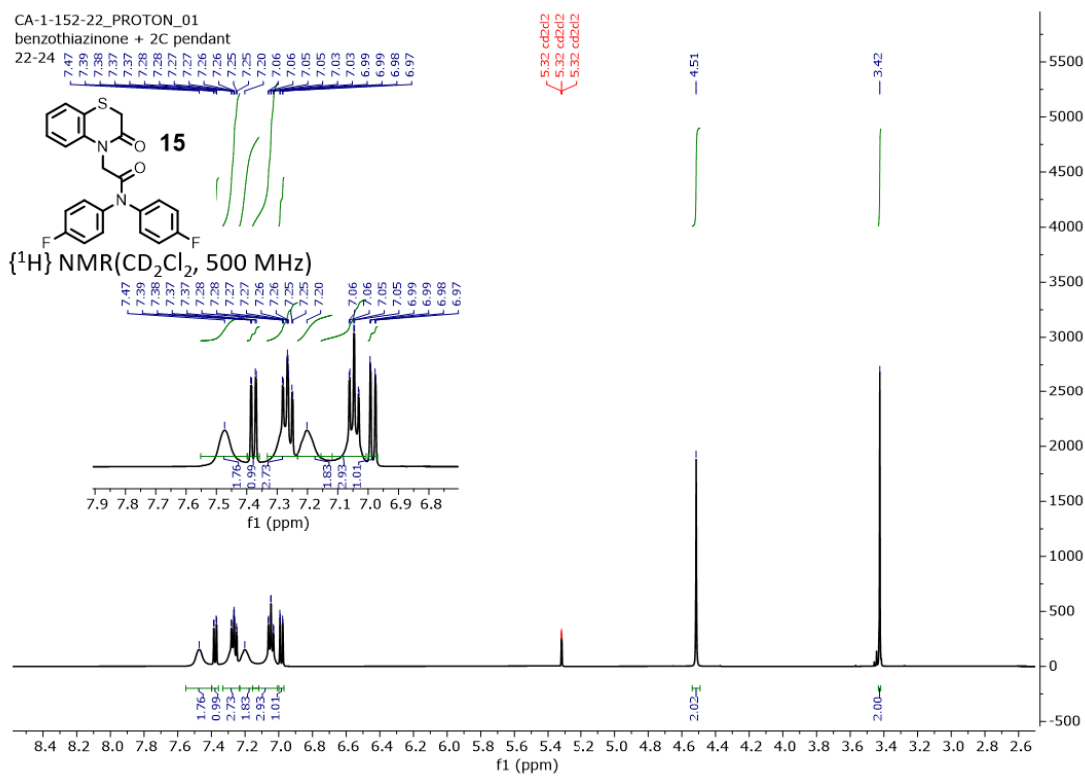


**Figure 2.22: Proton NMR of compound 15. Related to Scheme 2.1**

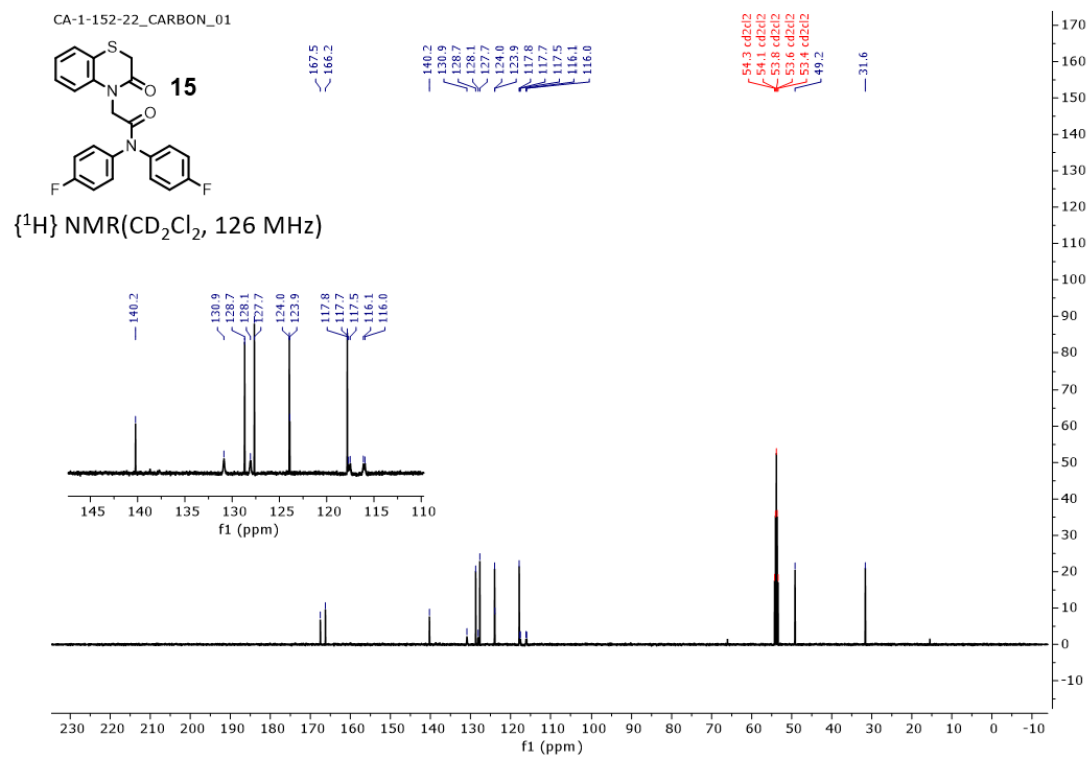


**Figure 2.23: Carbon-13 NMR of compound 15. Related to Scheme 2.1**

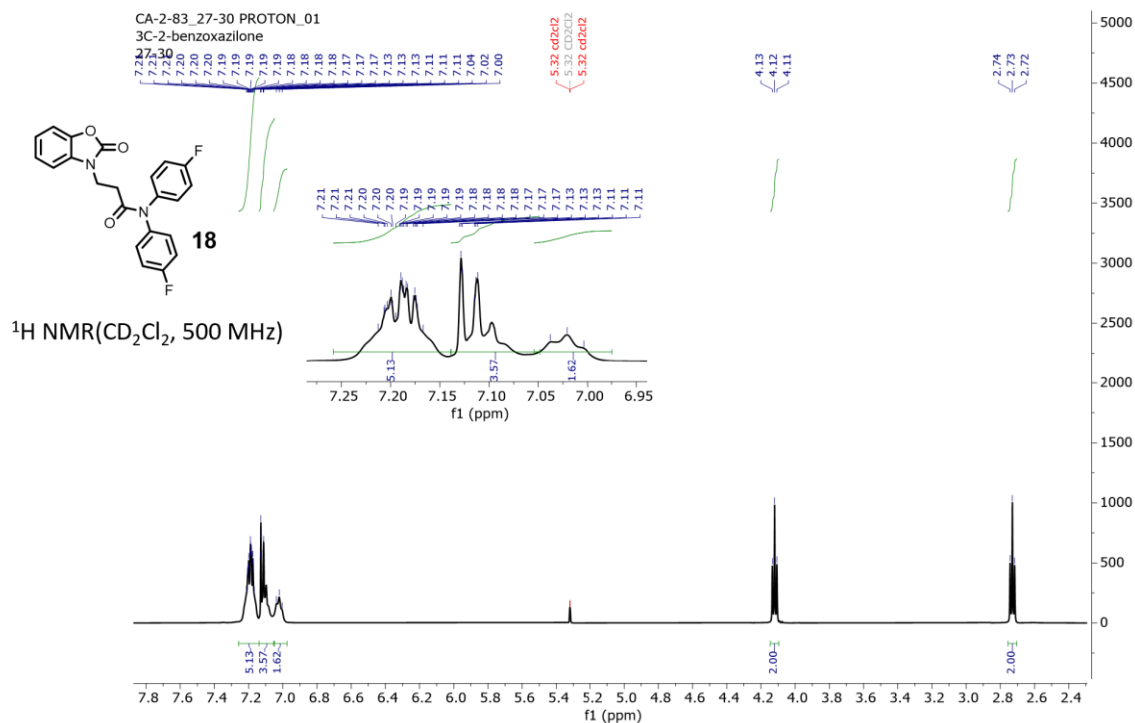


**Figure 2.24: Proton NMR of compound 18. Related to Scheme 2.1**



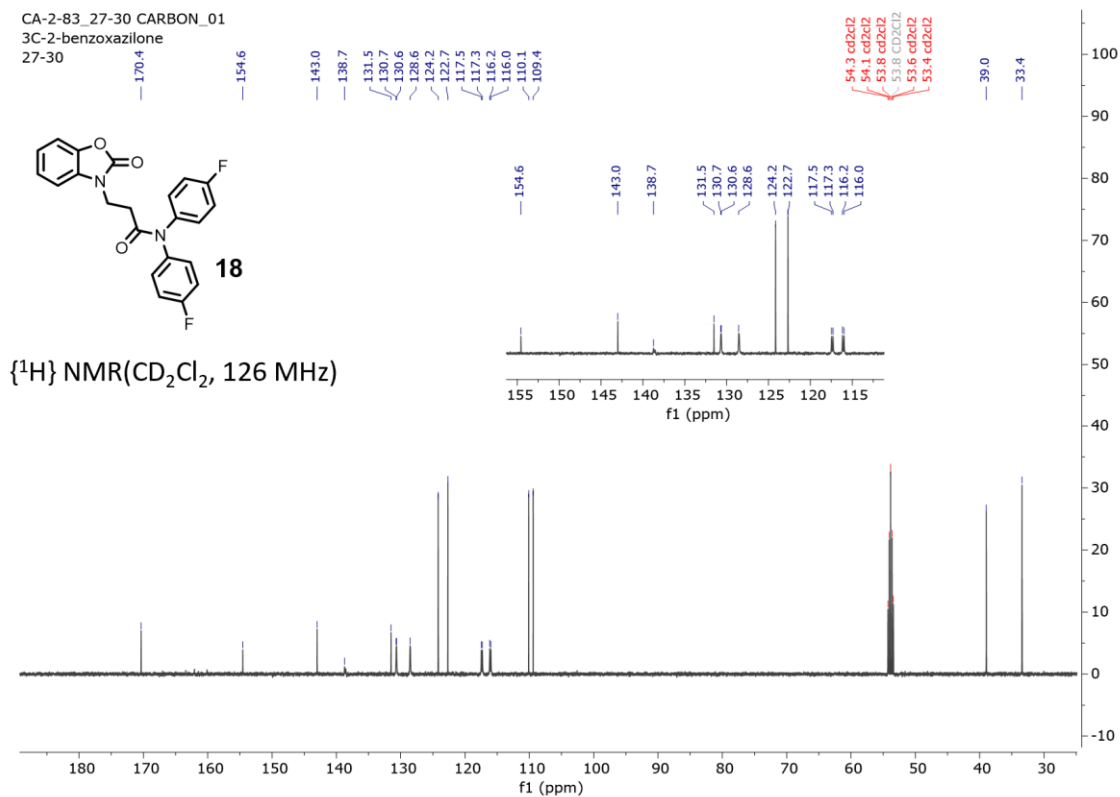


**Figure 2.25: Carbon-13 NMR of compound 18. Related to Scheme 2.1**

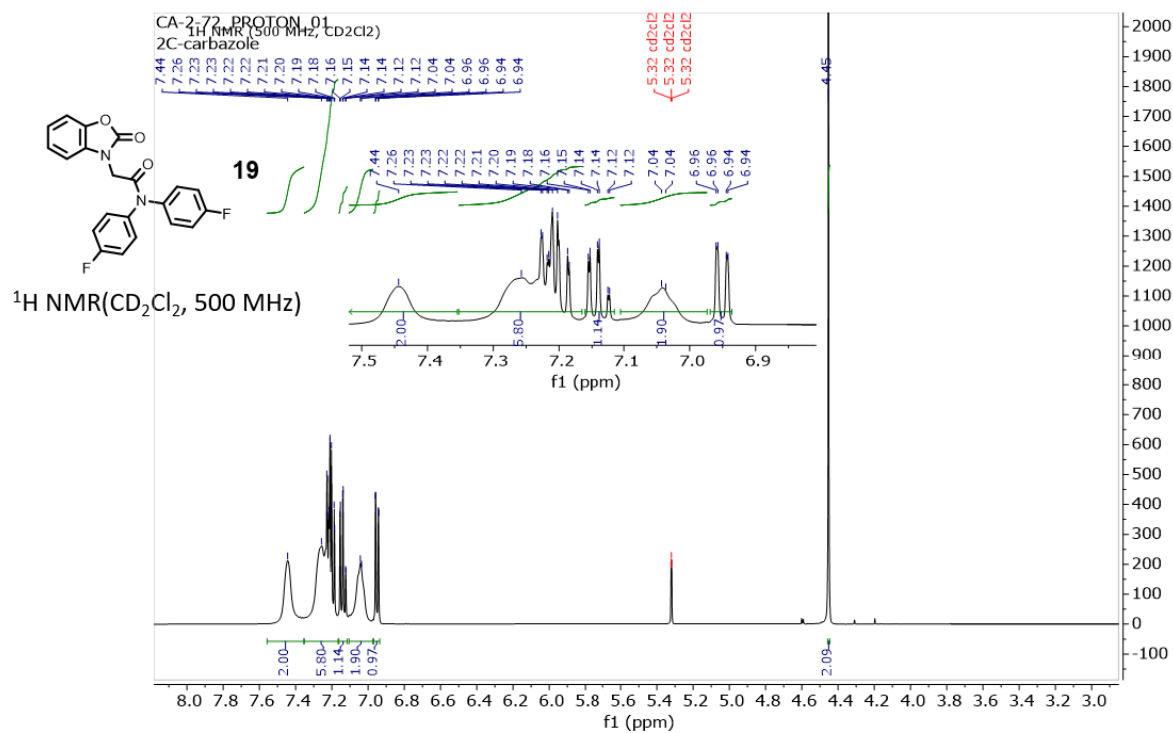


**Figure 2.26: Proton NMR of compound 19. Related to Scheme 2.1**

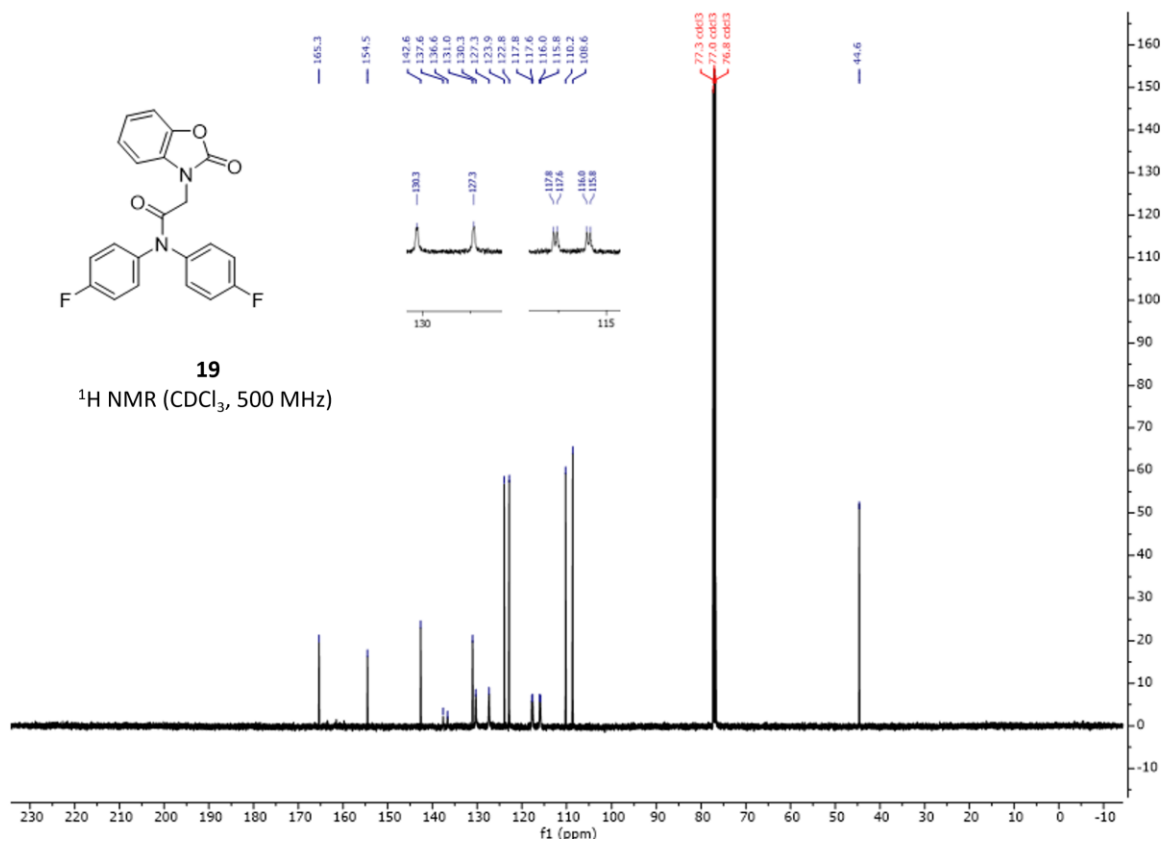


**Figure 2.27: Carbon-13 NMR of compound 19. Related to Scheme 2.1**

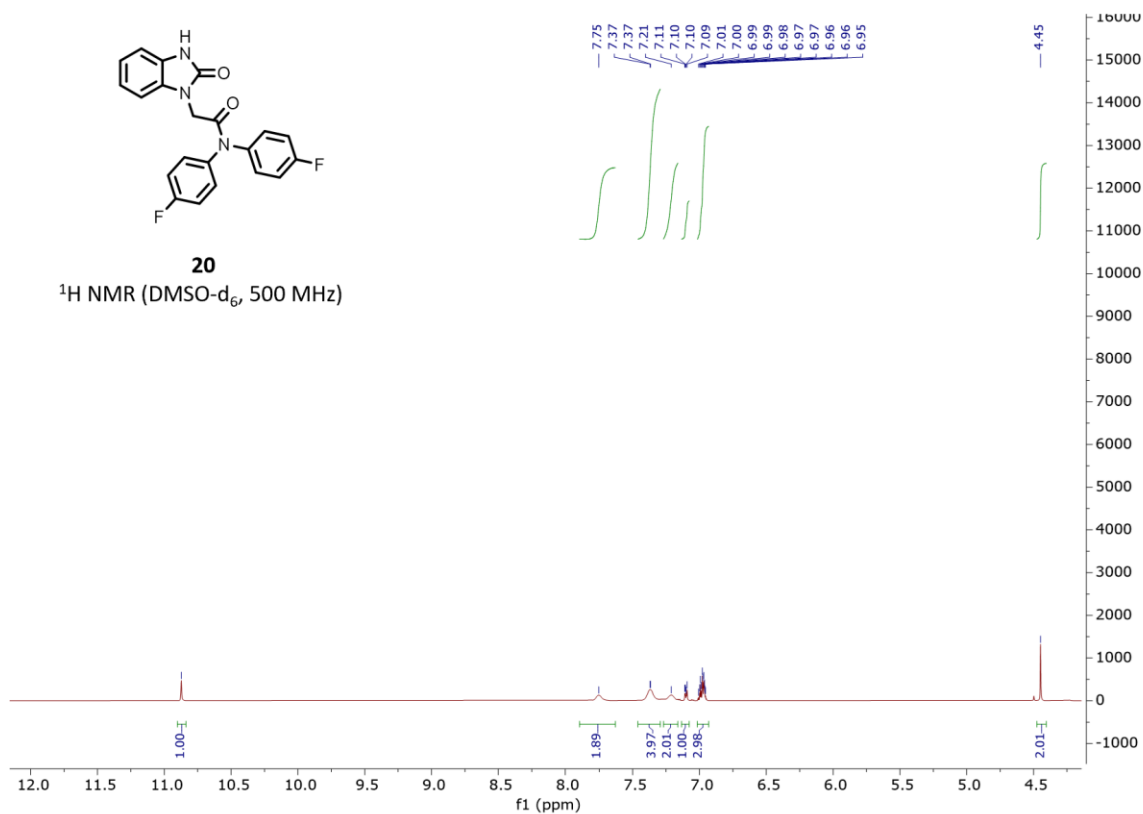


**Figure 2.28: Proton NMR of compound 20. Related to Scheme 2.1**

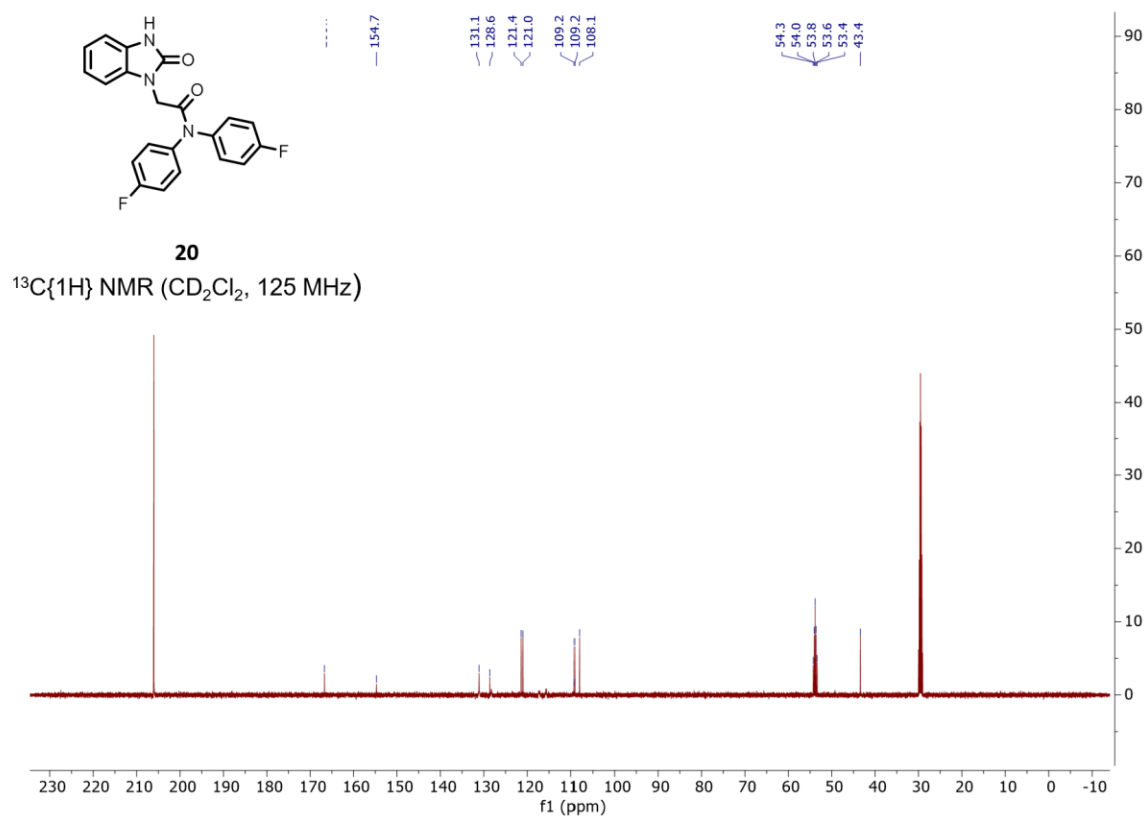


**Figure 2.29: Carbon-13 NMR of compound 20. Related to Scheme 2.1**

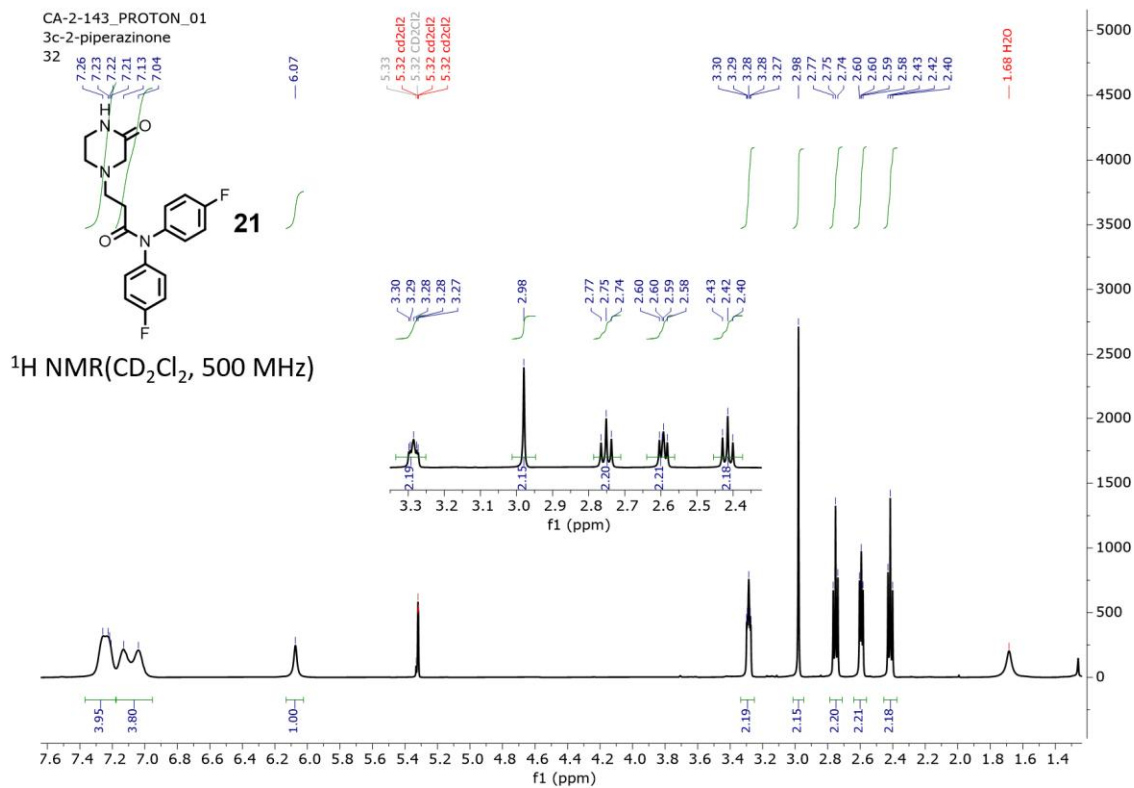


**Figure 2.30: Proton NMR of compound 21. Related to Scheme 2.1**

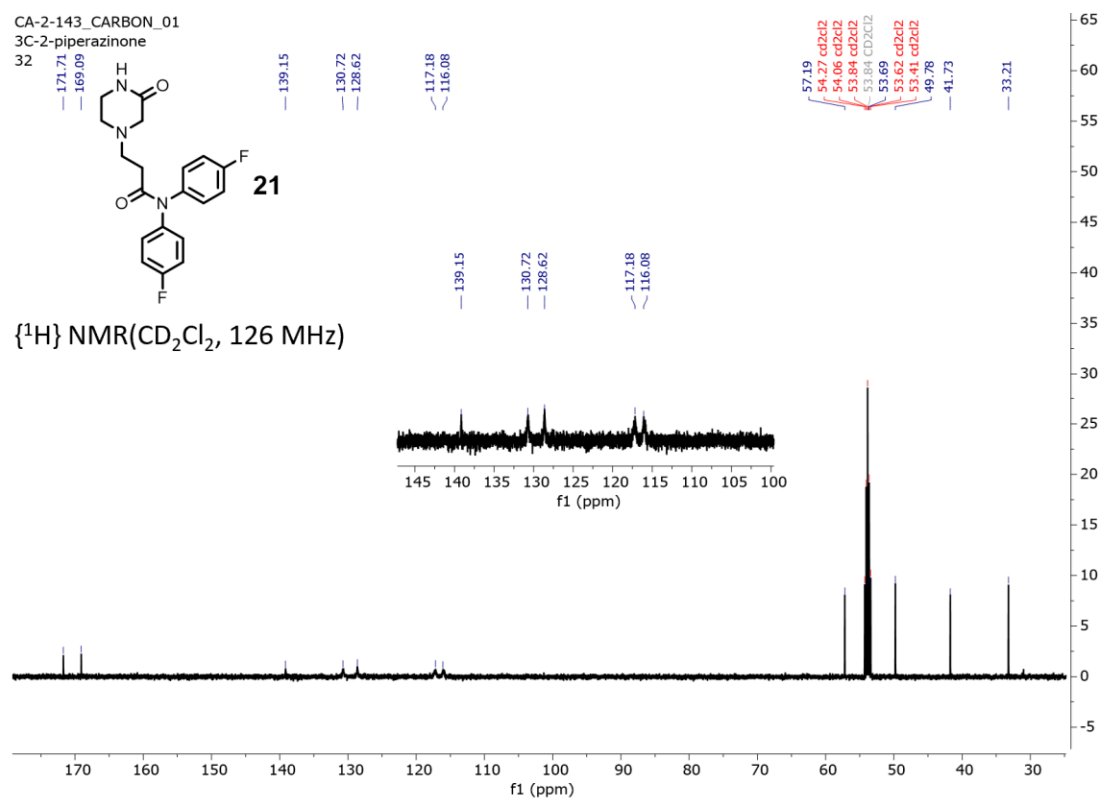


**Figure 2.31: Carbon-13 NMR of compound 21. Related to Scheme 2.1**

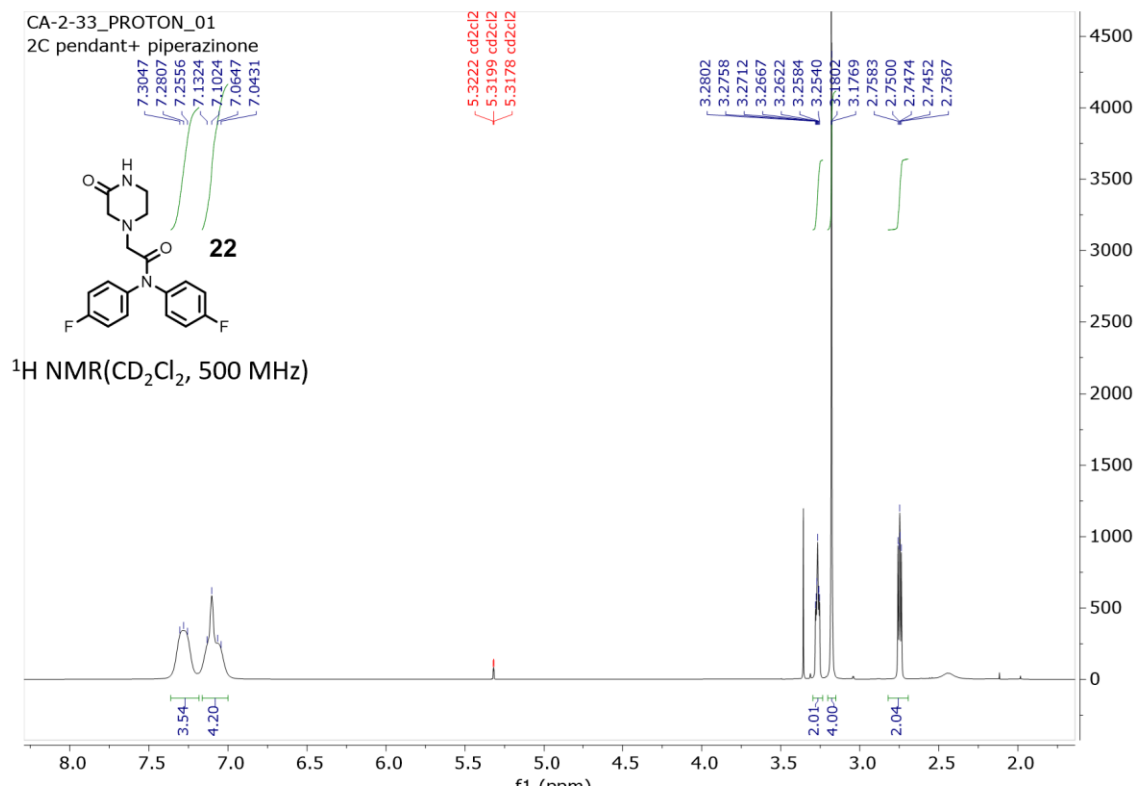


**Figure 2.32: Proton NMR of compound 22. Related to Scheme 2.1**



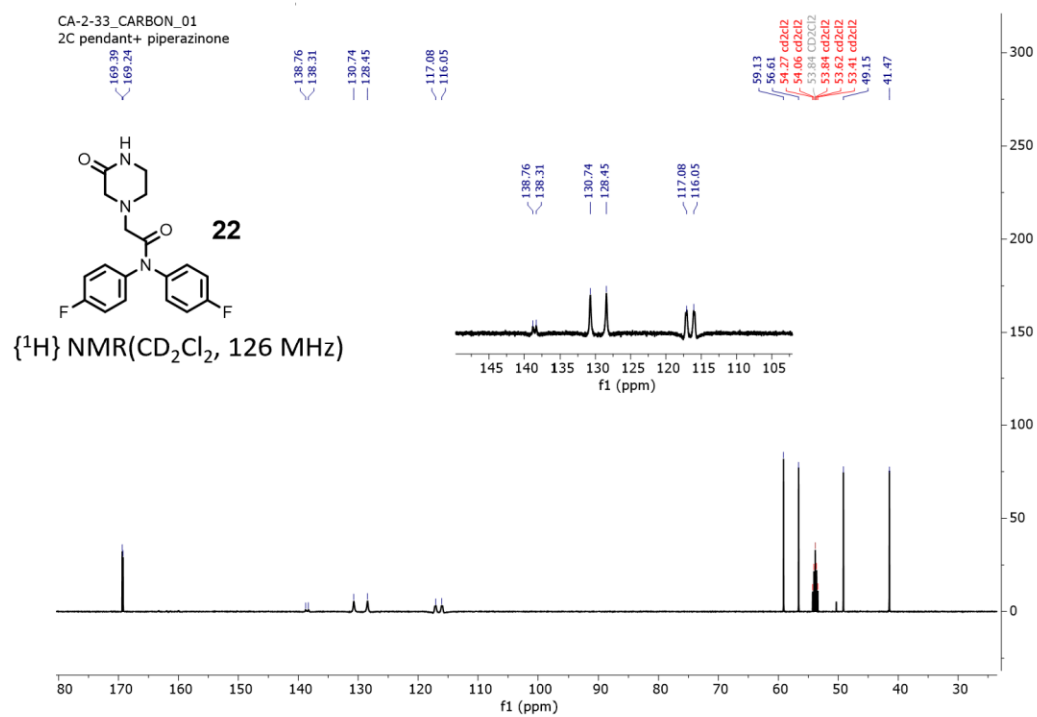


**Figure 2.33: Carbon-13 NMR of compound 22. Related to Scheme 2.1**

## **Biological Evaluations**

### **Fluorogenic Peptide Assay**

Purified enzymatic activity assays were performed in black flat-bottom, clear-bottom 96-well plates with a total reaction volume of 100  $\mu$ L per well. Varying concentrations of test compounds (3.75–30  $\mu$ M or 0.16–30  $\mu$ M) were added to wells containing 0.5 nM human constitutive 20S proteasome, diluted in buffer (38 mM Tris, 100 mM NaCl, pH 7.8). The drug-proteasome mixtures were incubated at 37 °C for 20 minutes. Following incubation, 10  $\mu$ L of a fluorogenic substrate solution was added to each well. The substrate solution consisted of Suc-LLVY-AMC, Z-LLE-AMC, and Boc-LRR-AMC, with a final concentration of 6.67  $\mu$ M for each substrate. The enzymatic activity was measured at 37 °C using a SpectraMax M5e spectrometer. Fluorescence intensity was recorded every minute for one hour, with excitation and emission wavelengths of 380 nm and 460 nm, respectively. The rate of substrate hydrolysis in vehicle control wells was normalized to 100%. The relative enzymatic activity of treated samples was calculated as the fold change in hydrolysis rate compared to the vehicle control.

### **Purified $\alpha$ -Synuclein Digestion with 20S Proteasome**

Proteolytic degradation assays for purified  $\alpha$ -synuclein were conducted in a total reaction volume of 25  $\mu$ L, prepared in a buffer containing 50 mM HEPES and 5 mM DTT (pH 7.2). Each reaction contained 300 nM of purified  $\alpha$ -synuclein, 10 nM of purified human 20S proteasome, and the test compound or vehicle control. The 20S proteasome was first diluted to a working concentration of 11.1 nM in HEPES buffer (22  $\mu$ L). Subsequently, 0.5  $\mu$ L of the test compound (dissolved in DMSO) or DMSO alone was added to the proteasome solution. The drug-proteasome mixture was incubated at 37 °C for 45 minutes. Following this initial incubation, 2.5  $\mu$ L of a 3  $\mu$ M stock solution of purified  $\alpha$ -synuclein was introduced into the reaction, and the mixture was incubated at 37 °C for an additional 3.5 hours. After the digestion phase, 0.5  $\mu$ M GAPDH was added as a loading control. The reaction was terminated by adding a concentrated SDS loading buffer, and the samples were boiled for 10 minutes at 95°C using a heating block. The digested samples were then analyzed by immunoblotting.

## **Western Blotting**

To prepare samples for immunoblotting, a concentrated Laemmli buffer containing 25%  $\beta$ -mercaptoethanol was added, and the mixture was boiled for 10 minutes. Proteins were separated using a 4–20% Tris-glycine SDS-PAGE gel and transferred onto PVDF membranes with a Mini Trans-Blot Electrophoretic Transfer Cell for 90 minutes. After transfer, membranes were blocked at room temperature for 30 minutes using a 5% blocking solution prepared in Tris-buffered saline containing Tween 20 (TBST). The membranes were then incubated for 1 hour at rt or overnight (16 hours) at 4°C with the appropriate primary antibody, diluted according to specifications, in TBST. Following primary antibody incubation, membranes were washed three times, each for 3 minutes, with TBST. They were then exposed to a secondary antibody for 1 hour at room temperature. Protein detection was performed using an ECL Western reagent, and signals were captured using the Azure Biosystems 300Q imaging system. When multiple proteins needed to be probed, membranes were stripped using a mild stripping buffer (200 mM glycine, 3.5 mM SDS, 8 mM Tween 20, pH 2.2) for 30 minutes. The membranes were then washed thrice with TBST, 5 minutes per wash, before re-probing using the same protocol. Protein band intensities were quantified using Bio-Rad Image Lab software.

## **Cell Culture**

HEK-293T cell lines were obtained from the American Type Culture Collection (ATCC). HEK-293T cells were maintained in Dulbecco's Modified Eagle's Medium supplemented with 10% fetal bovine serum and 1% penicillin-streptomycin. The cells were maintained at 37°C in a humidified incubator with 5% CO<sub>2</sub> on 10 cm tissue-culture-treated plates. Cells tested negative for mycoplasma contamination before use for assay.

### **Cellular degradation of $\alpha$ -synuclein in HEK cells**

HEK-293T cells were cultured in 60 mm plates until reaching approximately 80% confluency. Transient transfection was performed using Xtreme Gene transfection reagent (Sigma, 6366236001) and the desired plasmid DNA. A mixture of 5  $\mu$ g of plasmid DNA 10  $\mu$ L of transfection reagent, and Opti-MEM medium was prepared and added to the cells. Protein expression was allowed for 48 hours, followed by treatment with test compounds or DMSO for 16 hours. After treatment, the cells were detached from the plate

by scraping, collected in media and PBS, and washed with PBS. The plates were also rinsed with PBS. The cell suspensions were pelleted at 300 g for 5 minutes, and the supernatant was discarded. The pellets were resuspended in ice-cold PBS, pelleted again at 300 g for 5 minutes, and the supernatant was removed. Cell lysis was performed by resuspending the pellet in RIPA buffer supplemented with protease inhibitors. The lysates were incubated on ice for 15 minutes, followed by centrifugation at 500 g for 25 minutes. The supernatant containing the total protein extract was collected, while the debris pellet was discarded. Protein concentrations were measured using the bicinchoninic acid (BCA) assay. Total protein amounts were normalized across samples to match the lowest concentration among the set. A Laemmli buffer was added to each sample, and western blot analysis was performed using the above protocol.

## Technical Replicates

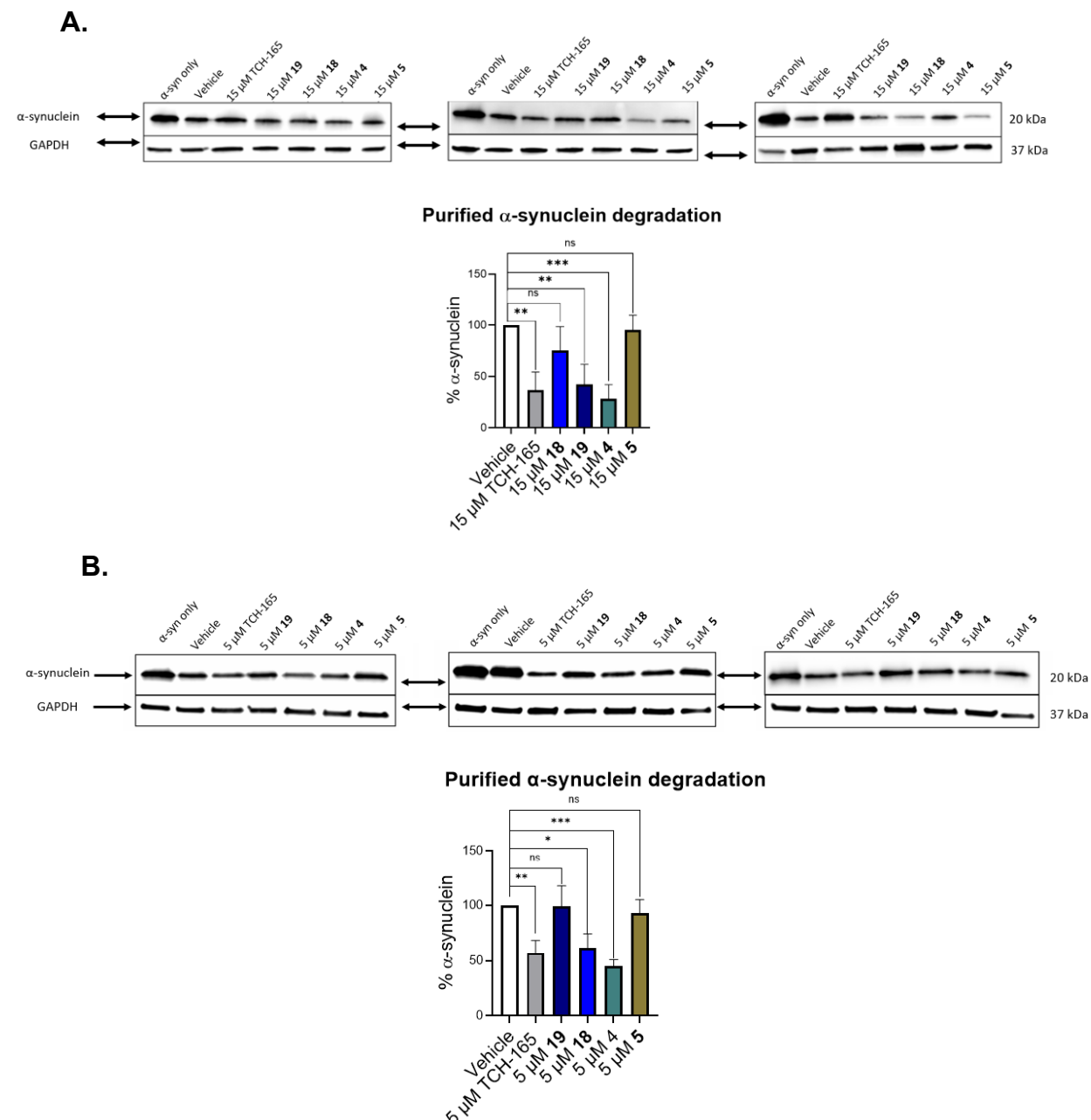


**Figure 2.34: Replicates of western blots of purified  $\alpha$ -synuclein degradation by the 20S proteasome.**

(Related to **Figure 2.3**). Westerns of  $\alpha$ -synuclein degradation by purified 20S proteasome treated with (A) 5  $\mu$ M and (B) 15  $\mu$ M of compounds 4, 5, 18, 19, and TCH-165. The quantification values were normalized to the GAPDH, and the gels shown indicate n=3 independent experiments.

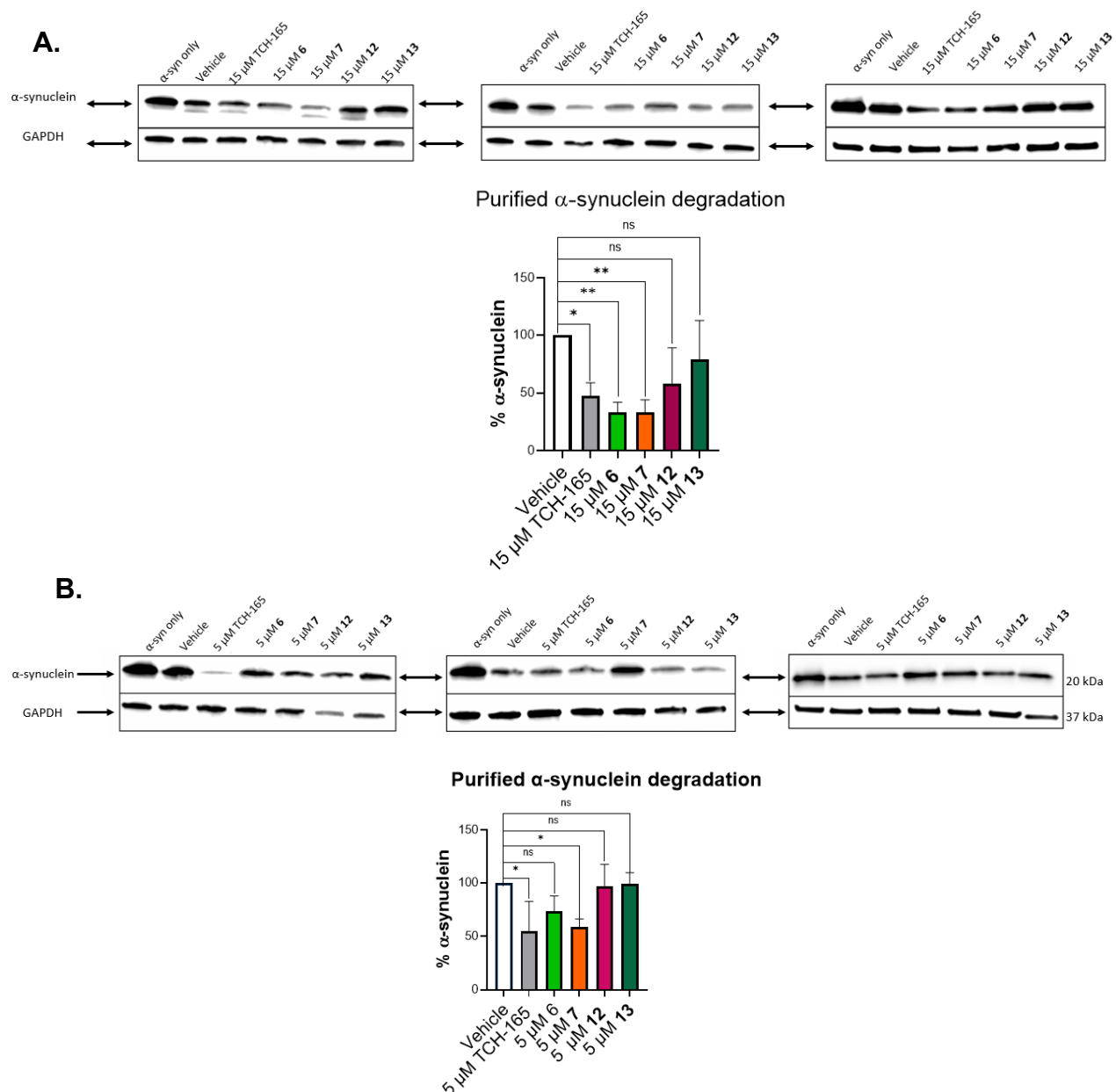


**Figure 2.35: Replicates of western blots of purified  $\alpha$ -synuclein degradation by the 20S proteasome.**

(Related to **Figure 2.3**). Westerns of  $\alpha$ -synuclein degradation by purified 20S proteasome treated with (A) 15  $\mu$ M and (B) 5  $\mu$ M of compounds **6**, **7**, **12**, **13**, and TCH-165. The quantification values were normalized to the GAPDH, and the gels shown indicate n=3 independent experiments.

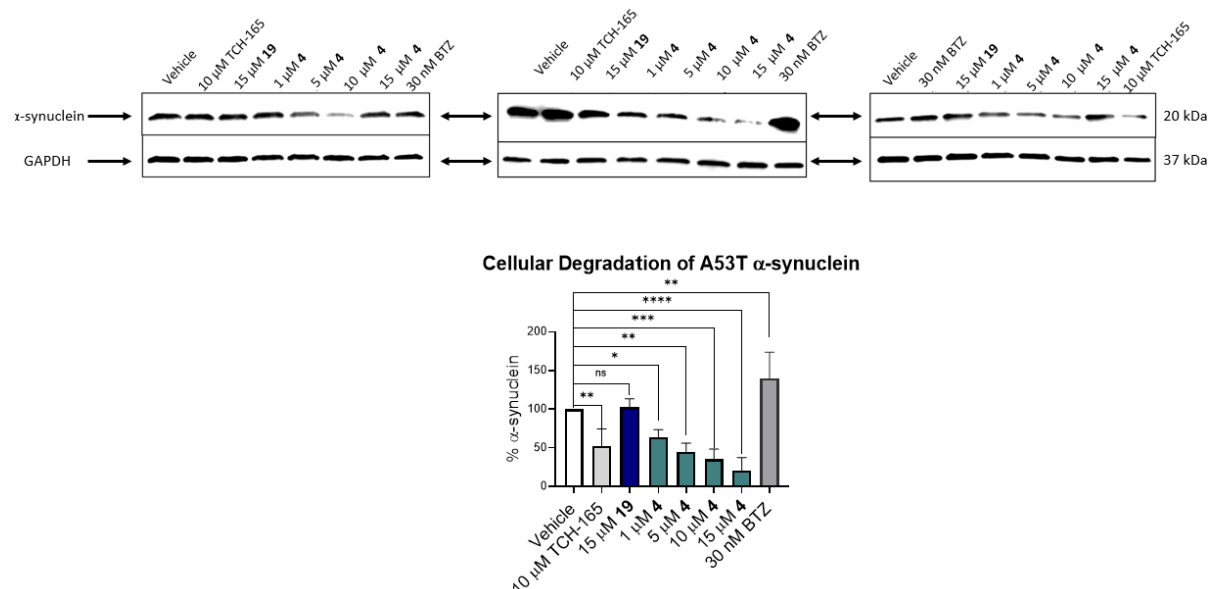


**Figure 2.36: Replicates of western blots of  $\alpha$ -synuclein degradation in HEK-293T cells.**

Related to **Figure 2.4B**. Western blots of A53T mutated  $\alpha$ -synuclein degradation in HEK-293T cells treated with vehicle (DMSO), bortezomib (BTZ), TCH-165, and compounds **4** and **19**. The quantification values were all normalized to the GAPDH, and the gels shown indicate n=3 independent experiments. Error bars are based on standard deviations.

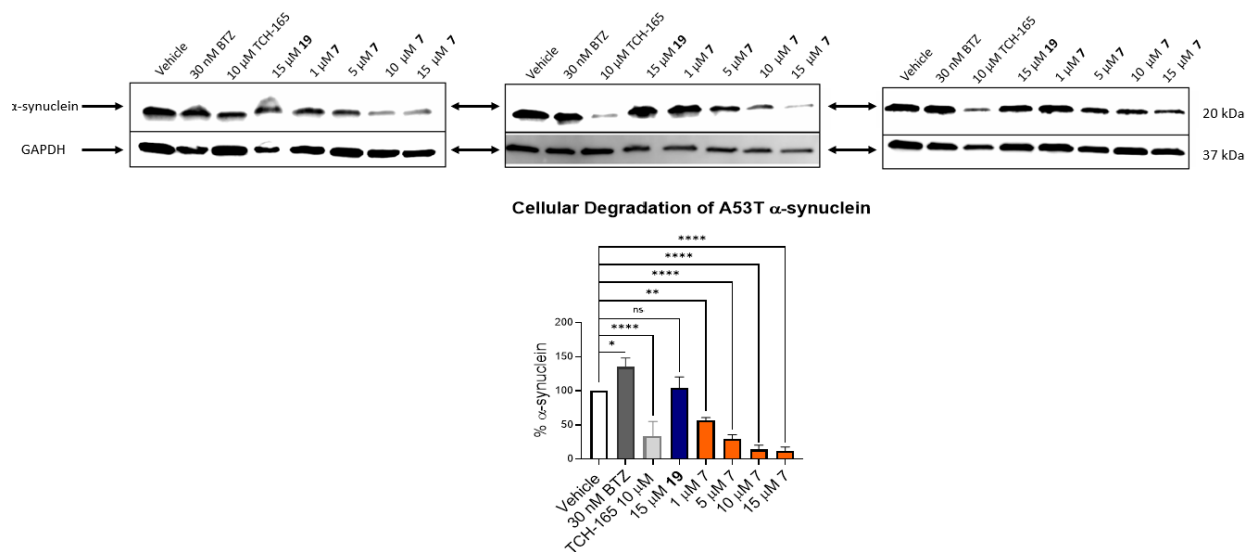


**Figure 2.37: Replicates of western blots of  $\alpha$ - synuclein degradation in HEK-293T cells.**

Related to **Figure 2.4C**. Western blots of A53T mutated  $\alpha$ -synuclein degradation in HEK-293T cells treated with vehicle (DMSO), bortezomib (BTZ), TCH-165, and compounds **7** and **19**. The quantification values were all normalized to the GAPDH, and the gels shown indicate n=3 independent experiments. Error bars are based on standard deviations.



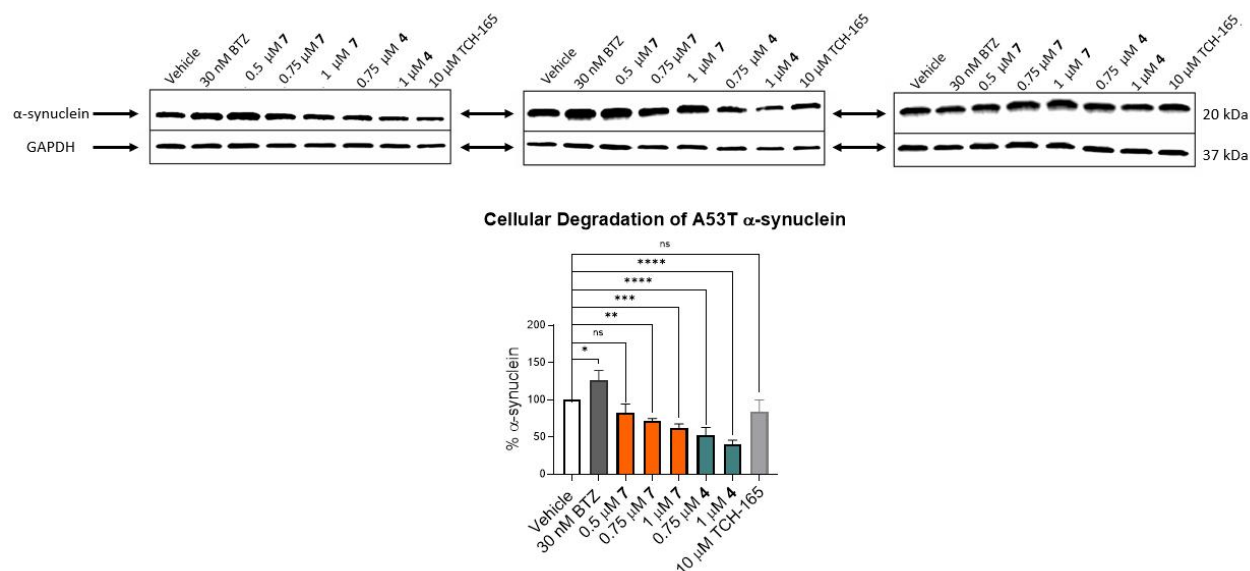


**Figure 2.38: Replicates of western blots of  $\alpha$ - synuclein degradation in HEK-293T cells.**

Related to **Figure 2.4D**. Western blots of A53T mutated  $\alpha$ -synuclein degradation in HEK-293T cells treated with vehicle (DMSO), bortezomib (BTZ), TCH-165, and compounds **4** and **7**. The quantification values were all normalized to the GAPDH, and the gels shown indicate n=3 independent experiments. Error bars are based on standard deviations.

**CHAPTER THREE:** 20S Proteasome Activation as a Therapeutic Strategy: Mitigating  
Oxidative Stress and Proteotoxicity in HT-22 cells

### 3.1 Introduction

Aging is an inevitable biological phenomenon characterized by a progressive decline in cellular and systemic functions, often culminating in increased vulnerability to various diseases.<sup>1–3</sup> The molecular and cellular underpinnings of aging encompass genomic instability,<sup>4</sup> telomere attrition<sup>5</sup>, epigenetic drift<sup>6</sup>, and a gradual breakdown in proteostasis<sup>1,2,7,8</sup>—the tightly regulated balance of protein synthesis, folding, and degradation. This decline in physiological robustness contributes significantly to the pathogenesis of numerous age-associated diseases. Age-related diseases and neurodegenerative disorders such as Alzheimer's disease (AD), Parkinson's disease (PD), and Huntington's disease (HD) stand as prominent examples.<sup>2,9</sup> These conditions diminish the quality of life for affected individuals and impose substantial societal and economic burdens on patients.

The hallmarks of these diseases are the accumulation and aggregation of misfolded proteins<sup>10,11</sup>, mitochondrial dysfunction<sup>12,13</sup>, oxidative stress<sup>12,14</sup>, and neuroinflammation<sup>13</sup>, all of which intersect with the broader mechanisms of aging. In AD, amyloid-beta plaques and hyperphosphorylated tau proteins disrupt synaptic communication.<sup>15,16</sup> In PD, the pathological aggregation of alpha-synuclein ( $\alpha$ -syn) in Lewy bodies causes dopaminergic neuronal loss.<sup>17–21</sup> Similarly, HD is characterized by the expansion of polyglutamine repeats in the huntingtin protein, leading to its aggregation and consequent neuronal toxicity.<sup>22</sup> Despite significant advances in understanding their molecular underpinnings, these disorders remain refractory to curative treatments, underscoring the pressing need for novel therapeutic strategies.

Proteostasis, the maintenance of protein homeostasis, is integral to cellular health, particularly in long-lived and metabolically active cells such as neurons. This equilibrium is maintained by a proteostasis network comprising molecular chaperones, the ubiquitin-proteasome system (UPS), and the autophagy-lysosome pathway.<sup>1,2,23</sup> These systems function synergistically to ensure the proper folding, trafficking, and degradation of proteins, thereby mitigating the accumulation of damaged or misfolded proteins.

However, with advancing age, the proteostasis network becomes increasingly compromised. Chaperones lose their efficiency, while the proteasome and autophagic systems exhibit diminished activity.<sup>24</sup> This decline is especially pronounced in neurons,

where the inability to clear misfolded proteins exacerbates the formation of toxic aggregates.<sup>15,25–27</sup> In neurodegenerative diseases, this loss of proteostasis control is a pivotal factor driving disease progression.

Oxidative stress, arising from an imbalance between reactive oxygen species (ROS), reactive nitrogen species (RNS) production, and antioxidant defenses, is another critical factor linking aging to neurodegenerative diseases. ROS and RNS are pivotal mediators in cellular physiology and pathology. They are chemically reactive molecules derived from oxygen and nitrogen, respectively, and include superoxide anion ( $O_2^-$ ), hydrogen peroxide ( $H_2O_2$ ), hydroxyl radicals ( $\bullet OH$ ), nitric oxide (NO), and peroxynitrite ( $ONOO^-$ ). While their regulated production plays critical roles in cellular signaling and homeostasis, excessive accumulation disrupts redox balance, leading to oxidative stress, a condition implicated in aging and various pathologies.<sup>28</sup> ROS are predominantly generated during aerobic respiration in the mitochondrial electron transport chain (ETC). During normal respiration, approximately 2–3% of electrons leak from the ETC and react with molecular oxygen to form superoxide, which is subsequently dismutated to  $H_2O_2$  by superoxide dismutase (SOD).<sup>10</sup>  $H_2O_2$  can be further reduced to water by catalase or glutathione peroxidase or can interact with metal ions, such as iron or copper, via the Fenton reaction to generate highly reactive  $\bullet OH$  radicals. Other cellular compartments, including the endoplasmic reticulum and peroxisomes, produce ROS during metabolic processes. RNS, on the other hand, are predominantly generated through enzymatic activity involving nitric oxide synthase (NOS).<sup>11,14,29,30</sup> This enzyme catalyzes NO production from L-arginine, which can interact with superoxide to form peroxynitrite, a potent oxidant. While NO is a key signaling molecule in vascular and immune responses, its excessive production under pathological conditions amplifies oxidative damage.<sup>28,31,32</sup>

Under physiological conditions, ROS and RNS are tightly regulated by antioxidant defenses, including enzymatic systems like SOD, catalase, and glutathione peroxidase, as well as non-enzymatic molecules such as vitamin E and glutathione.<sup>14,31,33–35</sup> These reactive species play critical roles in cellular signaling at moderate levels, influencing processes like proliferation, differentiation, and apoptosis. However, oxidative stress ensues when their production overwhelms antioxidant defenses, leading to proteins, lipids, and DNA oxidative modifications. These modifications disrupt cellular functions and

contribute to the pathogenesis of age-related diseases, including neurodegenerative disorders, cancer, and cardiovascular diseases.<sup>14</sup> Hence, the generation and regulation of ROS and RNS are integral to cellular function, but their dysregulation underpins oxidative stress. Understanding their dual role as signaling molecules and mediators of damage is essential for developing therapeutic strategies to mitigate oxidative stress-associated pathologies.

The central nervous system is particularly vulnerable to oxidative stress due to its high metabolic rate and relatively low antioxidant capacity. In the context of aging, chronic oxidative stress exacerbates proteostasis decline by impairing the function of molecular chaperones and proteolytic systems, creating a vicious cycle of protein aggregation and cellular dysfunction.<sup>27</sup> Moreover, oxidative stress-induced mitochondrial damage further amplifies ROS production, perpetuating neuronal degeneration.<sup>36</sup>

The convergence of aging-related proteostasis decline and oxidative stress establishes a fertile ground for the onset and progression of neurodegenerative diseases. As neurons age, their capacity to adapt to proteotoxic and oxidative stress diminishes, making them susceptible to AD, PD, and HD pathological features. Importantly, this susceptibility is not merely a consequence of chronological aging but is influenced by cumulative cellular damage and genetic predispositions. Emerging evidence highlights the therapeutic potential of targeting proteostasis and oxidative stress to mitigate neurodegeneration. Enhancing proteasome activity, for instance, has shown promise in reducing protein aggregation and improving cellular resilience.<sup>37–39</sup> Similarly, bolstering antioxidant defenses through pharmacological or dietary interventions holds potential for mitigating oxidative damage.<sup>12</sup> These approaches represent a paradigm shift in treating neurodegenerative diseases, moving from symptomatic management to addressing the underlying cellular dysfunctions.

Given the multifactorial nature of neuronal death in PD (**Chapter 1**), a multi-faceted strategy may offer the most promise for counteracting toxic protein aggregate accumulation and restoring proteostasis. Our recent work has demonstrated that 20S proteasome activators, specifically those based on bis(fluorophenyl)-amide scaffold with chlorocarbazole core (compound **7**, **chapter 2**), effectively reduce the accumulation of mutant A53T  $\alpha$ -synuclein in cellular models at sub-micromolar concentrations.<sup>40</sup> Here, we

extend these findings by showing that this 20S proteasome activator also confers protection against oxidative stress in HT-22 cells. This protective effect is achieved through enhanced proteolytic degradation of damaged proteins, high reduced/oxidized glutathione levels, and lower intracellular ROS levels, underscoring the therapeutic potential of proteasome activation in alleviating neurodegenerative disease pathology.

### **3.2 Rational**

The activation of the proteasome, particularly the 20S core proteasome, is emerging as a pivotal mechanism for combating age-related diseases, including neurodegenerative disorders. Proteasome activation enhances the degradation of misfolded and oxidatively damaged proteins, directly mitigating proteotoxic stress and preserving cellular homeostasis. By clearing protein aggregates, such as tau and alpha-synuclein, proteasome activation reduces cytotoxicity and improves neuronal functionality.<sup>40</sup> Reducing oxidative stress through enhanced proteasomal activity could alleviate the cellular burden of reactive oxygen species (ROS) and associated damage. These effects extend the organismal lifespan and health span, promoting resistance to stress and delaying the progression of aggregation-related pathologies. This dual intervention underscores proteasome activation as a transformative therapeutic strategy to address oxidative stress's molecular and systemic impacts.

Most interventions aimed at enhancing proteasomal activity have focused on genetic manipulations<sup>37,38</sup> or biochemical methods,<sup>41,42</sup> which, while effective in research contexts, lack pharmacological feasibility for therapeutic applications. A pharmacologically viable approach to activating the 20S proteasome holds significant promise, particularly in addressing the detrimental effects of oxidative stress. The 20S proteasome is uniquely positioned to degrade oxidized and damaged proteins in an ATP-independent manner, making it a critical component of the cellular defense against oxidative damage.<sup>43–46</sup> During oxidative stress, the 20S proteasome plays a compensatory role in maintaining proteostasis, as the ubiquitin-proteasome system often becomes overwhelmed. However, its natural activity can decline with age and under sustained oxidative conditions, accumulating proteotoxic aggregates and exacerbating cellular dysfunction.<sup>42,47,48</sup>

Developing and applying small-molecule activators targeting the 20S proteasome provides an innovative strategy to restore its proteolytic capacity. These activators are hypothesized to promote the proteasome's open-gate conformation, enhancing substrate accessibility to its catalytic core.<sup>40,49–53</sup> By facilitating the clearance of damaged or oxidized proteins, such molecules can mitigate proteotoxicity and improve cellular resilience under oxidative stress.

Furthermore, small-molecule 20S proteasome activators are advantageous due to their potential for systemic delivery, dose optimization, and target specificity. This pharmacological approach could effectively reduce the cellular burden of oxidative stress, thereby preventing or slowing the progression of age-related and oxidative stress-induced diseases, including neurodegenerative disorders like Alzheimer's and Parkinson's.

### **3.3 Results and Discussion**

#### **3.3.1 20S Proteasome Activator Does Not Offer Protection Against tBHP-Induced Toxicity in HT-22 Cells**

Research has shown increased oxidative stress could induce protein damage, ultimately leading to cell death. My first goal was to test the protective capacity of the 20S proteasome activator, compound **7**, against oxidative stress-induced cell death. To achieve this, the mouse hippocampal cell line HT-22 was used as a model system while *tert*-butyl hydroperoxide (tBHP) was used as an oxidant. TBHP is a lipid-soluble peroxide commonly used to induce oxidative stress. It generates hydroxyl radicals and superoxide upon metabolism by intracellular processes. I first performed a dose-response curve by treating HT-22 cells with varying concentrations of tBHP (160  $\mu$ M to 1.25  $\mu$ M) for 24 or 48 hours. Cell viability was assessed using the CellTiter-Glo® Luminescent Cell Viability Assay (Promega) following the manufacturer's protocol. Luminescence was measured using a microplate reader, and the results were normalized to untreated controls to determine relative cell viability.

The IC<sub>50</sub> values for the tBHP-mediated reduction of cell viability were 32.2  $\mu$ M and 40.8  $\mu$ M for 48 h and 24 h treatments, respectively (**Figure 3.1 B**).

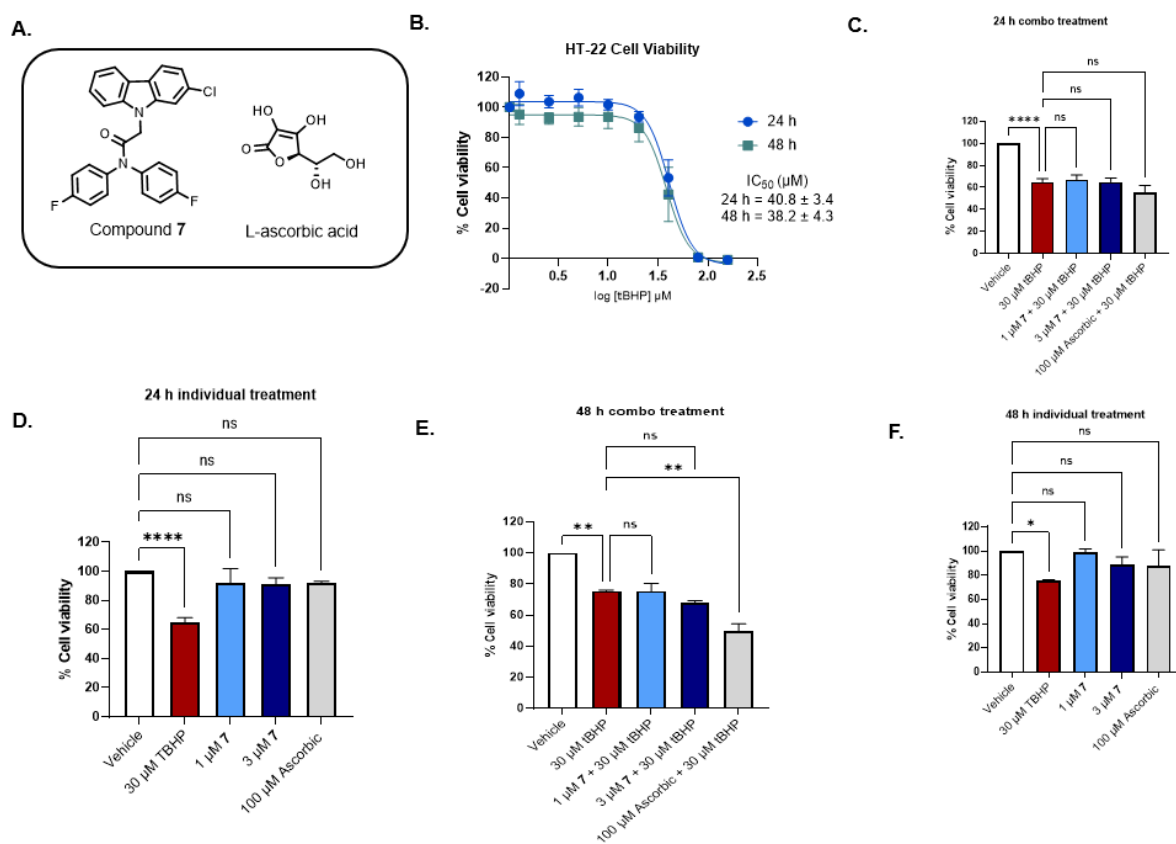


**Figure 3.1: 20S proteasome activator could not protect against tBHP-induced cell toxicity in HT-22 cells.**

(A) compound **7** and L-ascorbic acid structures. Viability of cells treated with (B) dose-response of tBHP (160 to 1.25  $\mu\text{M}$ ) for 24 and 48 h (C) cells were treated with compound **7** (1  $\mu\text{M}$  or 3  $\mu\text{M}$ ) and 100  $\mu\text{M}$  of L-ascorbic acid for 2 h before further treatment with tBHP (30  $\mu\text{M}$ ) for 24 h (D) Cells were treated individually with compound **7** (1  $\mu\text{M}$  or 3  $\mu\text{M}$ ), tBHP (30  $\mu\text{M}$ ) and 100  $\mu\text{M}$  of L-ascorbic acid for 24 h (E) cells were treated with compound **7** (1  $\mu\text{M}$  or 3  $\mu\text{M}$ ) and 100  $\mu\text{M}$  of L-ascorbic acid for 2 h before further treatment with tBHP (30  $\mu\text{M}$ ) for 48 h and (F) Cells were treated individually with compound **7** (1  $\mu\text{M}$  or 3  $\mu\text{M}$ ), tBHP (30  $\mu\text{M}$ ) and 100  $\mu\text{M}$  of L-ascorbic acid for 48 h. All experiments were done in triplicates. One-way ANOVA statistical analysis was used to determine statistical significance (ns = not significant, \* $p < 0.05$ , \*\* $p < 0.01$ , \*\*\* $p < 0.001$ , \*\*\*\* $p < 0.0001$ ). Error bars based on standard deviation.



With the dose-response of tBHP determined, the protective effect of compound **7** on oxidative stress was explored against oxidative stress induced by (tBHP). Pre-treatments with DMSO (vehicle) and compound **7** (1  $\mu$ M or 3  $\mu$ M) for 2 hours before tBHP exposure (30  $\mu$ M) provided an opportunity to evaluate dose-dependent protective effects over acute (24-hour) and prolonged (48-hour) oxidative challenges, with the inclusion of the putative antioxidant, L-ascorbic acid (100  $\mu$ M) serving as a positive control. Comparisons of cells treated with compound **7** or L-ascorbic acid alone for similar durations aimed to delineate their intrinsic antioxidative properties without exogenous oxidative insults. However, the data demonstrate that neither compound **7** (1  $\mu$ M and 3  $\mu$ M) nor L-ascorbic acid could exhibit protective effects against tBHP-induced oxidative stress in cells, as measured by cell viability (**Figure 3.1**). In the acute (24-hour) treatment groups, cells treated with tBHP alone exhibited 65.5% viability relative to the vehicle control, indicating significant oxidative damage. Co-treatment with compound **7** showed similar viability of 66.5% and 68% at 1  $\mu$ M and 3  $\mu$ M, respectively, suggesting no protective effect at these concentrations (**Figure 3.1 B**). L-ascorbic acid (100  $\mu$ M) could not overcome the oxidative damage by tBHP with a viability of 55%. When treated individually, both concentrations of compound **7** (1  $\mu$ M and 3  $\mu$ M) showed high viability (90% and 93%, respectively), comparable to L-ascorbic acid (91%), underscoring their inherent lack of toxicity. The limited improvement in cell viability upon co-treatment of compound **7** and L-ascorbic acid may somewhat mitigate oxidative stress. However, their effects are not significantly pronounced at these concentrations under acute conditions.

The 48-hour treatment outcomes reveal nuanced effects of compound **7** and L-ascorbic acid on cell viability under oxidative stress induced by (tBHP). Notably, cells treated with tBHP alone exhibited a viability of 75.5%, indicating a potential adaptive response to prolonged oxidative exposure. Co-treatment with compound **7** at 1  $\mu$ M maintained cell viability at 75.5%, mirroring the tBHP-only group, while the 3  $\mu$ M concentration reduced viability to 68%. However, these decreases in viability were not significant. Interestingly, L-ascorbic acid co-treatment significantly reduced cell viability by 49.5%, which could be attributed to its pro-oxidant activity at high concentrations, leading to increased oxidative stress and reduced cell survival (**Figure 3.1 E**). Without that, cells treated solely with compound **7** at 1  $\mu$ M and 3  $\mu$ M showed 98% and 85% viabilities, respectively, indicating

that higher concentrations may exert cytotoxic effects. L-ascorbic acid alone yielded 87% viability, consistent with its known cytoprotective properties at appropriate doses (**Figure 3.1 F**).

These findings suggest compound **7** could not exhibit protective effects against oxidative stress at the concentrations tested (1 and 3  $\mu\text{M}$ ). Conversely, L-ascorbic acid may exert pro-oxidant effects under certain conditions, leading to decreased cell viability.<sup>54</sup> Further attempts to explore the protective effect of compound **7** by varying the concentration of tBHP (20  $\mu\text{M}$  or 40  $\mu\text{M}$ ) proved unsuccessful. In addition, several factors, such as DNA damage<sup>55</sup>, mitochondrial dysfunction<sup>56</sup>, and protein misfolding or aggregation<sup>57</sup>, may precede cell death, complicating the interpretation of cell viability as a sole measure of protection. Thus, relying exclusively on cell death as a readout may fail to accurately capture the cellular mechanisms regulated by 20S proteasome activation. Complementary analyses are necessary to elucidate its role fully, such as assessing proteasomal activity, ROS levels, protein homeostasis, and the activation of stress-response pathways, to provide a comprehensive understanding of how 20S proteasome modulation impacts cellular resilience against oxidative stress.

### **3.3.2 The 20S Proteasome Activator Alleviates Oxidative Stress in HT-22 Cells by Decreasing Protein Damage and ROS Levels While Boosting Reduced Glutathione**

Protein carbonylation is an irreversible oxidative modification that introduces carbonyl groups (aldehydes and ketones) into the side chains.<sup>58</sup> This process occurs via direct oxidation of susceptible amino acids—primarily lysine (**Figure 3.2 A**), arginine, proline, and threonine—or secondary reactions with reactive carbonyl species derived from lipid peroxidation or glycoxidation. Protein carbonylation is a definitive marker of oxidative stress, indicative of irreversible protein oxidation that impairs cellular function and drives pathological states.<sup>59,60</sup> Its stability and disease relevance, especially in conditions like neurodegeneration and cancer, emphasize its diagnostic and mechanistic importance.<sup>11,61,62</sup> In this context, I investigated the impact of the 20S proteasome activator, compound **7**, on oxidative stress-induced protein damage, specifically targeting protein carbonylation. The aim is to elucidate potential proteostasis regulatory mechanisms under oxidative stress. This approach provides a direct link between

proteasome activity and mitigation of oxidative protein damage. To this end, HT-22 cells were cultured to 70% confluency and treated with DMSO or compound **7** (1  $\mu$ M or 3  $\mu$ M) for 24 or 48 hours. Cells were lysed by sonication, and protein lysates 250  $\mu$ L (1 mg/ml) were derivatized with dinitrophenyl hydrazine (DNPH). Derivatized proteins were resolved via SDS-PAGE, transferred to PVDF membranes, and probed with anti-DNP and anti- $\beta$ -actin antibodies to detect carbonylated proteins and loading control, respectively.

The results demonstrate the effect of 20S proteasome activation by compound **7** on oxidative stress-induced protein damage, as quantified by protein carbonylation levels (**Figure 3.2 B and C**). Compound **7** significantly reduced the total protein carbonylation in HT-22 cells at both 1  $\mu$ M and 3  $\mu$ M concentrations, with the reduction being more pronounced at the higher dose. After 24 hours, protein carbonylation was reduced to 67% and 53.5% of the vehicle control for 1  $\mu$ M and 3  $\mu$ M treatments, respectively (**Figure 3.2C**). This trend was sustained at 48 hours, with protein carbonylation levels of 69% for 1  $\mu$ M and 55% for 3  $\mu$ M treatments compared to the vehicle control. This suggests that compound **7**-mediated proteasome activation consistently lowers the accumulation of oxidized proteins over time (**Figure 3.2C**). The 20S proteasome, a critical component of the ubiquitin-independent proteolytic pathway, selectively degrades misfolded or carbonylated proteins, preventing aggregation and mitigating oxidative stress-induced cytotoxicity.<sup>63</sup> Additionally, Trader and coworkers reported that activation enhanced the 20S proteasome's degradation of intrinsically disordered and oxidatively damaged proteins without significantly affecting the 26S proteasome.<sup>64</sup> Compound **7** likely activates the 20S proteasome, accelerating the clearance of carbonylated proteins and reducing their steady-state levels of endogenous oxidants. This is consistent with prior studies indicating that 20S proteasome activation can act as a compensatory mechanism to maintain proteostasis in response to oxidative insults.<sup>43</sup>

Interestingly, the more significant reduction in protein carbonylation at 3  $\mu$ M suggests a dose-dependent enhancement of proteasomal activity. However, the marginal differences between 24-hour and 48-hour treatments suggest that while compound **7** increases proteasomal degradation, the initial reduction in carbonylated proteins may reach a threshold where further degradation becomes less pronounced. This may reflect a

balance between ongoing protein damage caused by oxidative stress and the proteasome's capacity to clear these modified proteins.

These findings highlight the potential of 20S proteasome activators like compound **7** as therapeutic strategies to alleviate oxidative stress-associated protein damage. By reducing the accumulation of carbonylated proteins, which are often implicated in the progression of neurodegenerative and age-related diseases, such compounds may improve cellular resilience to oxidative insults.<sup>29,65,66</sup> Future studies should explore whether sustained proteasome activation influences other aspects of proteostasis, such as the synthesis of antioxidant proteins, and whether its efficacy extends to models of chronic oxidative stress or disease.

Next, I analyzed the reduced (GSH) and oxidized glutathione (GSSG) ratio of HT-22 cells treated with compound **7**. The GSH/GSSG ratio has emerged as a promising biomarker for oxidative stress due to its central role in maintaining cellular redox balance and detoxifying reactive oxygen species (ROS).<sup>67</sup> Glutathione (GSH) directly neutralizes ROS by donating electrons, forming oxidized glutathione (GSSG), which is subsequently reduced back to GSH via glutathione reductase.<sup>68</sup> This dynamic redox cycle prevents oxidative damage to cellular components, including lipids, proteins, and DNA. Alterations in the GSH/GSSG ratio strongly correlate with oxidative stress in various conditions, such as drug-induced hepatotoxicity<sup>69,70</sup>, bacterial and viral infections, and redox imbalances in cryopreserved hepatocytes. Its sensitivity and specificity make it an invaluable tool for detecting early oxidative damage before irreversible cellular outcomes occur. HT-22 cells were seeded in 96-well plates and treated with DMSO (vehicle control) or compound **7** (1  $\mu$ M or 3  $\mu$ M) for 24 hours, and 40  $\mu$ M menadione (positive control) was added for an hour. GSH/GSSG levels were quantified using a luminescence-based assay with luciferin generation and detection reagents, and luminescence was measured on a multi-mode plate reader.

The study highlights the utility of the GSH/GSSG ratio as a biomarker for oxidative stress in HT-22 cells. It provides insights into the redox-modulating properties of compound **7**, a 20S proteasome activator. The vehicle-treated cells exhibited a baseline GSH/GSSG ratio of 47.8, representing the redox balance under normal conditions. Treatment with

compound **7** at 1  $\mu\text{M}$  and 3  $\mu\text{M}$  elevated the GSH/GSSG ratio to 56.1 and 57.1, respectively, indicating a reduction in oxidative stress (**Figure 3.2 D**).

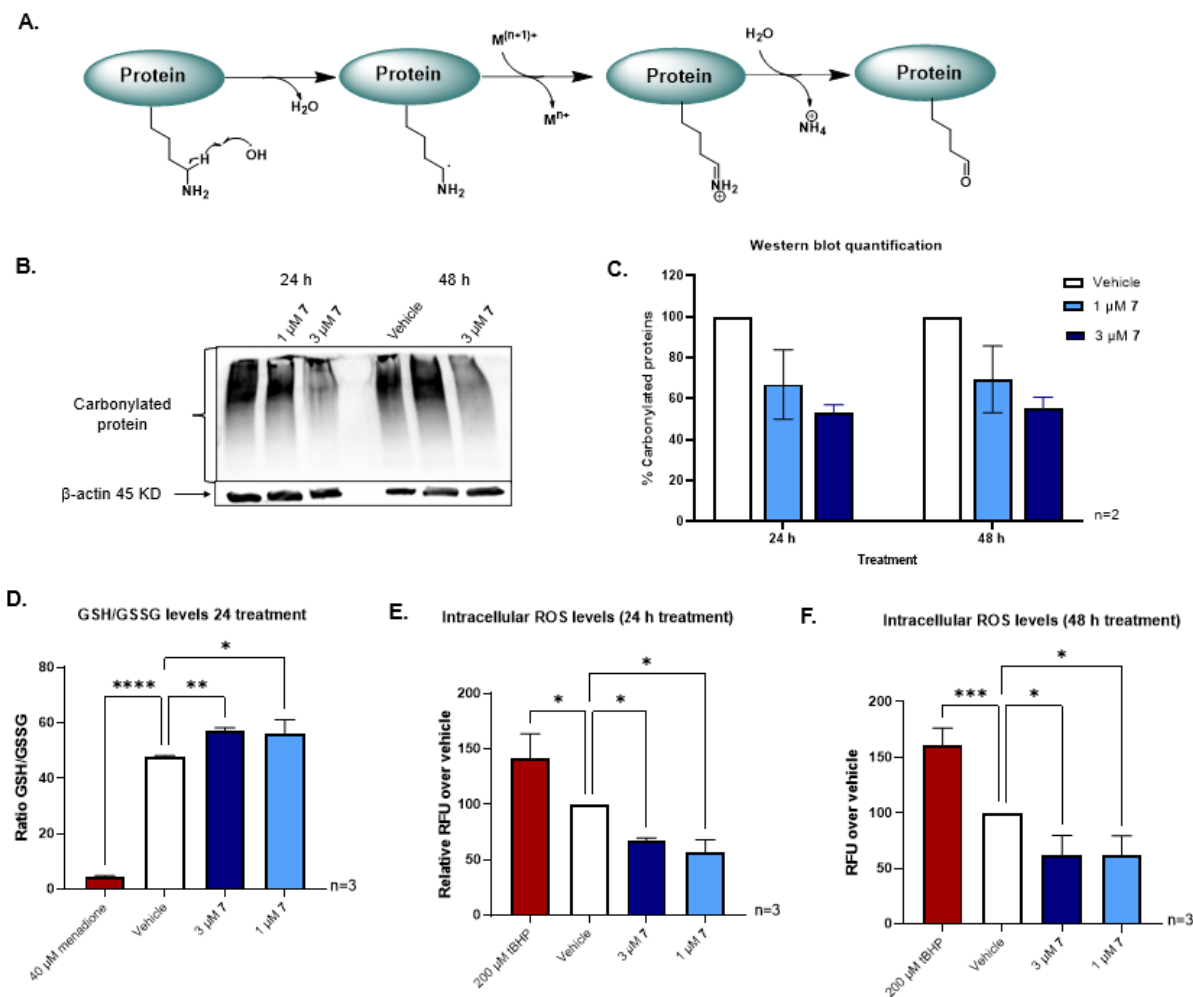


**Figure 3.2: 20S Proteasome Activator Mitigates Oxidative Stress by Reducing Protein Damage and Intracellular ROS Levels and Enhancing Reduced Glutathione in HT-22 Cells.**

(A) Mechanism of protein carbonylation on a lysine residue (B) Quantification of intracellular protein damage (carbonylation) in HT-22 cells treated with DMSO (vehicle) or compound **7** (1  $\mu\text{M}$  or 3  $\mu\text{M}$ ) for 24 or 48 h. The cell lysate was derivatized with DNPH, and derivatized samples were analyzed using Western blot. (B) Quantification of western blot (C) Quantification of GSH/GSSG ratio of HT-22 cells treated with DMSO (vehicle) or compound **7** (1  $\mu\text{M}$  or 3  $\mu\text{M}$ ) for 24 h.

### **Figure 3.2: (Cont'd)**

Quantification of intracellular ROS in HT-22 cells treated with DMSO (vehicle) or compound **7** (1  $\mu$ M or 3  $\mu$ M) for (D) 24 h or (E) 48 h. TBHP was used as positive control and was added 1 h before analysis. All experiments were done in triplicates unless otherwise stated. One-way ANOVA statistical analysis was used to determine statistical significance (ns = not significant, \* $p < 0.05$ , \*\* $p < 0.01$ , \*\*\* $p < 0.001$ , \*\*\*\* $p < 0.0001$ ). Error bars based on standard deviation.

This suggests compound **7** enhances redox homeostasis, likely through the proteasomal degradation of oxidized proteins and mitigation of oxidative damage, as supported by its demonstrated ability to reduce protein carbonylation (**Figure 3.2 B & C**). On the contrary, menadione, a potent oxidative stress inducer, caused a dramatic reduction in the GSH/GSSG ratio to 4.4, reflecting severe redox imbalance. Menadione generates ROS via redox cycling, depleting reduced glutathione and increasing oxidized glutathione levels, exacerbating oxidative stress (**Figure 3.2 D**).<sup>71,72</sup> The striking contrast between the effects of menadione and compound **7** underscores the sensitivity of the GSH/GSSG ratio in capturing cellular redox status and oxidative stress severity.

The increase in the GSH/GSSG ratio with compound **7** treatment can be attributed to its activation of the 20S proteasome, which facilitates the removal of oxidized and damaged proteins. This proteolytic mechanism prevents protein aggregation and reduces the cellular oxidative burden, indirectly preserving glutathione pools. The dose-dependent effects observed further suggest that 20S proteasome activation plays a significant role in maintaining cellular redox balance. These findings corroborate evidence that the GSH/GSSG ratio is a reliable indicator of oxidative stress and supports the therapeutic potential of 20S proteasome activators like compound **7** in mitigating oxidative damage.<sup>69,70,73</sup> Morikawa *et al.* showed that exposure of cultured human airway epithelial cells to ozone caused a transient shift in the intracellular glutathione redox state, decreasing the reduced glutathione (GSH) ratio to oxidized glutathione (GSSG). However, pretreatment with a reduced glutathione ester (GSH-OEt) suppressed IL-8 production, mitigating the inflammatory response.<sup>74</sup> Future studies should explore the long-term effects of compound **7** on redox balance and its efficacy under conditions of

chronic oxidative stress or *in vivo* models of neurodegenerative diseases, where protein aggregation and oxidative damage are key pathological features.

I next focused on evaluating intracellular ROS levels to elucidate the underlying factors contributing to the observed decrease in reduced GSH levels. This investigation will provide insights into whether the depletion of GSH is primarily driven by increased oxidative stress, enhanced ROS production, or other mechanisms, such as disrupted glutathione recycling or excessive protein oxidation. By quantifying ROS levels and correlating them with changes in the GSH/GSSG ratio, the analysis aims to identify the specific oxidative pathways at play and clarify the impact of compound **7** on cellular redox dynamics. This approach will further enhance our understanding of the redox-regulatory role of 20S proteasome activation on oxidative stress. The intracellular ROS levels in HT-22 cells were assessed by culturing cells in DMEM with sodium pyruvate until 70% confluency, followed by seeding in 96-well plates ( $10^4$  cells/well) and overnight incubation. Cells were treated with DMSO (control), compound **7** (1  $\mu$ M or 3  $\mu$ M), or tBHP (positive control) for 48 hours. After washing with HBSS, cells were incubated with CM-DCFDA dye at 37 °C for 30 minutes. Fluorescence (excitation: 487 nm; emission: 528 nm) was measured using a plate reader to quantify intracellular ROS.

After 24 hours of treatment, ROS levels were reduced to 57% and 67% at 1  $\mu$ M and 3  $\mu$ M concentrations of compound **7**, respectively, compared to control. However, tBHP-treated cells displayed a marked increase in ROS, reaching 141%. Similarly, at 48 hours, ROS levels with compound **7** treatment were maintained at 62% (1  $\mu$ M) and 61% (3  $\mu$ M), whereas tBHP-induced oxidative stress further elevated ROS to 161%. These results demonstrate the capacity of compound **7** to mitigate ROS accumulation over both time points despite varying concentrations.

Compound **7**'s ROS attenuation aligns with its action mechanism as a 20S proteasome activator. Compound **7** reduces the burden of damaged proteins by enhancing proteolytic degradation of carbonylated proteins, thereby alleviating ROS amplification pathways and maintaining intracellular redox balance. Increased carbonylated proteins can overwhelm the proteostasis network, contributing to cellular damage. This effect is particularly significant, given that oxidative stress, characterized by excessive ROS levels, disrupts

cellular homeostasis, damages biomolecules, and contributes to the pathology of neurodegenerative diseases, cancer, and aging.<sup>11,27,47,59</sup>

Furthermore, the observed stabilization of ROS levels with compound **7** treatment may be indirectly linked to glutathione (GSH) metabolism. Glutathione, a key cellular antioxidant, operates as a first line of defense against oxidative damage by scavenging ROS and maintaining redox homeostasis.<sup>77</sup> Excessive ROS levels deplete reduced GSH pools, shifting the GSH/GSSG ratio and exacerbating oxidative stress. By mitigating ROS, compound **7** may preserve intracellular GSH, preventing its overutilization and maintaining an optimal GSH/GSSG ratio. This preservation of glutathione pools further supports cellular resilience against oxidative insults.

In contrast, the pronounced ROS elevation in tBHP-treated cells underscores the pathological consequences of unregulated ROS production. tBHP-induced oxidative stress exemplifies the damage from an overwhelmed antioxidant system, reinforcing the significance of proteasomal degradation in managing oxidative damage. These findings position compound **7** as a potential therapeutic strategy for diseases driven by oxidative stress and protein aggregation, including Parkinson's disease, Alzheimer's disease, and amyotrophic lateral sclerosis. Future studies should explore the long-term efficacy of compound **7** under chronic oxidative stress conditions and its effects on broader antioxidant systems.

### **3.3.2 The 20S Proteasome Activator Induces Selective Proteolysis and Maintains Mitochondrial Integrity**

The activation of the 20S proteasome has emerged as a novel and promising therapeutic approach for combating neurodegenerative diseases, including Alzheimer's disease (AD), Parkinson's disease (PD), and multiple system atrophy (MSA). These disorders share common pathological hallmarks, such as the accumulation of misfolded or aberrant proteins, including tau, alpha-synuclein, which disrupt cellular homeostasis and lead to neurotoxicity.<sup>24–26,48</sup> By selectively enhancing the proteolytic degradation of such pathogenic proteins, 20S proteasome activation offers a targeted strategy to alleviate protein aggregation and restore cellular function.

However, a critical barrier to the clinical application of 20S proteasome activators lies in their ability to discriminate between aberrant proteins and those essential for normal



cellular processes. Non-selective degradation could disrupt proteostasis and compromise vital cellular pathways, leading to unintended consequences. This challenge underscores the importance of advancing our understanding of the selectivity mechanisms underlying 20S proteasome activation and its impact on the global proteome. Without ensuring specificity, the therapeutic potential of this approach remains limited.

To address this pivotal challenge, we undertook a detailed proteomic analysis of HT-22 cells treated compound **7** compared to vehicle-treated controls. Our objective was to evaluate the scope and specificity of proteolytic degradation induced by compound **7**. This investigation aimed to identify the subset of proteins targeted by 20S proteasome activation and assess the potential off-target effects that could compromise mitochondrial integrity, cellular signaling, or other critical functions. Such a targeted approach is essential to refine the therapeutic window of 20S proteasome activators and minimize their risk profile. HT-22 cells were treated with compound **7** (1  $\mu$ M) or vehicle control for 24 hours (n=3 per group). The collected samples were digested using trypsin and labeled with tandem mass tag (TMT) 6-plex reagents. After pooling the labeled peptide samples, the peptide mixture was subjected to two-dimensional LC-MS/MS for proteomic analysis. Statistically significant differences in protein expression between the treated and control groups identify proteins modulated by compound **7** exposure. I undertook cell culturing and lysate preparation. Subsequent sample preparation, proteomic data acquisition, and data processing were performed in collaboration with Professor Zhang's lab at the University of Virginia Medical School.

Additionally, this study sought to explore the broader impact of 20S proteasome activation on cellular processes, particularly its effect on mitochondrial function. Mitochondrial dysfunction is a hallmark of many neurodegenerative diseases, and ensuring the integrity of mitochondrial membrane potential under proteasome activation is crucial for developing safe therapies. By demonstrating that 20S proteasome activation preserves mitochondrial function while selectively targeting pathogenic proteins, this work provides critical insights into the feasibility of this approach for long-term clinical application.

In the current study, the global proteomic profiling of HT-22 cells treated with compound **7**, a 20S proteasome activator, revealed selective and significant modulation of protein expression. A total of 7,348 proteins were identified, among which 146 proteins exhibited

downregulation ( $>25\%$ ,  $p < 0.05$ ), with 11 proteins showing reductions  $\geq 50\%$ . In contrast, 26 proteins were upregulated ( $>25\%$ ,  $p < 0.05$ ), with 5 demonstrating  $\geq 50\%$  increase (**Figure 3.3 A**).

The proteomic profiling of HT-22 cells treated with compound **7**, a 20S proteasome activator, provides valuable insights into its selective modulation of protein expression. The identification of 7,348 proteins highlights the breadth of this analysis and underscores the wide-ranging potential effects of compound **7** within the cellular environment. Of particular interest is the selective nature of the observed protein expression changes.

The downregulation of 146 proteins, with 11 exceeding a reduction of 50%, suggests that compound **7** preferentially targets specific proteins for enhanced degradation (**Figure 3.3 C**). This aligns with the known activity of 20S proteasome activators, which promote the degradation of intrinsically disordered or damaged proteins without ubiquitin tagging.<sup>45,63</sup> Such specificity may have therapeutic implications, particularly in the context of neurodegenerative disorders where the accumulation of misfolded or damaged proteins plays a pivotal role.

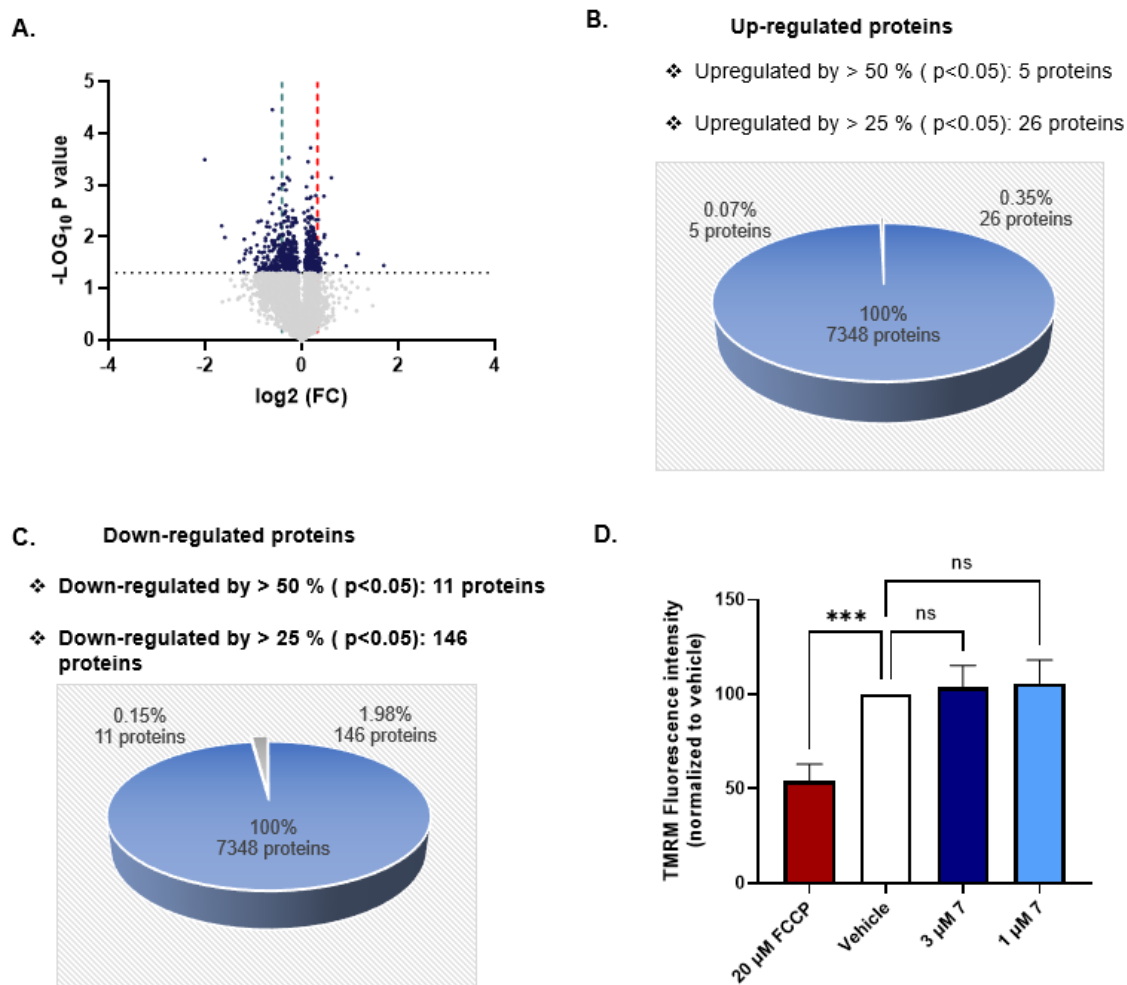


**Figure 3.3: Compound 7 Does Not Significantly Impact the General Proteome and Maintains Mitochondrial Integrity in HT-22 Cells.**

(A) The volcano plot shows the significantly changing proteins in trypsin digestion followed by tandem mass tags proteomic analysis. The red line delineates increased protein abundance upon (red,  $\log_2(\text{CF}) > 0.32$ , adj. P value  $< 0.05$ ) and a decrease in protein abundance (teal,  $\log_2(\text{CF}) < -0.42$ , adj. P value,  $0.05$ ) or no significant change (light gray) upon treatment with  $1 \mu\text{M}$  of compound **7** for 24 h. Pie chart showing the number of proteins that are significantly (B) up-regulated, (C) down-regulated, (D) Relative TMRM fluorescence intensity of HT-22 cells treated with DMSO (vehicle) of  $1 \mu\text{M}$  of compound **7** for 24 h.

### **Figure 3.3: (Cont'd)**

For positive control, cells were treated with 20  $\mu$ M of FCP 20 minutes before TMRM loading. One-way ANOVA statistical analysis was used to determine statistical significance (ns = not significant, \* $p < 0.05$ , \*\* $p < 0.01$ , \*\*\* $p < 0.001$ , \*\*\*\* $p < 0.0001$ ). Error bars based on standard deviation.

On the other hand, the upregulation of 26 proteins, with 5 showing increases greater than 50%, might reflect compensatory cellular responses to enhanced proteasomal activity (**Figure 3.3B**). These proteins could represent pathways activated to counterbalance the heightened degradation or may indicate indirect effects of compound **7** on cellular systems, such as stress response or metabolic reprogramming.

These results demonstrate that compound **7**'s activity is not indiscriminate, as only a small fraction of the proteome exhibits significant modulation. This selective action is a critical feature for therapeutic strategies aimed at targeting pathological proteins while minimizing unintended cellular disruptions. Future studies should focus on characterizing the identity and functional roles of the significantly affected proteins to elucidate the broader implications of these findings and to refine the therapeutic potential of 20S proteasome activators like compound **7**.

These findings align with prior studies suggesting that 20S proteasome activation primarily targets proteins with disordered regions or oxidative modifications for degradation while sparing structured, functional proteins.<sup>50,51</sup> This selectivity minimizes the risk of indiscriminate proteolysis, a critical factor in maintaining cellular integrity during therapeutic interventions. The modest subset of proteins affected by compound **7** highlights its specificity, as less than 2.5% of the proteome showed significant changes in expression. Such precision is essential for therapeutic applications, as the uncontrolled degradation of essential proteins could impair critical cellular functions. A similar study reported that HEK-293 cells treated with Btz caused many changes in protein levels, affecting 29% of proteins (>50%,  $P < 0.05$ ) compared to the vehicle control. However, 20S proteasome activators MO and AM had a much smaller impact, changing 11% and 5.8% of proteins (>50%,  $P < 0.05$ ), respectively.<sup>64</sup> This observation was attributed to the indiscriminate inhibition of all proteasome isoforms by Btz, causing widespread changes

in protein levels and cellular systems, while 20S CP activators are designed to specifically target only the 20S CP isoform of the proteasome.

The upregulation of specific proteins suggests that 20S proteasome activation may indirectly influence oxidative stress and proteostasis pathways. For instance, degradation of damaged proteins can alleviate oxidative burdens, as oxidized proteins act as secondary sources of reactive oxygen species (ROS) if not promptly cleared. Furthermore, the downregulation of proteins with a >50% decrease in abundance may reflect the 20S proteasome's role in selectively targeting proteins prone to aggregation, such as alpha-synuclein and p25 $\alpha$ , as supported by our previous studies.<sup>40,49–53</sup>

The proteomic analysis revealed that more than 50% of proteins downregulated were mitochondrial-associated proteins, many of which play crucial roles in oxidative stress regulation and cellular metabolism. This finding necessitated an investigation into the underlying mechanisms driving this downregulation. Specifically, it was essential to determine whether the reduction in these mitochondrial proteins resulted from compound **7**'s protective effects in mitigating oxidative stress or indicative of a detrimental impact on mitochondrial function.

Mitochondria are critical for maintaining cellular energy homeostasis, redox balance, and apoptosis regulation. Any compromise to mitochondrial health can precipitate widespread cellular dysfunction, including bioenergetic failure, increased reactive oxygen species (ROS) production, and activation of cell death pathways.<sup>78–80</sup> Thus, the downregulation of mitochondrial proteins raised a pertinent concern regarding the potential unintended effects of compound **7** on mitochondrial integrity. Given the dual role of mitochondria in both energy production and ROS generation, the proteasome's role in modulating mitochondrial-associated proteins could profoundly influence cellular homeostasis.

I evaluated mitochondrial integrity using mitochondrial membrane potential as a functional readout to elucidate whether the downregulation of mitochondrial proteins reflected a protective response or a pathological perturbation. Changes in mitochondrial membrane potential is a robust indicator of mitochondrial health, as it reflects the proton gradient across the inner mitochondrial membrane—a critical driver of ATP synthesis through oxidative phosphorylation.<sup>81</sup> A loss of mitochondrial membrane potential typically signifies

mitochondrial dysfunction, impaired bioenergetics, and increased susceptibility to oxidative stress.<sup>79,80,82</sup>

By measuring mitochondrial membrane potential, we sought to determine whether compound **7** preserved mitochondrial functionality while selectively reducing the abundance of stress-related mitochondrial proteins. This analysis is crucial, as maintaining mitochondrial integrity is a prerequisite for the therapeutic viability of 20S proteasome activators in oxidative stress and neurodegenerative disease models.

To assess mitochondrial membrane potential ( $\Delta\Psi_m$ ) in HT-22 cells treated with DMSO or compound **7** (1  $\mu$ M), cells were plated in 96-well plates, treated with either DMSO (vehicle control), compound **7** (1  $\mu$ M), or p-trifluoromethoxyphenylhydrazine, FCCP (20  $\mu$ M) as a positive control, and loaded with tetramethylrhodamine, methyl ester, perchlorate (TMRM). Fluorescence was measured using a plate reader, and data were normalized to vehicle control. Fluorescence intensities were compared between treatments to evaluate ( $\Delta\Psi_m$ ) changes, with FCCP serving as a validation control. Experiments were conducted in triplicate to ensure reliability.

The assessment of mitochondrial membrane potential ( $\Delta\Psi_m$ ) in HT-22 cells treated with compound **7** and FCCP revealed that compound **7** had no significant impact on  $\Delta\Psi_m$  at the tested concentrations, while the positive control, FCCP, caused a marked and statistically significant reduction. In vehicle-treated cells,  $\Delta\Psi_m$  was normalized to 100% as a comparison baseline. Treatment with compound **7** (1  $\mu$ M and 3  $\mu$ M) resulted in  $\Delta\Psi_m$  levels of 105% and 103%, respectively, both of which were not **statistically** significantly different ( $p > 0.005$ ) from the vehicle control (**Figure 3.3 D**). These results indicate that compound **7** does not affect mitochondrial membrane potential at the concentrations tested, suggesting that it lacks direct modulatory effects on mitochondrial function within this experimental context. In contrast, cells treated with FCCP, a known mitochondrial uncoupler, exhibited a substantial reduction in  $\Delta\Psi_m$  to 54%, which was statistically significant ( $P \leq 0.01$ ). FCCP acts by dissipating the proton gradient across the inner mitochondrial membrane, thereby reducing  $\Delta\Psi_m$  and validating the sensitivity and reliability of the TMRM assay.<sup>83</sup>

In summary, the data underscore the specificity of compound **7**, which does not impact mitochondrial membrane potential under the tested conditions, while highlighting the

robust response to FCCP, reinforcing the utility of this assay for detecting alterations in  $\Delta\Psi_m$ . Further studies may be required to evaluate the effects of compound **7** under different conditions or at higher concentrations. Still, these findings strongly suggest that it does not compromise mitochondrial function at the concentrations tested.

Furthermore, a lack of adverse effects on mitochondrial function would reinforce the specificity and safety of compound **7** as a modulator of proteostasis and oxidative balance. The results of this investigation could provide critical insights into the interplay between proteasome activation, mitochondrial health, and oxidative stress resilience, thereby informing the development of targeted therapeutic strategies.

### **3.4 Conclusions**

This study highlights the therapeutic potential and specificity of compound **7**, a small-molecule 20S proteasome activator, in modulating proteostasis and oxidative stress in neuronal cells. By selectively enhancing the degradation of damaged and oxidized proteins, compound **7** reduces oxidative protein damage and intracellular reactive oxygen species while preserving mitochondrial integrity, as evidenced by stable mitochondrial membrane potential. Notably, the compound demonstrated no significant off-target effects on mitochondrial function or general protein abundance, underscoring its safety profile. The proteomic analysis revealed targeted modulation of a small subset of proteins, with downregulation predominantly observed in oxidatively stressed and aggregation-prone proteins. This selectivity minimizes the risk of indiscriminate proteolysis, a critical consideration for therapeutic viability. Furthermore, the observed increase in the reduced/oxidized glutathione ratio supports the role of 20S proteasome activation in maintaining cellular redox balance under oxidative stress.

While compound **7** demonstrated significant protective effects at lower concentrations, its efficacy against acute oxidative challenges, such as tBHP-induced toxicity, was limited, suggesting a need for optimization in experimental conditions or combination therapies. The robust response to FCCP validates the assay sensitivity and reinforces the importance of mitochondrial health as a functional readout in assessing therapeutic interventions. These findings establish a foundation for further investigations into the long-term effects of 20S proteasome activation in models of chronic oxidative stress and neurodegenerative diseases. Future studies should explore the broader systemic impact

of proteasome activation, particularly in vivo, to elucidate its full therapeutic potential and safety profile. The selective and multifaceted actions of compound **7** position it as a promising candidate for mitigating oxidative damage and proteotoxic stress in neurodegenerative disorders and related pathologies.



## REFERENCES

- (1) Kaushik, S.; Cuervo, A. M. Proteostasis and Aging. *Nat. Med.* **2015**, *21* (12), 1406–1415. <https://doi.org/10.1038/nm.4001>.
- (2) Farooqui, T.; Farooqui, A. A. Aging: An Important Factor for the Pathogenesis of Neurodegenerative Diseases. *Mech. Ageing Dev.* **2009**, *130* (4), 203–215. <https://doi.org/10.1016/j.mad.2008.11.006>.
- (3) Santos, D. F.; Simão, S.; Nóbrega, C.; Bragança, J.; Castelo-Branco, P.; Araújo, I. M. Oxidative Stress and Aging: Synergies for Age Related Diseases. *FEBS Lett.* **2024**, *598* (2), 2074–2091. <https://doi.org/10.1002/1873-3468.14995>.
- (4) Maslov, A. Y.; Vijg, J. Genome Instability, Cancer and Aging. *Biochim. Biophys. Acta - Gen. Subj.* **2009**, *1790* (10), 963–969. <https://doi.org/10.1016/j.bbagen.2009.03.020>.
- (5) Rossiello, F.; Jurk, D.; Passos, J. F.; d’Adda di Fagagna, F. Telomere Dysfunction in Ageing and Age-Related Diseases. *Nat. Cell Biol.* **2022**, *24* (2), 135–147. <https://doi.org/10.1038/s41556-022-00842-x>.
- (6) Teschendorff, A. E.; West, J.; Beck, S. Age-Associated Epigenetic Drift: Implications, and a Case of Epigenetic Thrift? *Hum. Mol. Genet.* **2013**, *22* (R1), 7–15. <https://doi.org/10.1093/hmg/ddt375>.
- (7) Hipp, M. S.; Kasturi, P.; Hartl, F. U. The Proteostasis Network and Its Decline in Ageing. *Nat. Rev. Mol. Cell Biol.* **2019**, *20* (7), 421–435. <https://doi.org/10.1038/s41580-019-0101-y>.
- (8) Konovalova, J.; Gerasymchuk, D.; Parkkinen, I.; Chmielarz, P.; Domanskyi, A. Interplay between MicroRNAs and Oxidative Stress in Neurodegenerative Diseases. *Int. J. Mol. Sci.* **2019**, *20* (23). <https://doi.org/10.3390/ijms20236055>.
- (9) Baker, D. J.; Petersen, R. C. Cellular Senescence in Brain Aging and Neurodegenerative Diseases: Evidence and Perspectives. *J. Clin. Invest.* **2018**, *128* (4), 1208–1216. <https://doi.org/10.1172/JCI95145>.
- (10) Ulfig, A.; Jakob, U. Cellular Oxidants and the Proteostasis Network: Balance between Activation and Destruction. *Trends Biochem. Sci.* **2024**, *49* (9), 761–774. <https://doi.org/10.1016/j.tibs.2024.07.001>.
- (11) Baraibar, M. A.; Liu, L.; Ahmed, E. K.; Friguet, B. Protein Oxidative Damage at the Crossroads of Cellular Senescence, Aging, and Age-Related Diseases. *Oxid. Med. Cell. Longev.* **2012**, *2012*. <https://doi.org/10.1155/2012/919832>.
- (12) Maharjan, S.; Oku, M.; Tsuda, M.; Hoseki, J.; Sakai, Y. Mitochondrial Impairment Triggers Cytosolic Oxidative Stress and Cell Death Following Proteasome Inhibition. *Sci. Rep.* **2014**, *4*, 1–11. <https://doi.org/10.1038/srep05896>.
- (13) Marchi, S.; Guilbaud, E.; Tait, S. W. G.; Yamazaki, T.; Galluzzi, L. Mitochondrial Control of Inflammation. *Nat. Rev. Immunol.* **2023**, *23* (3), 159–173. <https://doi.org/10.1038/s41577-022-00760-x>.

- (14) Cenini, G.; Lloret, A.; Cascella, R. Oxidative Stress in Neurodegenerative Diseases: From a Mitochondrial Point of View. *Oxid. Med. Cell. Longev.* **2019**, 2019. <https://doi.org/10.1155/2019/2105607>.
- (15) Sadigh-Eteghad, S.; Sabermarouf, B.; Majdi, A.; Talebi, M.; Farhoudi, M.; Mahmoudi, J. Amyloid-Beta: A Crucial Factor in Alzheimer's Disease. *Med. Princ. Pract.* **2015**, 24 (1), 1–10. <https://doi.org/10.1159/000369101>.
- (16) Hampel, H.; Hardy, J.; Blennow, K.; Chen, C.; Perry, G.; Kim, S. H.; Villemagne, V. L.; Aisen, P.; Vendruscolo, M.; Iwatsubo, T.; Masters, C. L.; Cho, M.; Lannfelt, L.; Cummings, J. L.; Vergallo, A. The Amyloid- $\beta$  Pathway in Alzheimer's Disease. *Molecular Psychiatry*. 2021, pp 5481–5503. <https://doi.org/10.1038/s41380-021-01249-0>.
- (17) Gibb WRG; Lees AJ. Occasional Review: The Relevance of the Lewy Body to the Pathogenesis of Idiopathic Parkinson's Disease. *J Neurol Neurosurg Psychiatry* **1998**, 51 (6), 745–752.
- (18) Osterhaus, A.; Groen, J.; Bildt, M. Van De; Martina, B.; Vos, J.; Egmond, H. Van. A -Synuclein In Lewy Bodies. *Nature* **1997**, 388, 839–840.
- (19) Gómez-Benito, M.; Granado, N.; García-Sanz, P.; Michel, A.; Dumoulin, M.; Moratalla, R. Modeling Parkinson's Disease With the Alpha-Synuclein Protein. *Front. Pharmacol.* **2020**, 11 (April), 1–15. <https://doi.org/10.3389/fphar.2020.00356>.
- (20) Fields, C. R.; Bengoa-Vergniory, N.; Wade-Martins, R. Targeting Alpha-Synuclein as a Therapy for Parkinson's Disease. *Front. Mol. Neurosci.* **2019**, 12 (December), 1–14. <https://doi.org/10.3389/fnmol.2019.00299>.
- (21) Espay, A. J.; McFarthing, K. Alpha-Synuclein and the Parkinson's Disease Drug Pipeline. *Park. Relat. Disord.* **2023**, 111 (April), 105432. <https://doi.org/10.1016/j.parkreldis.2023.105432>.
- (22) Illarioshkin, S. N.; Klyushnikov, S. A.; Vigont, V. A.; Seliverstov, Y. A.; Kaznacheyeva, E. V. Molecular Pathogenesis in Huntington's Disease. *Biochem.* **2018**, 83 (9), 1030–1039. <https://doi.org/10.1134/s0006297918090043>.
- (23) Keller, J. N.; Hanni, K. B.; Markesbery, W. R. Possible Involvement of Proteasome Inhibition in Aging: Implications for Oxidative Stress. *Mech. Ageing Dev.* **2000**, 113 (1), 61–70. [https://doi.org/10.1016/S0047-6374\(99\)00101-3](https://doi.org/10.1016/S0047-6374(99)00101-3).
- (24) Thibaut, T. A.; Anderson, R. T.; Smith, D. M. A Common Mechanism of Proteasome Impairment by Neurodegenerative Disease-Associated Oligomers. *Nat. Commun.* **2018**, 9 (1), 1–13. <https://doi.org/10.1038/s41467-018-03509-0>.
- (25) Soto, C.; Estrada, L. D. Protein Misfolding and Neurodegeneration. *Arch. Neurol.* **2008**, 65 (2), 184–189. <https://doi.org/10.1001/archneurol.2007.56>.
- (26) Chi, H.; Chang, H. Y.; Sang, T. K. Neuronal Cell Death Mechanisms in Major Neurodegenerative Diseases. *Int. J. Mol. Sci.* **2018**, 19 (10). <https://doi.org/10.3390/ijms19103082>.

- (27) Martínez, A.; Portero-Otin, M.; Pamplona, R.; Ferrer, I. Protein Targets of Oxidative Damage in Human Neurodegenerative Diseases with Abnormal Protein Aggregates. *Brain Pathol.* **2010**, *20* (2), 281–297. <https://doi.org/10.1111/j.1750-3639.2009.00326.x>.
- (28) Puspita, L.; Chung, S. Y.; Shim, J. W. Oxidative Stress and Cellular Pathologies in Parkinson's Disease. *Mol. Brain* **2017**, *10* (1), 1–12. <https://doi.org/10.1186/s13041-017-0340-9>.
- (29) Trist, B. G.; Hare, D. J.; Double, K. L. Oxidative Stress in the Aging Substantia Nigra and the Etiology of Parkinson's Disease. *Aging Cell* **2019**, *18* (6), 1–23. <https://doi.org/10.1111/accel.13031>.
- (30) Iakovou, E.; Kourti, M. A Comprehensive Overview of the Complex Role of Oxidative Stress in Aging, The Contributing Environmental Stressors and Emerging Antioxidant Therapeutic Interventions. *Front. Aging Neurosci.* **2022**, *14* (June), 1–29. <https://doi.org/10.3389/fnagi.2022.827900>.
- (31) Aborode, A. T.; Pustake, M.; Awuah, W. A.; Alwerdani, M.; Shah, P.; Yarlagadda, R.; Ahmad, S.; Silva Correia, I. F.; Chandra, A.; Nansubuga, E. P.; Abdul-Rahman, T.; Mehta, A.; Ali, O.; Amaka, S. O.; Zuñiga, Y. M. H.; Shkodina, A. D.; Inya, O. C.; Shen, B.; Alexiou, A. Targeting Oxidative Stress Mechanisms to Treat Alzheimer's and Parkinson's Disease: A Critical Review. *Oxid. Med. Cell. Longev.* **2022**, *2022*. <https://doi.org/10.1155/2022/7934442>.
- (32) Niedzielska, E.; Smaga, I.; Gawlik, M.; Moniczewski, A.; Stankowicz, P.; Pera, J.; Filip, M. Oxidative Stress in Neurodegenerative Diseases. *Mol. Neurobiol.* **2016**, *53* (6), 4094–4125. <https://doi.org/10.1007/s12035-015-9337-5>.
- (33) Afzal, S.; Abdul Manap, A. S.; Attiq, A.; Albokhadaim, I.; Kandeel, M.; Alhojaily, S. M. From Imbalance to Impairment: The Central Role of Reactive Oxygen Species in Oxidative Stress-Induced Disorders and Therapeutic Exploration. *Front. Pharmacol.* **2023**, *14* (October), 1–22. <https://doi.org/10.3389/fphar.2023.1269581>.
- (34) Pisoschi, A. M.; Pop, A.; Iordache, F.; Stanca, L.; Predoi, G.; Serban, A. I. Oxidative Stress Mitigation by Antioxidants - An Overview on Their Chemistry and Influences on Health Status. *Eur. J. Med. Chem.* **2021**, *209*, 112891. <https://doi.org/10.1016/j.ejmech.2020.112891>.
- (35) Korovesis, D.; Rubio-Tomás, T.; Tavernarakis, N. Oxidative Stress in Age-Related Neurodegenerative Diseases: An Overview of Recent Tools and Findings. *Antioxidants* **2023**, *12* (1). <https://doi.org/10.3390/antiox12010131>.
- (36) Deger, J. M.; Gerson, J. E.; Kaye, R. The Interrelationship of Proteasome Impairment and Oligomeric Intermediates in Neurodegeneration. *Aging Cell* **2015**, *14* (5), 715–724. <https://doi.org/10.1111/accel.12359>.
- (37) Choi, W. H.; De Poot, S. A. H.; Lee, J. H.; Kim, J. H.; Han, D. H.; Kim, Y. K.; Finley, D.; Lee, M. J. Open-Gate Mutants of the Mammalian Proteasome Show Enhanced Ubiquitin-Conjugate Degradation. *Nat. Commun.* **2016**, *7*. <https://doi.org/10.1038/ncomms10963>.

- (38) Anderson, R. T.; Bradley, T. A.; Smith, D. M. Hyperactivation of the Proteasome in *Caenorhabditis Elegans* Protects against Proteotoxic Stress and Extends Lifespan. *J. Biol. Chem.* **2022**, 298 (10), 102415. <https://doi.org/10.1016/j.jbc.2022.102415>.
- (39) Han, D. H.; Na, H. K.; Choi, W. H.; Lee, J. H.; Kim, Y. K.; Won, C.; Lee, S. H.; Kim, K. P.; Kuret, J.; Min, D. H.; Lee, M. J. Direct Cellular Delivery of Human Proteasomes to Delay Tau Aggregation. *Nat. Commun.* **2014**, 5. <https://doi.org/10.1038/ncomms6633>.
- (40) Staerz, S. D.; Anamoah, C.; Tepe, J. J. 20S Proteasome Enhancers Prevent Cytotoxic Tubulin Polymerization-Promoting Protein Induced  $\alpha$ -Synuclein Aggregation. *iScience* **2024**, 27 (7), 110166. <https://doi.org/10.1016/j.isci.2024.110166>.
- (41) Chondrogianni, N.; Georgila, K.; Kourtis, N.; Tavernarakis, N.; Gonos, E. S. 20S Proteasome Activation Promotes Life Span Extension and Resistance to Proteotoxicity in *Caenorhabditis Elegans*. *FASEB J.* **2015**, 29 (2), 611–622. <https://doi.org/10.1096/fj.14-252189>.
- (42) Jung, S. H.; Jae, S. H.; Chang, I.; Kim, S. Age-Associated Decrease in Proteasome Content and Activities in Human Dermal Fibroblasts: Restoration of Normal Level of Proteasome Subunits Reduces Aging Markers in Fibroblasts from Elderly Persons. *Journals Gerontol. - Ser. A Biol. Sci. Med. Sci.* **2007**, 62 (5), 490–499. <https://doi.org/10.1093/gerona/62.5.490>.
- (43) Reinheckel, T.; Sitte, N.; Ullrich, O.; Kuckelkorn, U.; Davies, K. J. A.; Grune, T. Comparative Resistance of the 20 S and 26 S Proteasome to Oxidative Stress. *Biochem. J.* **1998**, 335 (3), 637–642. <https://doi.org/10.1042/bj3350637>.
- (44) Sahu, I.; Mali, S. M.; Sulkshane, P.; Xu, C.; Rozenberg, A.; Morag, R.; Sahoo, M. P.; Singh, S. K.; Ding, Z.; Wang, Y.; Day, S.; Cong, Y.; Kleifeld, O.; Brik, A.; Glickman, M. H. The 20S as a Stand-Alone Proteasome in Cells Can Degrade the Ubiquitin Tag. *Nat. Commun.* **2021**, 12 (1), 1–61. <https://doi.org/10.1038/s41467-021-26427-0>.
- (45) Deshmukh, F. K.; Yaffe, D.; Olshina, M. A.; Ben-Nissan, G.; Sharon, M. The Contribution of the 20s Proteasome to Proteostasis. *Biomolecules* **2019**, 9 (5). <https://doi.org/10.3390/biom9050190>.
- (46) Pickering, A. M.; Staab, T. A.; Tower, J.; Sieburth, D.; Davies, K. J. A. A Conserved Role for the 20S Proteasome and Nrf2 Transcription Factor in Oxidative Stress Adaptation in Mammals, *Caenorhabditis Elegans* and *Drosophila Melanogaster*. *J. Exp. Biol.* **2013**, 216 (4), 543–553. <https://doi.org/10.1242/jeb.074757>.
- (47) Vilchez, D.; Saez, I.; Dillin, A. The Role of Protein Clearance Mechanisms in Organismal Ageing and Age-Related Diseases. *Nat. Commun.* **2014**, 5. <https://doi.org/10.1038/ncomms6659>.
- (48) Ciechanover, A.; Kwon, Y. T. Degradation of Misfolded Proteins in Neurodegenerative Diseases: Therapeutic Targets and Strategies. *Exp. Mol. Med.* **2015**, 47 (3), e147. <https://doi.org/10.1038/EMM.2014.117>.

- (49) Jones, C. L.; Njomen, E.; Sjögren, B.; Dexheimer, T. S.; Tepe, J. J. Small Molecule Enhancement of 20S Proteasome Activity Targets Intrinsically Disordered Proteins. *ACS Chem. Biol.* **2017**, *12* (9), 2240–2247. <https://doi.org/10.1021/acschembio.7b00489>.
- (50) Njomen, E.; Osmulski, P. A.; Jones, C. L.; Gaczynska, M.; Tepe, J. J. Small Molecule Modulation of Proteasome Assembly. *Biochemistry* **2018**, *57* (28), 4214–4224. <https://doi.org/10.1021/acs.biochem.8b00579>.
- (51) Staerz, S. D.; Jones, C. L.; Tepe, J. J. Design, Synthesis, and Biological Evaluation of Potent 20S Proteasome Activators for the Potential Treatment of  $\alpha$ -Synucleinopathies. *J. Med. Chem.* **2022**, *65* (9), 6631–6642. <https://doi.org/10.1021/acs.jmedchem.1c02158>.
- (52) Fiolek, T. J.; Magyar, C. L.; Wall, T. J.; Davies, S. B.; Campbell, M. V.; Savich, C. J.; Tepe, J. J.; Mosey, R. A. Dihydroquinazolines Enhance 20S Proteasome Activity and Induce Degradation of  $\alpha$ -Synuclein, an Intrinsically Disordered Protein Associated with Neurodegeneration. *Bioorganic Med. Chem. Lett.* **2021**, *36*. <https://doi.org/10.1016/j.bmcl.2021.127821>.
- (53) Fiolek, T. J.; Keel, K. L.; Tepe, J. J. Fluspirilene Analogs Activate the 20S Proteasome and Overcome Proteasome Impairment by Intrinsically Disordered Protein Oligomers. *ACS Chem. Neurosci.* **2021**, *12* (8), 1438–1448. <https://doi.org/10.1021/acschemneuro.1c00099>.
- (54) Przybyło, M.; Langner, M. On the Physiological and Cellular Homeostasis of Ascorbate. *Cell. Mol. Biol. Lett.* **2020**, *25* (1). <https://doi.org/10.1186/s11658-020-00223-y>.
- (55) Iqbal, M. J.; Kabeer, A.; Abbas, Z.; Siddiqui, H. A.; Calina, D.; Sharifi-Rad, J.; Cho, W. C. Interplay of Oxidative Stress, Cellular Communication and Signaling Pathways in Cancer. *Cell Commun. Signal.* **2024**, *22* (1), 1–16. <https://doi.org/10.1186/s12964-023-01398-5>.
- (56) Orthopaedic Surgery - 2022 - Wang - Mitochondrial Dysfunction in Oxidative Stress-Mediated Intervertebral Disc Degeneration.Pdf.
- (57) Xin, X.; Gong, T.; Hong, Y. Hydrogen Peroxide Initiates Oxidative Stress and Proteomic Alterations in Meningothelial Cells. *Sci. Rep.* **2022**, *12* (1), 1–10. <https://doi.org/10.1038/s41598-022-18548-3>.
- (58) Kehm, R.; Baldensperger, T.; Raupbach, J.; Höhn, A. Protein Oxidation - Formation Mechanisms, Detection and Relevance as Biomarkers in Human Diseases. *Redox Biol.* **2021**, *42*. <https://doi.org/10.1016/j.redox.2021.101901>.
- (59) Weitzel, K.; Chemie, F.; Rev, M. S.; Introduction, I.; Reference, C. Bond-Dissociation Energies of Cations — Pushing The. *WHO Libr. Cat. Data* **2011**, No. i, 221–235. <https://doi.org/10.1002/mas>.
- (60) Martínez-Orgado, J.; Martínez-Vega, M.; Silva, L.; Romero, A.; de Hoz-Rivera, M.; Villa, M.; del Pozo, A. Protein Carbonylation as a Biomarker of Oxidative Stress and

- a Therapeutic Target in Neonatal Brain Damage. *Antioxidants* **2023**, *12* (10), 1–13. <https://doi.org/10.3390/antiox12101839>.
- (61) Rodríguez-García, A.; García-Vicente, R.; Morales, M. L.; Ortiz-Ruiz, A.; Martínez-López, J.; Linares, M. Protein Carbonylation and Lipid Peroxidation in Hematological Malignancies. *Antioxidants* **2020**, *9* (12), 1–30. <https://doi.org/10.3390/antiox9121212>.
  - (62) Akagawa, M. Protein Carbonylation: Molecular Mechanisms, Biological Implications, and Analytical Approaches. *Free Radic. Res.* **2021**, *55* (4), 307–320. <https://doi.org/10.1080/10715762.2020.1851027>.
  - (63) Sahu, I.; Mali, S. M.; Sulkshane, P.; Xu, C.; Rozenberg, A.; Morag, R.; Sahoo, M. P.; Singh, S. K.; Ding, Z.; Wang, Y.; Day, S.; Cong, Y.; Kleifeld, O.; Brik, A.; Glickman, M. H. The 20S as a Stand-Alone Proteasome in Cells Can Degrade the Ubiquitin Tag. *Nat. Commun.* **2021**, *12* (1). <https://doi.org/10.1038/s41467-021-26427-0>.
  - (64) Coleman, R. A.; Mohallem, R.; Aryal, U. K.; Trader, D. J. Protein Degradation Profile Reveals Dynamic Nature of 20S Proteasome Small Molecule Stimulation. *RSC Chem. Biol.* **2021**, *2* (2), 636–644. <https://doi.org/10.1039/d0cb00191k>.
  - (65) Lee, M. H.; Hyun, D. H.; Marshall, K. A.; Ellerby, L. M.; Bredesen, D. E.; Jenner, P.; Halliwell, B. Effect of Overexpression of Bcl-2 on Cellular Oxidative Damage, Nitric Oxide Production, Antioxidant Defenses, and the Proteasome. *Free Radic. Biol. Med.* **2001**, *31* (12), 1550–1559. [https://doi.org/10.1016/S0891-5849\(01\)00633-5](https://doi.org/10.1016/S0891-5849(01)00633-5).
  - (66) Salmon, A. B.; Richardson, A.; Pérez, V. I. Update on the Oxidative Stress Theory of Aging: Does Oxidative Stress Play a Role in Aging or Healthy Aging? *Free Radic. Biol. Med.* **2010**, *48* (5), 642–655. <https://doi.org/10.1016/j.freeradbiomed.2009.12.015>.
  - (67) Frijhoff, J.; Winyard, P. G.; Zarkovic, N.; Davies, S. S.; Stocker, R.; Cheng, D.; Knight, A. R.; Taylor, E. L.; Oettrich, J.; Ruskovska, T.; Gasparovic, A. C.; Cuadrado, A.; Weber, D.; Poulsen, H. E.; Grune, T.; Schmidt, H. H. H. W.; Ghezzi, P. Clinical Relevance of Biomarkers of Oxidative Stress. *Antioxidants Redox Signal.* **2015**, *23* (14), 1144–1170. <https://doi.org/10.1089/ars.2015.6317>.
  - (68) Deponte, M. Glutathione Catalysis and the Reaction Mechanisms of Glutathione-Dependent Enzymes. *Biochim. Biophys. Acta - Gen. Subj.* **2013**, *1830* (5), 3217–3266. <https://doi.org/10.1016/j.bbagen.2012.09.018>.
  - (69) Gumprich, E.; Devereaux, M. W.; Dahl, R. H.; Sokol, R. J. Glutathione Status of Isolated Rat Hepatocytes Affects Bile Acid-Induced Cellular Necrosis but Not Apoptosis. *Toxicol. Appl. Pharmacol.* **2000**, *164* (1), 102–111. <https://doi.org/10.1006/taap.2000.8894>.
  - (70) Cao, L.; Waldon, D.; Teffera, Y.; Roberts, J.; Wells, M.; Langley, M.; Zhao, Z. Ratios of Biliary Glutathione Disulfide (GSSG) to Glutathione (GSH): A Potential Index to Screen Drug-Induced Hepatic Oxidative Stress in Rats and Mice. *Anal. Bioanal. Chem.* **2013**, *405* (8), 2635–2642. <https://doi.org/10.1007/s00216-012-6661-8>.

- (71) Criddle, D. N.; Gillies, S.; Baumgartner-wilson, H. K.; Jaffar, M.; Chinje, E. C.; Passmore, S.; Chvanov, M.; Barrow, S.; Gerasimenko, O. V; Tepikin, A. V; Sutton, R.; Petersen, O. H. Menadione-Induced Reactive Oxygen Species Generation via Redox Cycling Promotes Apoptosis of Murine Pancreatic Acinar Cells \*. *J. Biol. Chem.* **2006**, *281* (52), 40485–40492. <https://doi.org/10.1074/jbc.M607704200>.
- (72) Malorni, W.; Iosi, F.; Santini, M. T.; Testa, U.; Ultrastructures, D.; Superiore, I.; Elena, V. R. Menadione-Induced Oxidative Stress Leads to a Rapid down-Modulation of Transferrin Receptor Recycling. **1993**, *318*, 309–318.
- (73) Sentellas, S.; Morales-Ibanez, O.; Zanuy, M.; Albertí, J. J. GSSG/GSH Ratios in Cryopreserved Rat and Human Hepatocytes as a Biomarker for Drug Induced Oxidative Stress. *Toxicol. Vitro.* **2014**, *28* (5), 1006–1015. <https://doi.org/10.1016/j.tiv.2014.04.017>.
- (74) Todokoro, M.; Mochizuki, H.; Tokuyama, K.; Utsugi, M.; Dobashi, K.; Mori, M.; Morikawa, A. Effect of Ozone Exposure on Intracellular Glutathione Redox State in Cultured Human Airway Epithelial Cells. **2004**, *28* (2), 0–9.
- (75) Ezraty, B.; Gennaris, A.; Barras, F.; Collet, J. F. Oxidative Stress, Protein Damage and Repair in Bacteria. *Nat. Rev. Microbiol.* **2017**, *15* (7), 385–396. <https://doi.org/10.1038/nrmicro.2017.26>.
- (76) Goldberg, A. L. Protein Degradation and Protection against Misfolded or Damaged Proteins. *Nature* **2003**, *426* (6968), 895–899. <https://doi.org/10.1038/nature02263>.
- (77) Kwon, D. H.; Cha, H.; Lee, H.; Hong, S.; Park, C.; Park, S.; Kim, G.; Kim, S.; Kim, H.; Hwang, H.; Choi, Y. H. Protective Effect of Glutathione against Oxidative Macrophages through Activating the Nuclear Factor Oxygenase-1 Pathway. **2019**, *2*. <https://doi.org/10.3390/antiox8040082>.
- (78) San-Millán, I. The Key Role of Mitochondrial Function in Health and Disease. *Antioxidants* **2023**, *12* (4). <https://doi.org/10.3390/antiox12040782>.
- (79) Osellame, L. D.; Blacker, T. S.; Duchon, M. R. Cellular and Molecular Mechanisms of Mitochondrial Function. *Best Pract. Res. Clin. Endocrinol. Metab.* **2012**, *26* (6), 711–723. <https://doi.org/10.1016/j.beem.2012.05.003>.
- (80) Suomalainen, A.; Nunnari, J. Mitochondria at the Crossroads of Health and Disease. *Cell* **2024**, *187* (11), 2601–2627. <https://doi.org/10.1016/j.cell.2024.04.037>.
- (81) Zorova, L. D.; Popkov, V. A.; Plotnikov, E. J.; Silachev, D. N.; Pevzner, I. B.; Jankauskas, S. S.; Zorov, S. D.; Babenko, V. A.; Zorov, D. B. Functional Significance of the Mitochondrial Membrane Potential. *Biochem. Suppl. Ser. A Membr. Cell Biol.* **2018**, *12* (1), 20–26. <https://doi.org/10.1134/S1990747818010129>.
- (82) Madeira, V. M. C. *Overview of Mitochondrial Bioenergetics*; 2012; Vol. 810. [https://doi.org/10.1007/978-1-61779-382-0\\_1](https://doi.org/10.1007/978-1-61779-382-0_1).
- (83) Connolly, N. M. C.; Theurey, P.; Adam-Vizi, V.; Bazan, N. G.; Bernardi, P.; Bolaños,

J. P.; Culmsee, C.; Dawson, V. L.; Deshmukh, M.; Duchen, M. R.; Düssmann, H.; Fiskum, G.; Galindo, M. F.; Hardingham, G. E.; Hardwick, J. M.; Jekabsons, M. B.; Jonas, E. A.; Jordán, J.; Lipton, S. A.; Manfredi, G.; Mattson, M. P.; McLaughlin, B. A.; Methner, A.; Murphy, A. N.; Murphy, M. P.; Nicholls, D. G.; Polster, B. M.; Pozzan, T.; Rizzuto, R.; Satrústegui, J.; Slack, R. S.; Swanson, R. A.; Swerdlow, R. H.; Will, Y.; Ying, Z.; Joselin, A.; Gioran, A.; Moreira Pinho, C.; Watters, O.; Salvucci, M.; Llorente-Folch, I.; Park, D. S.; Bano, D.; Ankarcrona, M.; Pizzo, P.; Prehn, J. H. M. *Guidelines on Experimental Methods to Assess Mitochondrial Dysfunction in Cellular Models of Neurodegenerative Diseases*; Springer US, 2018; Vol. 25. <https://doi.org/10.1038/s41418-017-0020-4>.



## **APPENDIX**

### **Methods**

#### **Cell culture**

HT-22 cells, a murine hippocampal cell line, were cultured in Dulbecco's Modified Eagle Medium (DMEM) supplemented with 10% (v/v) fetal bovine serum (FBS) and 1% (v/v) penicillin-streptomycin. Cells were maintained in a humidified incubator at 37°C with 5% CO<sub>2</sub> to ensure optimal growth conditions. For passaging, cells at approximately 70% confluency were rinsed with sterile phosphate-buffered saline (PBS) to remove residual medium and detached using 0.25% trypsin-EDTA. The trypsinization reaction was terminated by adding complete DMEM medium, and the cell suspension was centrifuged at 300×g for 3 minutes. The pellet was resuspended in fresh complete medium, and cells were seeded into new culture vessels at an appropriate density.

Cells were routinely monitored under a phase-contrast microscope to assess confluency and morphology. Medium was replaced every 48 hours, and cells were passed every 3–4 days to maintain healthy, actively growing cultures. All experiments were conducted using cells at passage numbers 4–10 to ensure consistency and reproducibility. Cells tested negative for mycoplasma contamination prior to being used for experiments.

#### **Cell viability assay**

HT-22 cells were cultured in Dulbecco's Modified Eagle Medium (DMEM) supplemented with sodium pyruvate under standard culture conditions (37°C, 5% CO<sub>2</sub>). For experiments, cells were seeded in 96-well plates at densities of  $1.0 \times 10^4$  or  $1.5 \times 10^4$  cells per well (100 µL) and allowed to adhere overnight. The medium was then replaced with DMEM without sodium pyruvate, and cells were incubated for 30 minutes prior to treatment. Cells were subsequently exposed to DMSO (vehicle control) or tert-butyl hydroperoxide (tBHP) for 24 or 48 hours. Cell viability was quantified using the CellTiter-Glo® luminescence assay, following the manufacturer's protocol, with luminescence measured using a microplate reader.

#### **Quantification of protein damage (carbonylation)**

HT-22 cells were cultured . Once cells reached 70% confluency, they were treated with DMSO or compound 7 (1 and 3 µM) for 24 or 48 h. Adherent cells were detached using 0.25% trypsin-EDTA, neutralized with complete DMEM, or directly scraped following PBS

washing. The cell suspension was collected in a centrifuge tube and pelleted by centrifugation at 300×g for 5 minutes at 4°C. The supernatant was discarded, and the pellet was washed once with ice-cold PBS. Cells were lysed using iced cold PBS supplemented with protease and phosphatase inhibitors (Roche). The pellet was resuspended in 100 µl of ice-cold lysis buffer and lysed by sonication. The lysates were clarified by centrifugation at 2,000×g for 15 minutes at 4°C, and the supernatant containing soluble proteins was transferred to a fresh pre-chilled microcentrifuge tube. Protein concentrations were determined using a BCA or Bradford assay, and samples were normalized for downstream applications. Lysates were stored at –80°C for long-term storage or kept on ice for immediate use in assays.

Protein carbonylation was assessed using a dinitrophenylhydrazine (DNPH) derivatization method. Protein samples (1 mg/ml) were mixed with 10 mM DNPH solution (100 µl to 500 µl protein) and incubated in the dark at room temperature for 60 minutes, with vortexing every 15 minutes. Proteins were precipitated by adding 20% trichloroacetic acid (TCA, 600 µl), incubating on ice for 15 minutes, followed by centrifugation at 10,000 × g for 10 minutes at 4°C. The supernatants were discarded, and pellets were washed once with 20% TCA (500 µl) and vortexed before further centrifugation under identical conditions. The pellets were subsequently washed with 1:1 ethanol: ethyl acetate (v/v, 500 µl) three times to remove free DNPH and air-dried for 5 minutes to ensure complete solvent evaporation.

Protein pellets were resuspended in 0.2% SDS prepared in 20 mM Tris–HCl (pH 6.8, 100 µl) and heated at 95°C for 5 minutes to ensure complete solubilization. Protein concentrations were determined using a BCA assay and normalized to 0.31 µg/ml (40 µl) for electrophoresis. Samples were mixed with 5 µl of loading buffer, heated at 95°C for 5 minutes, and separated on a 4–20% Tris-glycine SDS-PAGE gel. Proteins were transferred to a PVDF membrane using the iBlot-3 semidry transfer system. The membrane was blocked with 5% milk in TBST at room temperature for 1 hour and probed with a mouse anti-DNP antibody (1:1000 dilution in 2% milk/TBST) for 1 hour. After two 10-minute washes in TBST, an anti-mouse HRP-conjugated secondary antibody (1:1000 in 2% milk/TBST) was applied for 1 hour. Chemiluminescence was detected using Radiance Plus reagent (Azure Biosystems).

The membrane was washed twice with water and stripped using mild stripping buffer for 30 minutes at room temperature. After washing in TBST for 30 minutes, the membrane was re-probed with a mouse  $\beta$ -actin-HRP antibody (1:1000 in 2% milk/TBST) for 1 hour. Imaging was performed as described above, and protein levels were quantified by densitometric analysis using ImageLab software (Bio-Rad).

### **Quantification of intracellular ROS**

HT-22 cells at 70% confluence were seeded at  $1.0 \times 10^4$  cells per well overnight in 96-well plates with opaque side walls, followed by treatment with DMSO or Compound 7 (1  $\mu$ M and 3  $\mu$ M) for 24 h or 48 h. For positive control, cells were treated with 200  $\mu$ M tBHP for 30 minutes. After treatment, cells were loaded with 10  $\mu$ M CM-H<sub>2</sub>DCFDA in prewarmed HBSS. The cells were then incubated in the dark for 30 min at 37 °C in a humidified 5% CO<sub>2</sub> atmosphere. The wells were then washed three times with warm HBSS, and the fluorescence was measured using a Biotek Synergy Neo 3 plate reader with an excitation wavelength of 487 nm and an emission wavelength of 529 nm. The fluorescence of the DMSO treated sample was set to 100%.

### **Measurement of GSH/GSSH levels**

HT-22 cells were cultured in DMEM supplemented with sodium pyruvate until reaching approximately 70% confluency. Cells were plated in 96-well plates at a density of  $1 \times 10^4$  cells per well (100  $\mu$ L) and allowed to adhere overnight. Treatments were performed using DMSO (vehicle control) or SS-4-15 at concentrations of 1  $\mu$ M or 3  $\mu$ M for 24 hours. For the positive control, cells were exposed to 40  $\mu$ M menadione for 1 hour. Following treatment, cells were washed once with cold HBSS buffer to remove residual compounds. Cell lysis was performed using 50  $\mu$ L of either total or oxidized glutathione reagent, incubating for 5 minutes at room temperature. Subsequently, 50  $\mu$ L of luciferin generation reagent was added, and the plate was incubated for 30 minutes. To complete the reaction, 100  $\mu$ L of luciferin detection reagent was added, and the plate was equilibrated at room temperature for 15 minutes. Luminescence was measured using the Synergy Neo3 multi-mode plate reader at room temperature.

**CHAPTER FOUR:** Development of Novel Small Molecule Activators of the 20S  
Proteasome Based on Piperazinone Scaffold

## 4.1 Introduction

The proteostasis network orchestrates a delicate equilibrium between protein synthesis and degradation, encompassing ribosomal machinery, molecular chaperones, and proteolytic systems.<sup>1–4</sup> This network exhibits remarkable adaptability and robustness under homeostatic conditions, swiftly counteracting proteomic perturbations to preserve cellular stability. However, proteostasis becomes progressively impaired with age, culminating in the accumulation of misfolded or aggregation-prone proteins and ensuing proteotoxicity.<sup>1,5,6</sup> Such disruptions are strongly implicated in the pathogenesis of neurodegenerative disorders, as the aggregation of intrinsically disordered proteins (IDPs) such as tau and  $\alpha$ -synuclein perturbs neuronal function in Alzheimer's and Parkinson's diseases, respectively.<sup>7–9</sup> Therapeutic strategies to mitigate IDP concentrations present a promising avenue for addressing these conditions, particularly as they remain refractory to conventional small-molecule interventions.<sup>10,11</sup>

Central to proteostasis are two degradation pathways: the ubiquitin-proteasome system (UPS) and the autophagy-lysosome pathway.<sup>12</sup> The proteasome, a pivotal component of the UPS, comprises the 26S holoenzyme, which includes the 20S core particle (CP) and one or two 19S regulatory particles (RPs).<sup>12–14</sup> The 20S CP adopts a barrel-like architecture formed by four heptameric rings: two outer  $\alpha$ -rings and two inner  $\beta$ -rings. Among the seven  $\beta$  subunits, three ( $\beta$ 1,  $\beta$ 2, and  $\beta$ 5) confer distinct proteolytic activities—caspase-like, trypsin-like, and chymotrypsin-like, respectively.<sup>15,16</sup> The 19S RP modulates proteasomal activity via ATP-dependent conformational changes, which enable substrate recognition, unfolding, and translocation into the 20S catalytic chamber.<sup>17,18</sup> Polyubiquitinated substrates require 19S-mediated processing for degradation, whereas the 20S CP, in the absence of the 19S RP, preferentially degrades IDPs due to their inherently unfolded states.<sup>19</sup>

Traditionally, protein function has been tightly linked to a defined three-dimensional structure, yet the discovery of functional IDPs challenges this paradigm. These proteins lack a stable tertiary conformation under physiological conditions, with their structural plasticity integral to their function.<sup>20,21</sup> calcineurin—a serine/threonine phosphatase—activates upon interaction with the  $\text{Ca}^{2+}$ -calmodulin complex through its intrinsically disordered region.<sup>22,23</sup> IDPs are ubiquitous across all domains of life, serving

indispensable roles in cellular signaling, transcriptional and translational regulation, and cell cycle control.<sup>8,20,24</sup> Their conformational flexibility underpins their functional versatility, enabling dynamic interactions with multiple partners and facilitating their involvement in complex regulatory networks. The activation domain of p53 exemplifies the functional versatility of intrinsically disordered proteins (IDPs), engaging in interactions with a diverse array of binding partners, including mouse double minute 2 (Mdm2), replication protein A (RPA), and histone acetyltransferase p300.<sup>25–27</sup> This multifaceted interactome underscores the structural plasticity inherent to IDPs. Notably, their disordered nature renders them intrinsically unstable, necessitating stringent regulation. Basal levels of IDPs are maintained by stabilizing proteolytically resistant complexes formed with molecular chaperones, 'nanny' proteins, and other macromolecular assemblies, which mitigate their susceptibility to degradation.<sup>28,29</sup>

Perturbations in IDP homeostasis, characterized by elevated cellular concentrations, predispose these proteins to promiscuous interactions, culminating in aberrant signaling cascades. Such dysregulation has been causally implicated in the etiology of diverse pathologies, including oncogenesis and neurodegenerative disorders.<sup>5,7,9</sup> The functional dysregulation of p53, driven by its aberrant interaction landscape, exemplifies the pathological potential of IDP imbalance, underscoring the necessity of maintaining proteostasis for cellular integrity.<sup>26,27</sup>

In 2018, the development of TCH-165, a 20S proteasome activator based on an imidazoline scaffold, marked a significant advancement in the selective modulation of proteasomal activity (**Figure 4.1**). TCH-165 was demonstrated to enhance 20S proteasome-mediated degradation of intrinsically disordered proteins (IDPs), including  $\alpha$ -synuclein, in both in vitro systems and cellular models.<sup>30</sup> Notably, this activation exhibited remarkable selectivity, as the degradation of the housekeeping protein glyceraldehyde 3-phosphate dehydrogenase (GAPDH) remained unaffected. Furthermore, in collaboration with the Gaczynska laboratory, biophysical studies provided compelling evidence for small molecule-induced gate-opening of the 20S proteasome. Atomic force microscopy (AFM) imaging corroborated this mechanistic hypothesis (**Figure 4.1**).<sup>30</sup>

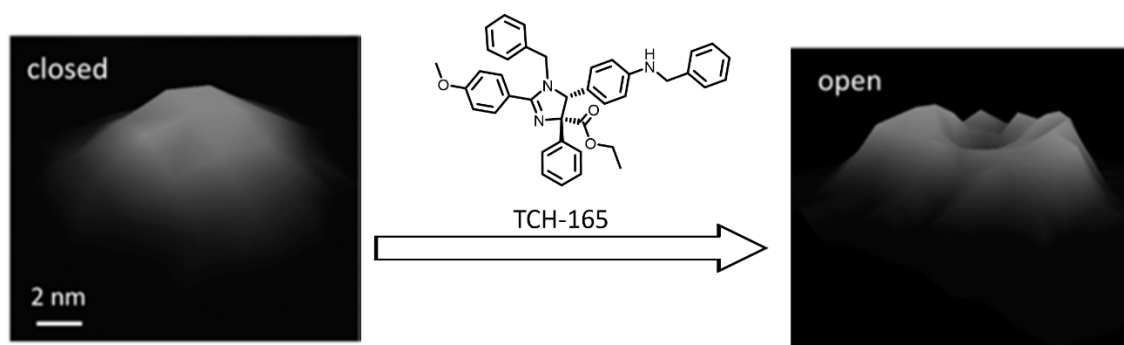


**Figure 4.1: Top view atomic force microscopy (AFM) images of closed and open-gate 20S proteasome before and after treatment with TCH-165, respectively.**

Despite its promise, TCH-165 is hindered by physicochemical limitations that preclude its therapeutic utility. The compound's molecular weight of 595 g/mol and a calculated partition coefficient (ClogP) of 8.35 violate two criteria of Lipinski's 'Rule of Five,' thereby undermining its drug-like properties.<sup>31</sup> Moreover, evaluations using the multi-parameter optimization framework developed by Wager and colleagues predict suboptimal suitability for central nervous system (CNS) applications, further limiting its translational potential.<sup>32</sup> Although extensive efforts have been directed towards optimizing the imidazoline scaffold to address these deficits, such endeavors have thus far yet to be successful. These findings underscore the pressing need to design novel scaffolds with enhanced physicochemical profiles to facilitate effective and selective 20S proteasome activation for therapeutic purposes.

## **4.2 Rational**

The trans-imidazoline analog TCH-165 represents the first potent 20S proteasome activator identified by the Tepe group. This small molecule activates all three catalytic sites of the 20S proteasome, demonstrating its unparalleled efficacy. Despite its potent activity, TCH-165 suffers from poor physicochemical properties, which restrict its translational potential. Consequently, TCH-165 has primarily been employed as a positive control in pursuing novel 20S proteasome activators. This raises a pivotal question: can structurally distinct scaffolds be designed to replicate the proteasome-activating properties of trans-imidazolines while exhibiting superior drug-like characteristics?

The discovery of *cis*-imidazolines, such as nutlins, as inhibitors of protein-protein interactions (PPIs) can serve as a precedent for scaffold diversification.<sup>33</sup> This sparked extensive research interest, and subsequent studies revealed that alternative scaffolds, including pyrrolidines and piperidinones, could mimic *cis*-imidazoline's inhibitory activity on the same PPIs (**Figure 4.2**).<sup>34</sup>

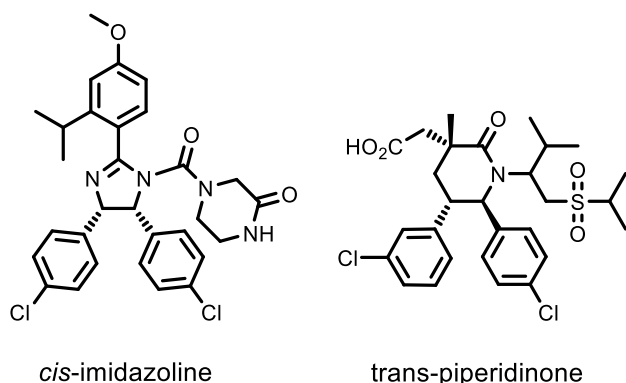


**Figure 4.2: The Protein-Protein Interaction (PPI) Inhibitor nutlin-3a (*cis*-imidazoline) and its *trans*-piperidinone Mimic.<sup>34</sup>**

This structural adaptability suggests that rationally designed scaffolds could replicate the *trans*-imidazoline-mediated activation of the 20S proteasome while addressing their limitations. Among candidate scaffolds, piperazinones emerge as particularly compelling. Regarded as “privileged scaffolds” in medicinal chemistry, piperazinone derivatives feature prominently in various biologically active small molecules, including antidepressants, antibiotics, and anticancer agents.<sup>35,36</sup> Their structural similarity to amino acids renders piperazinones valuable as conformationally constrained peptidomimetics, which protect peptides from enzymatic degradation and modulate physicochemical properties by reducing hydrogen bond donor groups.<sup>37,38</sup> The carbonyl functionality of piperazinones further facilitates synthetic versatility, enabling the generation of diverse derivatives, including reduced piperazine analogs, through straightforward chemical transformations.<sup>39</sup>



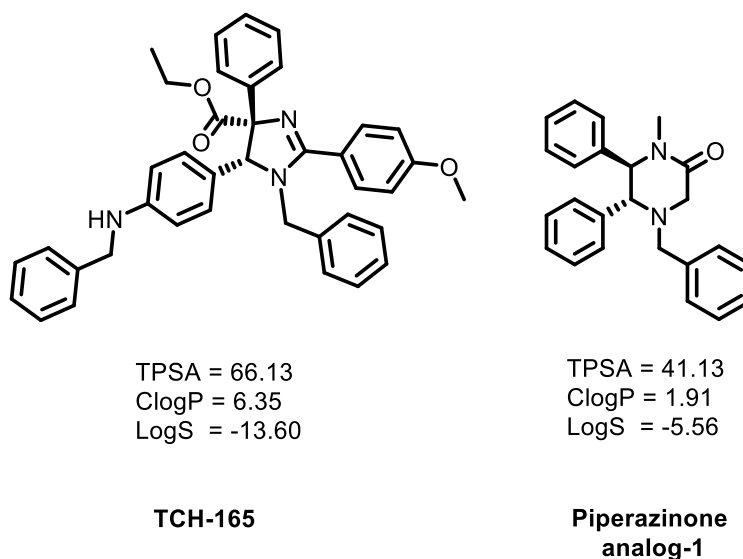


**Figure 4.3: Structures of TCH-165 and an Analog of its Piperazinone Mimic.**

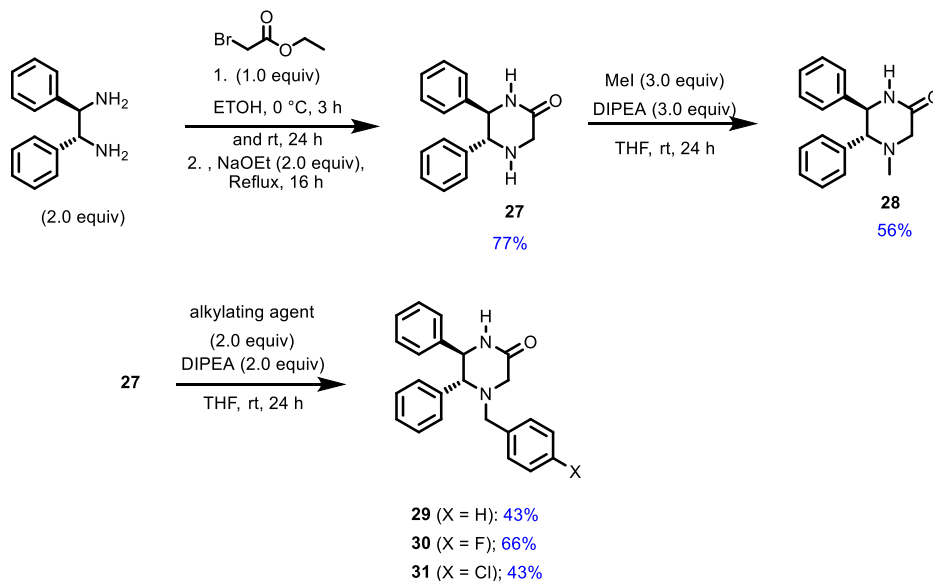
We proposed the synthesis of piperazinone-based analogs as trans-imidazoline mimics. These compounds will incorporate strategic functionalization at nitrogen atoms to orient phenyl groups in a trans configuration, closely emulating the stereochemistry of TCH-165 (**Figure. 4.3**). Preliminary in silico analyses support the viability of this scaffold: a prototype piperazinone analog (compound **27**) exhibits a calculated logP of 1.91 and a logS of -5.56.<sup>31</sup> These parameters align with the multi-parameter optimization guidelines proposed by Wager et al. for CNS drug candidates.<sup>32</sup> Furthermore, these properties suggest that the analogs will likely traverse the blood-brain barrier, a critical criterion for addressing proteostasis dysregulation in neurodegenerative diseases.<sup>40</sup>

The potential of piperazinone-based scaffolds is underpinned by their documented utility in medicinal chemistry and their compatibility with rational design principles. By synthesizing and optimizing these analogs, we aim to develop next-generation 20S proteasome activators that combine the efficacy of TCH-165 with enhanced drug-like characteristics, providing a promising therapeutic avenue for diseases linked to proteostasis impairment.

### 4.3 Design and synthesis of analogs

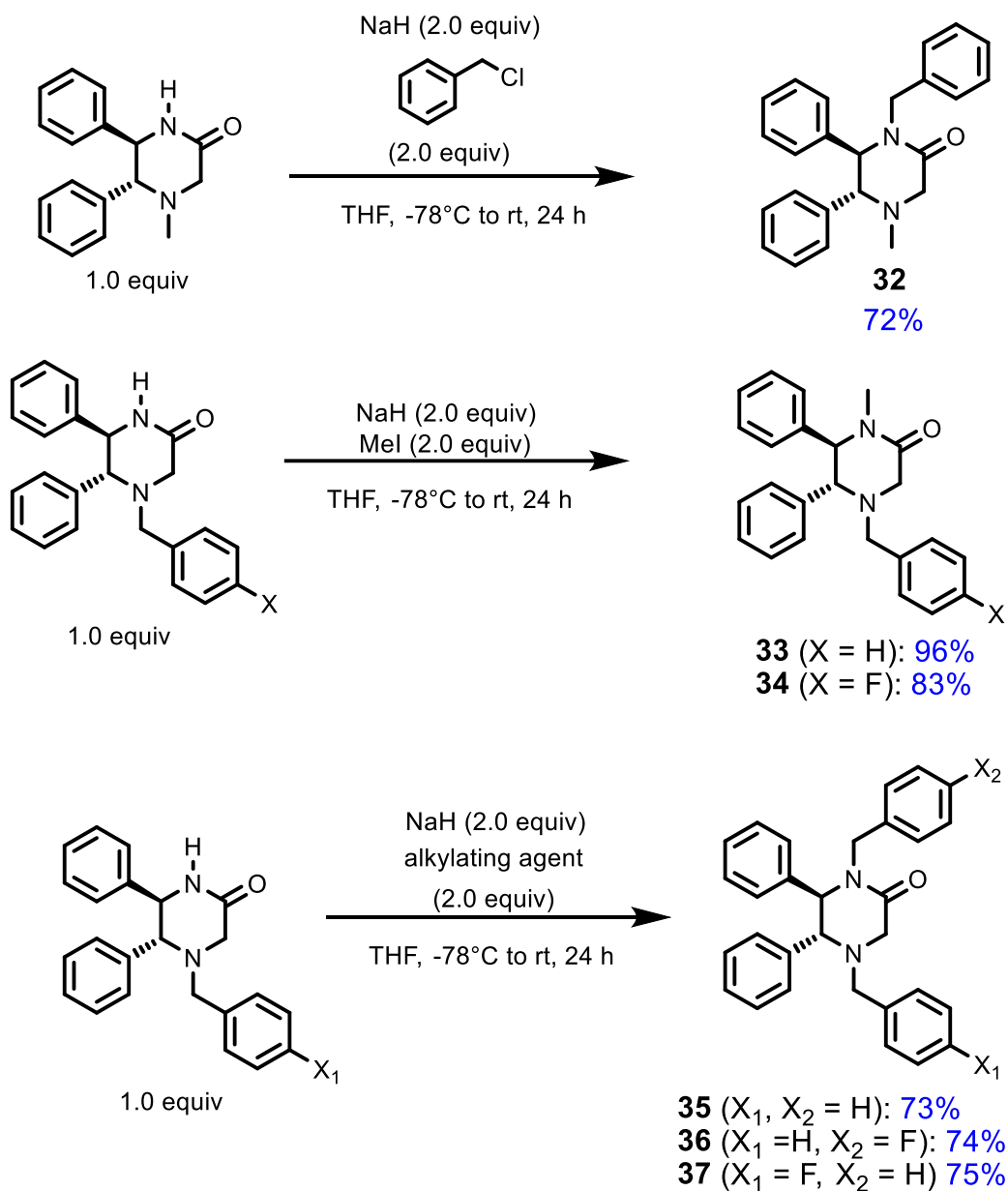
The synthesis of the piperazinone core was achieved by reacting  $\alpha$ -halo ester (ethyl 2-bromoacetate) with (1R,2R)-1,2-diphenylethane-1,2-diamine in the presence of sodium ethoxide. Initially, the reaction at room temperature yielded compound **27** in 31% and the side product S1 in 16%. Optimization of the reaction conditions by introducing ethyl 2-

bromoacetate dropwise over 3 h at 0 °C, followed by refluxing the reaction mixture for 16 h, significantly improved the yield of compound **27** to 77%, with no side product detected. These findings suggest that the controlled addition of ethyl 2-bromoacetate at reduced temperature minimizes double alkylation of the diamine nitrogen, thus favoring the desired cyclization step.



**Scheme 4.1: Synthesis of compounds 27-31. Alkylating agents used; 29: benzyl chloride, 30: *p*-fluorobenzyl bromide and 31: *p*-chlorobenzyl bromide).**

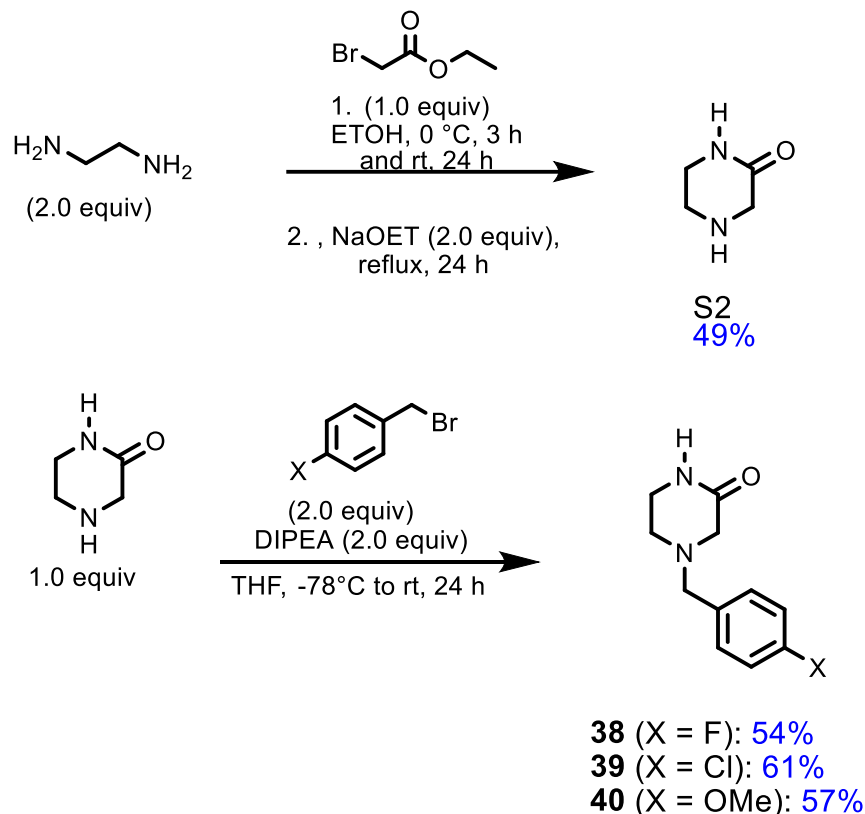
Following the optimization of the cyclization step, attention shifted to the methylation of the amine nitrogen in compound **27**. The methylation was achieved by reacting one equivalent of compound **27** with three equivalents each of diisopropylamine and methyl iodide in tetrahydrofuran (THF) at room temperature for 20 h, affording compound **28** in a yield of 56%. This methylation protocol was subsequently extended to other alkylation reactions, including benzylation, para-fluorobenzylation, and para-chlorobenzylation, to furnish compounds **29**, **30**, and **31**, respectively. When benzyl chloride was employed as the alkylating agent, the desired product was obtained with a yield of 41%. A slightly improved yield of 66% was observed with *p*-fluorobenzyl bromide, while *p*-chlorobenzyl bromide afforded the product a 43% yield (**Scheme 4.1**). These results demonstrate that the nature of the alkylating agent significantly influences the reaction outcome, with bulkier or less reactive reagents leading to diminished yields under the same conditions.



**Scheme 4.2: Synthesis of Compounds 33-36. Alkylating Agents Used; 35-36: *p*-fluorobenzyl bromide and 37: *p*-chlorobenzyl chloride).**

Having successfully achieved the alkylation of the amine nitrogen, efforts were directed toward the alkylation of the amide nitrogen to generate a series of analogs (compounds **33-37**). These transformations were achieved by treating the corresponding intermediates with three equivalents, each sodium hydride, and the chosen alkylating agent, in dry tetrahydrofuran (THF) for 48 h. The product yields displayed a clear dependence on the steric and electronic properties of the alkylating agent. Using methyl iodide as the alkylating agent yielded compound **33** in an excellent 96%. In comparison,

using the bulkier para-fluorobenzyl bromide reduced yield by approximately 74% (compounds **34- 37**).



#### **Scheme 4.3: Synthesis Route to Access Compounds 38-40.**

The effect of their removal from the molecular core was systematically evaluated to investigate the role of the phenyl groups in the activity of 20S proteasome activators. To this end, a series of analogs bearing identical alkyl substitutions on the amine nitrogen were synthesized and tested using small fluorogenic peptide substrates. This approach aimed to assess the contribution of the phenyl groups to proteasome-mediated peptide degradation. Additionally, removing the phenyl groups results in a smaller core structure with retained biological activity, which may offer enhanced potential for structural optimization. The 2-piperazinone core was synthesized by reacting ethylenediamine with ethyl-2-bromoacetate in the presence of sodium ethoxide, following previously established methods. Subsequently, alkylation of the amine nitrogen within the 2-piperazinone framework yielded a series of derivatives with moderate efficiency. As shown in Scheme 4, these derivatives were subjected to further analysis to elucidate

structure-activity relationships and evaluate the functional significance of the phenyl groups.

#### **4.4 Biological Evaluation of Synthesized Analogs**

Having accessed the piperazinone analogs, I moved on to evaluate them for their ability to activate the 20S proteasome. The primary assay was small fluorogenic peptide substrates. The peptide substrates are conjugated to a 7-amino-4-methylcoumarin (AMC) fluorescent probe, a widely accepted method for evaluating proteasome function in vitro.<sup>41–43</sup> The assay relies on the proteasome's catalytic sites cleaving these substrates, releasing AMC, which emits fluorescence upon excitation. Monitoring this fluorescence provides a direct measure of proteasome activity. This method has been extensively used to characterize proteasome dynamics under various conditions and treatments, providing reliable insights into catalytic site-specific activity.<sup>44,45,46</sup>

In this study, varying concentrations of each analog (80  $\mu$ M to 1.25  $\mu$ M) were pre-incubated with purified 1 nM of purified 20S proteasome, allowing sufficient interaction time (15 minutes) to modulate proteasome activity. After substrate addition, fluorescence was recorded over 1 h with an excitation and emission wavelength of 280 and 460 nm, respectively. This offers a quantitative assessment of the rate of substrate cleavage.

The substrates for the three catalytic sites were used at the following concentrations: Z-LLE-AMC (Casp-L activity, 10  $\mu$ M), Suc-LLVY-AMC (CT-L activity, 10  $\mu$ M), and Boc-LRR-AMC (T-L activity, 20  $\mu$ M, due to the low activity of the trypsin-like site). This combination of all three substrates reflects the overall impact on the 20S proteasome activity. This approach minimizes temporal variability and provides a robust platform for determining fold changes in proteasome activation.

The untreated sample (vehicle) fluorescence was standardized to 100%, and each compound's fold change in proteasome activity was calculated. This normalization facilitates a clear comparison between treated and untreated samples, a practice previously validated in proteasome modulation studies. TCH-165, a known proteasome activator, was used as a positive control to benchmark the extent of activation induced by the synthesized analogs.<sup>47</sup> Analog-induced activation exceeding two-fold over the vehicle control was considered significant and warranted further investigation into site-specific activity.

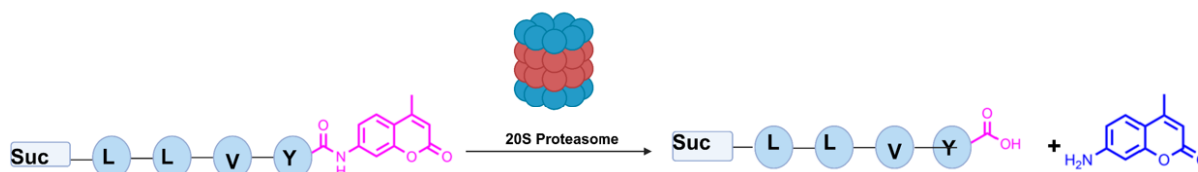


**Figure 4.4: Schematic Diagram for Small Peptide Assay.**

The 26S proteasome cleaves the AMC probe, releasing the AMC fluorophore, which is monitored by a plate reader at 480 nm.

The preliminary data indicate that compounds **27** and **28** could not activate the 20S proteasome to facilitate the degradation of small peptide substrates (Figure 4.4). The EC<sub>200</sub> values for these analogs exceeded 80  $\mu$ M, while their maximum fold-activation of the proteasome remained below 2 relative to the benchmark compound TCH-165. The max fold of activation for compounds **27** and **28** was 1.3, showing poor activity.

The subsequent introduction of an additional benzyl group at the amide nitrogen (**29**) slightly improved the activity level, with an EC<sub>200</sub> of 38.9  $\mu$ M and a max fold of 3.3 (**Figure 4.5A**). These results suggest additional interactions between the added benzyl ring and key residues in the proteasome's binding pockets.

Previous studies from our laboratory suggested that halogenation could enhance proteasome activation.<sup>1</sup> Prior studies on phenothiazine-based analogs reinforced this hypothesis. For example, para-substituted halogen derivatives of phenothiazines have demonstrated notable efficacy as 20S proteasome activators. Halogenation modulates bioactivity by altering electronic properties, hydrophobicity, and binding affinity, as observed in various proteasome activators.<sup>22</sup> Thus, compounds **30** and **7** were designed to incorporate halogen substitutions to leverage these properties to enhance activity. These modifications warrant further investigation to delineate their impact on the proteasome activation profile.

Following established protocols, the newly synthesized analogs (compounds **30** and **31**) were evaluated for their ability to enhance 20S proteasome proteolytic activity.

The incorporation of Fluorine and chlorine at the para positions of the benzyl moiety dramatically increased proteasome activity. The EC<sub>200</sub> of the fluorinated analog (**30**) was 8.7, whereas the chlorinate analog (**31**) had an EC<sub>200</sub> of 8.5  $\mu$ M (**Figure 4.5A**).

I hypothesize that adding these halogens could create additional hydrogen bonds not seen in the previous analogs. Interestingly, methylation of the amide nitrogen (**33** and **34**) decreased activity with an EC<sub>200</sub> of 18.7 and 26.3, respectively.

Halogens' positive impact on 20S proteasome activation made me develop new analogs with more halogen groups to improve interactions. Analogs with amide and amine nitrogen benzylated were developed (**35-37**).

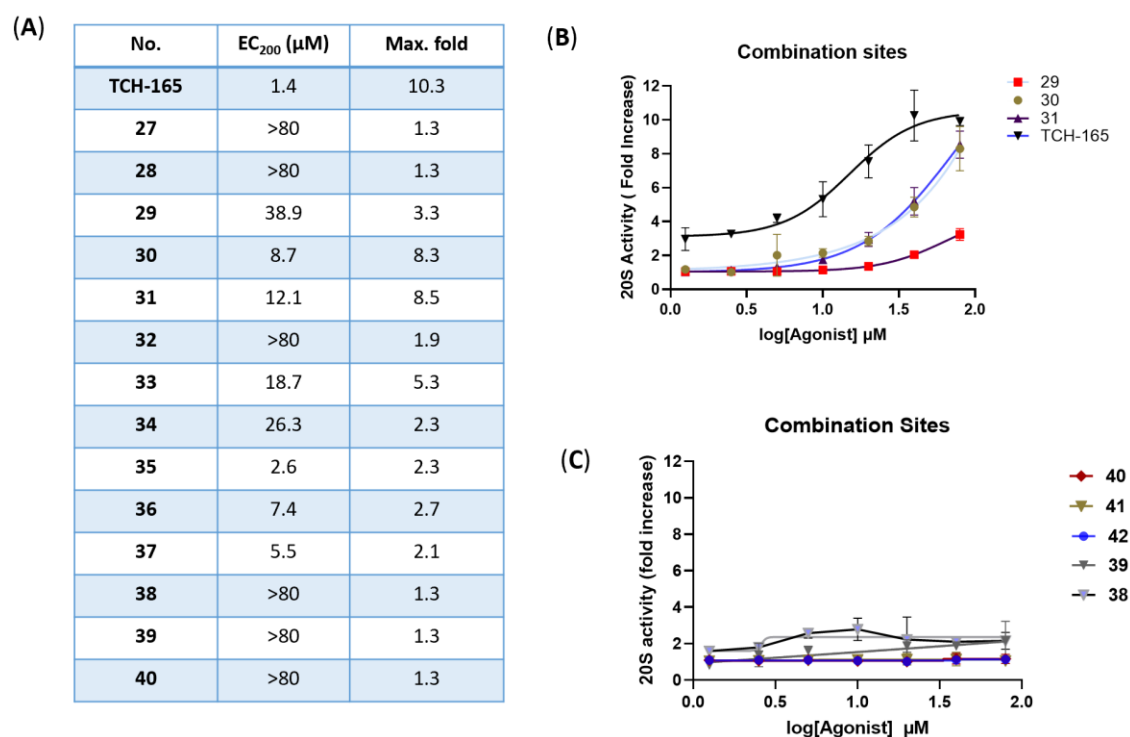


**Figure 4.5: Enhancement of 2S Proteasome activity by Synthesized Analogs**

(A) The concentration of compounds needed to activate the proteasome by 200% (EC<sub>200</sub> values) for compounds 21-41. Activity graphs for compounds (B) **29-31** and positive control, TCH-165 and (C) **38-42**.

These analogs showed increased activity with lower EC<sub>200</sub> values (**Figure 4.5 A**). Compounds **35** and **36** had EC<sub>200</sub> of 2.6 μM and 7.4 μM, respectively. However, these analogs (**35-37**) had lower max fold values due to their poor solubility at higher concentrations. Those results suggest the propensity for the 20S proteasome to interact with analogs with bulky aromatic groups.

Finally, the impact of the phenyl rings on the piperazine was evaluated (**40-41**). Interestingly, none of these analogs (**40-42**) could activate the 20S proteasome to degrade the small fluorogenic peptides.

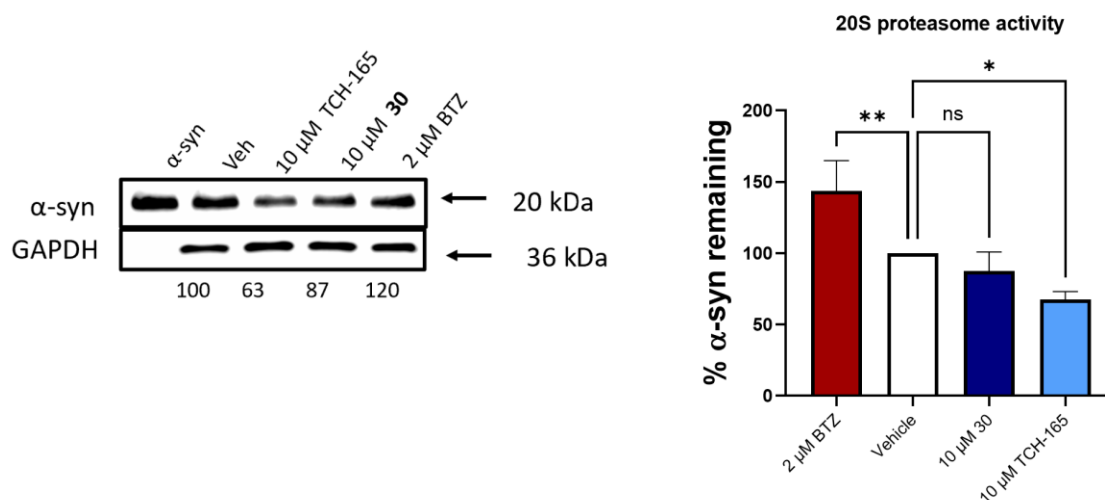


**Figure 4.6: Evaluation of in vitro 20S proteasome-mediated degradation of α-synuclein degradation.**

The degradation of purified α-synuclein by the 20S proteasome treated with 10 μM of compound 30 and TCH-165 or the proteasome inhibitor, BTZ. GAPDH was added as a loading control. Each set of assays was done in triplicate. Error bars denote standard deviation. One-way ANOVA statistical analysis was used to determine statistical significance (ns = not significant, \*p < 0.05, \*\*p < 0.01,). Error bars based on standard deviation. n denotes the number of replicates.

The subsequent phase of this study aimed to investigate the biological efficacy of compounds 30 as activators of the 20S proteasome, focusing specifically on their ability to facilitate the degradation of a disease-relevant intrinsically disordered protein (IDP). α-syn, an established substrate of the 20S proteasome and a protein implicated in the pathogenesis of Parkinson's disease, was selected for this evaluation due to its critical role in proteostasis imbalance and neurotoxicity when aggregated.

To assess the activity of the compounds, purified human 20S proteasome (10 nM) was pre-incubated with DMSO (2%) or 10 μM of compound **30** or the positive control TCH-



165. After incubation with  $\alpha$ -syn (300 nM) for three and a half hours, reaction mixtures were analyzed using protein gel electrophoresis followed by western blotting to quantify the remaining  $\alpha$ -syn. These assays were designed to determine whether the compounds could enhance proteasomal degradation of  $\alpha$ -syn, potentially reducing its pathological accumulation and alleviating proteotoxic stress.

Results indicated compound **30** could not significantly enhance the degradation of  $\alpha$ -syn, with 87% of the protein remaining under this treatment conditions. This lack of activity may reflect inadequate compound-induced structural changes in the 20S proteasome to promote efficient substrate engagement and catalysis. In contrast, TCH-165, the benchmark compound, facilitated a marked degradation of  $\alpha$ -syn, leaving only 72% of the substrate intact. These findings underscore the superior efficacy of TCH-165 in modulating proteasome activity against IDP substrates.

As expected, the proteasome inhibitor bortezomib abrogated  $\alpha$ -syn degradation, confirming the proteasome's role in substrate turnover during these assays. These results emphasize the specificity of the 20S proteasome in degrading  $\alpha$ -syn and highlight the importance of identifying small-molecule activators capable of enhancing this process.

The findings suggest that while the halogenated derivative, compound 30, exhibits promising physicochemical properties, further optimization is necessary to improve their biological activity. Refinement of molecular interactions and enhancement of proteasomal engagement may be required to achieve degradation profiles comparable to TCH-165. These insights provide valuable guidance for the continued development of therapeutic agents targeting proteostasis pathways in neurodegenerative diseases

#### **4.5 Conclusion**

Exploring piperazinone-based small molecules as activators of the 20S proteasome offers significant insights into the therapeutic potential for targeting neurodegenerative disorders characterized by proteostasis impairment. This study successfully synthesized and evaluated a range of piperazinone derivatives, demonstrating that structural modifications, particularly halogenation and specific alkyl substitutions, can substantially enhance proteasome activation. Compounds with para-halogen substitutions on benzyl moieties exhibited improved EC200 values and increased activation profiles, affirming the critical role of these modifications in facilitating proteasomal engagement. Conversely,

analogs lacking key structural features, such as phenyl rings, could not induce proteasomal activity, highlighting the specificity of these interactions.

While the analogs showed promise in enhancing proteasome-mediated peptide degradation, their efficacy in promoting the degradation of disease-relevant intrinsically disordered proteins such as  $\alpha$ -synuclein was limited compared to the benchmark activator TCH-165. This underscores further the need to optimize these compounds for substrate specificity and translational relevance. Challenges related to solubility and physicochemical properties also emerged as critical factors limiting the functional potential of the synthesized analogs, suggesting that future efforts should focus on balancing potency with drug-like characteristics.

In conclusion, the findings from this study provide a robust foundation for the rational design of next-generation 20S proteasome activators. By leveraging the structural adaptability of piperazinones and incorporating advanced optimization strategies, clinically viable compounds capable of restoring proteostasis and mitigating the progression of neurodegenerative diseases may be possible. These insights contribute to the broader understanding of proteasome biology and its therapeutic implications, paving the way for innovative interventions in managing proteostasis-related pathologies.

## REFERENCES

- (1) Kaushik, S., and Cuervo, A.M. (2015). Proteostasis and aging. *Nat. Med.* **21**, 1406–1415. 10.1038/nm.4001.
- (2) Powers, E.T., and Balch, W.E. (2013). Diversity in the origins of proteostasis networks-a driver for protein function in evolution. *Nat. Rev. Mol. Cell Biol.* **14**, 237–248. 10.1038/nrm3542.
- (3) McCarthy, A. (2010). Probing the Proteostasis Network. *Chem. Biol.* **17**, 1163–1164. 10.1016/j.chembiol.2010.11.006.
- (4) Whittemore, S.R., Saraswat Ohri, S., Forston, M.D., Wei, G.Z., and Hetman, M. (2022). The Proteostasis Network: A Global Therapeutic Target for Neuroprotection after Spinal Cord Injury. *Cells* **11**, 1–25. 10.3390/cells11213339.
- (5) Vilchez, D., Saez, I., and Dillin, A. (2014). The role of protein clearance mechanisms in organismal ageing and age-related diseases. *Nat. Commun.* **5**. 10.1038/ncomms6659.
- (6) Mattson, M.P., and Magnus, T. (2006). Ageing and neuronal vulnerability. *Nat. Rev. Neurosci.* **7**, 278–294. 10.1038/nrn1886.
- (7) Labbadia, J., and Morimoto, R.I. (2015). The biology of proteostasis in aging and disease. *Annu. Rev. Biochem.* **84**, 435–464. 10.1146/annurev-biochem-060614-033955.
- (8) Tompa, P., Schad, E., Tantos, A., and Kalmar, L. (2015). Intrinsically disordered proteins: Emerging interaction specialists. *Curr. Opin. Struct. Biol.* **35**, 49–59. 10.1016/j.sbi.2015.08.009.
- (9) Ciechanover, A., and Kwon, Y.T. (2015). Degradation of misfolded proteins in neurodegenerative diseases: therapeutic targets and strategies. *Exp. Mol. Med.* **47**, e147. 10.1038/EMM.2014.117.
- (10) Dang, C. V., Reddy, E.P., Shokat, K.M., and Soucek, L. (2017). Drugging the “undruggable” cancer targets. *Nat. Rev. Cancer* **17**, 502–508. 10.1038/nrc.2017.36.
- (11) Ruan, H., Sun, Q., Zhang, W., Liu, Y., and Lai, L. (2019). Targeting intrinsically disordered proteins at the edge of chaos. *Drug Discov. Today* **24**, 217–227. 10.1016/j.drudis.2018.09.017.
- (12) Ozawa, T. (1992). Analysis of a multiqueue model for an ISDN access interface. *Perform. Eval.* **15**, 65–75. 10.1016/0166-5316(92)90055-L.
- (13) Krüger, E., Kloetzel, P.M., and Enenkel, C. (2001). 20S proteasome biogenesis. *Biochimie* **83**, 289–293. 10.1016/S0300-9084(01)01241-X.
- (14) Tanaka, K. (2009). The proteasome: Overview of structure and functions. *Proc. Japan Acad. Ser. B Phys. Biol. Sci.* **85**, 12–36. 10.2183/pjab.85.12.
- (15) Groll, M., Heinemeyer, W., Jäger, S., Ullrich, T., Bochtler, M., Wolf, D.H., and

- Huber, R. (1999). The catalytic sites of 20S proteasomes and their role in subunit maturation: A mutational and crystallographic study. *Proc. Natl. Acad. Sci. U. S. A.* **96**, 10976–10983. 10.1073/pnas.96.20.10976.
- (16) Huber, E.M., Heinemeyer, W., Li, X., Arendt, C.S., Hochstrasser, M., and Groll, M. (2016). A unified mechanism for proteolysis and autocatalytic activation in the 20S proteasome. *Nat. Commun.* **7**, 1–10. 10.1038/ncomms10900.
  - (17) Rabl, J., Smith, D.M., Yu, Y., Chang, S.C., Goldberg, A.L., and Cheng, Y. (2008). Mechanism of Gate Opening in the 20S Proteasome by the Proteasomal ATPases. *Mol. Cell* **30**, 360–368. 10.1016/j.molcel.2008.03.004.
  - (18) Etlinger, J.D., and Goldberg, A.L. (1977). A soluble ATP dependent proteolytic system responsible for the degradation of abnormal proteins in reticulocytes. *Proc. Natl. Acad. Sci. U. S. A.* **74**, 54–58. 10.1073/pnas.74.1.54.
  - (19) Opoku-Nsiah, K.A., and Gestwicki, J.E. (2018). Aim for the core: suitability of the ubiquitin-independent 20S proteasome as a drug target in neurodegeneration. *Transl. Res.* **198**, 48–57. 10.1016/j.trsl.2018.05.002.
  - (20) Iakoucheva, L.M., Brown, C.J., Lawson, J.D., Obradović, Z., and Dunker, A.K. (2002). Intrinsic disorder in cell-signaling and cancer-associated proteins. *J. Mol. Biol.* **323**, 573–584. 10.1016/S0022-2836(02)00969-5.
  - (21) Babu, M.M., van der Lee, R., de Groot, N.S., and Gsponer, J. (2011). Intrinsically disordered proteins: Regulation and disease. *Curr. Opin. Struct. Biol.* **21**, 432–440. 10.1016/j.sbi.2011.03.011.
  22. King, M.M., and Huang, C.Y. (1983). Activation of calcineurin by nickel ions. *Biochem. Biophys. Res. Commun.* **114**, 955–961. 10.1016/0006-291X(83)90653-8.
  - (23) Kissinger, C.R., Parge, H.E., Knighton, D.R., Lewis, C.T., Pelletier, L.A., Tempczyk, A., Kalish, V.J., Tucker, K.D., Showalter, R.E., Moomaw, E.W., et al. (1995). Crystal structures of human calcineurin and the human FKBP12–FK506–calcineurin complex. *Nature* **378**, 641–644. 10.1038/378641a0.
  - (24) Wright, P.E., and Dyson, H.J. (2015). Intrinsically disordered proteins in cellular signalling and regulation. *Nat. Rev. Mol. Cell Biol.* **16**, 18–29. 10.1038/nrm3920.
  - (25) Wright, P.E., and Dyson, H.J. (2009). Linking folding and binding. *Curr. Opin. Struct. Biol.* **19**, 31–38. 10.1016/j.sbi.2008.12.003.
  - (26) Oldfield, C.J., Meng, J., Yang, J.Y., Qu, M.Q., Uversky, V.N., and Dunker, A.K. (2008). Flexible nets: Disorder and induced fit in the associations of p53 and 14-3-3 with their partners. *BMC Genomics* **9**, 1–20. 10.1186/1471-2164-9-S1-S1.
  - (27) Anderson, C.W., and Appella, E. (2009). Signaling to the p53 Tumor Suppressor through Pathways Activated by Genotoxic and Non-Genotoxic Stresses Second Edi. (Elsevier Inc.) 10.1016/B978-0-12-374145-5.00264-3.
  - (28) Tsvetkov, P., Reuven, N., and Shaul, Y. (2009). The nanny model for IDPs. *Nat.*

Chem. Biol. 5, 778–781. 10.1038/nchembio.233.

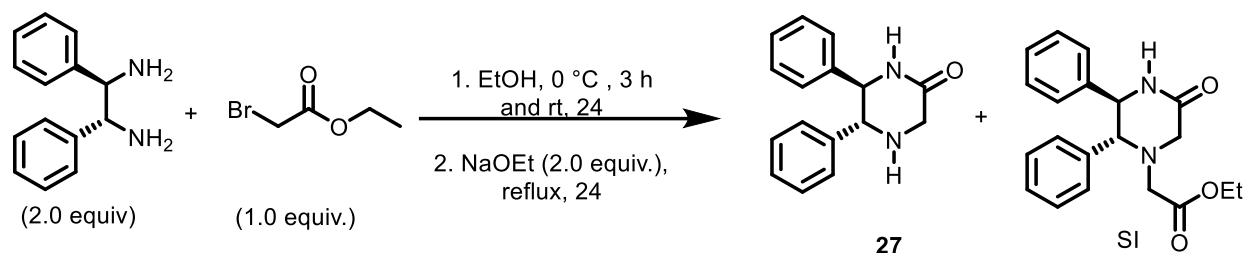
- (29) Kwon, Y.T., and Ciechanover, A. (2017). The Ubiquitin Code in the Ubiquitin-Proteasome System and Autophagy. *Trends Biochem. Sci.* 42, 873–886. 10.1016/j.tibs.2017.09.002.
- (30) Njomen, E., Osmulski, P.A., Jones, C.L., Gaczynska, M., and Tepe, J.J. (2018). Small Molecule Modulation of Proteasome Assembly. *Biochemistry* 57, 4214–4224. 10.1021/acs.biochem.8b00579.
- (31) Lipinski, C.A., Lombardo, F., Dominy, B.W., and Feeney, P.J. (2012). Experimental and computational approaches to estimate solubility and permeability in drug discovery and development settings. *Adv. Drug Deliv. Rev.* 64, 4–17. 10.1016/j.addr.2012.09.019.
- (32) Wager, T.T., Hou, X., Verhoest, P.R., and Villalobos, A. (2010). Moving beyond rules: The development of a central nervous system multiparameter optimization (CNS MPO) approach to enable alignment of druglike properties. *ACS Chem. Neurosci.* 1, 435–449. 10.1021/cn100008c.
- (33) Ding, Q., Zhang, Z., Liu, J.J., Jiang, N., Zhang, J., Ross, T.M., Chu, X.J., Bartkovitz, D., Podlaski, F., Janson, C., et al. (2013). Discovery of RG7388, a potent and selective p53-MDM2 inhibitor in clinical development. *J. Med. Chem.* 56, 5979–5983. 10.1021/jm400487c.
- (34) Zhao, Y., Aguilar, A., Bernard, D., and Wang, S. (2015). Small-molecule inhibitors of the MDM2-p53 protein-protein interaction (MDM2 inhibitors) in clinical trials for cancer treatment. *J. Med. Chem.* 58, 1038–1052. 10.1021/jm501092z.
- (35) Mohd Imran, and Mohammad Asif (2020). Biologically Active Pyridazines and Pyridazinone Derivatives: A Scaffold for the Highly Functionalized Compounds. *Russ. J. Bioorganic Chem.* 46, 726–744. 10.1134/S1068162020050155.
- (36) Valdivielso, Á.M., García-López, M.T., Gutiérrez-Rodríguez, M., and Herranz, R. (2014). Exploring the Phe-Gly Dipeptide-derived Piperazinone Scaffold in the search for Antagonists of the Thrombin receptor PAR1. *Molecules* 19, 4814–4846. 10.3390/molecules19044814.
- (37) Yu, K., Rajakumar, G., Srivastava, L.K., Mishra, R.K., and Johnson, R.L. (1988). I<sup>1</sup> UonhO. 1430–1436.
- (38) Gante, J. Peptidomimetics-Tailored Enzyme Inhibitors.
- (39) Dinsmore, C.J., and Beshore, D.C. (2002). Syntheses and transformations of piperazinone rings. A review. *Org. Prep. Proced. Int.* 34, 367–404. 10.1080/00304940209458075.
- (40) Daina, A., Michielin, O., and Zoete, V. (2017). SwissADME: A free web tool to evaluate pharmacokinetics, drug-likeness and medicinal chemistry friendliness of small molecules. *Sci. Rep.* 7, 1–13. 10.1038/srep42717.
- (41) Gaczynska, M., and Osmulski, P.A. (2005). Characterization of noncompetitive

- regulators of proteasome activity. *Methods Enzymol.* 398, 425–438. 10.1016/S0076-6879(05)98035-X.
- (42) Trader, D.J., Simanski, S., Dickson, P., and Kodadek, T. (2017). Establishment of a suite of assays that support the discovery of proteasome stimulators. *Biochim. Biophys. Acta - Gen. Subj.* 1861, 892–899. 10.1016/j.bbagen.2017.01.003.
  - (43) Kisselev, A.F., and Goldberg, A.L. (2005). Monitoring activity and inhibition of 26S proteasomes with fluorogenic peptide substrates. *Methods Enzymol.* 398, 364–378. 10.1016/S0076-6879(05)98030-0.
  - (44) Fiolek, T.J., Keel, K.L., and Tepe, J.J. (2021). Fluspirilene Analogs Activate the 20S Proteasome and Overcome Proteasome Impairment by Intrinsically Disordered Protein Oligomers (*Neurosci*) 10.1021/acscchemneuro.1c00099.
  - (45) Staerz, S.D., Jones, C.L., and Tepe, J.J. (2022). Design, Synthesis, and Biological Evaluation of Potent 20S Proteasome Activators for the Potential Treatment of  $\alpha$ -Synucleinopathies. *J. Med. Chem.* 65, 6631–6642. 10.1021/acs.jmedchem.1c02158.
  - (46) Jones, C.L., Njomen, E., Sjögren, B., Dexheimer, T.S., and Tepe, J.J. (2017). Small Molecule Enhancement of 20S Proteasome Activity Targets Intrinsically Disordered Proteins. *ACS Chem. Biol.* 12, 2240–2247. 10.1021/acscchembio.7b00489.
  - (47) Njomen, E., Osmulski, P.A., Jones, C.L., Gaczynska, M., and Tepe, J.J. (2018). Small Molecule Modulation of Proteasome Assembly 10.1021/acs.biochem.8b00579.

## APPENDIX

### Synthesis:

#### (5*R*,6*R*)-6,6-diphenylpiperazin-2-one (**27**)



The compound was synthesized by following previously described method.<sup>3</sup> To a clean, dry 100 mL round bottom flask was added, (1*R*, 2*R*) 1,2 diphenyl ethylenediamine (2.0 equiv, 3.0 mmol) followed by 30 mL of absolute ethanol. The reaction mixture was cooled to 0 °C. Ethyl bromoacetate (1.0 equiv, 1.5 mmol) was dissolved in 10.0 mL of absolute ethanol and added to the reaction mixture dropwise over 3 hours. The mixture was allowed to warm to room temperature and stirred overnight under nitrogen gas. Sodium ethoxide (2.0 equiv, 3.0 mmol) was added to the reaction mixture and then refluxed for 24 hours. After that, the reaction mixture was cooled to room temperature and the solvent evaporated under reduced pressure. The purification was achieved using automated Combiflash chromatography (silica gel, 20-40 microns, gradient 5-10% methanol in dichloromethane). The compound was isolated as a white fluffy solid. Yield: 276 *mg* (72%). MP: 165-166 °C. IR: 3321, 3060, 1683 cm<sup>-1</sup>. <sup>1</sup>H NMR (500 MHz, CDCl<sub>3</sub>) δ 7.18-7.24 (m, 6H), 7.05 (dd, *J* = 7.7, 1.6 Hz, 2H), 6.93 (dt, *J* = 8.2, 2.2 Hz, 2H), 6.11 (br s, 1H), 4.54 (d, *J* = 9.2 Hz, 1H), 3.80 (s, 2H), 3.78 (d, *J* = 9.2 Hz, 1H), 2.1 (s, 1H). <sup>13</sup>C{<sup>1</sup>H} NMR (125 MHz, CDCl<sub>3</sub>) δ 169.5, 138.4, 138.4, 128.4, 128.4, 128.4, 128.3, 127.8, 127.4, 66.1, 64.7, 50.3. HRMS (ESI-TOF) *m/z*: [(*M*+*H*)<sup>+</sup>] calcd for (C<sub>16</sub>H<sub>17</sub>N<sub>2</sub>O<sup>+</sup>) 253.1341; Found 253.1341.

#### Side Product

Yield: 26.0 *mg* (21%). <sup>1</sup>H NMR (500 MHz, CDCl<sub>3</sub>) δ 7.25 – 7.09 (m, 6H), 7.05 (dd, *J* = 7.7, 1.6 Hz, 2H), 6.93 (dt, *J* = 8.2, 2.2 Hz, 2H), 6.07 (s, 1H), 4.64 (d, *J* = 9.4 Hz, 1H), 4.07 – 4.00 (m, 3H), 3.84 (d, *J* = 16.9 Hz, 1H), 3.74 (d, *J* = 16.9 Hz, 1H), 3.26 (d, *J* = 17.5 Hz, 1H), 3.14 (d, *J* = 17.5 Hz, 1H), 1.15 (t, *J* = 7.1 Hz, 3H). <sup>13</sup>C{<sup>1</sup>H} NMR (125 MHz, CDCl<sub>3</sub>) δ 170.3, 168.8, 138.5, 136.4, 129.2, 128.7, 128.5, 128.4, 18.4, 127.6, 69.3, 64.2, 60.5, 55.5,

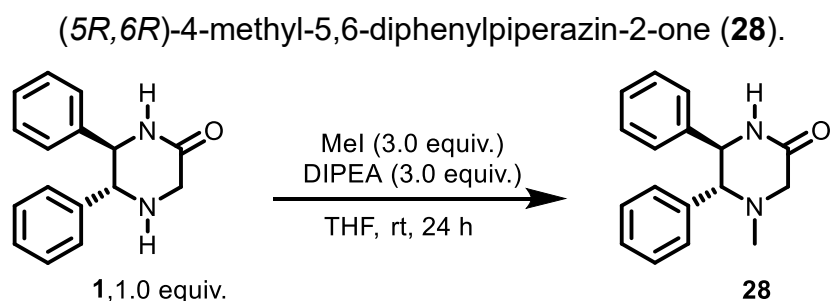
53.9, 14.3. HRMS (ESI-TOF)  $m/z$ :  $[(M+H)^+]$  calcd for  $(C_{20}H_{23}N_2O_3^+)$  339.1709; Found 339.1709.3

General procedure the synthesis of compounds **28-31**, **33**

To a clean, dry 25 mL, round bottom flask was charged with (5*R*,6*R*)-6,6-diphenylpiperazin-2-one (1.0 equiv.), different alkylating agents (3.0 equiv), and 10.0 mL of dry tetrahydrofuran. After stirring the mixture at room temperature for 90 minutes, diisopropylethylamine (3.0 equiv) was added to the reaction mixture and stirred at the same temperature for 24-48 hours under nitrogen gas. After that, the reaction was stopped, and the solvent evaporated under reduced pressure. The mixture was purified using automated Combiflash chromatography (silica gel, 20-40 microns, gradient 70-0% hexane in ethyl acetate).

General procedure for synthesizing compounds **32**, **34**, **34** and **37**.

Various amine alkylated (5*R*,6*R*)-6,6-diphenylpiperazin-2-one (1.0 equiv) was dissolved in 10 mL of anhydrous tetrahydrofuran. The reaction mixture was cooled to -78 °C and added sodium hydride (3.0 equiv). After 90 minutes, different alkylating agents (3.0 equiv, 1.08 mmol) were dissolved in 2.0 mL of tetrahydrofuran and added to the reaction mixture dropwise. The reaction was quenched with 10 mL of H<sub>2</sub>O and extracted with EtOAc (4 x 10 mL). The organics were combined, washed once with brine, dried over anhydrous sodium sulfate, and concentrated under reduced pressure. The crude solid was purified using automated *Combiflash chromatography* (silica gel, 20-40 microns, gradient 90-10% hexane in ethyl acetate).

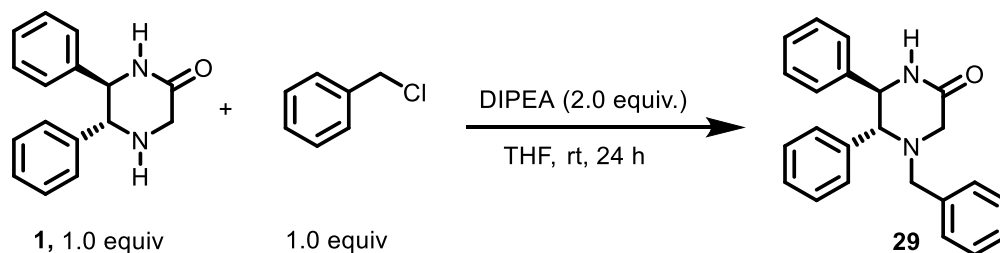


Isolated with 5% methanol in ethyl acetate. Flaky pale brown solid (0.28 g, 56%). MP: 110-111 °C. IR: 3250, 3027, 2781, 1668  $\text{cm}^{-1}$ . <sup>1</sup>H NMR (500 MHz, CDCl<sub>3</sub>)  $\delta$  7.12-7.22 (m, 6H), 7.05 (dd,  $J$  = 7.7, 1.9 Hz, 2H), 6.90 (dt,  $J$  = 6.6, 2.2 Hz, 2H), 6.19 (br s, 1H), 4.60 (d,  $J$  =



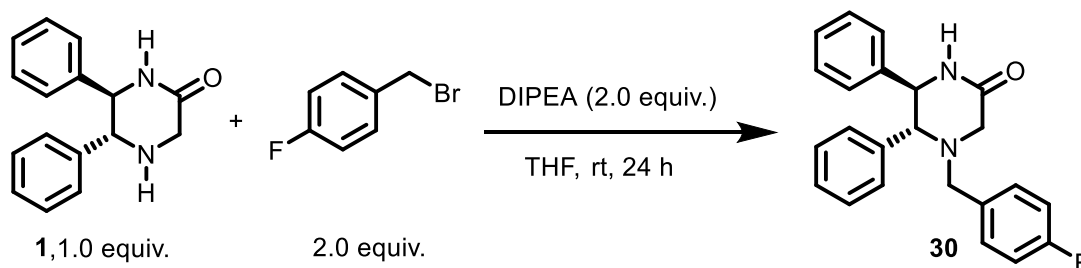
9.3 Hz, 1H), 3.13 (d,  $J = 17.0$  Hz, 1H), 3.13 (d,  $J = 9.3$  Hz, 1H), 2.20 (s, 3H).  $^{13}\text{C}\{^1\text{H}\}$  NMR (125 MHz,  $\text{CDCl}_3$ )  $\delta$  168.9, 138.7, 137.4, 128.9, 128.5, 128.4, 128.3, 128.2, 127.6, 73.7, 64.1, 59.2, 43.2. HRMS (ESI-TOF)  $m/z$ :  $[(M+H)^+]$  calcd for  $(\text{C}_{17}\text{H}_{19}\text{N}_2\text{O}^+)$  267.1492; Found. 267.1499.

(5*R*,6*R*)-4-benzyl-1-methyl-5,6-diphenylpiperazin-2-one (**29**).



Isolated with 50% hexane in ethyl acetate. White solid (112.7 mg, 41%). MP: 174-175 °C. IR: 3231, 3030, 1682  $\text{cm}^{-1}$ .  $^1\text{H}$  NMR (500 MHz,  $\text{CDCl}_3$ )  $\delta$  7.20-7.16 (m, 14H), 6.96 (dd,  $J=8.4$ , 1.6 Hz, 2H), 6.00 (s, 1H), 4.70 (d,  $J = 8.7$  Hz, 1H), 3.81 (d,  $J = 13.2$  Hz, 1H), 3.56 (d,  $J = 17.2$  Hz, 1H), 3.49 (d,  $J = 8.7$  Hz, 1H), 3.06 (d,  $J = 17.2$  Hz, 1H), 2.88 (d,  $J = 13.2$  Hz, 1H).  $^{13}\text{C}\{^1\text{H}\}$  NMR (125 MHz,  $\text{CDCl}_3$ )  $\delta$  169.1, 139.0, 137.6, 137.4, 129.0, 128.9, 128.7, 128.5, 128.4, 128.4, 128.3, 127.6, 127.5, 71.9, 64.2, 59.1, 55.7. HRMS (ESI-TOF)  $m/z$ :  $[(M+H)^+]$  calcd for  $(\text{C}_{23}\text{H}_{23}\text{N}_2\text{O}^+)$  343.1805; found, 343.1836.

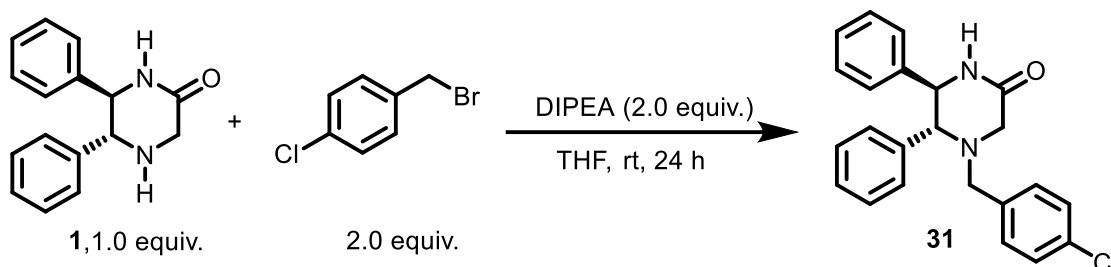
(5*R*,6*R*)-4-(4-fluorobenzyl)-5,6-diphenylpiperazin-2-one (**30**).



Isolated with 75% hexane in ethyl acetate. White solid (173.8 mg, 66%). MP: 161-162 °C. IR: 3238, 3030, 1687  $\text{cm}^{-1}$ .  $^1\text{H}$  NMR (500 MHz,  $\text{CD}_2\text{Cl}_2$ )  $\delta$  7.26 – 7.13 (m, 10H), 7.01-6.93 (m, 4H), 5.99 (s, 1H), 4.69 (d,  $J = 8.7$  Hz, 1H), 3.69 (d,  $J = 13.2$  Hz, 1H), 3.50 (d,  $J = 8.7$  Hz, 1H), 3.40 (d,  $J = 17.0$  Hz, 1H), 3.01 (d,  $J = 17.0$  Hz, 1H), 2.86 (d,  $J = 13.2$  Hz, 1H).  $^{13}\text{C}\{^1\text{H}\}$  NMR (125 MHz,  $\text{CDCl}_3$ )  $\delta$  169.0, 162.2 (d,  $J_{\text{CF}}=243.8$  Hz), 161.2, 138.9, 137.4,

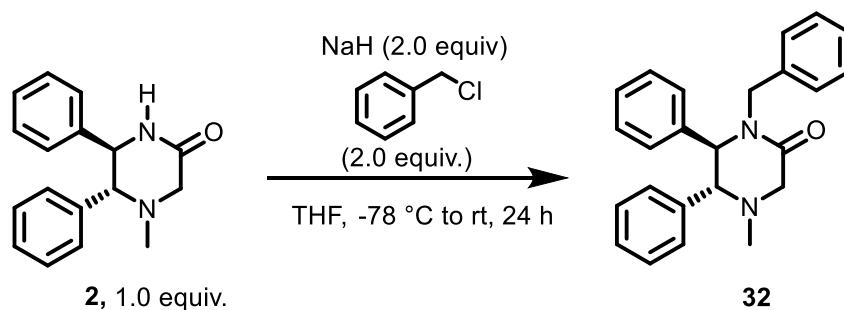
133.0 (d,  $J_{CF} = 2.5$  Hz), 130.3 (d,  $J_{CF} = 8.8$  Hz) 128.9, 128.7, 128.4, 128.4, 128.4, 127.6, 115.3 (d,  $J_{CF} = 21.3$  Hz), 71.7, 64.0, 58.3, 55.5. HRMS (ESI-TOF)  $m/z$ :  $[(M+H)^+]$  calcd for  $(C_{23}H_{22}FN_2O^+)$  361.1711; found, 361.1721.

(5*R*,6*R*)-4-(4-chlorobenzyl)-5,6-diphenylpiperazin-2-one (**31**)



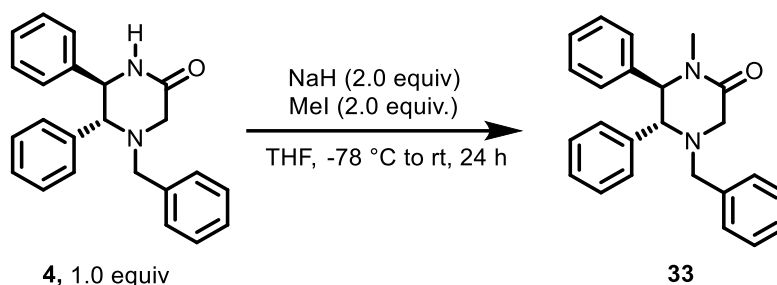
Isolated with 50% hexane in ethyl acetate. White solid (156.6 mg, 43%). MP: 151-152 °C. IR: 3250, 1683  $cm^{-1}$ .  $^1H$  NMR (500 MHz,  $CDCl_3$ )  $\delta$  7.26-7.23 (m, 5H) 7.22-7.13 (m, 7H), 6.95 (dt,  $J = 6.6, 1.6$  Hz, 2H), 6.19 (s, 1H), 4.69 (d,  $J = 8.5$  Hz, 1H), 3.74 (d,  $J = 13.3$  Hz, 1H), 3.50 (d,  $J = 17.1$  Hz, 1H), 3.47 (d,  $J = 8.5$  Hz, 1H), 3.05 (d,  $J = 17.1$  Hz, 1H), 2.87 (d,  $J = 13.3$  Hz, 1H).  $^{13}C\{^1H\}$  NMR (125 MHz,  $CDCl_3$ )  $\delta$  168.9, 138.9, 137.3, 135.9, 133.2, 130.1, 128.9, 128.8, 128.6, 128.4, 128.4, 127.6, 71.6, 64.0, 58.3, 55.5. HRMS (ESI-TOF)  $m/z$ :  $[(M+H)^+]$  calcd for  $(C_{23}H_{22}ClN_2O^+)$  377.1415; found :377.1431.

(5*R*,6*R*)-1-benzyl-4-methyl-5,6-diphenylpiperazin-2-one (**32**).



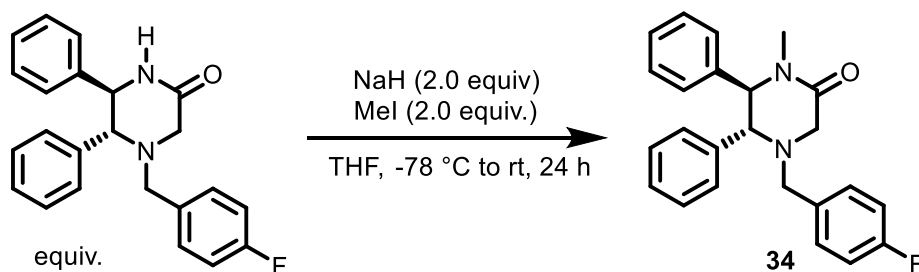
Isolated with 5% methanol in ethyl acetate. White solid (30.3 mg, 16%). MP: 159-161 °C. IR: 3030, 2800, 1650  $cm^{-1}$ .  $^1H$  NMR (500 MHz,  $CDCl_3$ )  $\delta$  7.29-7.08 (m, 11H), 6.91-6.88 (m, 2H), 6.83-6.81 (m, 2H), 5.50 (d,  $J = 14.8$  Hz 1H), 4.37 (d,  $J = 8.7$  Hz, 1H), 3.74 (d,  $J = 16.5$  Hz, 1H), 3.38 (d,  $J = 14.8$  Hz, 1H), 3.28 (d,  $J = 8.7$  Hz, 1H), 3.26 (d,  $J = 16.5$  Hz, 1H), 1.99 (s, 3H).  $^{13}C\{^1H\}$  NMR (125 MHz,  $CDCl_3$ )  $\delta$  168.1, 138.0, 137.9, 136.4, 128.8, 128.6, 128.5, 128.4, 128.3, 128.1, 128.1, 127.4, 74.6, 67.2, 59.6, 46.4, 43.0. HRMS (ESI-TOF)  $m/z$ :  $[(M+H)^+]$  calcd for  $(C_{24}H_{25}N_2O^+)$  357.1961; found 357.1968.

(5*R*,6*R*)-4-benzyl-1-methyl-5,6-diphenylpiperazin-2-one (**33**).



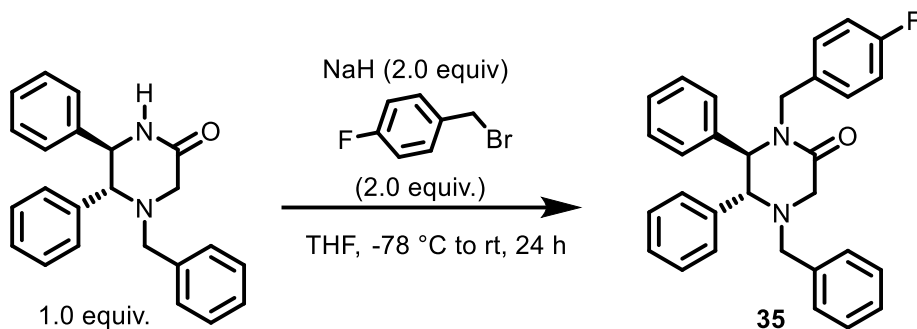
Isolated with 50% hexane in ethyl acetate. White solid (81.8 mg, 96%). MP: 114-115 °C. IR: 3030, 2800, 1650  $\text{cm}^{-1}$ .  $^1\text{H}$  NMR (500 MHz,  $\text{CDCl}_3$ )  $\delta$  7.31 – 7.20 (m, 8H), 7.17 – 7.12 (m, 4H), 7.01 – 6.97 (m, 2H). 4.54 (d,  $J$  = 7.1 Hz, 1H), 3.66 (d,  $J$  = 13.3 Hz, 1H), 3.60 (d,  $J$  = 7.1 Hz, 1H), 3.47 (d,  $J$  = 16.8 Hz, 1H), 3.15 (d,  $J$  = 16.8 Hz, 1H), 2.94 (d,  $J$  = 13.3 Hz, 1H), 2.76 (s, 3H).  $^{13}\text{C}\{^1\text{H}\}$  NMR (125 MHz,  $\text{CDCl}_3$ )  $\delta$  168.2, 138.8, 137.5, 137.3, 128.9, 128.8, 128.7, 128.5, 128.4, 128.3, 128.1, 127.8, 127.4, 71.5, 70.0, 58.7, 55.2, 32.6. HRMS (ESI-TOF)  $m/z$ :  $[(M+H)^+]$  calcd for ( $\text{C}_{24}\text{H}_{25}\text{N}_2\text{O}^+$ ) 357,1961; found, 357.1963.

(5*R*,6*R*)-4-(4-fluorobenzyl)-1-methyl-5,6-diphenylpiperazin-2-one (**34**)



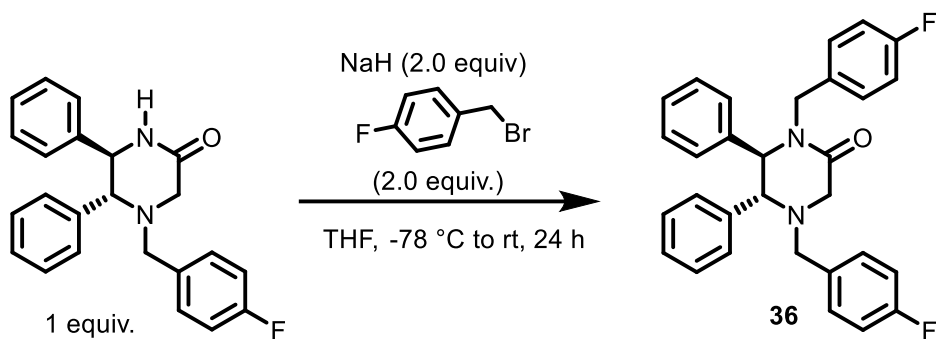
Isolated with 30% hexane in ethyl acetate. White solid (87.4 mg, 83%). MP: IR:3060, 2953, 1654  $\text{cm}^{-1}$ .  $^1\text{H}$  NMR (500 MHz,  $\text{CD}_2\text{Cl}_2$ )  $\delta$  7.31 – 7.25 (m, 5H), 7.14- 7.09 (m, 4H), 7.00-6.92 (m, 2H), 6.94-6.90 (m, 2H), 4.55 (d,  $J$  = 7.0 Hz, 1H), 3.60 (d,  $J$  = 13.3 Hz, 1H), 3.59 (d,  $J$  = 7.0 Hz, 1H), 3.44 (d,  $J$  = 16.7 Hz, 1H), 3.16 (d,  $J$  = 16.7 Hz, 1H), 2.93 (d,  $J$  = 13.3 Hz, 1H).  $^{13}\text{C}\{^1\text{H}\}$  NMR (125 MHz,  $\text{CDCl}_3$ )  $\delta$  169.0, 162.2 (d,  $J_{\text{CF}}$  = 243.8 Hz), 161.2, 138.9, 137.4, 133.0 (d,  $J_{\text{CF}}$  = 2.5 Hz), 130.3 (d,  $J_{\text{CF}}$  = 8.8 Hz) 128.9, 128.7, 128.4, 128.4, 128.4, 127.6, 115.3 (d,  $J_{\text{CF}}$  = 21.3 Hz), 71.7, 64.0, 58.3, 55.5. HRMS (ESI-TOF)  $m/z$ :  $[(M+H)^+]$  calcd for ( $\text{C}_{24}\text{H}_{24}\text{FN}_2\text{O}^+$ ) 357.1961; found, 357.1958.

(5*R*, 6*R*)-4-benzyl-1-(4-fluorobenzyl)-5,6-diphenylpiperazin-2-one (**35**)



Isolated with 75 % hexane in ethyl acetate. White solid (130.7 mg, 74%). MP: 163-164 °C. IR: 3030, 1653  $\text{cm}^{-1}$ .  $^1\text{H}$  NMR (500 MHz,  $\text{CD}_2\text{Cl}_2$ )  $\delta$  7.30-7.10 (m, 13H), 7.03 (td,  $J$  = 5.0, 3.0 Hz 2H), 7.00-6.91 (m, 4H), 5.28 (d,  $J$  = 14.6 Hz, 1H), 4.46 (d,  $J$  = 6.3 Hz, 1H), 3.69 (d,  $J$  = 6.3 Hz, 1H), 3.56 (d,  $J$  = 13.4 Hz, 1H), 3.48 (d,  $J$  = 14.6 Hz, 1H), 3.38 (d,  $J$  = 16.8 Hz, 1H), 3.24 (d,  $J_{\text{CF}}$  = 16.8 Hz, 1H), 3.02 (d,  $J$  = 13.4 Hz, 1H).  $^{13}\text{C}\{^1\text{H}\}$  NMR (125 MHz,  $\text{CDCl}_3$ )  $\delta$  168.2, 163.3 (d,  $J_{\text{CF}}$  = 245 Hz), 138.7, 137.2 (d,  $J_{\text{CF}}$  = 10.0 Hz), 132.3 d,  $J_{\text{CF}}$  = 2.5 Hz, 130.8, 130.7, 128.8, 128.7, 128.5, 128.5, 128.4, 128.2, 128.2, 128.1, 127.4, 115.4 (d,  $J_{\text{CF}}$  = 21.3 Hz), 70.3, 66.3, 58.5, 54.7, 46.2. HRMS (ESI-TOF)  $m/z$ :  $[(\text{M}+\text{H})^+]$  calcd for  $(\text{C}_{30}\text{H}_{28}\text{FN}_2\text{O}^+)$  451.2180; found, 451.2193.

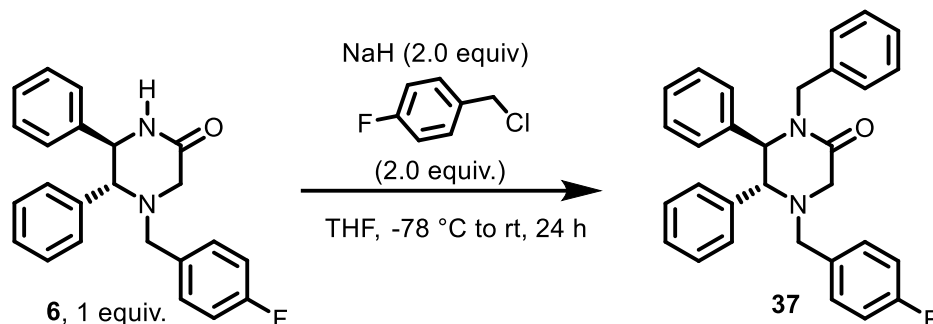
(5*R*,6*R*)-1,4-bis(4-fluorobenzyl)-5,6-diphenylpiperazin-2-one (**36**).



Isolated with 70% hexane in ethyl acetate. White solid (84.8 mg, 73%). MP: 143-145 °C. IR: 3064, 1653  $\text{cm}^{-1}$ .  $^1\text{H}$  NMR (500 MHz,  $\text{CDCl}_3$ )  $\delta$  7.33-7.27 (m, 3H), 7.25-7.18 (m, 3H), 7.13 (dd,  $J$  = 8.5, 5.5 Hz, 2H), 7.07 (dd,  $J$  = 8.4, 5.6 Hz, 2H), 7.01 (dd,  $J$  = 7.6, 1.8 Hz, 2H), 6.96-6.90 (m, 6H), 5.42 (d,  $J$  = 14.5 Hz, 1H), 4.45 (d,  $J$  = 6.0 Hz, 1H), 3.65 (d,  $J$  = 6.0 Hz, 1H), 3.5(d,  $J$  = 13.3 Hz), 3.47 (d,  $J$  = 14.5 Hz), 3.43 (d,  $J$  = 16.9 Hz), 3.27 (d,  $J$  = 16.9 Hz, 1H), 3.02 (d,  $J$  = 13.3 Hz, 1H).  $^{13}\text{C}\{^1\text{H}\}$  NMR (125 MHz,  $\text{CDCl}_3$ )  $\delta$  168.0, 163.3 (d,  $J_{\text{CF}}$  = 244 Hz), 162.2 (d,  $J_{\text{CF}}$  = 244 Hz), 161.4, 161.2, 138.8, 137.0, 133.0, 132.9 (d,  $J_{\text{CF}}$  = 3. Hz), 132.2 (d,  $J_{\text{CF}}$  = 3.0 Hz), 130.8 (d,  $J_{\text{CF}}$  = 8.0 Hz), 130.3 (d,  $J_{\text{CF}}$  = 8.0 Hz),

130.8, 130.3, 130.3, 128.7, 128.6, 128.6, 128.3, 128.0, 115.6 (d,  $J_{CF} = 21.4$  Hz), 115.3 (d,  $J_{CF} = 21.4$  Hz), 69.9, 66.1, 57.7, 54.5, 46.3. HRMS (ESI-TOF)  $m/z$ :  $[(M+H)^+]$  calcd for  $(C_{30}H_{27}F_2N_2O^+)$  469.2086; found, 469.2098.

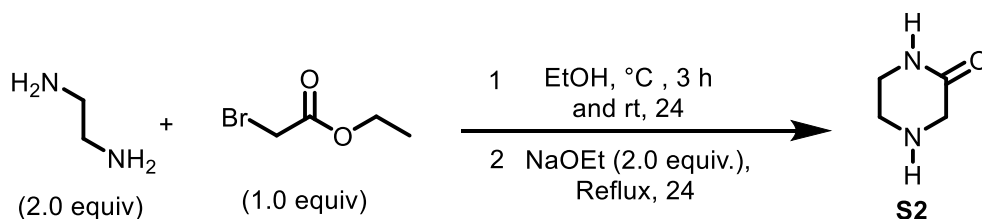
(5*R*,6*R*)-1-benzyl-4-(4-fluorobenzyl)-5,6-diphenylpiperazi-2-one (**37**)



Isolated with 75 % hexane in ethyl acetate. White solid (21 mg, 21%).

. IR: 3030, 1653  $cm^{-1}$ .  $^1H$  NMR (500 MHz,  $CD_2Cl_2$ )  $\delta$  7.30-7.10 (m, 13H), 7.03 (td,  $J = 5.0$ , 3.0 Hz 2H), 7.00-6.91 (m, 4H), 5.44 (d,  $J = 14.6$  Hz, 1H), 4.52 (d,  $J = 6.0$  Hz, 1H), 3.70 (d,  $J = 6.3$  Hz, 1H), 3.52 (d,  $J = 13.5$  Hz, 1H), 3.46 (d,  $J = 14.7$  Hz, 1H), 3.39 (d,  $J = 16.8$  Hz, 1H), 3.28 (d,  $J_{CF} = 16.8$  Hz, 1H), 3.05 (d,  $J = 13.5$  Hz, 1H).  $^{13}C\{^1H\}$  NMR (125 MHz,  $CDCl_3$ )  $\delta$  168.2, 163.3 (d,  $J_{CF} = 245$  Hz), 138.7, 137.2 (d,  $J_{CF} = 10.0$  Hz), 132.3 d,  $J_{CF} = 2.5$  Hz, 130.8, 130.7, 128.8, 128.7, 128.5, 128.5, 128.4, 128.2, 128.2, 128.1, 127.4, 115.4 (d,  $J_{CF} = 21.3$  Hz), 70.3, 66.3, 58.5, 54.7, 46.2. HRMS (ESI-TOF)  $m/z$ :  $[(M+H)^+]$  calcd for  $(C_{30}H_{28}FN_2O^+)$  451.2180; found, 451.2193.

Piperazin-2-one (**S2**)



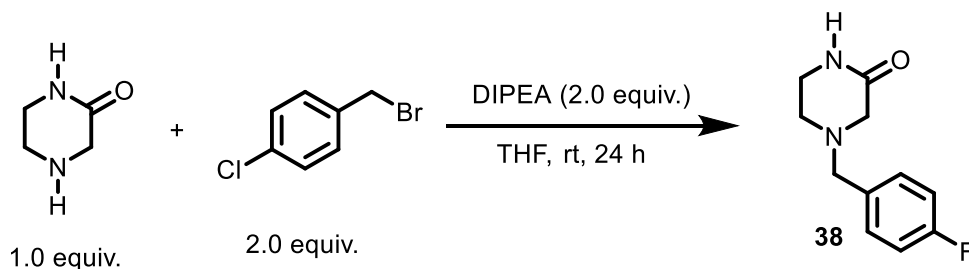
To a solution of ethylenediamine (3.34 mL, 50.0 mmol) in EtOH (40 mL) at 0 °C was added ethyl bromoacetate (2.76 mL, 25.0 mmol) dropwise. The solution was allowed to warm to room temperature and stirred overnight. The resulting white solid was removed by filtration, and the filtrate was transferred to a flame-dried flask containing sodium ethoxide (3.74 g, 55.0 mmol) under nitrogen gas. The solution was then refluxed overnight. The

reaction was cooled to room temperature and concentrated. The solid residue was purified *using an automated combiflash chromatography* (silica gel, 20-40 microns, gradient 5-10% methanol in dichloromethane). The product identity was confirmed by comparing it to previously reported data.<sup>4</sup> White solid (977 mg, 39%). MP: 133-134°C. IR: 3325, 3062, 1684 cm<sup>-1</sup>. <sup>1</sup>H NMR (500 MHz, CD<sub>2</sub>Cl<sub>2</sub>) δ 1.62 (s, 1H), 2.96 (d, *J* = 5.4 Hz, 2H), 3.30 (td, *J* = 5.4, 2.4 Hz, 2H). <sup>13</sup>C{<sup>1</sup>H} NMR (125 MHz, CD<sub>2</sub>Cl<sub>2</sub>) δ 170.2, 50.3, 43.3, 42.7 HRMS (ESI-TOF) *m/z*: [(M+H)<sup>+</sup>] calcd for (C<sub>4</sub>H<sub>9</sub>N<sub>2</sub>O<sup>+</sup>) 101.0709; found, 101.0713.

General procedure for the synthesis of compounds **38-40**.

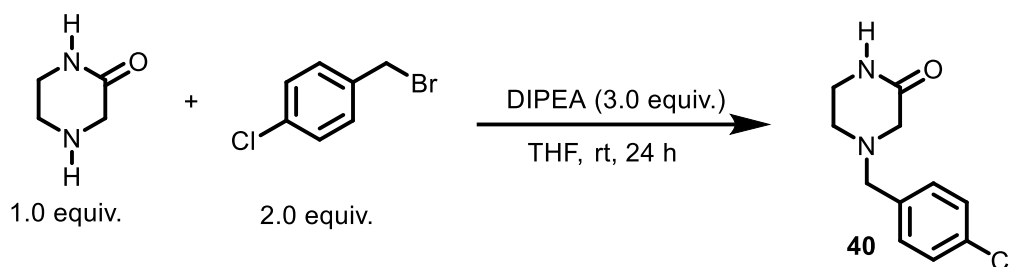
To a solution of piperazin-2-one (2-3 mmol, 1 equiv) was added diisopropyl ethylamine (4-6 mmol, 2 equiv), the corresponding alkylating agent and 10 mL of dry THF. The solution was allowed to stir at room temperature for 24 hours. The reaction mixture was concentrated and dissolved in 10 mL of saturated aqueous NaHCO<sub>3</sub> solution. The resulting solution was extracted with 20 mL (3x) of EtOAc and the organic layers were concentrated until a white solid start precipitating out of solution. The solid was then collected by filtration.

4-(4-fluorobenzyl)piperazin-2-one (**38**)



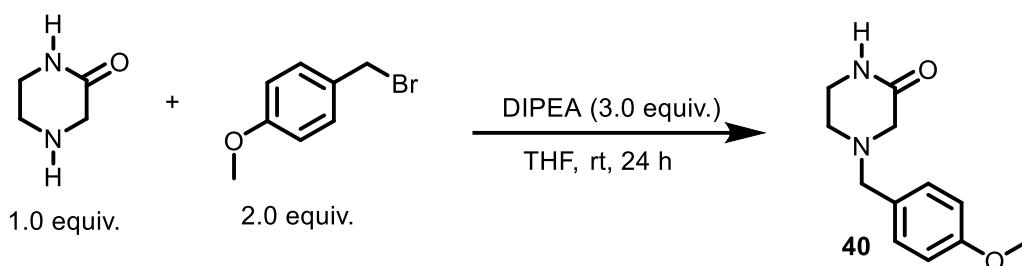
White solid (263.7 mg, 54%). MP: 128-129 °C. IR: 3256, 1676 cm<sup>-1</sup>. <sup>1</sup>H NMR (500 MHz, CD<sub>2</sub>Cl<sub>2</sub>) δ 7.45 – 7.19 (m, 2H), 7.08 – 6.92 (m, 2H), 6.09 (s, 1H), 3.51 (s, 2H), 3.39 – 3.19 (m, 2H), 3.04 (s, 2H), 2.71 – 2.28 (m, 2H). <sup>13</sup>C{<sup>1</sup>H} NMR (125 MHz, CD<sub>2</sub>Cl<sub>2</sub>) δ 169.2, 162.5 (d, *J*<sub>CF</sub> = 243.8 Hz), 133.7 (d, *J*<sub>CF</sub> = 2.5 Hz), 130.5 (d, *J*<sub>CF</sub> = 7.5 Hz), 115.4 d (*J*<sub>CF</sub> = 21.3 Hz), 61.3, 57.3, 49.0, 41.8. HRMS (ESI-TOF) *m/z*: [(M+H)<sup>+</sup>] calcd for (C<sub>11</sub>H<sub>14</sub>FN<sub>2</sub>O<sup>+</sup>) 209.1085; found, 209.1079.

4-(4-chlorobenzyl)piperazin-2-one (**39**)



White solid (265.8 mg, 61%). MP: 156-157 °C. IR: 3406, 3063, 1671  $\text{cm}^{-1}$ .  $^1\text{H}$  NMR (500 MHz,  $\text{CD}_2\text{Cl}_2$ )  $\delta$  7.63 – 7.35 (m, 4H), 6.88 (s, 1H), 3.73 (s, 2H), 3.63 – 3.44 (m, 2H), 3.26 (s, 2H), 2.82 – 2.78 (m, 2H).  $^{13}\text{C}\{^1\text{H}\}$  NMR (125 MHz,  $\text{CD}_2\text{Cl}_2$ )  $\delta$  169.5, 136.5, 133.2, 130.7, 130.7, 128.8, 61.3, 57.3, 49.0, 41.7. HRMS (ESI-TOF)  $m/z$ :  $[(\text{M}+\text{H})^+]$  calcd for  $(\text{C}_{11}\text{H}_{14}\text{ClN}_2\text{O}^+)$  255.0789; found, 255.0796.

4-(4-methoxybenzyl)piperazin-2-one (**40**)



White solid (169.8 mg, 57%). MP: 156-157 °C. IR: 3261, 2837, 1670  $\text{cm}^{-1}$ .  $^1\text{H}$  NMR (500 MHz,  $\text{CD}_2\text{Cl}_2$ )  $\delta$  7.36 – 6.96 (m, 2H), 6.84 (d,  $J$  = 8.6 Hz, 3H), 5.89 (s, 1H), 3.76 (s, 3H), 3.48 (s, 2H), 3.39 – 3.20 (m, 2H), 3.03 (s, 2H), 2.67 – 2.45 (m, 2H).  $^{13}\text{C}$  NMR (125 MHz,  $\text{CD}_2\text{Cl}_2$ )  $\delta$  169.3, 159.4, 130.6, 129.7, 114.0, 61.5, 57.3, 55.6, 48.9, 41.9. HRMS (ESI-TOF)  $m/z$ :  $[(\text{M}+\text{H})^+]$  calcd for  $(\text{C}_{12}\text{H}_{17}\text{N}_2\text{O}_2^+)$  221.1285; found, 221.1278.

## REFERENCES

- (1) Kisselev, A. F.; Goldberg, A. L. Monitoring Activity and Inhibition of 26S Proteasomes with Fluorogenic Peptide Substrates. *Methods Enzymol.* **2005**, 398, 364–378.
- (2) Jones, C. L.; Njomen, E.; Sjögren, B.; Dexheimer, T. S.; Tepe, J. J. Small Molecule Enhancement of 20S Proteasome Activity Targets Intrinsically Disordered Proteins. *ACS Chem. Biol.* **2017**, 12, 2240–2247.
- (3) Jia, M. Q.; Li, Y.; Rong, Z. Q.; You, S. L. Synthesis of (1R,2R)-DPEN-Derived Triazolium Salts and Their Application in Asymmetric Intramolecular Stetter Reactions. *Org. Biomol. Chem.* **2011**, 9, 2072–2074.
- (4) Korch, K. M.; Eidamshaus, C.; Behenna, D. C.; Nam, S.; Horne, D.; Stoltz, B. M. Enantioselective Synthesis of  $\alpha$ -Secondary and  $\alpha$ -Tertiary Piperazin-2- Ones and Piperazines by Catalytic Asymmetric Allylic Alkylation. *Angew. Chemie - Int. Ed.* **2015**, 54, 179–183.



## APPENDIX

### NMR Spectra:

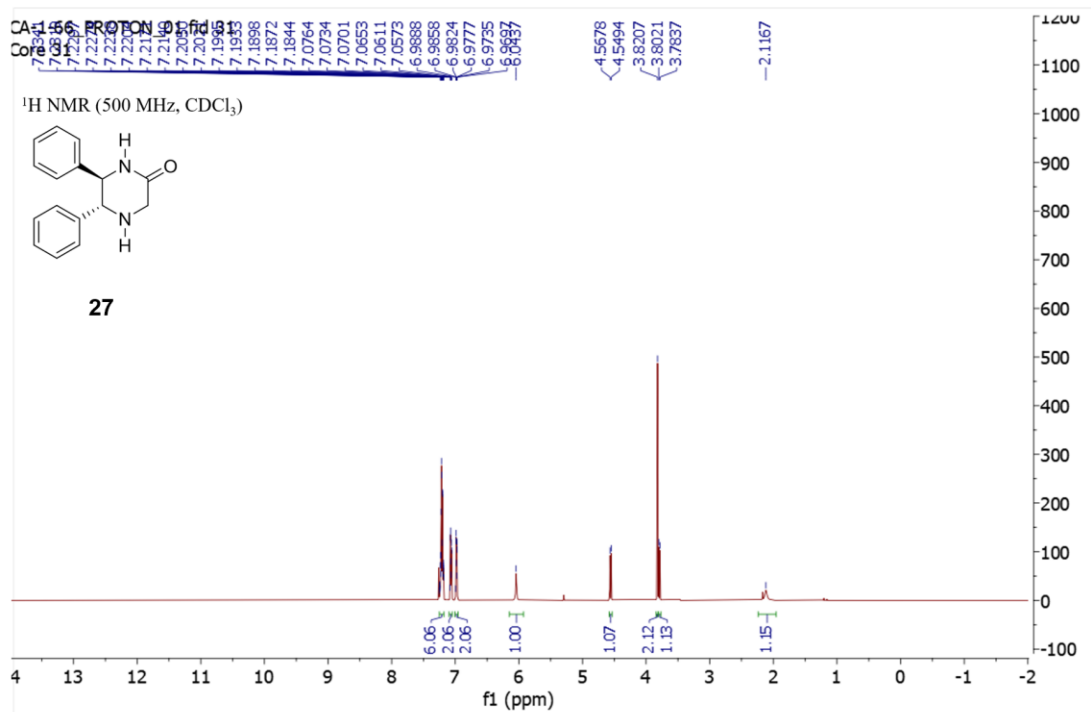


**Figure 4.7: Proton NMR of compound 27. Related to scheme 4.1.**

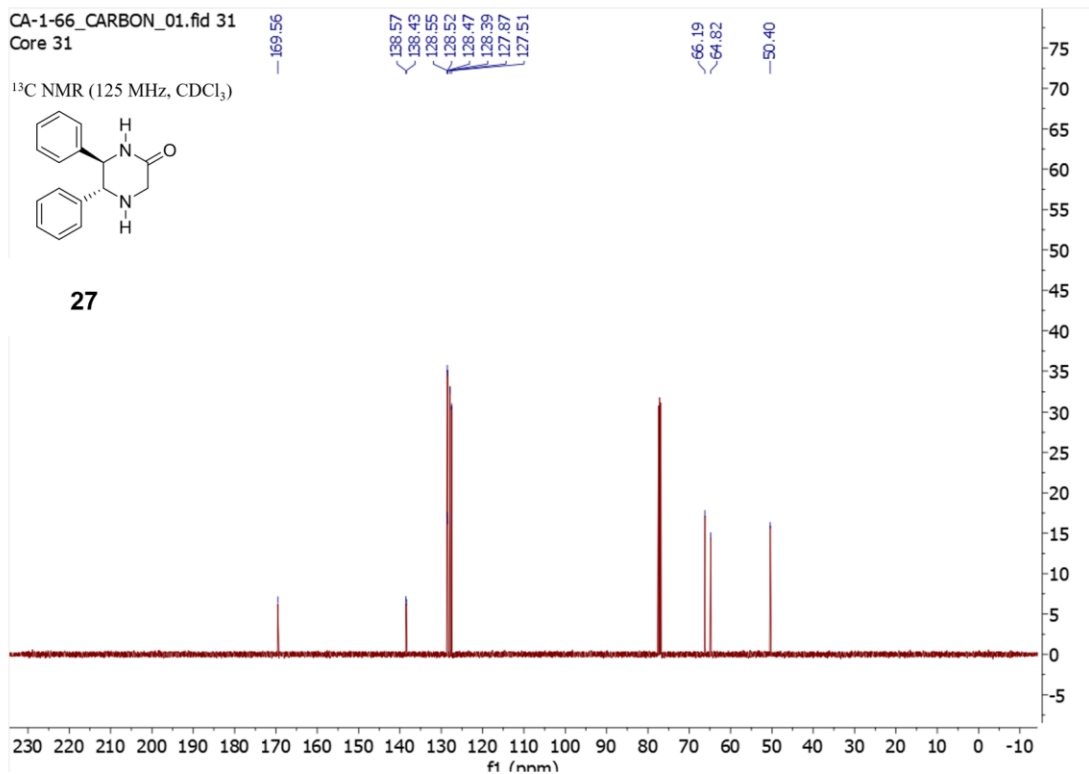


**Figure 4.8: Carbon-13 NMR of compound 27. Related to scheme 4.1.**

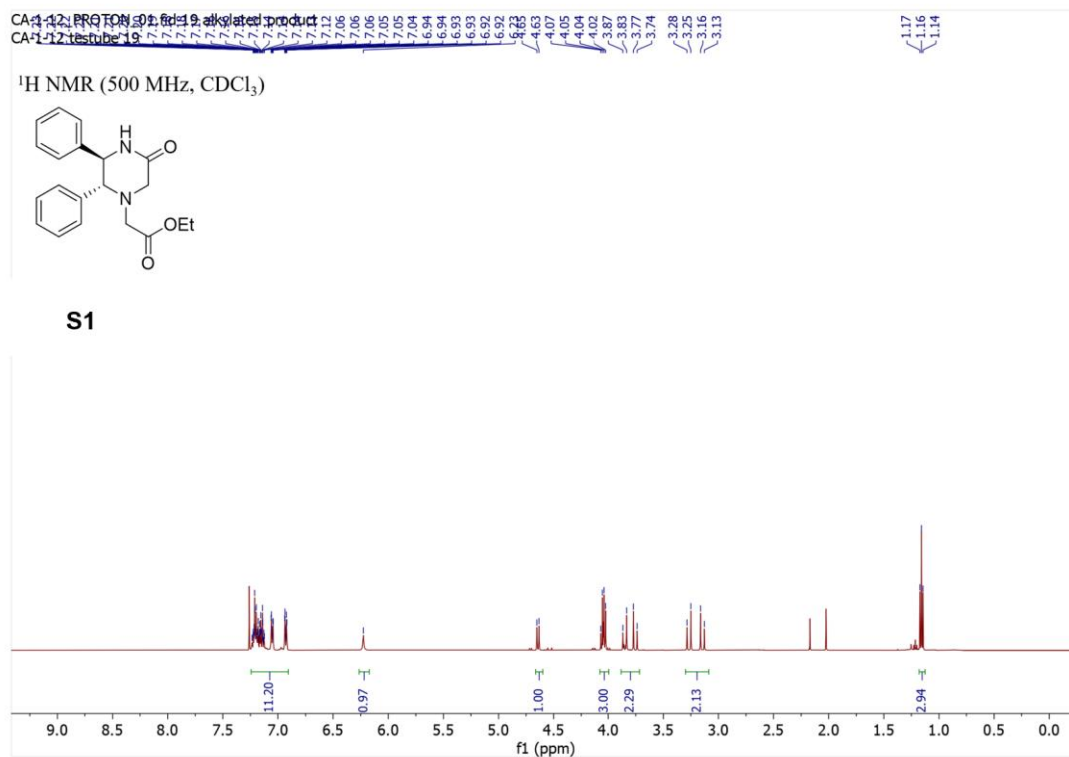


**Figure 4.9: Proton NMR of compound S1. Related to scheme 4.1.**

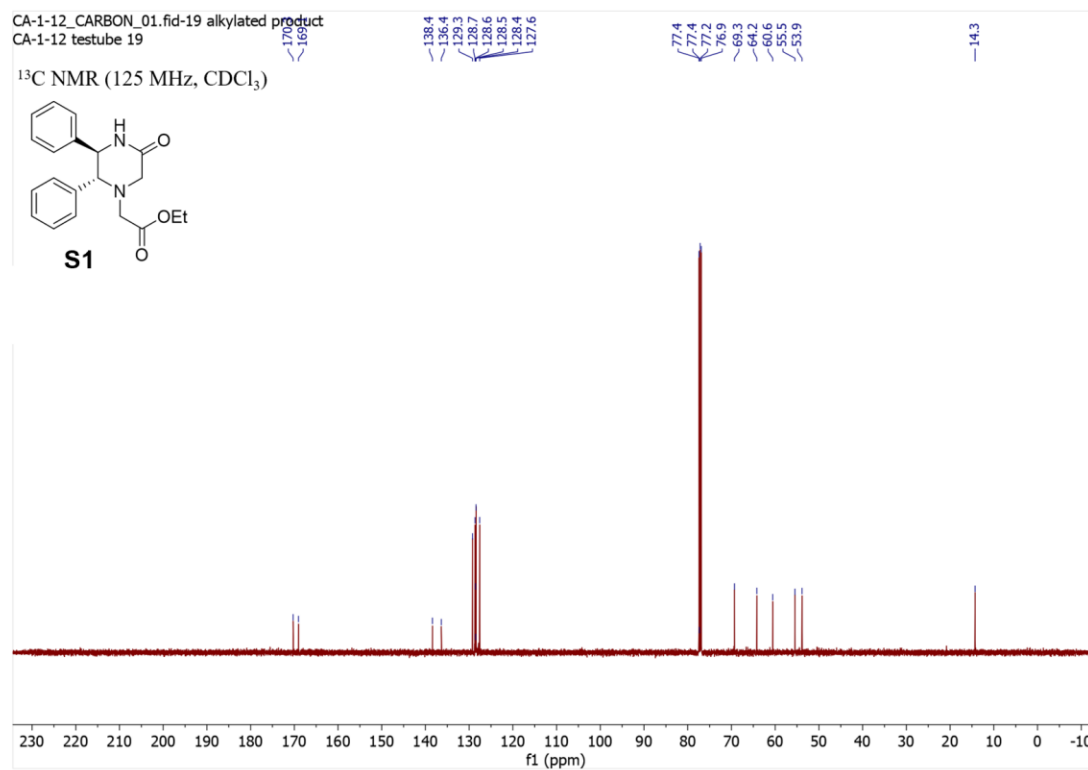


**Figure 4.10: Carbon-13 NMR of compound S1. Related to scheme 4.1.**



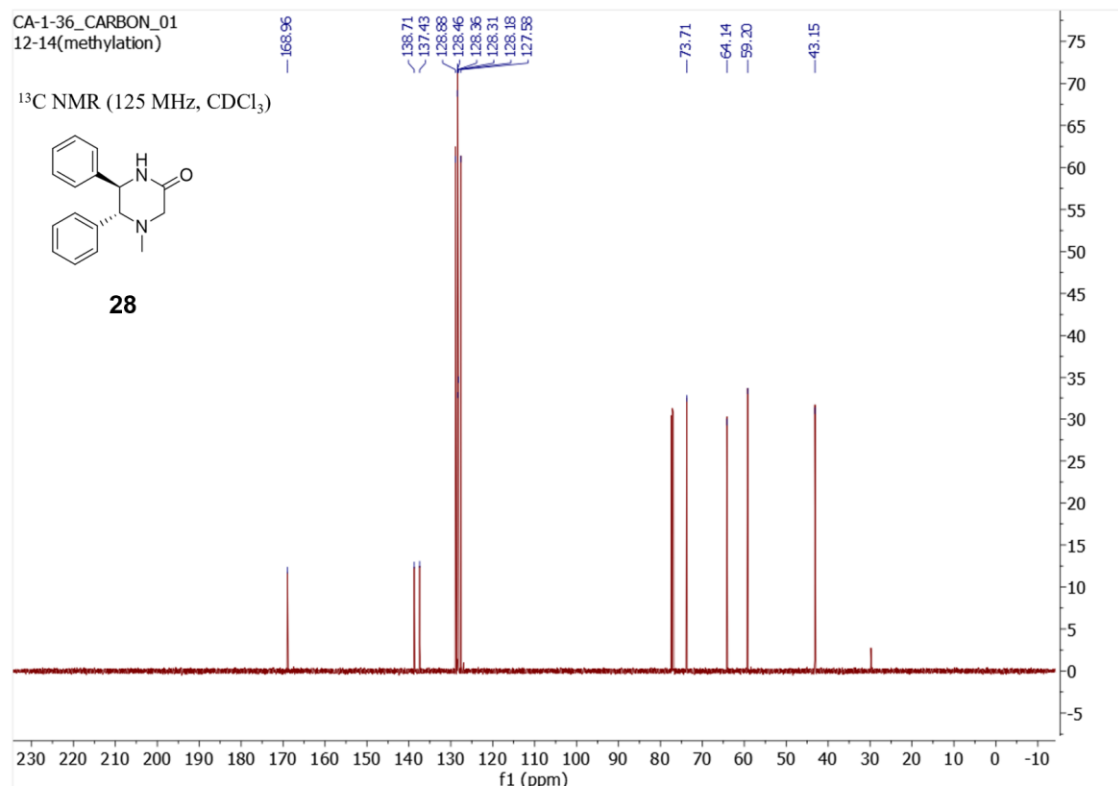


**Figure 4.12: Carbon-13 NMR of compound 28. Related to scheme 4.1.**

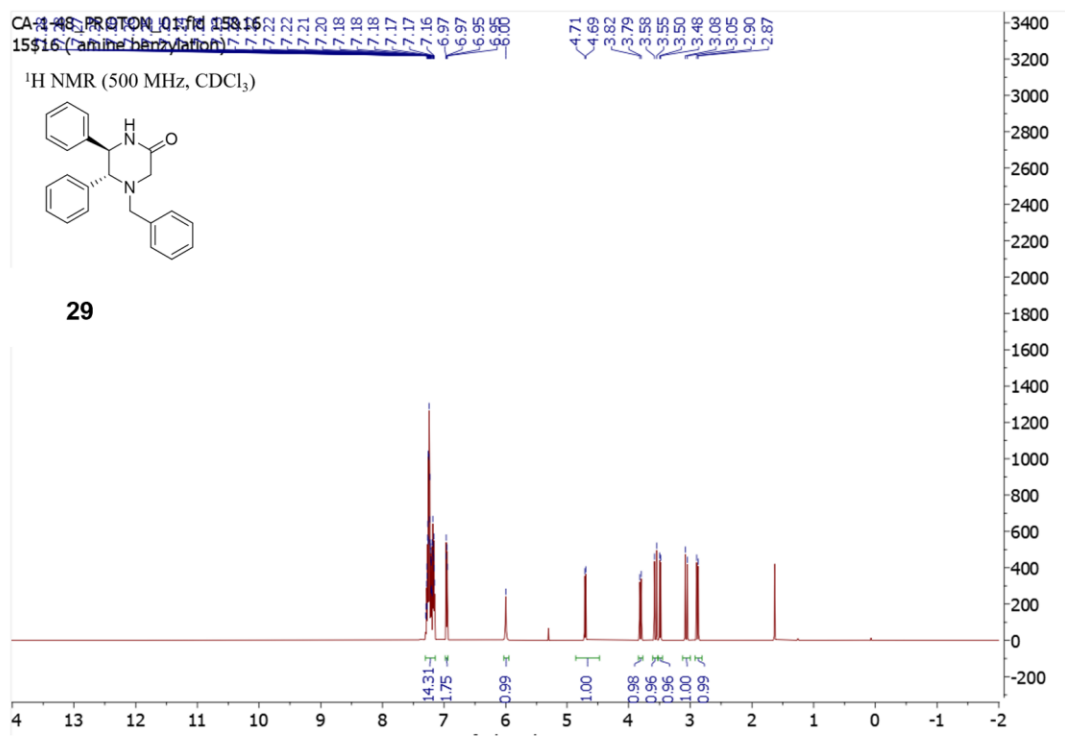


**Figure 4.13: Proton NMR of compound 29. Related to scheme 4.1.**

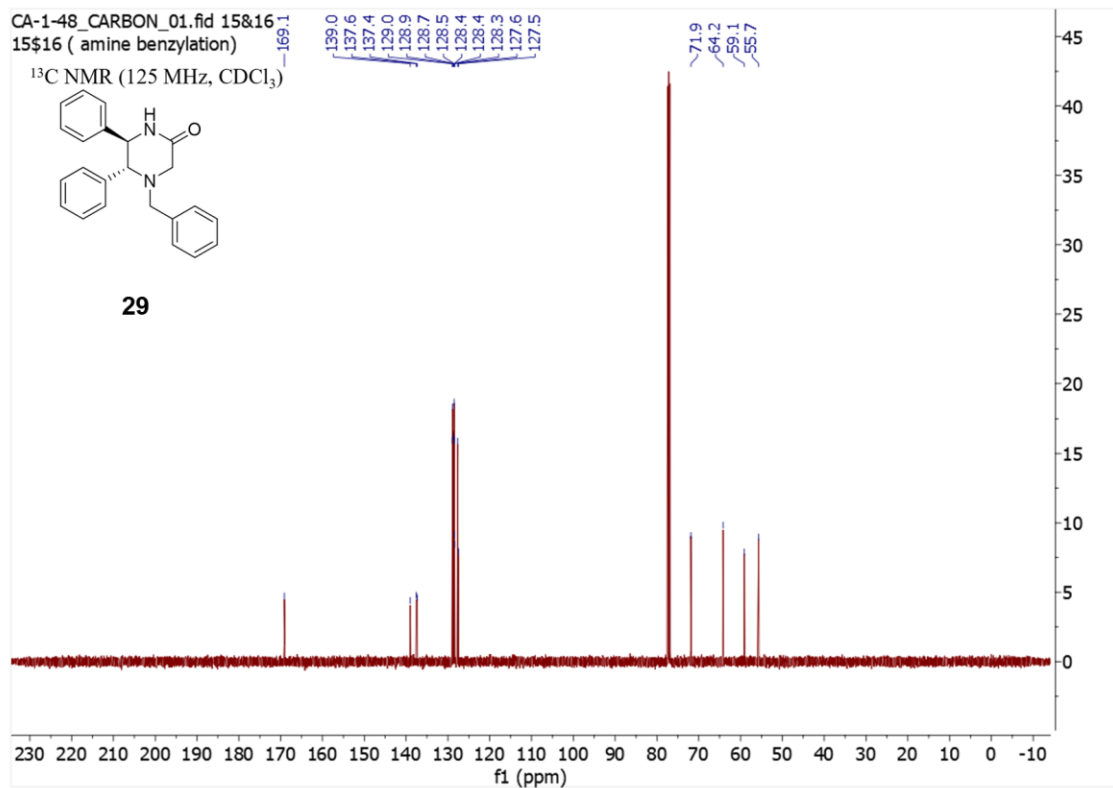


**Figure 4.14: Carbon-13 NMR of compound 29. Related to scheme 4.1.**





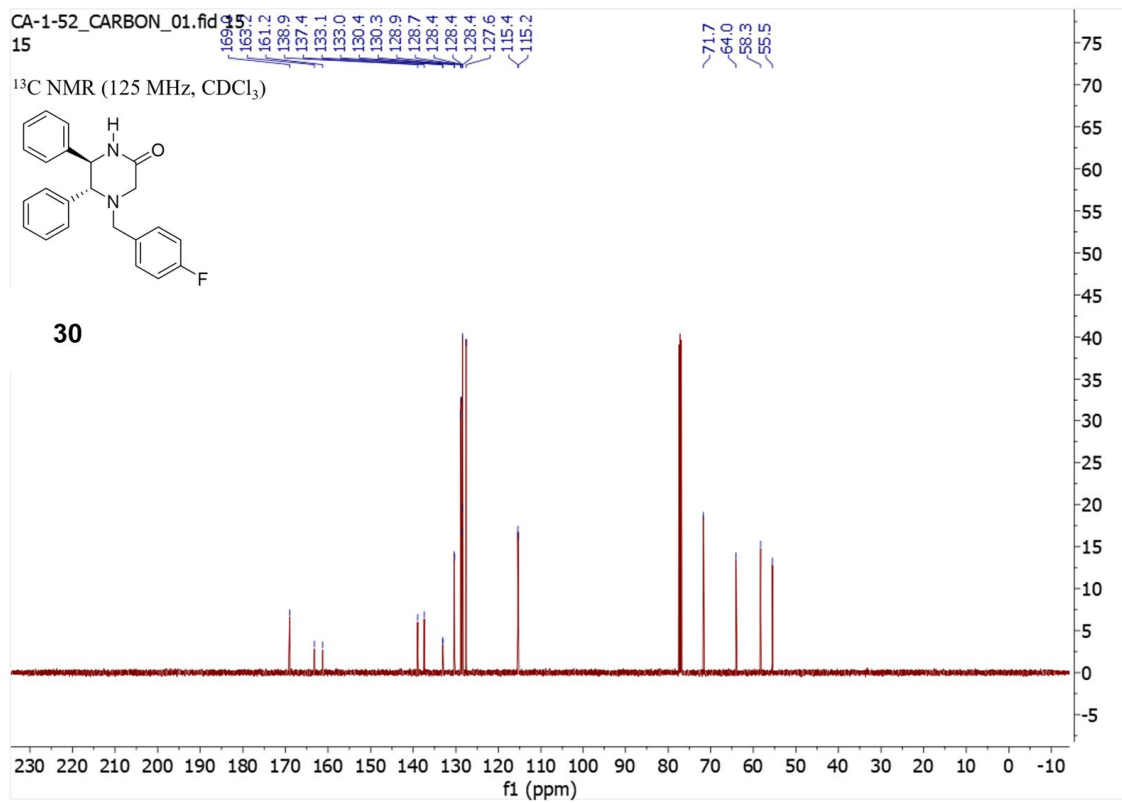


**Figure 4.16: Carbon-13 NMR of compound 30. Related to scheme 4.1.**

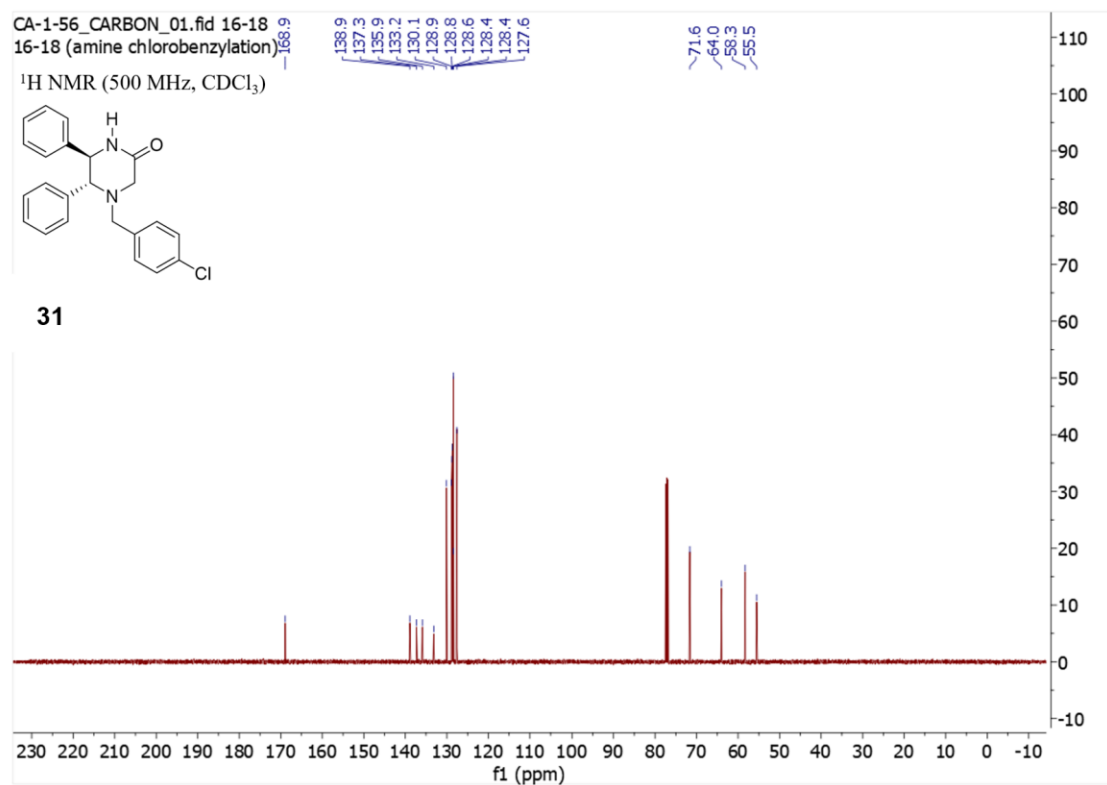


**Figure 4.17: Proton NMR of compound 31. Related to scheme 4.1.**

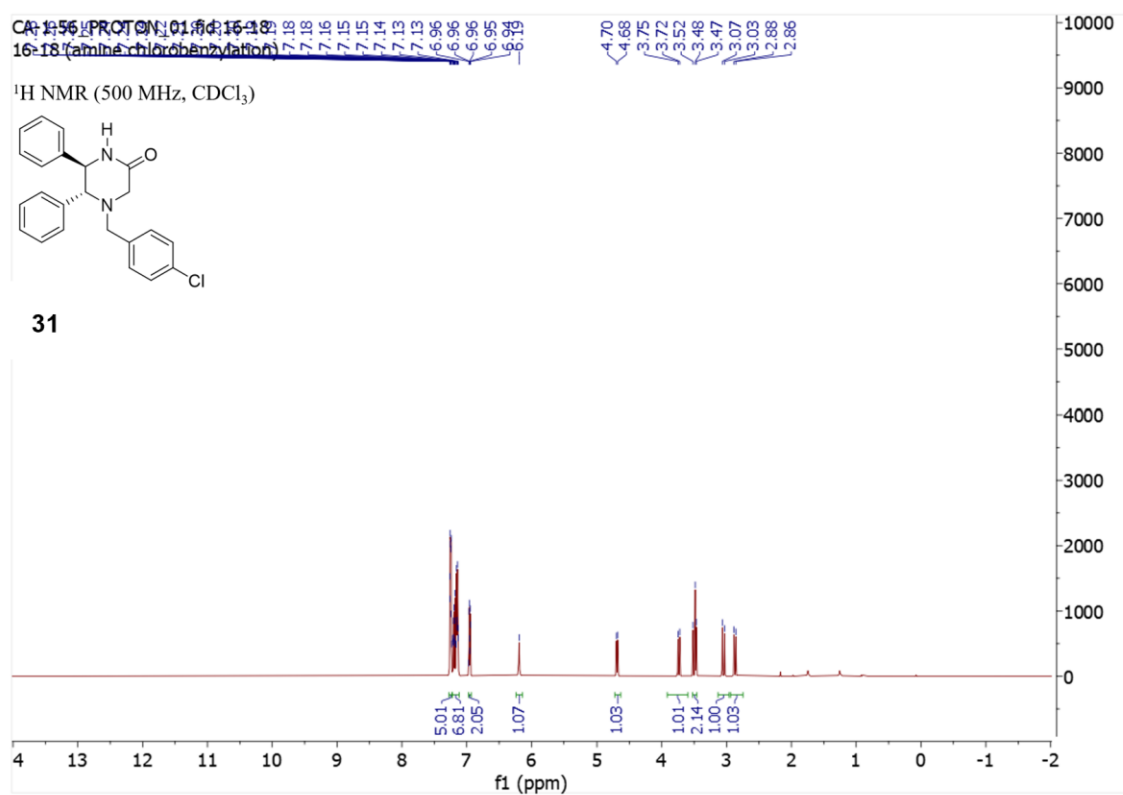


**Figure 4.18: Carbon-13 NMR of compound 31. Related to scheme 4.1.**

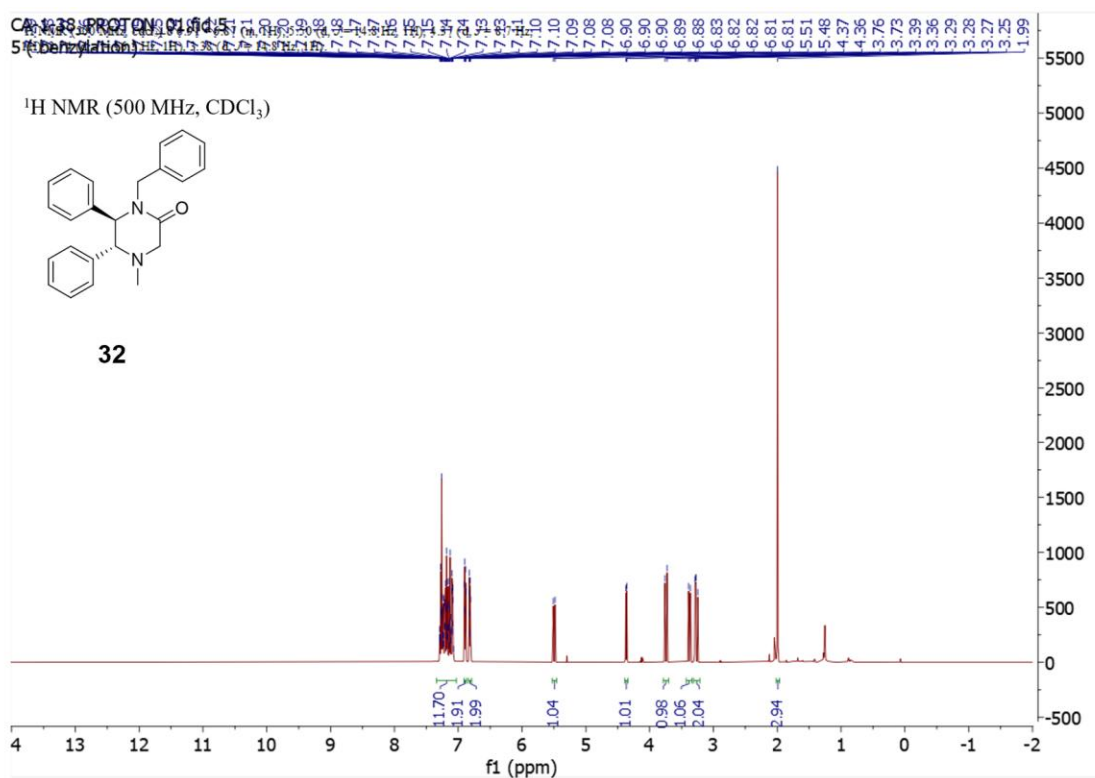


**Figure 4.19: Proton NMR of compound 32. Related to scheme 4.2.**

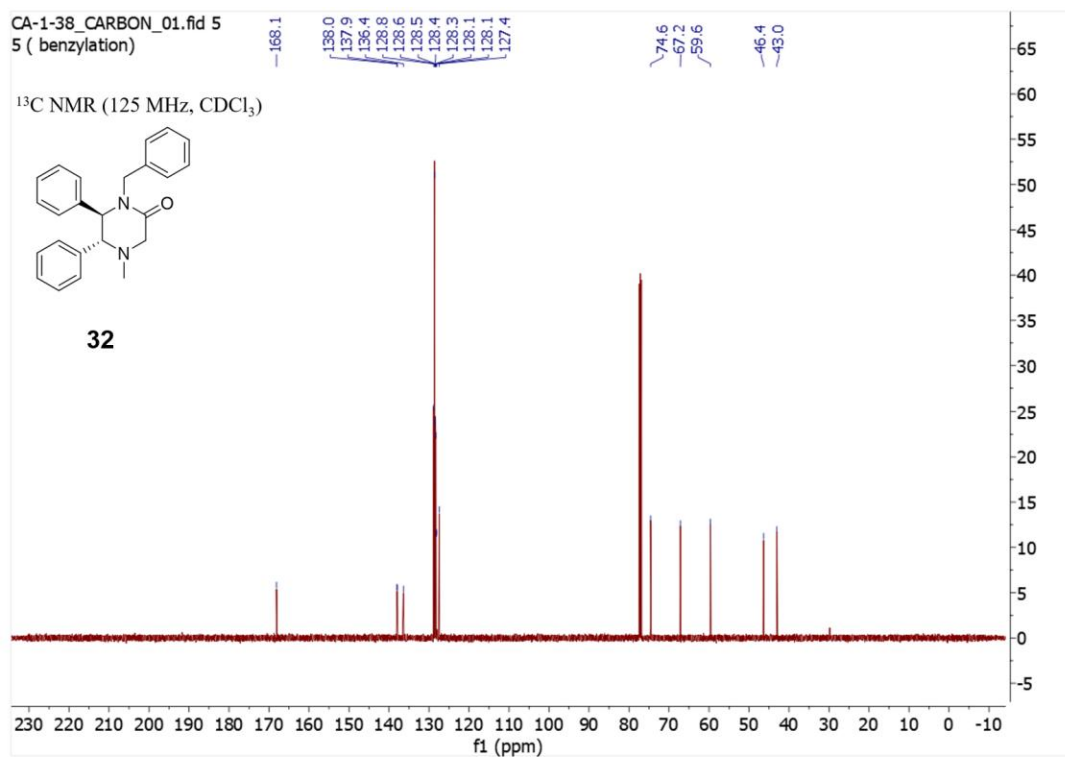


**Figure 4.20: Carbon-13 NMR of compound 32. Related to scheme 4.2.**



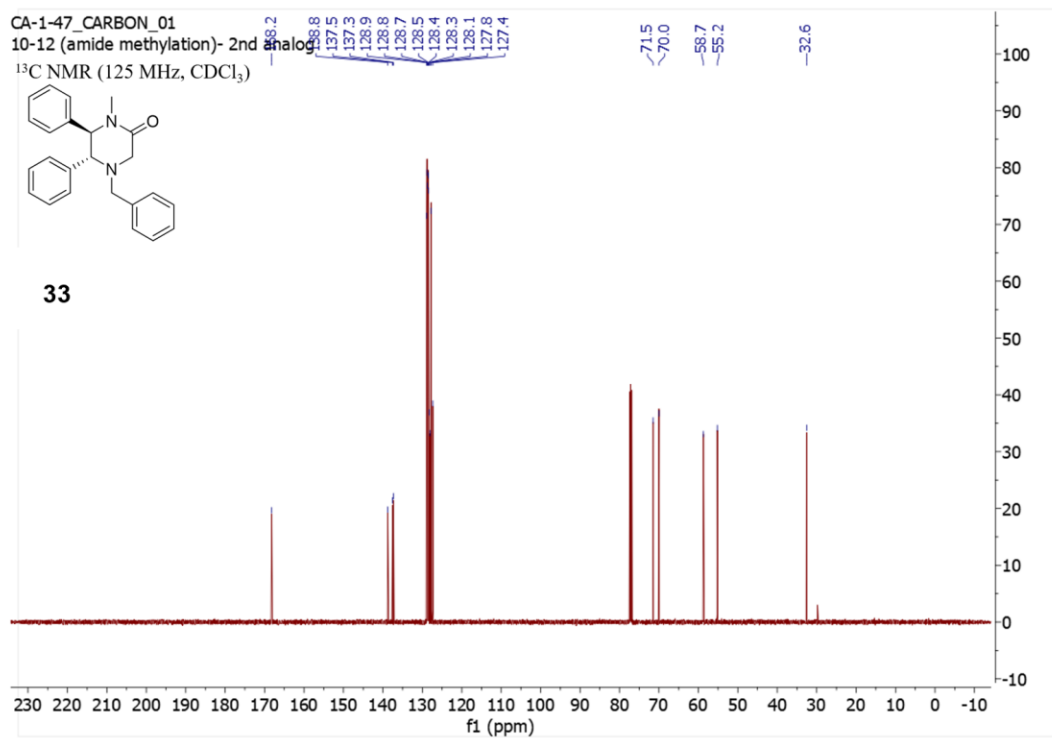


**Figure 4.22: Carbon-13 NMR of compound 33. Related to scheme 4.2.**



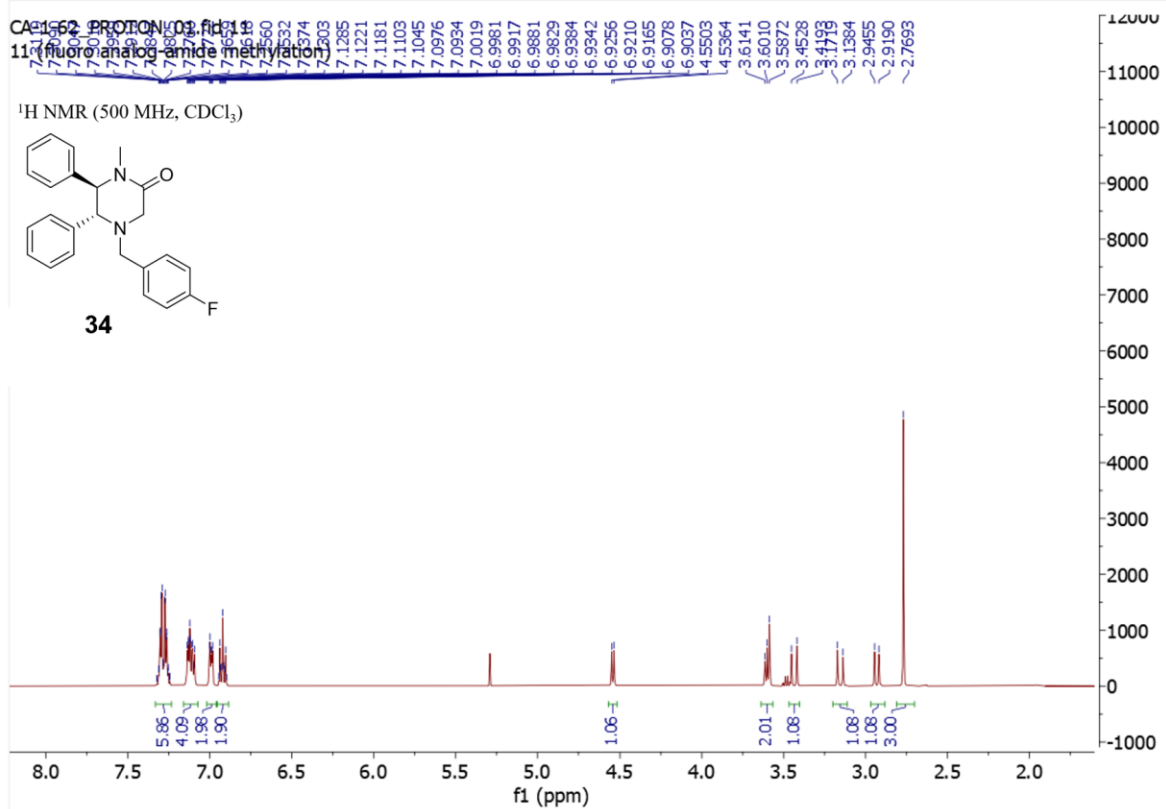


**Figure 4.23: Proton NMR of compound 33. Related to scheme 4.2.**

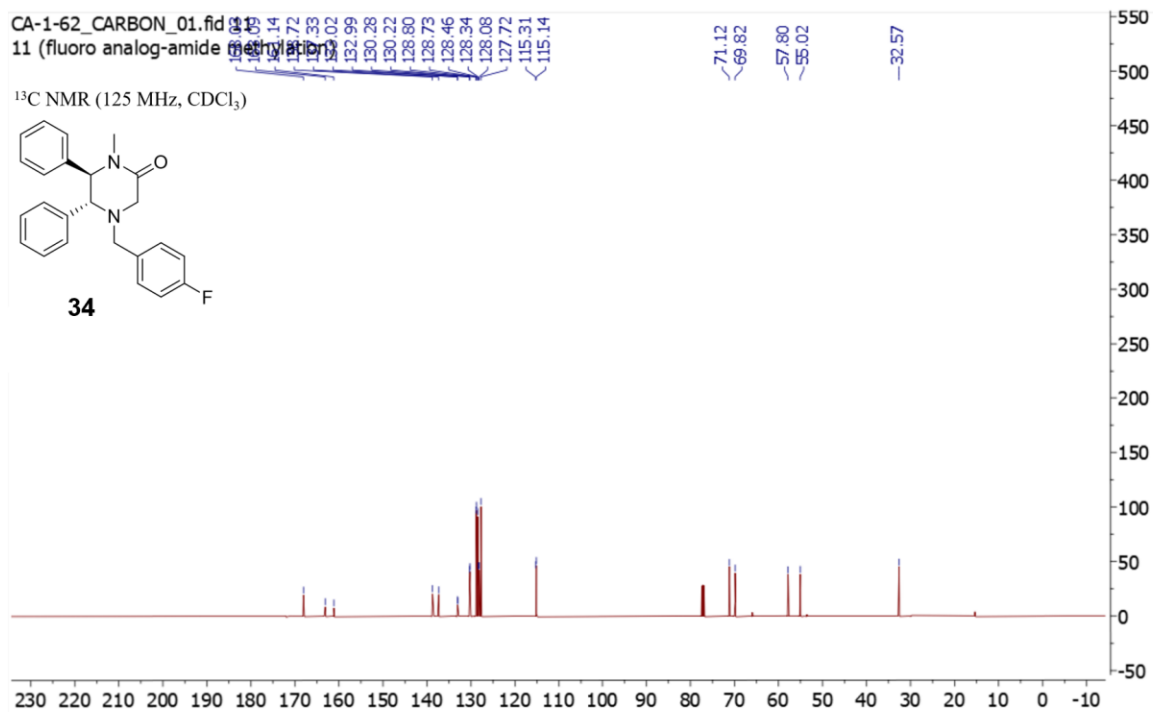


**Figure 4.24: Carbon-13 NMR of compound 34. Related to scheme 4.2.**



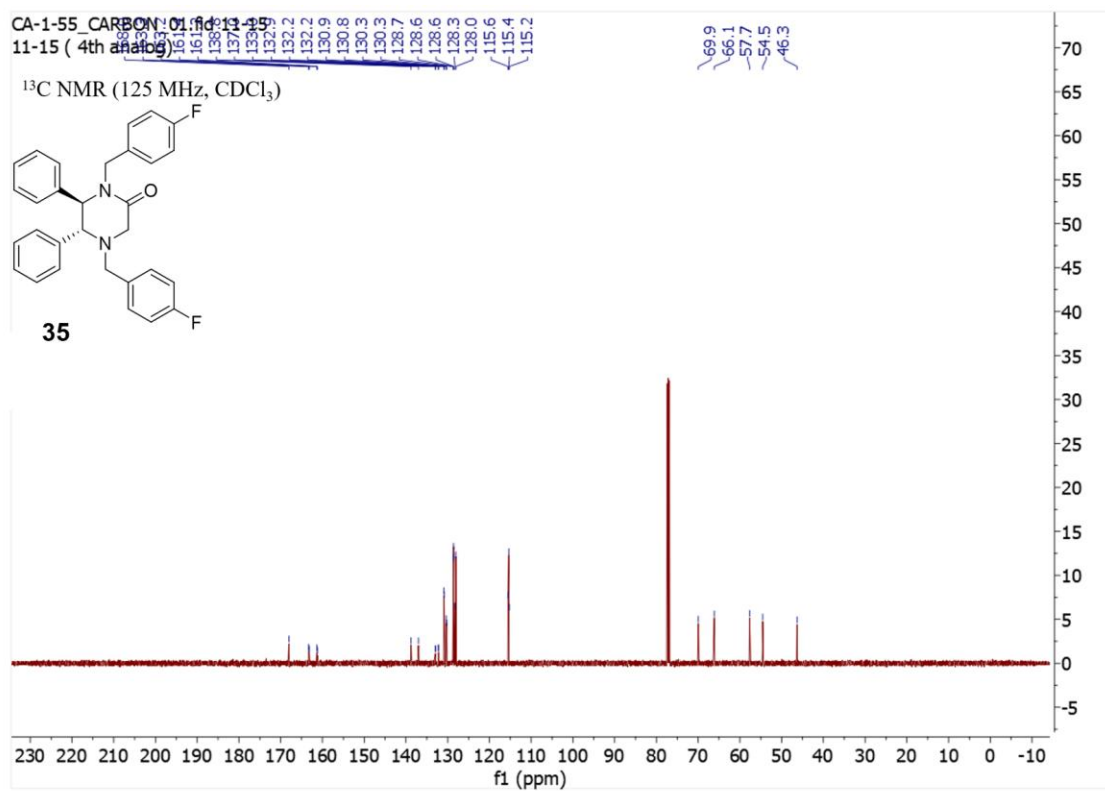


**Figure 4.26: Carbon-13 NMR of compound 35. Related to scheme 4.2.**

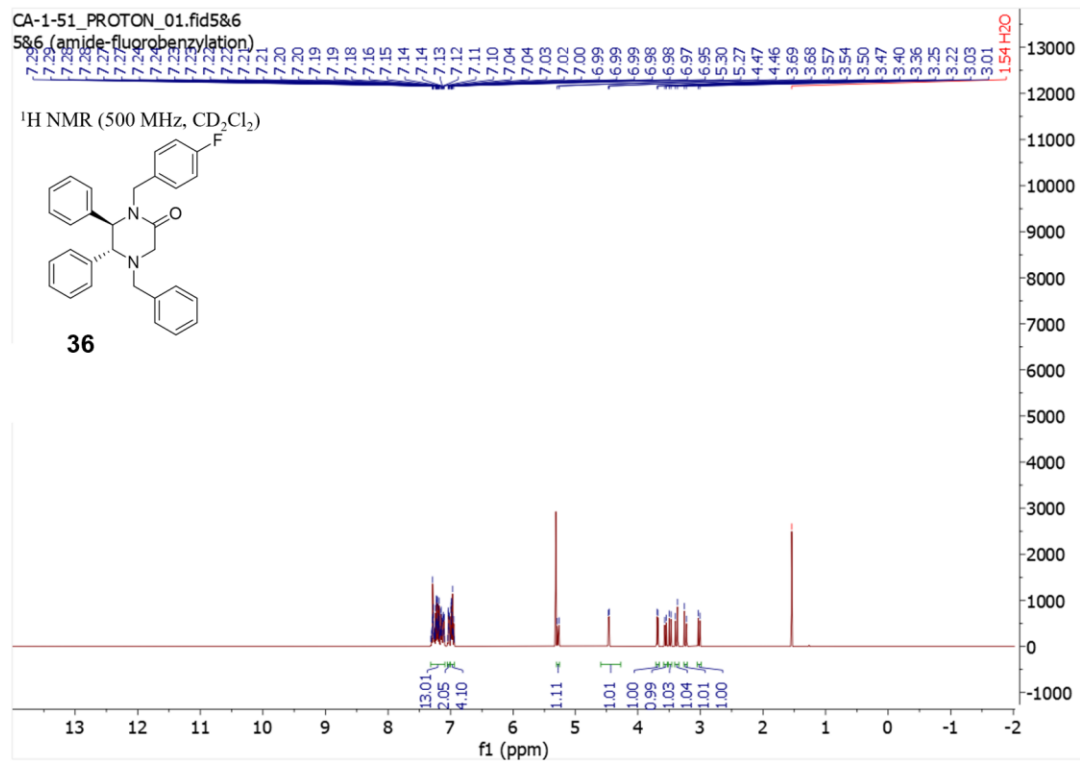


**Figure 4.27: Proton NMR of compound 36. Related to scheme 4.2.**

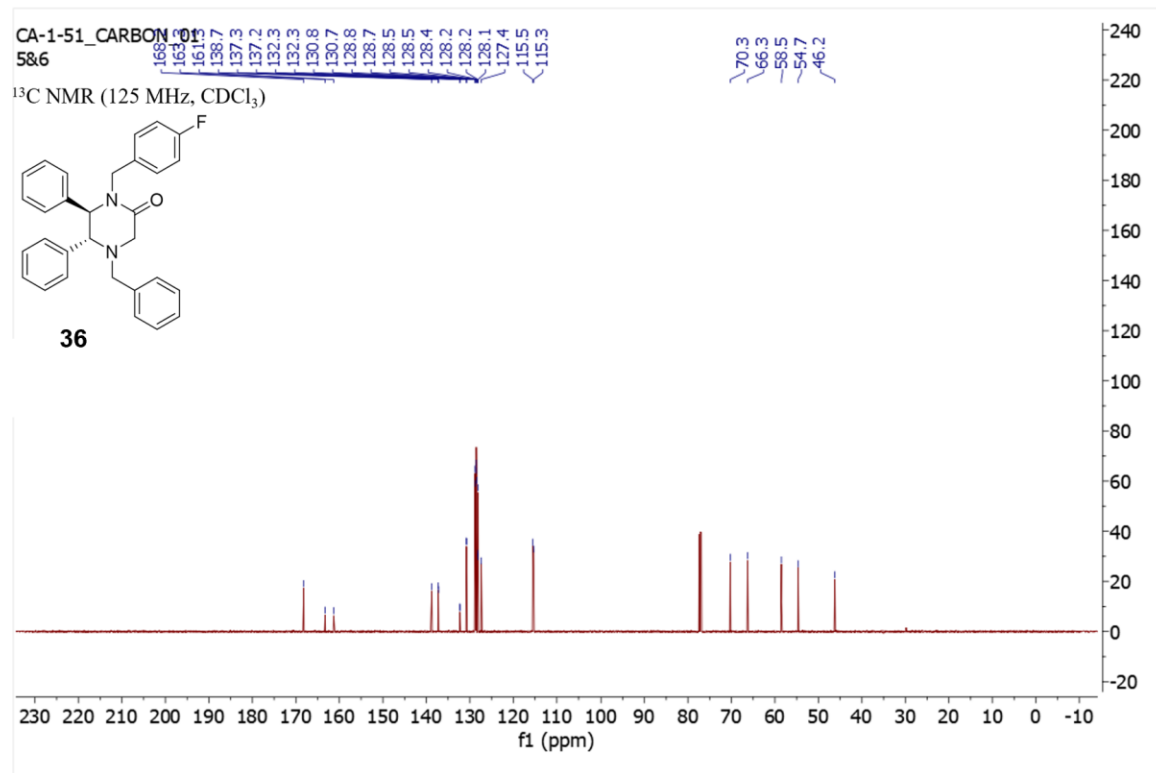


**Figure 4.28: Carbon-13 NMR of compound 36. Related to scheme 4.2.**

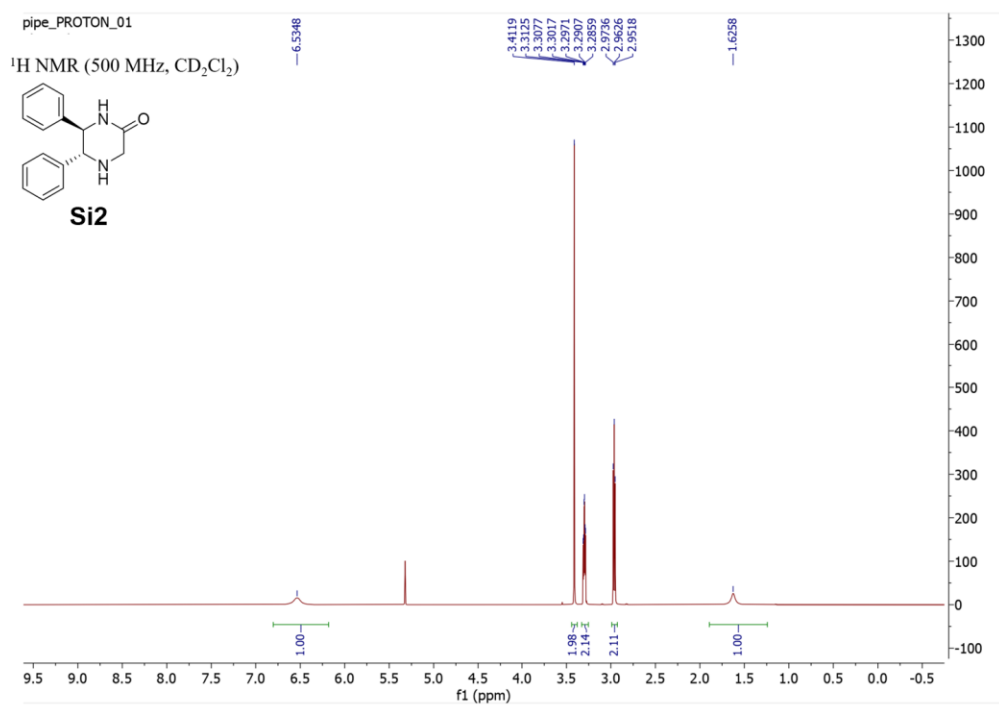


**Figure 4.29: Proton NMR of compound SI2. Related to scheme 4.3.**

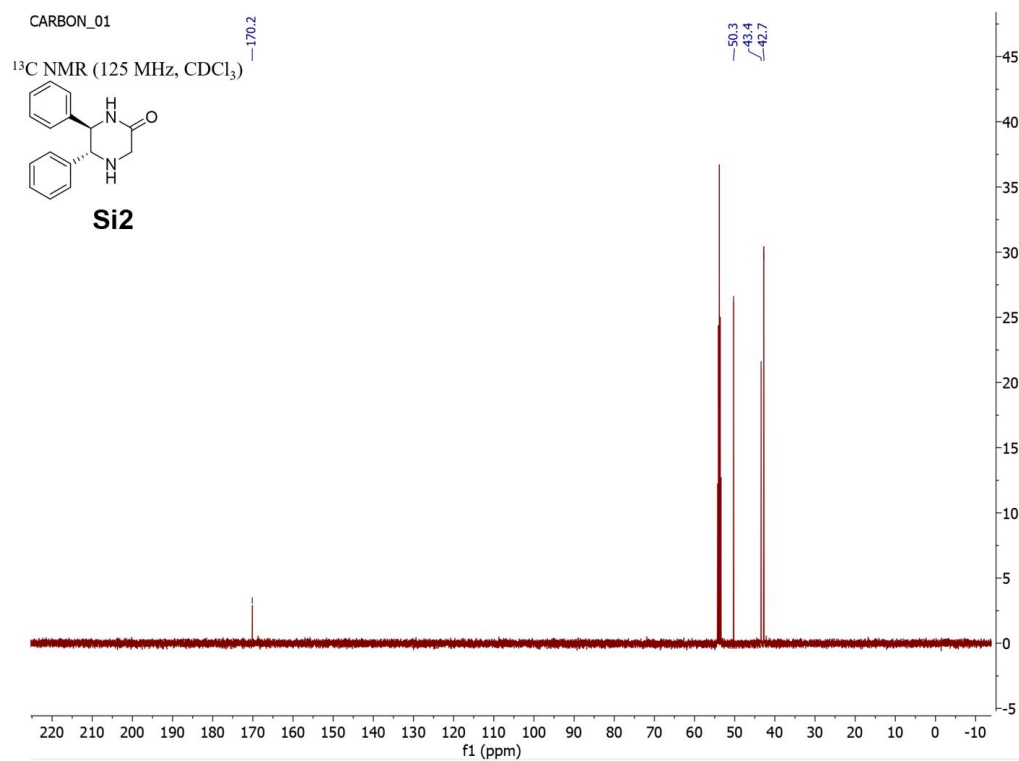


**Figure 4.30: Carbon-13 NMR of compound SI2. Related to scheme 4.3.**



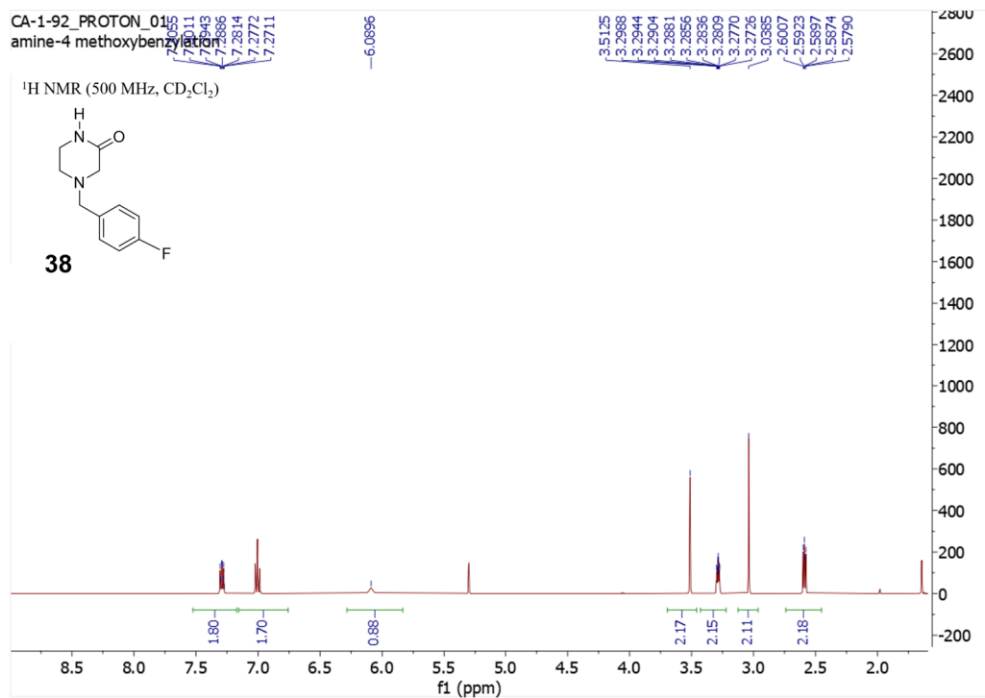


**Figure 4.31: Proton NMR of compound 38. Related to scheme 4.3.**

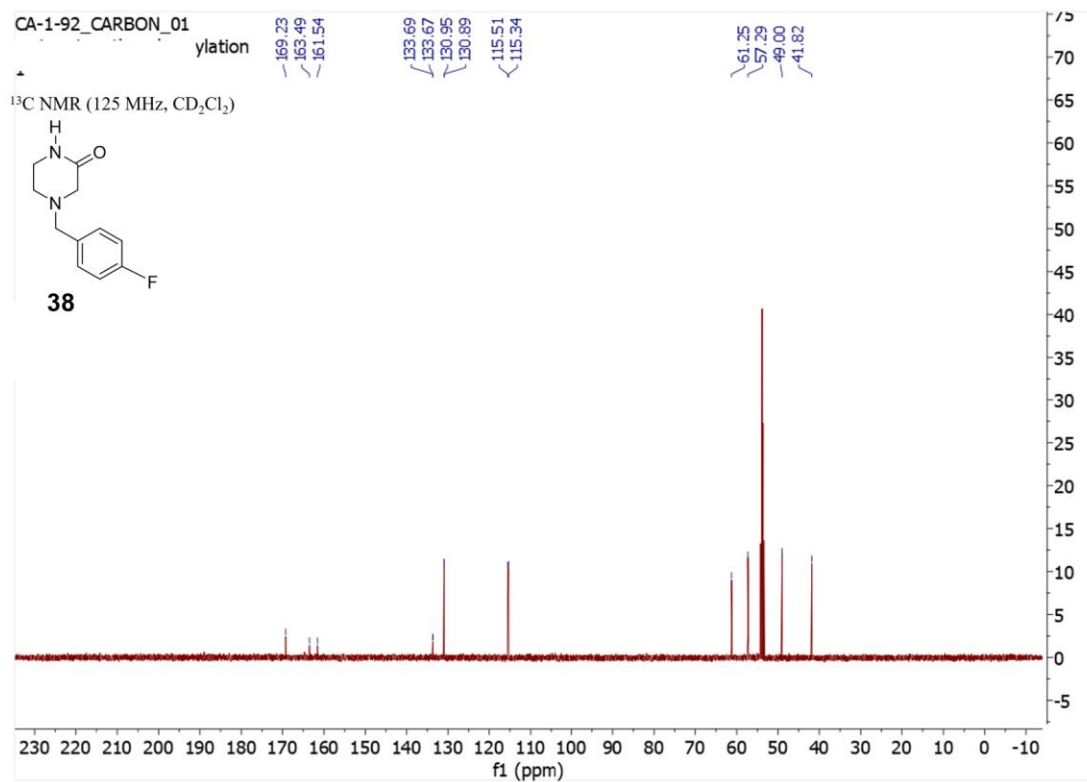


**Figure 4.32: Carbon-13 NMR of compound 38. Related to scheme 4.3.**

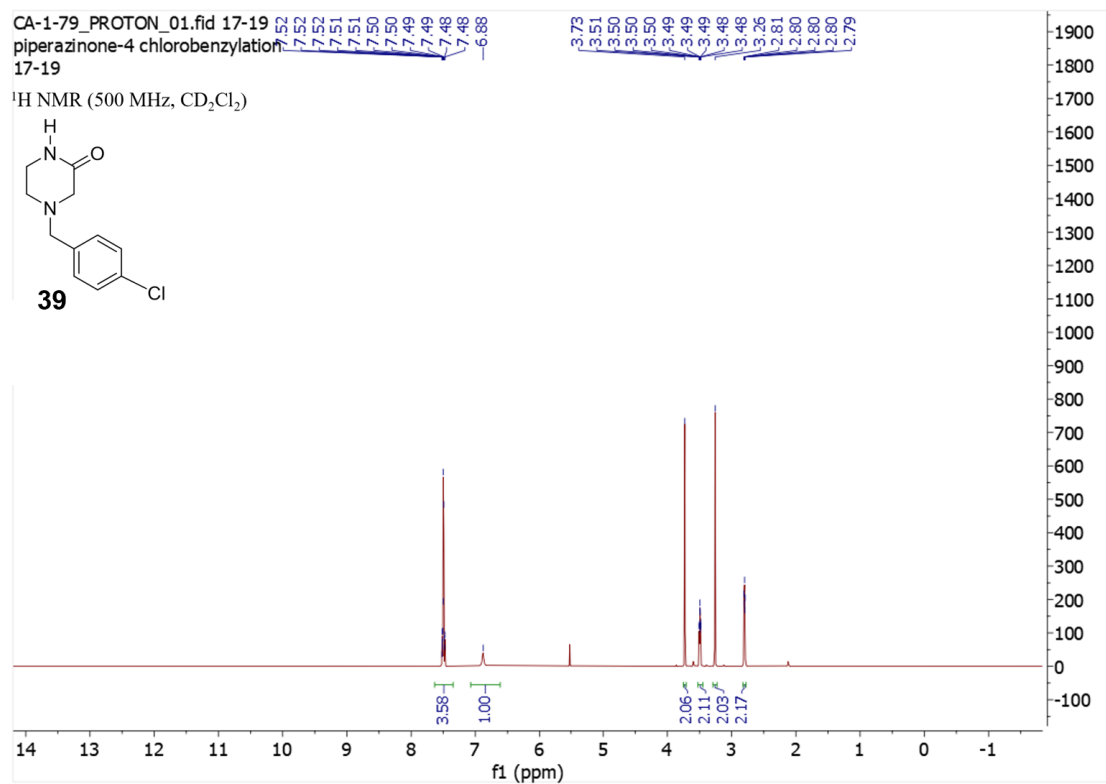


**Figure 4.33: Proton NMR of compound 39. Related to scheme 4.3.**

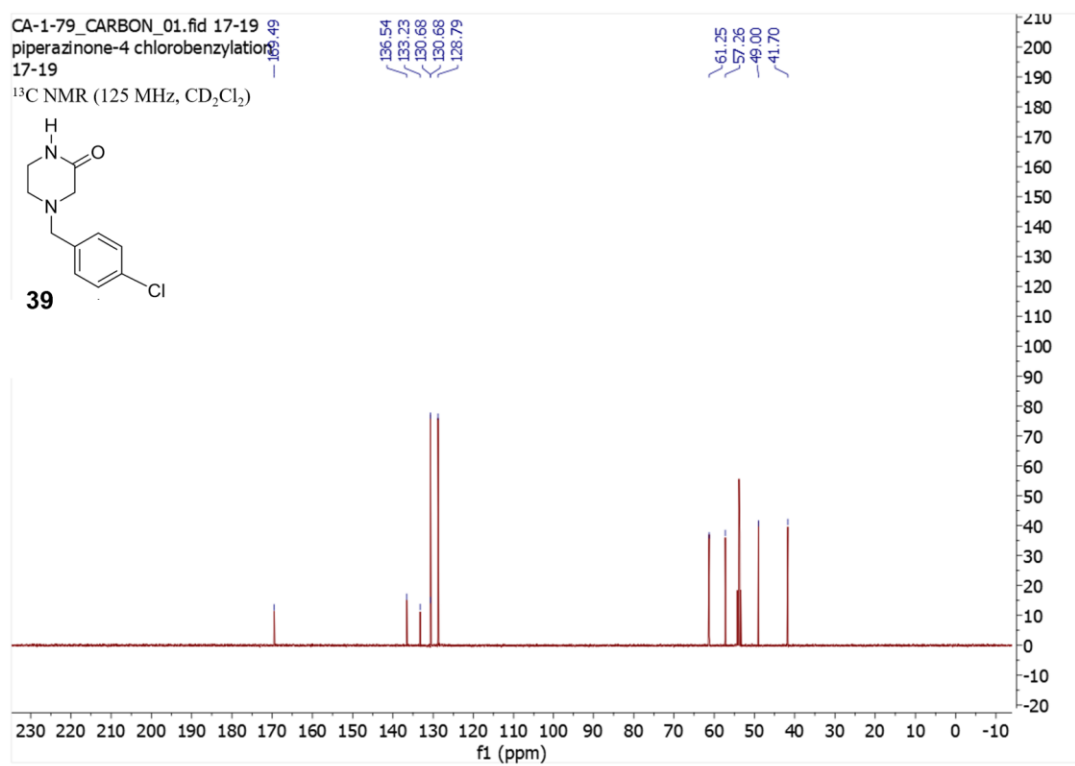


**Figure 4.34: Carbon-13 NMR of compound 39. Related to scheme 4.3.**

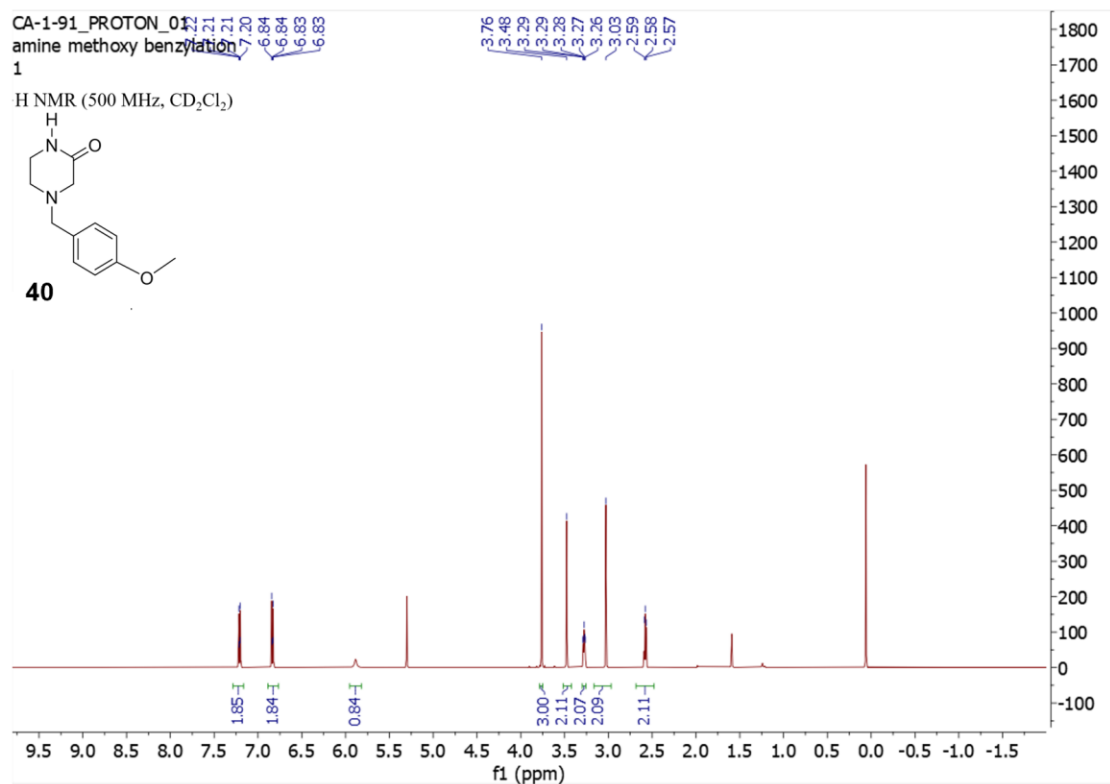


**Figure 4.35: Proton NMR of compound 40. Related to scheme 4.3.**

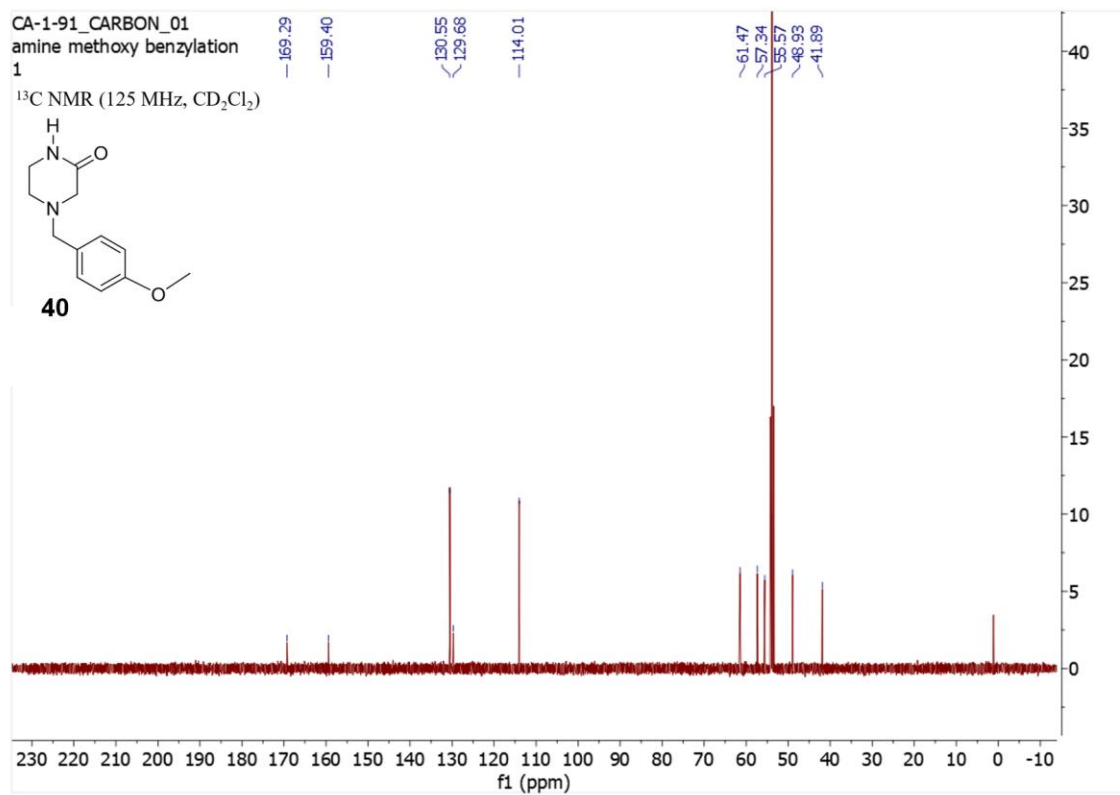


**Figure 4.36: Carbon-13 NMR of compound 40. Related to scheme 4.3.**

### **Small peptide assay:**

As described previously, the small peptide assay was carried out in a black flat/transparent bottom 96-well plate with a 100  $\mu$ L volume.<sup>1,2</sup> Different concentrations of compounds (between 80  $\mu$ M to 1.25  $\mu$ M) to be tested were incubated with 1 nM 20S proteasome (Enzo Life Sciences) in a 50 mM Tris-HCl and 100 mM NaCl buffer at a pH of 7.8 for 15 minutes at 37 °C. After incubation, **Aminomethylcoumarin (AMC)**-conjugated substrates corresponding to each catalytic site were added. The enzymatic activity was measured at 37 °C on a SpectraMax M5e spectrometer by measuring the increase in fluorescence units per minute for one hour at excitation and emission wavelengths of 380 and 460 nm, respectively. The fluorescence of the vehicle was set at 100%. The tested compounds' fold activity was then plotted as a function of drug concentration using GraphPad Prism. The fluorogenic substrates Z-LLE-AMC (Casp-L activity, 10  $\mu$ M), Suc-LLVY-AMC (CT-L activity, 10  $\mu$ M), and Boc-LRR-AMC (T-L activity, 20  $\mu$ M, due to the low activity of the trypsin-like site) used were all obtained from Bosten Biochem.

### **In vitro $\alpha$ -synuclein degradation assay**

Proteolytic digestions of  $\alpha$ -synuclein assays were carried out in a 25  $\mu$ L reaction volume of 50 mM HEPES and 5 mM DTT buffer at a pH of 7.2, 300 nM of purified  $\alpha$ -synuclein, and 10 nM purified human 20S proteasome. The 20S proteasome was first diluted to 11.1 nM in the HEPES buffer, and 0.5  $\mu$ L of the test compounds in DMSO or DMSO alone were added. The drug: proteasome solution was incubated for 45 minutes at 37 °C. After this incubation, 2.5  $\mu$ L of a 3  $\mu$ M stock of  $\alpha$ -synuclein was added, and the mixture was incubated at 37 °C for an additional 3.5 hours. After the second incubation, 0.5  $\mu$ M of GAPDH was added as a loading control. A concentrated SDS loading buffer was also added, and then the samples were boiled for 10 minutes to stop the digestion and immunoblotted.

To prepare samples for immunoblotting, a concentrated Laemmli buffer containing 25%  $\beta$ -mercaptoethanol was added, and the mixture was boiled for 10 minutes. Proteins were separated using a 4–20% Tris-glycine SDS-PAGE gel and transferred onto PVDF membranes with a Mini Trans-Blot Electrophoretic Transfer Cell for 90 minutes. After

transfer, membranes were blocked at room temperature for 30 minutes using a 5% blocking solution prepared in Tris-buffered saline containing Tween 20 (TBST). The membranes were then incubated for 1 hour at rt or overnight (16 hours) at 4°C with the appropriate primary antibody, diluted according to specifications, in TBST. Following primary antibody incubation, membranes were washed three times, each for 3 minutes, with TBST. They were then exposed to a secondary antibody for 1 hour at room temperature. Protein detection was performed using an ECL Western reagent, and signals were captured using the Azure Biosystems 300Q imaging system. When multiple proteins needed to be probed, membranes were stripped using a mild stripping buffer (200 mM glycine, 3.5 mM SDS, 8 mM Tween 20, pH 2.2) for 30 minutes. The membranes were then washed thrice with TBST, 5 minutes per wash, before re-probing using the same protocol. Protein band intensities were quantified using Bio-Rad Image Lab software.



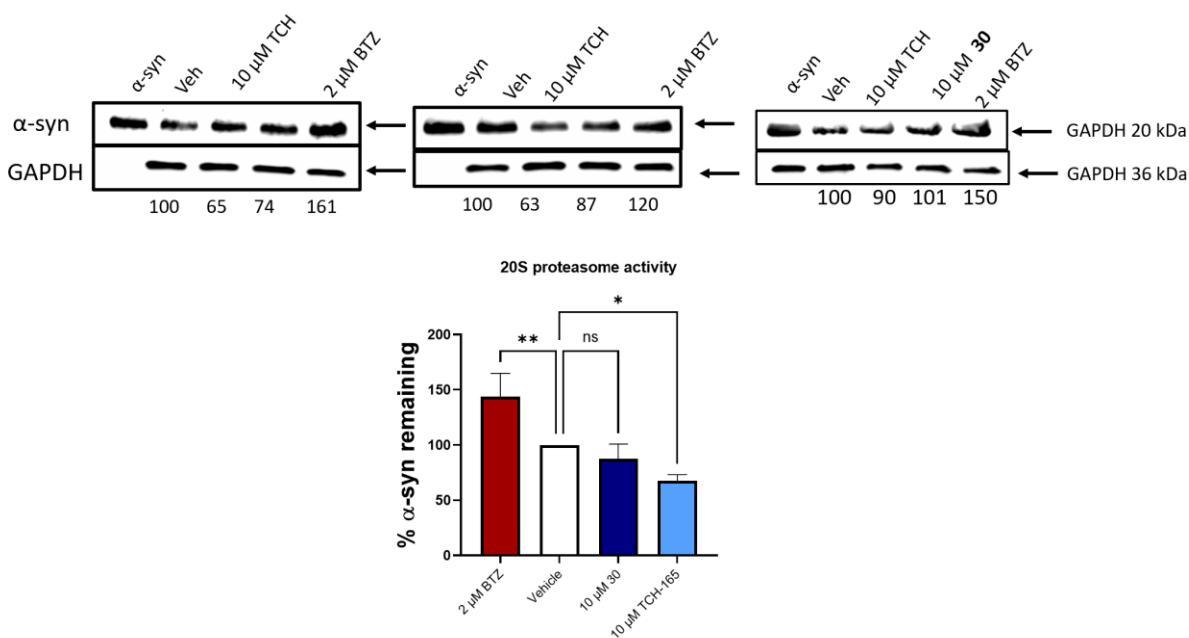


**Figure 4.37: Westerns of a-synuclein degradation by purified 20S proteasome treated with 10 μM of compound 30 ,and TCH-165. The quantification values were all normalized to the GAPDH, and the gels shown are indicative of n=3 independent experiments. Related to Figure 4.6.**

## **CHAPTER FIVE: Materials and Miscellaneous**

## 5.1 Materials

### 5.1.1 Antibodies

| Antibodies                                      | Source          | Catalog number |
|---|-----------------|----------------|
| Mouse Monoclonal Anti- $\alpha$ -synuclein      | Novus Biologics | NBP2-15365     |
| Rabbit Monoclonal Anti-p25 $\alpha$             | Novus Biologics | NBP1-91613     |
| Mouse HRP Tagged Anti-GAPDH                     | Novus Biologics | NBP2-27103H    |
| Anti-Rabbit HRP-Linked                          | Cell Signaling  | 7074S          |
| Anti-Mouse HRP-Linked                           | Cell Signaling  | 70745          |
| Rabbit Anti- $\alpha$ -synuclein                | Abcam           | ab212184       |
| Mouse HRP Tagged Anti-DNP                       | Santa Cruz      | Sc-69698 HRP   |
| Mouse HRP Tagged Anti-Ubiquitin                 | Santa Cruz      | sc-8017        |
| Rabbit HRP Tagged Monoclonal ant- $\beta$ Actin | Cell Signaling  | 5125           |

**Table 5.1: List of antibodies used herein.**

### 5.1.2 Proteins and Peptides

| Proteins and peptides                             | Source           | Catalog number |
|---|------------------|----------------|
| Boc-LLR-AMC (trifluoroacetate salt)               | Cayman Chemicals | 26642          |
| Z-LLR-AMC   | Cayman Chemicals | 10008117       |
| Suc-LLVY-AMC                                      | R&D Systems      | S-280-05M      |
| Human 20S Proteasome protein, CF                  | R&D Systems      | E-360-050      |
| Recombinant Human $\alpha$ -synuclein protein, CF | R&D Systems      | SP-485-500     |
| Recombinant Human GAPDH protein                   | Novus Biologics  | NBP2-52615     |
| Rabbit HRP Tagged Monoclonal ant- $\beta$ Actin   | Cell Signaling   | 5125           |

**Table 5.2: List of proteins and peptides used in this work.**

### 5.1.3 Mammalian Cell Lines

| Reagents | Source | Catalog number |
|----------|--------|----------------|
| HET-293T | ATCC   | CRL-3216       |
| HT-22    | Cytion | 305158         |

**Table 5.3: List of cell lines used in this work.**

### 5.1.4 Reagents and Chemicals

| Reagent  | Source                  | Identifier  |
|--|-------------------------|-------------|
| Dulbecco's Modified Eagle's Medium                     | Gibco                   | 11995-065   |
| Penicillin–Streptomycin                                | Gibco                   | 15140-122   |
| Fetal Bovine Serum                                     | Gibco                   | 26140-079   |
| RPMI 1640  | Gibco                   | 11875-093   |
| Horse Serum Donor Herd                                 | Sigma-Aldrich           | H1270       |
| Opti-mem   | Gibco                   | 31985-070   |
| 0.25% Trypsin-EDTA (1x)                                | Gibco                   | 25200-056   |
| DMEM, high glucose, no glutamine, no phenol red        | ThermoFisher Scientific | 31053036    |
| cOmplete™, Mini, EDTA-free Protease Inhibitor Cocktail | Sigma-Aldrich           | 11836170001 |
| X-tremeGENE siRNA Transfection Reagent                 | Sigma-Aldrich           | 4476093001  |
| X-tremeGENE HP DNA Transfection Reagent                | Sigma-Aldrich           | 6366236001  |
| PBS  | Sigma-Aldrich           | D8537       |
| RIPA Buffer  | Sigma-Aldrich           | R0278       |
| HBSS   | ThermoFisher Scientific | 882484      |
| TMRM   | ThermoFisher Scientific | T668        |
| Pierce BCA Protein Analysis Kit                        | ThermoFisher Scientific | 23225       |
| Laemmli Sample Buffer                                  | Bio-Rad                 | 1610747     |
| 2-Mercaptoethanol                                      | Sigma-Aldrich           | M6250       |
| 4-20% Tris-glycine SDS-PAGE gel                        | Bio-Rad                 | 4561096     |
| PVDF membrane  | Bio-Rad                 | 1620177     |
| Blotting Grade Blocker                                 | Bio-Rad                 | 1706404     |

**Table 5.4: List of chemicals and reagents used in this work.**

|   |   |              |
|---|---|--------------|
| Radiance plus                                     | Azure Biosystems                        | AC2103       |
| Cell Titer Glo Reagent                            | Promega                                 | G3580        |
| GSH/GSSG-Glo™ Assay                               | Promega                                 | V6611        |
| TCH-165   | Njomen, E.; <i>et al.</i> <sup>42</sup> | N/A          |
| TMRM  | ThermoFisher Scientific                 | T668         |
| Bortezomib  | Cayman Chemicals                        | 10008822     |
| Flowmi® Cell Strainers (with a porosity of 40 µm) | Sigma-Aldrich                           | BAH136800040 |

**Table 5.4: (Cont'd).**

### 5.1.5 Instrumentation

| Instrumentation                               | Source            | Identifier  |
|---|-------------------|-------------|
| Q500 Sonicator                                | Qsonica           | Q500-110    |
| Mini Trans-Blot Electrophoretic Transfer Cell | Bio-Rad           | 1703930     |
| Azure Biosystems 300Q imager                  | Azure Biosystems  | AZI300-01   |
| SpectraMax® M5e Microplate Reader             | Molecular Devices | Refurbished |
| BioTek Synergy Neo                            | Agilent           | N/A         |

**Table 5.5: List of instruments used in this work.**

### 5.1.6. Software

| Software                   | Source            | Identifier   |
|----------------------------|-------------------|--|
| Bio-Rad Image Lab software | Bio-Rad           | Bio-Rad: <a href="https://www.bio-rad.com/en-us/product/image-lab-software?ID=KRE6P5E8Z">https://www.bio-rad.com/en-us/product/image-lab-software?ID=KRE6P5E8Z</a>   |
| GraphPad Prism 8           | GraphPad          | GraphPad: <a href="https://www.graphpad.com/scientific-software/prism/">https://www.graphpad.com/scientific-software/prism/</a>  |
| SoftMax Pro 7.1            | Molecular Devices | Molecular Devices: <a href="https://support.moleculardevices.com/s/article/SoftMax-Pro-7-1-software-Download-page">https://support.moleculardevices.com/s/article/SoftMax-Pro-7-1-software-Download-page</a> |

**Table 5.6: List of software utilized in this work.**

## **5.2 Miscellaneous**

### **5.2.1 Quantification and statistical analysis**

All data presented in this work are as mean  $\pm$  standard deviation (SD) unless otherwise stated in the legend. For each figure, the number of replicates is indicated in the figure legends. Statistical analysis was only performed on experiments with three or more replications or "n's. Western blot quantifications were performed with Bio-Rad Image Lab software. Statistical analysis was performed with GraphPad Prism 8 software. One-way ANOVA analysis, along with appropriate post-hoc tests, was used for multiple comparisons of means. Effect was considered significant for \* $p < 0.05$ , \*\* $p < 0.01$ , \*\*\* $p < 0.001$ , \*\*\*\* $p < 0.0001$ .

### **5.2.2 Note**

Sections 2.2-2.5 of chapter 2 were reproduced with permission from *iScience* 2024, 27 (7), 110166-110166. Publication date: July 19, 2024: Copyright 2024 Elsevier Inc. <https://doi.org/10.1016/j.isci.2024.110166>.